1-1-1999

The morphological behavior of miktoarm star and multiple-graft block copolymers.

Frederick Louis Beyer
University of Massachusetts Amherst

THE MORPHOLOGICAL BEHAVIOR OF MIKTOARM STAR AND MULTIPLE-GRAFT BLOCK COPOLYMERS

A Dissertation Presented

by

FREDERICK LOUIS BEYER III

Submitted to the Graduate School of the
University of Massachusetts Amherst in partial fulfillment
of the requirements for the degree of

DOCTOR OF PHILOSOPHY

September 1999

Polymer Science and Engineering

THE MORPHOLOGICAL BEHAVIOR OF MIKTOARM STAR AND MULTIPLE-GRAFT BLOCK COPOLYMERS

A Dissertation Presented

by

FREDERICK LOUIS BEYER III

Approved as to style and content by:

Samuel P. Gido, Chair

Alan J. Lesser, Member

H. Henning Winter, Member

Richard J. Farris, Head
Polymer Science & Engineering

DEDICATION

To my grandfather, Lucian Allen Peacock.

ACKNOWLEDGEMENTS

Much of the credit for my current level of academic achievement belongs to the educators I've encountered over the course of the last 22 years. A few names come immediately to mind. Prof. J. M. A. Danby and Prof. S. O. Paur, of North Carolina State University, taught me how to think rationally, a skill which I fear will never again be as sharp as it was when I was an undergraduate. Dr. Nora Beck Tan, of the Army Research Laboratory, took an active interest in my graduate career at an early stage, and has provided me with valuable experience and encouragement. Dr. Andrew Peacock, of Exxon Chemical, and Prof. Alan Lesser, of the UMass Polymer Science & Engineering department, both lent encouragement and guidance for many months following my first involvement with the CUMIRP program. It has been my distinct pleasure to work with both Prof. Lesser and Prof. Henning Winter of UMass during the course of my dissertation research, and I owe them thanks for their valuable time and input.

I must also pay due credit to those who have contributed formally to the five studies described in this manuscript. From the University of Athens, Greece, Yiannis Poulos, Apostolos Avergeropoulos, Maria Xenidou, Hermis Iatrou, Gabriel Velis, and Prof. Nikos Hadjichristidis contributed invaluable time and effort in the realm of sample synthesis. From the University of Alabama at Birmingham, David Uhrig and Prof. Jimmy Mays also contributed many hours to the synthetic portion of this work, and I am privileged to count them also as friends. Mei Ling Chiang, Prof. Bruce Garetz, and Prof. Nitash Balsara contributed greatly to the work on regular multigrafts. Finally, Sam Trevino of NIST in Gaithersburg, MD, deserves much credit for his help in collecting SANS data and for a lot of laughs in the process.

ABSTRACT

THE MORPHOLOGICAL BEHAVIOR OF MIKTOARM STAR AND MULTIPLE-GRAFT BLOCK COPOLYMERS

SEPTEMBER 1999

FREDERICK LOUIS BEYER III

B.S., NORTH CAROLINA STATE UNIVERSITY

M.S., UNIVERSITY OF MASSACHUSETTS AMHERST

Ph.D., UNIVERSITY OF MASSACHUSETTS AMHERST

Directed by: Professor Samuel P. Gido

The effects of molecular architecture on block copolymer morphological behavior for two distinct types of architectures have been investigated. The first, A_nB_m-type stars, have a single, centrally located junction point from which blocks of two polymer species radiate, and are referred to as miktoarm stars. The extremes of a model proposed by Milner were investigated using three miktoarm systems, A_2B_2 stars, A_8B_8 "Vergina" stars, and A_5B stars. Samples having a low molecular asymmetry agreed in general with the predictions of this model, although bicontinuous morphologies were not observed. The A_5B miktoarm samples, which have a high level of molecular asymmetry, exhibited behavior not predicted by the model, but which was consistent with a trend of discrepancies observed in prior studies. The effect of the junction point on chain stretching behavior in miktoarm stars was noted by comparing the lamellar period of several A_2B_2 and A_8B_8 stars to comparable AB diblocks. These materials were found to

have significantly increased lamellar periods, thought to result from the increased chain stretching at and near the junction point.

The second type of molecular architecture investigated was the multiple-graft architecture. Three series of multigrafts were characterized: regular multigrafts with tetrafunctional branch points, random multigrafts with trifunctional branch points, and random multigrafts with tetrafunctional branch points. Using the constituting block copolymer hypothesis, the behavior of these molecules was predicted using existing theories for block copolymers with simpler architectures. Use of this hypothesis is justified herein, and illustrates that the behavior of block copolymers with complex architectures is dictated by the preferred behavior of smaller architectural subunits from which the multigraft is comprised. The morphological behavior of multiple-graft block copolymers was shown to be influenced by branch point functionality, branch point location, and the number of branch points per molecule. Architectural heterogeneity was found to impair self-assembly behavior of the multigrafts. Small-angle scattering data indicating the formation of microphase separated domains of specific shapes were observed for non-lamellar morphologies, which are able to form and fill space without ordering on a lattice.

Finally, lamellar grain size and shape a the series of regular multigrafts was investigated. Grain size was seen to be influenced by the total molecular weight of the multigraft. Grain anisotropy was found to increase as the lamellar grains increase in size, indicating that the growth of lamellar grains is anisotropic, occurring more readily in the direction normal to the plane of the lamellae.

TABLE OF CONTENTS

LIST OF TABLES

LIST OF FIGURES

CHAPTER 1

INTRODUCTION

1.1 Miktoarm Stars

Study of the morphological behavior of block copolymers with non-linear, grafted architectures has been extensive over the last five years.[1-6] This work originated in part from an interest in finding new ways to control the formation of block copolymer mesophases other than by variations in temperature and relative volume fractions of the component materials.[1] Results of an early study examining the morphological behavior of a limited set of A_nB_m–type stars indicated that molecular architecture could significantly affect morphological behavior.[2] Figure 1.1 illustrates a model A_nB_m-type block copolymer, in this case having $n = 3$ and $m = 2$. This work was facilitated by developments in chlorosilane chemistry techniques which allowed the coupling of blocks of living polymers in new ways.[7]

Soon after Hadjichristidis and coworkers[2] published their preliminary findings, Milner presented a mean-field model predicting the combined effects of architectural asymmetry, a difference in the number of arms of components A and B, and conformational asymmetry, the difference in space-filling characteristics of components A and B, on the morphological behavior of A_nB_m-type stars.[8] This work provided a guide to experimentalists examining the morphological behavior of these materials, newly christened "miktoarm" stars by Hadjichristidis. Miktoarm is a combination of the Greek *μικτοσ*, meaning "mixed", and arm. Both miktoarm star and A_nB_m-type star will be used through out this work to refer to block copolymers with this architecture.

The Milner model was successfully used to predict the behavior of two series of miktoarm stars.[1,9] These materials, A_2B stars and A_3B stars, confirmed the general

predictions of the Milner model. However, several samples were found to exhibit morphological behaviors differing from the predictions of the Milner model. These discrepancies suggested that while the model correctly predicted the basic effects of architecture on morphological behavior, the specific details of the miktoarm star molecular architecture and its impact on morphology might not be properly described.

A second area of interest in the model was the effect on morphological behavior of architecturally symmetric, A_nB_n-type miktoarm stars. These materials were predicted to behave essentially as linear AB diblocks of the same overall volume fraction. Such samples were of interest because they provided an opportunity to examine the effect of the star architecture on conformational asymmetry while ignoring architectural asymmetry, and were becoming useful in the prediction of the behavior of multiple-graft block copolymers.

1.2 Multiple-Graft Block Copolymers

The status of research and use of graft block copolymers at the outset of this work was beginning to change after many years of limited activity. Previously, research into graft block copolymer physical behavior was severely limited by the synthetic techniques which were available.[10,11] These techniques produced graft copolymers having highly heterogeneous architectures, such as that illustrated in Figure 1.2. This molecule has a backbone of one polymer, with arms of a second polymer grafted to the backbone. A sample of a typical graft copolymer produced by common methods might contain many different architectural species. The sample could be characterized as having polydisperse backbones, polydisperse arms, randomly placed branch points, and no control over the

number of branch points per molecule. The architectural heterogeneity of these materials completely prohibited a comprehensive study of their morphological behavior.

However, the interest in graft block copolymers was rising. Modeling by Shinozaki and coworkers found that the architectural variables described above affected the order-disorder transition of such materials.[12] Lyatskaya and Balazs found that mixtures of diblock copolymers and graft copolymers might be very useful as blend compatibilizing agents.[13-15]

Recent developments in living anionic polymer chemistry and chlorosilane coupling techniques now allowed the synthesis of graft copolymers with well-defined architectures.[16,17] Several possible architectures which were newly possible are illustrated in Figure 1.3. Two architectural variables are illustrated in this figure. The first, functionality of the branch point, is derived from the synthetic techniques by which multigrafts are produced, and reflects the number of reactive sites on the chlorosilane junction point molecule. A trichloromethylsilane molecule is used to attach a single arm to the multigraft backbone; multigrafts with one arm grafted to the backbone per branch point are referred to as having trifunctional branch points. A tetrachlorosilane molecule is used to attach two arms to the multigraft backbone; multigrafts with two arms per branch point are called tetrafunctional multigrafts.

The second architectural variable is location of the branch points along the backbone. Branch points can either be located at regular intervals along the backbone, in which case the multigraft is termed "regular", or at random locations along the backbone, in which case the multigraft is termed "random". Branch point location is also controlled directly through synthetic techniques.[16,17] Regular multigrafts are synthesized using a macromolecular, polycondensation type reaction, where preformed polyisoprene (PI)

Finally and certainly not least among my academic colleagues, I am indebted to my dissertation advisor, Prof. Sam Gido. Without doubt I have learned much from Sam, sometimes not of my choice, but always to my advantage. Sam has taught me much about academia, scientific research, block copolymers, and the many practical matters which are involved in acquiring a doctorate, lessons which will surely serve me well in the future.

I have been lucky to count many among my friends during the last five years, but a handful of these I know will be pestering me for years to come. Darrin and Buddy helped me keep my sanity as we blasted each other playing Marathon. Mark and Dale kept my firmly in touch with my roots in North Carolina throughout my tenure in Massachusetts. I would have been lost without Suellen Sack, who showed me how much fun two feet of snow and sub-zero temperatures could really be. Vinnie has been great for showing me that life does exist outside of the Polymer Science department, and Vivek and Sid have taught me much in the last few months about conquering the world. True friends are rare, and I am fortunate to have so many.

To my family, I owe a debt I cannot express much less repay. Without fail, they have always been supportive of my academic undertakings; my success has been a family project from kindergarten through the current stage.

Finally, I would like to thank my girlfriend Kristi. Her love and friendship are true blessings having no explanation nor requiring one. My only regret in graduate school has to be that we didn't meet sooner, because our relationship has become the foundation on which I've stood during the last two years. Her love has made me a better person, and that may be the best result of my time in graduate school.

backbone "connector units" are linked together using preformed macromolecular polystyrene (PS) coupling agents. This process assures regular placement of branch points. Random multigrafts are synthesized in an entirely different method: polybutadiene (PB) backbones are synthesized in their entirety using living anionic polymerization. The backbones are then modified relying on precisely controlled stoichiometry to control the number of branch points per molecule. The branching agent (a functionalized chlorosilane molecule) reacts specifically with pendant vinyl groups on the PB backbone resulting from limit 1,2- polymerization of the 1,4-butadiene. In this manner, the placement of branch points is randomized.

These two synthetic techniques now allowed a systematic study of multiple-graft block copolymers with well-defined architectures. Examination of the effects of the architectural variables illustrated in Figure 1.3, branch point location and functionality, on the morphological behavior of multiple-graft block copolymers with precisely defined architectures was possible for the first time.

1.3 Background

The following sections are offered as a brief introduction to the basic principles applied in this dissertation. The reader is advised to refer to the cited references for a more complete discussion of these topics.

1.3.1 Self-Assembly of Linear Diblocks

The mechanism for self-assembly of linear (AB) diblocks into ordered mesophases derives from the basic tendency of immiscible systems to phase separate when unfavorable enthalpic interactions overcome the entropic benefits of mixing.[18] In

block copolymers, however, the joining of immiscible blocks into one molecule prevents conventional, macroscopic phase separation. Instead, the driving force to minimize unfavorable A-B contacts produces a system which forms mesomorphic structures on the nanoscopic level.[19,20]

A variety of interesting morphologies are formed when block copolymers self-assemble. These include alternating lamellae of A and B, cylinders of one component in a matrix of the other, and spheres of one component in a matrix of the other. Other morphologies which have been observed include complex bicontinuous morphologies, perforated lamellae, and undulating lamellae.[21-28]

The selection of morphology is based simply on the free energy of the system. The total free energy of a block copolymer system which has microphase separated is a sum of competing effects, the energy required to create a surface between microphase separated domains, and the energy resulting from the stretching of the polymer chains away from the newly formed interface.

Figure 1.4 shows a morphology diagram recently calculated by Matsen and Bates.[29] This diagram predicts AB diblock copolymer morphology as a function of f, the relative volume fraction of one component of an AB diblock copolymer, and the product χN, where χ is the Flory-Huggins binary segmental interaction parameter[30] and N is the total degree of polymerization of the block copolymer. Polymers A and B in this case have identical conformational behavior, leading to a morphology diagram symmetric about $f = 0.5$. This morphology diagram reflects the results of nearly 30 years of both theoretical and experimental work toward understanding the morphological behavior of block copolymers, beginning with a model proposed by Helfand,[31-36] and with significant refinements by Leibler[37] and Semenov.[38] It predicts the formation of the "classical"

morphologies, alternating lamellae (L), hexagonally packed cylinders (H), spheres ($Q_{Im\bar{3}m}$) on a body-centered cubic (BCC) lattice, as well as more complicated morphologies such as the "gyroid" cubic bicontinuous morphology ($Q_{Ia\bar{3}d}$).[24,26] Below a critical level of $\chi N = 10.5$ for a block copolymer with equal volume fractions of A and B, a diblock copolymer is predicted to form a homogenous, disordered morphology.

Three regimes in Figure 1.4 are commonly defined. These are the weak segregation regime (WSR), the intermediate segregation regime (ISR), and the strong segregation regime (SSR). The divisions between these regimes are based on the change in scaling behavior of mesophase period with degree of polymerization.[20] Typically, the WSR is defined by $\chi N < 15$, the ISR by $15 < \chi N < 100$, and the SSR by $\chi N > 100$. For the purposes of most block copolymer morphology studies, samples that fall in the SSR are preferred as their behavior has been most extensively modeled and examined. In the SSR, the interface between the microphase separated domains is a sharp division between essentially pure domains of components A and B. This condition, utilized by Helfand as the narrow interphase approximation,[34] is only possible when the unfavorable enthalpic interactions dominate the free energy of the system, such as occurs at high χN.

1.3.2 The Milner Model

Microphase separated block copolymers have been successfully represented as polymer brushes grafted to the dividing surface between mesophases.[39-44] The model proposed by Milner applies these arguments to construct a self-consistent, mean-field theory for miktoarm star morphological behavior.[8,45] The free energy of a mesophase is calculated for a single molecule confined in a wedge representing the Wigner-Seitz unit cell for each morphology,[36] and is the sum of the interfacial energy required to create the

interface between microphase separated domains of A and B, and the stretching energy resulting from the incompressibility boundary condition for a bulk polymer.

The shape of the wedge is determined by the mesophase, as illustrated in Figure 1.5. The height of the wedge is the radius of the round unit cell. The location of the dividing surface between microphase separated A and B domains is shown as a shaded plane. Wedge height is determined by a technique developed for polymer brushes, and is limited only by the number of chains confined to the wedge at a given surface density (chains per unit area). Chains are added incrementally until the appropriate number are present on each side of the wedge. The height of the interface determines the surface area of the interface, and is governed by the conformational properties of the constituent materials. Such round unit cell models are recognized as giving non-physical results in certain limits,[46] but are successful in predicting general behavior.

The stretching free energy contribution to the free energy is also determined using models developed for polymer brushes. The chain ends for each arm of the star are assumed to be found at any distance from the dividing surface within the wedge. This assumption justifies use of a quadratic chemical potential function with distance from the interface.[40] To calculate the stretching energy, chemical potential is integrated with respect to interface surface area.

Combining the stretching free energy component with the interfacial free energy term yields a set of equations giving free energy for the four morphologies considered, lamellae, hexagonal cylinders, BCC spheres, and the ordered, bicontinuous double-diamond (OBDD) morphology.[27] These are given as equations 1, 2, and 3,

$$\frac{f_{lam}}{f_0} = \left[\varepsilon(1-\phi) + \frac{\phi}{\varepsilon} \right]^{1/3} \qquad (1)$$

$$\frac{f_{cyl}}{f_0} = \left[\frac{2\varepsilon\phi(1-\phi^{1/3})^3(3+\phi^{1/2})}{(1-\phi)^2} + \frac{2\phi}{\varepsilon} \right]^{1/3} \tag{2}$$

$$\frac{f_{sph}}{f_0} = \left[\frac{27\varepsilon\phi^{4/3}(1-\phi^{1/3})^3(\phi^{2/3}+3\phi^{1/3}+6)}{10(1-\phi)^2} + \frac{27\phi}{10\varepsilon} \right]^{1/3} \tag{3}$$

where f is free energy, f_0 is the free energy of a lamellar morphology for a sample with 50 volume % of each component, ϕ is the volume fraction of the minority component, and ε is a unified molecular asymmetry parameter describing the architectural and conformational characteristics of the molecule. An analytical solution in terms of f and ε for the OBDD morphology is not possible; free energy must be calculated numerically in this case.

Milner's model in fact finds the OBDD morphology to be unstable.[8,45,47] Recent work by Matsen and Bates has verified this result, and attributes the instability of both the OBDD and the gyroid morphologies to packing frustration[29,48,49] arising from a combination of the confinement of the block copolymer junction point to the interface between A and B domains, and the incompressibility boundary condition. The geometries of the gyroid and OBDD morphologies are such that for the polymers to fill space as required, the junction point between blocks must deviate from its preferred position at the interface. This raises the total free energy of the morphology, and makes it unstable when the penalty for this deviation is great (in the SSR). The solution for the OBDD phase in the Milner model is multiplied by a small constant prefactor (0.99) to generate a window of stability.

Figure 1.6 shows the morphology diagram generated using the Milner model, including the unstable OBDD phase. Morphology is given for A_nB_m stars characterized by volume fraction, ϕ_B, and the unified molecular asymmetry, ε. The molecular

asymmetry parameter, ε, combines architectural asymmetry, the difference in number of arms of components A and B, with conformational asymmetry, the disparity in the space-filling characteristics of components A and B. The molecular asymmetry parameter is given as

$$\varepsilon = \left(\frac{n_A}{n_B}\right)\cdot\left(\frac{l_A}{l_B}\right)^{1/2} = \left(\frac{n_A}{n_B}\right)\cdot\left(\frac{\frac{V_A}{R_A^{\,2}}}{\frac{V_B}{R_B^{\,2}}}\right)^{1/2} = \left(\frac{n_A}{n_B}\right)\cdot\left(\frac{\frac{v_A}{b_A^{\,2}}}{\frac{v_B}{b_B^{\,2}}}\right)^{1/2} \qquad (4)$$

where n_i is the number of arms of component i, and l_i is a material parameter describing the conformational behavior of component i. This material parameter is defined as $l_i = V_i/(R_i^2)$, where V_i is the volume of component i having radius of gyration, R_i. Both terms are proportional to chain length, N, and the equation defining ε reduces to a function of arm number, n_i, segmental volume, v_i, and statistical segment length, b_i.

The model predicts that the volume fraction range in which a given morphology is predicted to be observed shift to higher volume fraction with increasing molecular asymmetry. This arises from the effect of confining multiple arms to one side of an interface. To illustrate, consider a conformationally symmetric linear diblock of equal volume fractions A and B ($\phi_B = 0.5$), such as illustrated in Figure 1.7a. If the single arm of A is then replaced by two arms of A exactly ½ the length of the original arm of A, to maintain a flat interface (lamellar morphology), the two arms must be stretched more than the single arm of A in the AB diblock (Figure 1.7b). This results in an increase in free energy, which may be partially alleviated by curvature of the interface away from the two A arms (Figure 1.7c). Volume fraction remains unchanged, but morphology has been dramatically altered by architecture. This effect produces the shift to higher volume fractions, with increasing molecular asymmetry, ε, of the volume fraction ranges in which

block copolymer morphologies are predicted. As illustrated in Figure 1.6, for a series of A_nB stars, as *n* increases the change in predicted morphological behavior is significant.

1.3.3 The Constituting Block Copolymer Hypothesis

While the Milner model predicts morphological behavior directly for A_nB_m-type block copolymer stars, and several models have been developed for linear diblocks, no such model exists for multiple-graft block copolymers. The effects of number and location of branch points on multigraft order-disorder transition behavior have been considered,[50] but no theory for the morphological behavior of such molecules has been forthcoming. During the course of investigating the morphological behavior of double-graft block copolymers, Gido and coworkers developed an empirical model which allows the prediction of morphological behavior of block copolymers with complex architectures using existing theory.[4,5,51]

Figures 1.8 illustrates the two double-graft architectures examined by Gido *et al.*, the π double-graft and H double-graft block copolymers. The double-graft architectures can be thought of as combinations of single-graft, A_2B star block copolymers. Figure 1.9 illustrates this concept for the π double-graft block copolymer. The π double-graft can be thought of as two A_2B miktoarm stars joined together at the ends of their backbones. These A_2B miktoarm stars which comprise the π double-graft are thus termed "constituting block copolymers". Gido and coworkers reasoned that, assuming the appropriate A_2B constituting block copolymers were of sufficient molecular weight to be in the SSR, the behavior of the double-grafts would be the governed by the behavior of the A_2B constituting block copolymers. Using the Milner model to predict the

morphological behavior of the appropriate A_2B miktoarm stars, the behavior of the double-grafts was correctly predicted to within the limit of the Milner model.[4,5]

For multiple-graft block copolymers such as those illustrated in Figure 1.3, the extension of the constituting block copolymer hypothesis is straightforward, illustrated by Figure 1.10. A regular multigraft with trifunctional branch points can be envisioned as a combination a A_2B miktoarm stars, connected by the ends of their A component arms. A regular multigraft with tetrafunctional branch points can be similarly envisioned as a combination of A_2B_2 miktoarm star block copolymers, joined together in series.

Determining the molecular characteristics of the constituting block copolymer for a given sample depends implicitly on collection of reliable molecular characterization data. For any multigraft, the length of the B component arm of the constituting block copolymer is simply the length of the grafted arm. Calculating the length of the A component arm for the constituting block copolymer is simply a matter of dividing the length of the multigraft backbone by the twice number of branch points. For a multigraft with regularly placed branch points, the constituting block copolymer calculated in this way is nearly exact, given accurate characterization of the multigraft molecular weight characteristics and the number of branch points per molecule. For a random multigraft, this technique produces an average constituting block copolymer, neglecting the local variation in constituting block copolymer composition due to variation in branch point location. This local variation, if able to be considered, would be equivalent to using a variety of constituting block copolymers to compose the multigraft, rather than a single constituting block copolymer. Thus, to predict the morphological behavior of random multigrafts using this technique involves the recognition that while the average behavior of the multigraft (on a μm scale) may be modeled in this way, on a much more local level

(on an Å scale) the individual molecules will be driven to behave differently in different locations.

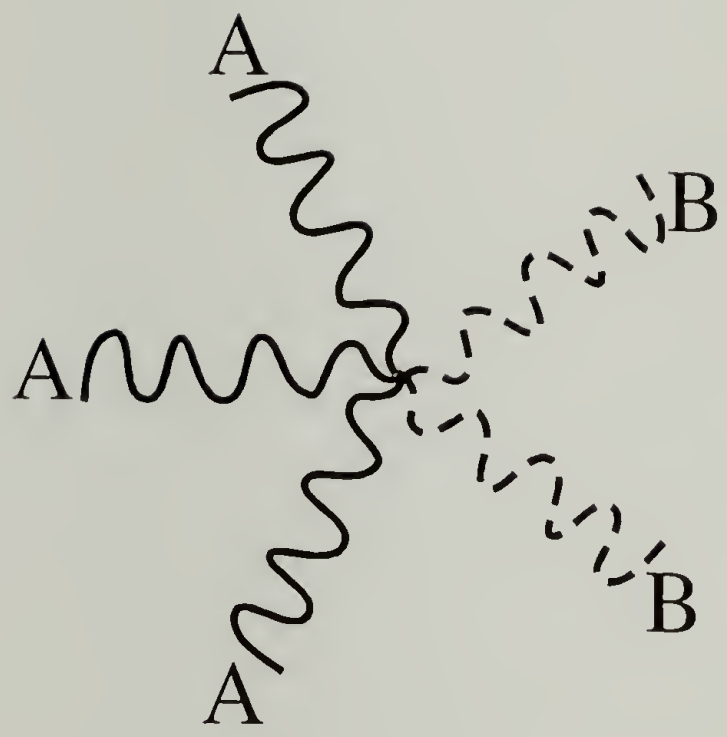

Figure 1.1. Schematic of an A_3B_2 miktoarm star comprised of three arms of polymer A and two arms of polymer B.

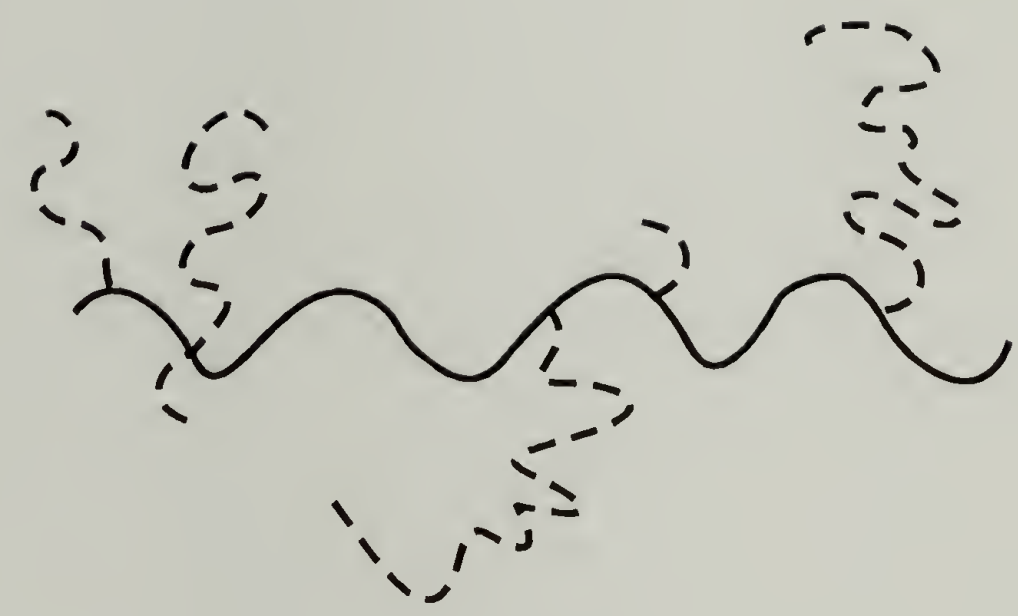

Figure 1.2. Illustration of a multiple-graft block copolymer with a heterogeneous, ill-defined molecular architecture, such as is produced by most common synthetic techniques.

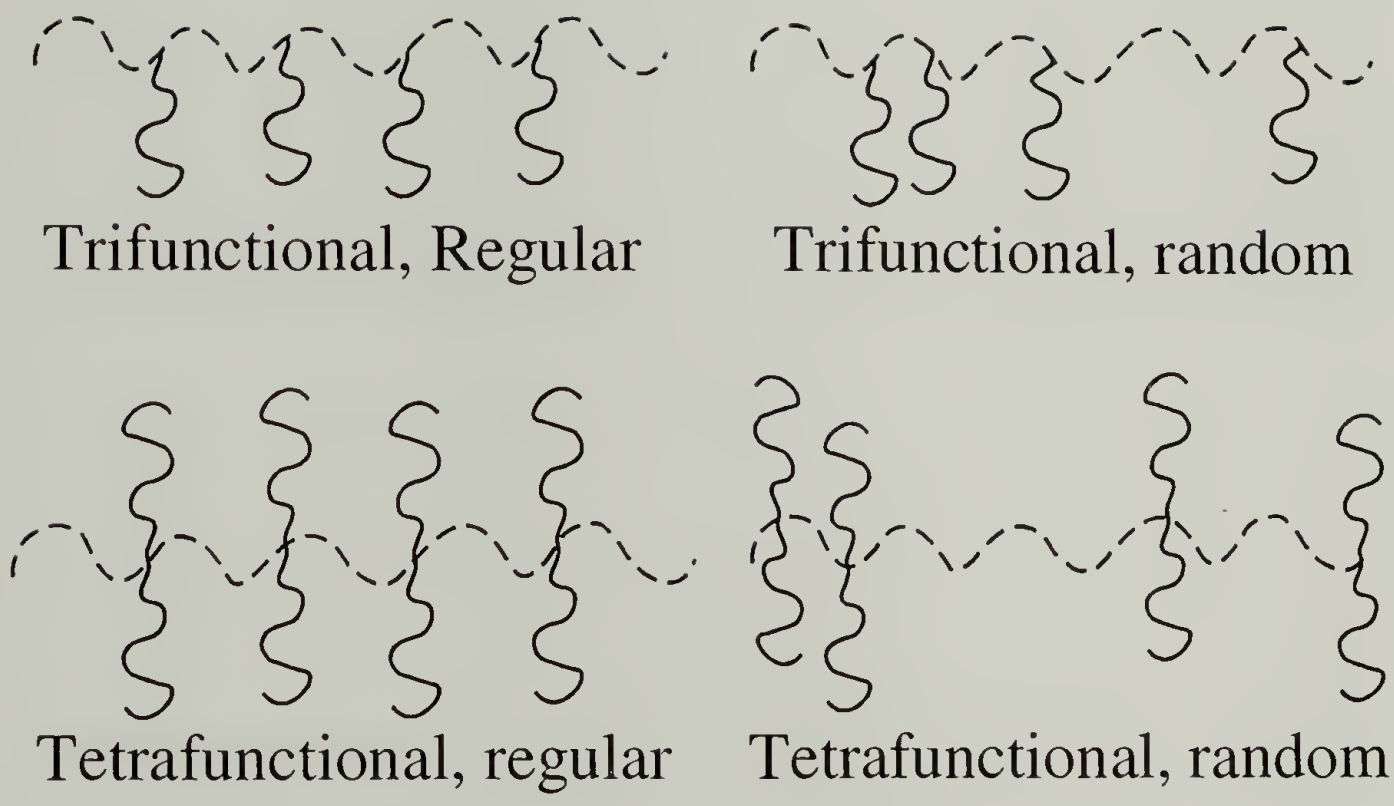

Figure 1.3. Four examples of multiple-graft architectures, illustrating the effects of two architectural variables, branch point location and branch point functionality.

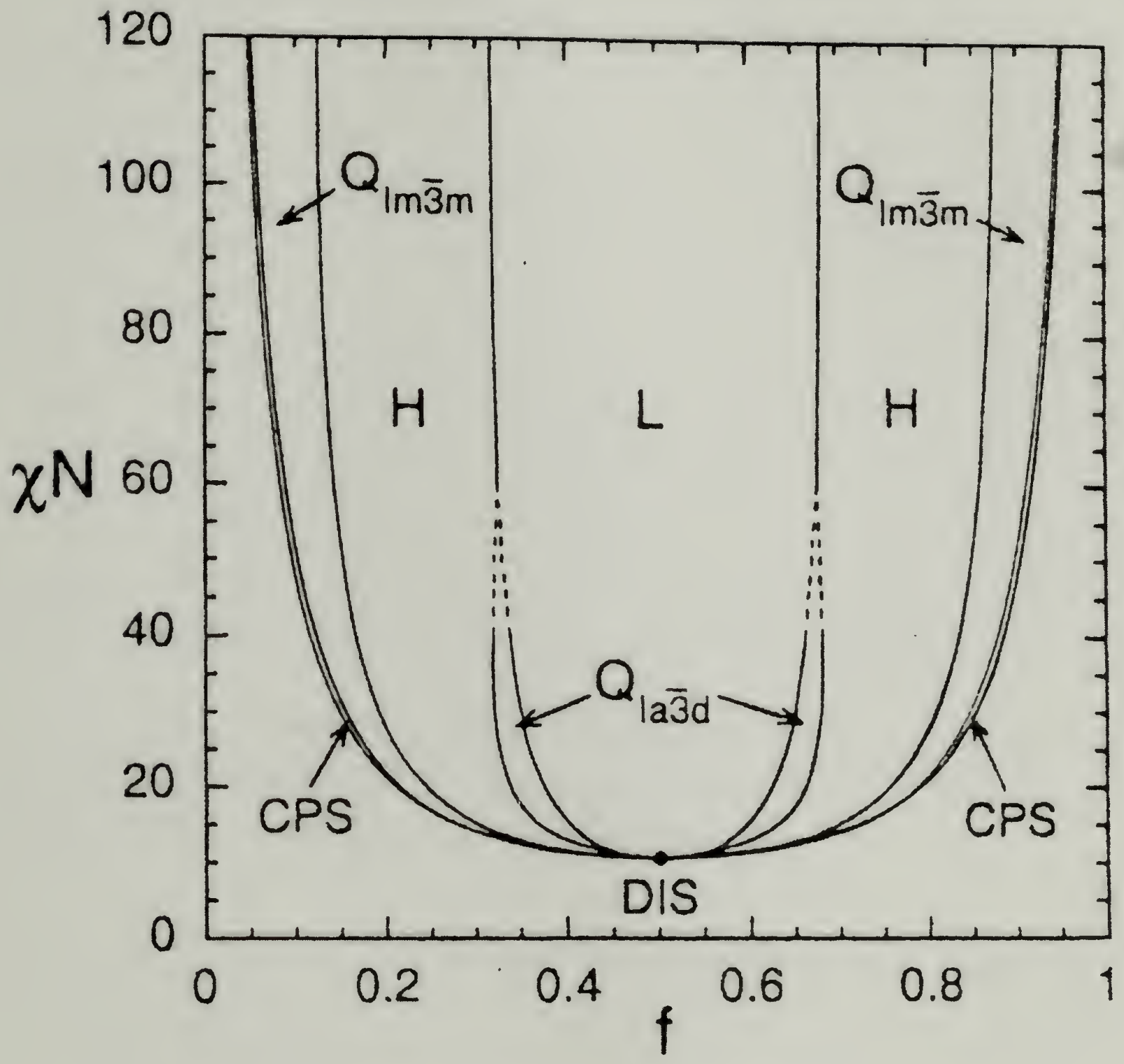

Figure 1.4. Morphology diagram for a linear AB diblock copolymer calculated by Matsen and Bates, spanning from the order-disorder transition into the strong segregation regime.

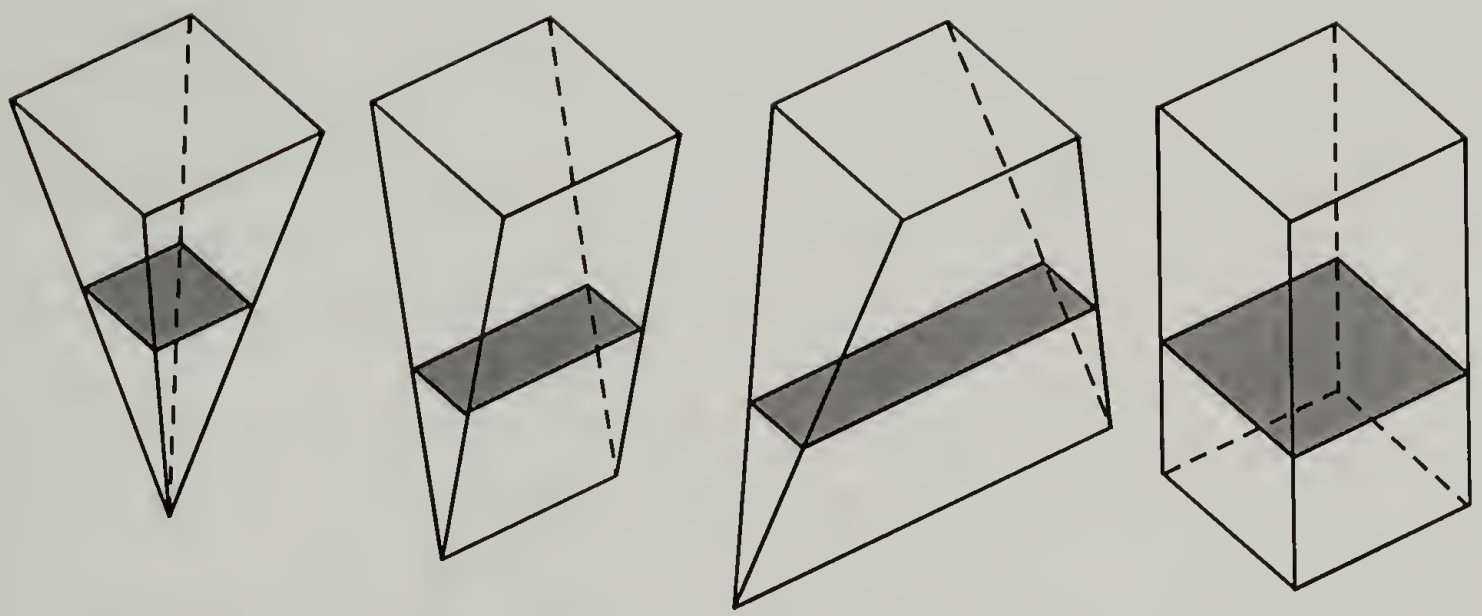

Figure 1.5. Gaussian wedges for lamellar, cylindrical, spherical, and OBDD bicontinuous morphologies used in the Milner model for calculating morphological behavior of miktoarm star block copolymers. The shaded planes represent the interface between microphase separated domains of components A and B.

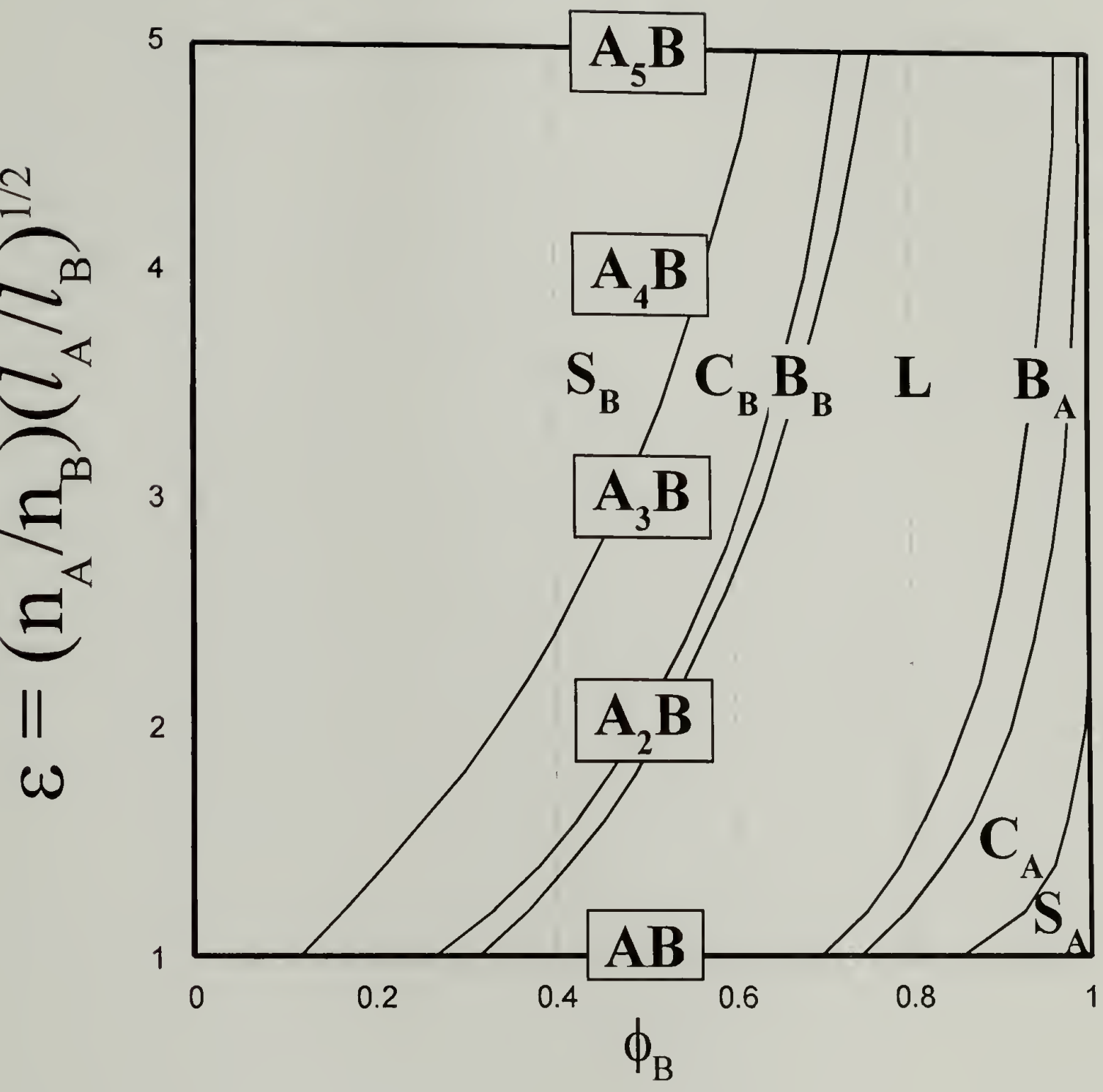

Figure 1.6. Strong segregation regime morphology diagram generated using the Milner model. Miktoarm star morphology is given as a function of volume fraction, ϕ_B, and molecular asymmetry. Boxes with A_nB stars indicate the level of molecular asymmetry for conformationally symmetric A_nB miktoarm stars, illustrating the effect of architectural asymmetry on morphological behavior.

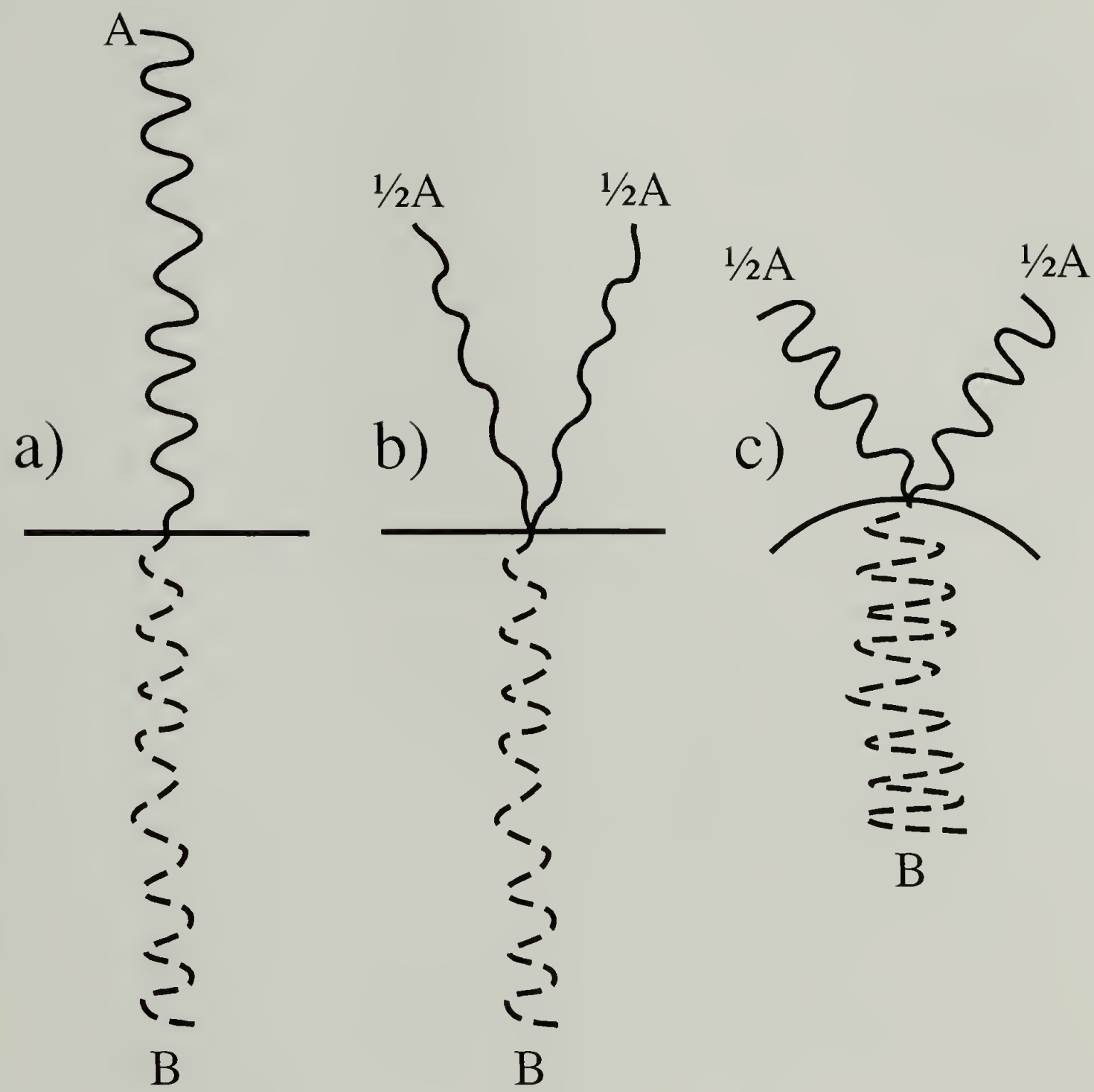

Figure 1.7. Illustration of the effect of changing from an AB linear diblock (a) to an $(½A)_2B$ miktoarm star (b and c). To reduce the increased chain stretching caused by adding a second A arm to the molecule, the interface between the two microphase separated domains curves away from the side with the larger number of arms (c).

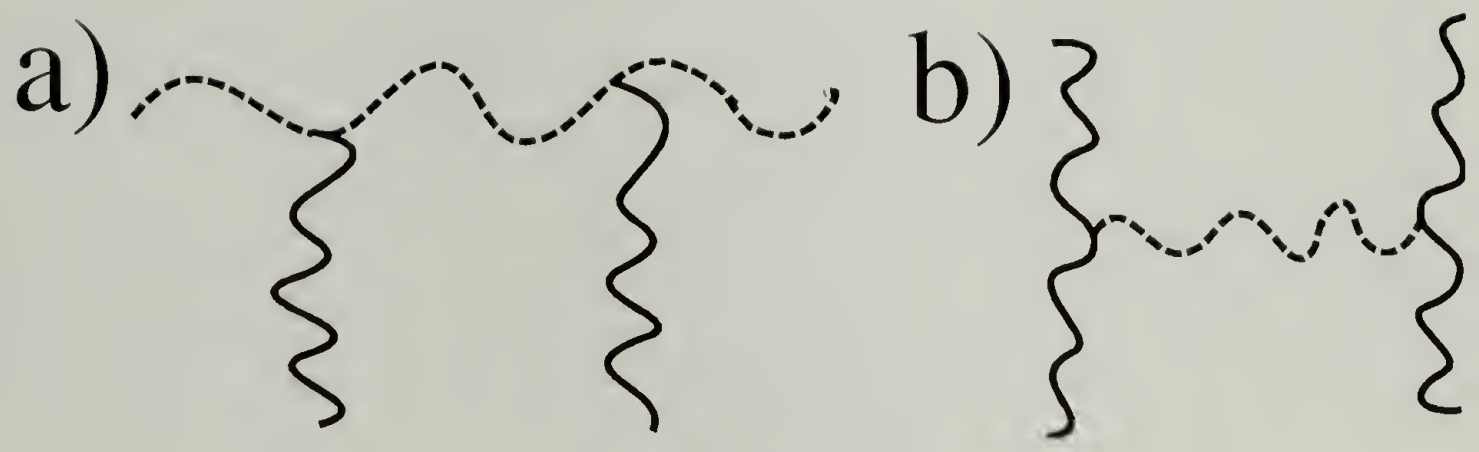

Figure 1.8. Illustrations of a) a π double-graft block copolymer, and b) an H double-graft block copolymer.

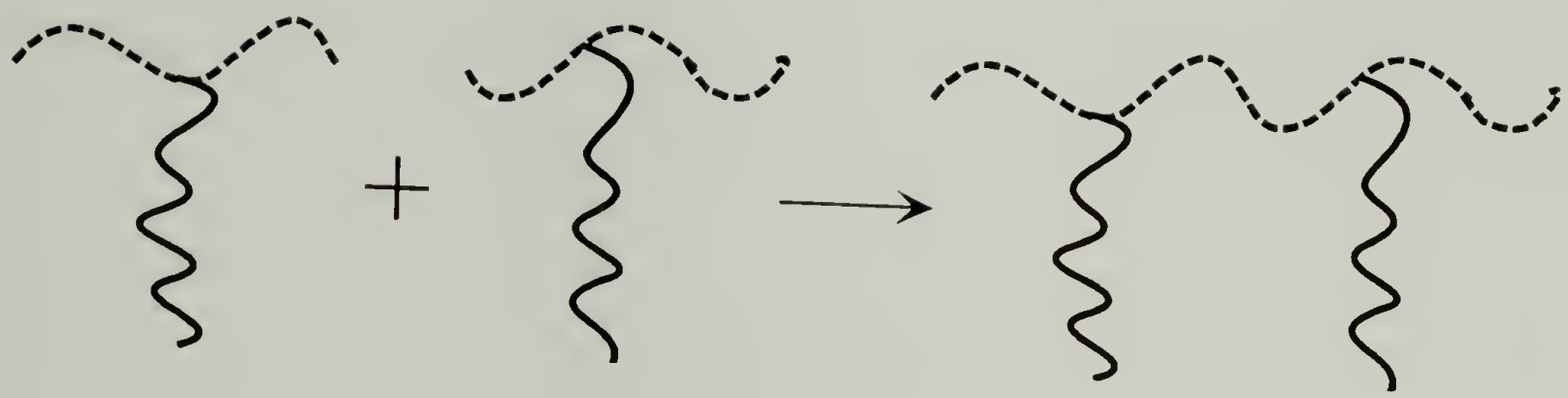

Figure 1.9. Illustration of the manner in which a π double-graft block copolymer may be imagined to be comprised of two A_2B miktoarm stars joined together by the ends of their A arms.

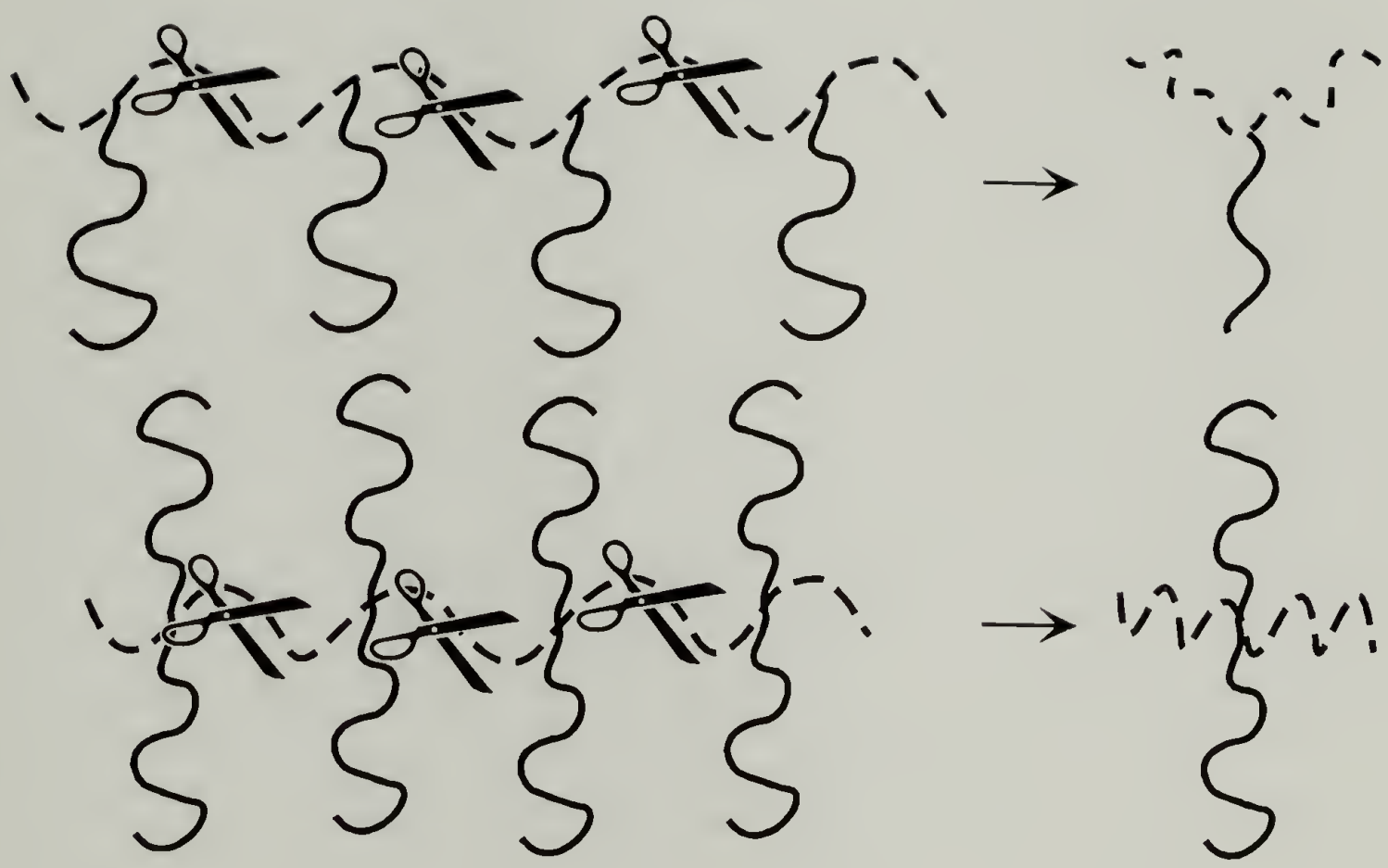

Figure 1.10. Illustration of the hypothetical decomposition of trifunctional and tetrafunctional multiple-graft block copolymers into the appropriate constituting block copolymers, an A_2B miktoarm star and an A_2B_2 miktoarm star, respectively.

CHAPTER 2

MORPHOLOGICAL BEHAVIOR OF A_8B_8 MIKTOARM STAR BLOCK COPOLYMERS

2.1 Abstract

The morphological behavior of three well-defined, miktoarm star block copolymers having sixteen arms per molecule was characterized using transmission electron microscopy, small-angle X-ray scattering, and small-angle neutron scattering techniques. The molecules, called "Vergina" stars, have eight arms of polyisoprene and eight arms of polystyrene radiating from a single junction point. The samples, with polystyrene volume fractions of 0.37, 0.44, and 0.47, and total molecular weights ranging from 330,000 to 894,000 g/mol, were all found to microphase separate into lamellar morphologies. In this respect all three samples, in agreement with theory, behave in the same way as linear diblock copolymers of the same relative volume fractions. Incorporating results from previous studies in the literature of miktoarm block copolymers containing trifunctional and tetrafunctional branch points, as well as the new Vergina star data, the scaling behavior of the area per junction versus junction functionality was investigated.

2.2 Introduction

Star block copolymers are a class of non-linear block copolymers which, like other block copolymers, microphase separate due to incompatibility between the two polymer materials comprising the distinct blocks. In recent work, the effect of controlled chain grafting architecture on microphase separated morphology through several series of

architecturally controlled materials has been investigated.[1,51,52] As illustrated in Figure 2.1, the Vergina stars have a total of 16 arms, 8 arms of polystyrene (PS) and 8 arms of polyisoprene (PI), which are joined together at a single junction. As the figure implies, the junction chemistry is such that the PS and PI arms both radiate in all directions. In the microphase separated state, however, the arms a short distance from the junction point have segregated by material type. In the notation of Olvera de la Cruz and Sanchez, the Vergina star block copolymers are of the type A_nB_n, with A = PS, B = PI, and n = 8.[50] Hadjichristidis has termed this general type of architecture, which has multiple arms radiating from a central junction point, "miktoarm" stars meaning "mixed-arm". The name "Vergina" comes from the town in northern Greece near which the ancient tomb of King Phillipos of Macedonia was discovered by Prof. M. Andronikos, of the University of Thessaloniki. Inside the tomb was a depiction of a 16-rayed star, from which the Vergina star architecture was conceived.

The multiarm, Vergina star copolymers investigated in this work form morphologies in which the relationship between domain dimensions and molecular weight is significantly altered from what is commonly observed in linear block copolymers. Due to the highly branched structure of the Vergina star molecules, the spacing of junction points along the interface is significantly larger than for any previously studied linear or miktoarm diblock copolymer.

Based on the weak segregation theory predictions of Olvera de la Cruz and Sanchez, it was expected that the Vergina stars would microphase separate into the same morphologies as those observed in linear diblocks of the same relative volume fractions, due to the overall symmetry of the Vergina molecules.[50] This prediction is also consistent with the strong segregation theory for microphase separated miktoarm star

copolymers formulated by Milner.[8] Milner's theory predicts shifting of the observed morphologies from those observed for a simple linear diblock as a result of asymmetry in the number of arms of components A and B and of asymmetry the chain characteristics (stiffness and volume per segment) of the A and B materials. Milner's model uses the ε parameter, defined by $\varepsilon = (n_A/n_B)(l_A/l_B)^{1/2}$, where n_i is the number of graft arms of block type *i* (A or B) and $l_i = V_i/R_i^2$. Here V_i is the volume of an entire arm of material *i* and R_i^2 is the mean square radius of gyration of an arm of material *i*. The parameter l_i gives a measure of the space filling characteristics of the polymer chain. In the case of the symmetric Vergina stars, ε reduces to $(l_{PS}/l_{PI})^{1/2}$. For blocks of PI and PS, one calculates a value for ε that is close to unity (1.16). Therefore, the predicted morphologies are essentially the same as those of PS-PI linear diblocks.

A total of three samples were prepared for the present study; detailed molecular characterization of these materials is given by Avgeropoulos and coworkers.[53] Two of these Vergina star materials have nearly the same relative volume fractions of PS and PI, but different overall molecular weights 330,000 g/mol and 710,000g/mol. The lower molecular weight sample, VS1, has a PS volume fraction of 0.44, and the larger molecular weight sample, VS2, has a PS volume fraction of 0.47. These two samples were expected to exhibit lamellar morphologies. The third sample, VS3, has a PS volume fraction of 0.37 and a molecular weight of 894,000g/mol.

2.3 Experimental

Synthesis of the Vergina star block copolymers has been described in a previous publication.[53] The PS and PI arms are synthesized separately using high vacuum, anionic

polymerization techniques. These arms are then linked together using chlorosilane coupling chemistry to form the final Vergina star molecule.

Solid films approximately 1 mm thick of the Vergina star polymers were cast from 2 wt. % toluene solution in 30 ml Pyrex beakers. Toluene is a nonselective solvent for PS and PI.[54] The rate at which the solvent evaporated was regulated so that the polymer films formed slowly over a two week period. The films were kept at room temperature and atmospheric pressure for several more days to allow continued evaporation of solvent. The samples were then placed under high vacuum at room temperature to allow further evaporation of residual solvent. They were then annealed for one week at 115˚C, following a two day period in which the oven temperature was slowly increased from room temperature. The samples were then allowed to cool slowly to room temperature over a period of two days.

All samples studied by transmission electron microscopy (TEM) were microtomed using a Leica cryoultramicrotome. Sections approximately 500 Å thick were cut from bulk films of sample mounted in epoxy using a Diatome cryogenic diamond knife. During sectioning, the samples were held at -110˚C while the knife was kept at -95˚C. Sections were collected on TEM grids and then stained for four hours in OsO_4, which reacts with the double bonds of the PI blocks and renders the PI domains dark relative to the PS domains in mass-thickness contrast imaging. TEM imaging was performed using a JEOL 100CX electron microscope operated at an accelerating voltage of 100kV.

Small angle X-ray scattering (SAXS) experiments were performed on both annealed and unannealed specimens using a Rigaku-Denki camera with Cu-K_α sealed-tube X-ray radiation and pinhole collimation. Patterns were recorded photographically

with Kodak direct-exposure X-ray film (DEF5). SAXS patterns were digitized with an Agfa Arcus II flat bed scanner and analyzed with custom-written software. Small angle neutron scattering (SANS) was performed at the Cold Neutron Research Facility at the National Institute of Standards and Technology in Gaithersburg, MD. Although our samples were not deuterated, their well-ordered structures produced sufficient neutron scattering for structural analysis. Samples were placed in the beam of the NG3-SANS with the incident radiation parallel to the surface of the cast films. Camera lengths of 3 m and 13 m were used at a wavelength of 5 Å. The NG3 uses pinhole collimation of the monochromated beam.

2.3 Results

All three Vergina stars formed lamellar morphologies. Table 2.1 gives molecular characteristics and lamellar long periods determined by SANS.

Figure 2.2 shows a TEM image of the lamellar microstructure of VS1, in which extremely well-ordered microdomains are evident. Large coherently ordered regions of lamellar structure were commonly seen in all TEM experiments on VS1. The SANS data for VS1 in Figure 2.3 show two orders of reflections from the lamellar long period, L, of 371 ± 6 Å. VS2 was similar to VS1 in many respects, including the nearly equal volume fractions of both constituent blocks. Figure 2.4 shows a typical example of the VS2 lamellar morphology observed in TEM. SAXS and SANS both provided conclusive evidence of the lamellar morphology with L = 515 ± 6 Å. Three orders of reflection are visible in the SANS pattern shown in Figure 2.5. VS3, with significantly more asymmetric volume fractions, also exhibited a lamellar morphology. Figure 2.6 shows a TEM image of the VS3 lamellar morphology. SANS results, shown also in Figure 2.7,

clearly demonstrates the lamella character of the microphase separated domains, displaying four orders of reflection from L = 641 ± 6 Å.

2.4 Discussion

The three Vergina star samples characterized in this work, when combined with data from previous studies of linear diblocks and less highly branched miktoarm star architectures, permit the examination of the effect of graft point functionality on microphase separated domain dimensions. Table 2.1 lists molecular characteristics and microphase separated lamellar long spacings for a number of PS-PI diblocks, I_2S and S_2I tri-branched architectures, I_3S tetra-branched architectures, as well as the Vergina stars. The data on the other materials is obtained from our previous work and from the literature.[1,9,55] Of particular interest is how the graft point functionality effects the interfacial area per molecule. From previous results on diblock copolymers, we are accustomed to block copolymers stretching normal to the interface between microphase separated domains so that $L \sim N^{2/3}$ is obtained in strongly segregated systems. Through conservation of volume in these incompressible materials, the molecular dimensions in the plane of the interface, and thus the area per molecule, A, must be correspondingly reduced such that $A \sim N^{1/3}$.

The behavior of the dimensionless area per molecule as a function of junction functionality is now examined. The dimensionless area per molecule is defined as A/R_g^2, the ratio of the area to the mean square radius of gyration of the entire star shaped molecule. The area per molecule is simply the volume of a molecule divided by half the long spacing, where the volume of the molecule is estimated based on known density values for bulk PS and PI. Values of this parameter are given for all the materials in

Table 2.1. For diblocks, R_g is calculated according to the standard relationship for linear chains using a number weighted average Kuhn length. For three-arm and four-arm miktoarm star block copolymers, R_g is determined using the Zimm-Stockmeyer approach for the calculation of $g = R_g/R_L$, where R_L is the radius of gyration of a linear polymer chain with the same total number of repeat units as the entire star molecule.[56] This approach, which is based on Gaussian statistics, does not properly account for the high degree of crowding and the resultant chain stretching near the junction point of a star molecule with a large number of arms like the Vergina stars. Thus this standard calculation underestimates R_g for many-arm stars. Published comparisons of experimentally determined and calculated R_g values for 12-arm and 18-arm stars[57] allow estimation, by interpolation, that calculated values of g, and thus R_g, for the Vergina stars must be increased by a factor of 1.45 to account for expansion due to arm crowding. The resulting R_g values for the Vergina stars are consistent with experimental determinations of R_g for the same series of Vergina stars. Also, the g values we obtained are consistent with an extrapolation of the experimental data in Table III of Daoud and Cotten's paper[58] to 16 arm stars utilizing the theta condition scaling relationship in their equation 25. The dimensionless area per molecule still has a molecular weight (degree of polymerization) dependence which, in the strong segregation limit, scales as $N^{-2/3}$. Thus the molecular weight corrected, dimensionless area per molecule is defined as $AN^{2/3}/R_g^2$. This parameter is also given for each material in Table 2.1.

Figure 2.8 shows a log-log plot of $AN^{2/3}/R_g^2$ versus graft point functionality, where f is the total number of arms. A least squares fit yields the power law expression $AN^{2/3}/R_g^2 = 3.4f^{1.19}$. Excluding the Vergina star data, the points for diblocks, three- and four-armed stars can be better fit by the expression $AN^{2/3}/R_g^2 = 4.6f^{0.82}$. This

discrepancy may be caused by an underestimation of R_g for the Vergina stars even after application of an expansion factor of 1.45. It could also result from the fact that the diblocks, three and four armed stars all have only one arm of at least one of the two component materials, resulting in asymmetric architectures in the three and four armed stars. This is different from the Vergina stars which have an equal number of arms of both components. It may be better to look at the scaling behavior of two different series: a series of A_nB_n materials, and a series of A_nB materials, both with increasing n. Neither the data nor the materials are currently available to do such a detailed study.

A prediction for the scaling behavior can be obtained by minimizing a simple Alexander-de Gennes scaling free energy per molecule with n_1 arms of block 1 and n_2 arms of block 2. This yields equation 1,

$$\frac{A}{R_g^{\,2}} = \frac{1}{R_g^{\,2}}\left(\frac{2}{\gamma}\right)^{1/3}\left\{n_1^{\,3}\left(\frac{V_1}{R_1}\right)^2 + n_2^{\,3}\left(\frac{V_2}{R_2}\right)^2\right\}^{1/3} \qquad (1)$$

where V_i is the volume of an arm of material i, R_i is the unperturbed root mean square end-to-end distance of a single arm of material i, γ is the interfacial energy per unit area, and R_g is the radius of gyration of the entire star shaped molecule. If only systems such as the Vergina stars, which are symmetric with respect to arm number, are considered, the expression becomes equation 2,

$$\frac{A}{R_g^{\,2}} = \frac{f}{2}\frac{1}{R_g^{\,2}}\left(\frac{2}{\gamma}\right)^{1/3}\left\{\left(\frac{V_1}{R_1}\right)^2 + \left(\frac{V_2}{R_2}\right)^2\right\}^{1/3} \qquad (2)$$

from which it is evident $AN^{2/3}/R_g^{\,2}$ is expected to scale as $f^{1.0}$. This predicted behavior certainly falls within the range of experimentally determined scaling as delimited by the two curve fits in Figure 2.6. Physically, the spacing between molecules at the interface increases with increasing graft functionality. This results in further spreading of the arm

trajectories parallel to the interface in molecules like the Vergina stars, which have high numbers of arms, relative to what is observed for linear diblocks.

2.5 Conclusions

The three Vergina star samples investigated in this study all formed lamellar morphologies. For VS1 and VS2 with PS volume fractions of 0.44 and 0.47 respectively, the lamellar morphology was expected based on the theoretically predicted similarity of symmetric, multiarm block copolymer behavior to that of simple diblocks. VS3, with a PS volume fraction of 0.37, is still in the region where diblocks would form lamella. The scaling of dimensionless, degree of polymerization corrected, interfacial area per molecule as a function of graft functionality was investigated across a series of diblocks, three armed miktoarm stars, four arm miktoarm stars, and Vergina stars. It was found that $AN^{2/3}/R_g^2$ scales roughly as the first power of the graft point functionality. This reflects an increased spacing between the molecules at the interface and more spreading of at least some of the arm trajectories parallel to the interface.

Sample	M_n (g/mol)	PDI	ϕ_{PS}	PS arm M_n (g/mol)	PS arms/ junct.	PI arm M_n (g/mol)	PI arms/ junct.	L (nm)	A/R_g^2	$AN^{2/3}/R_g^2$
L1[55]	21000	1.13	0.50	11000	1	10000	1	17	0.211	8.43
L2[55]	31000	1.13	0.37	12000	1	19000	1	24	0.145	7.75
L3[55]	49000	1.13	0.42	22000	1	27000	1	28	0.112	8.01
L4[55]	55000	1.18	0.43	25000	1	30000	1	34	0.105	8.11
L5[55]	97000	1.18	0.48	45000	1	52000	1	46	0.077	8.66
L6[55]	102000	1.18	0.58	62000	1	40000	1	51	0.074	8.26
S_2I-49[9]	75400	1.06	0.51	20800	2	33800	1	36.1	0.121	11.3
I_3S-55[9]	101900	1.05	0.55	59300	1	14200	3	39.2	0.133	15.0
I_3S-61[9]	94400	1.05	0.61	59300	1	11700	3	38.0	0.134	14.1
I_2S-3[1]	83000	1.04	0.62	61200	1	14800	2	39.0	0.113	11.5
VS1	330000 (M_w)	1.07	0.44	20900 (M_w)	7.7	20200 (M_w)	8.4	37.1	0.362	91.9
VS2	710000 (M_w)	1.05	0.47	43600 (M_w)	7.9	48200 (M_w)	4.6	51.5	0.244	103
VS3	894000 (M_w)	1.05	0.37	43600 (M_w)	7.9	71200 (M_w)	7.7	64.1	0.174	87.8

Table 2.1. Molecular characteristics and scaling behavior of lamellae-forming miktoarm star block and diblock copolymers.

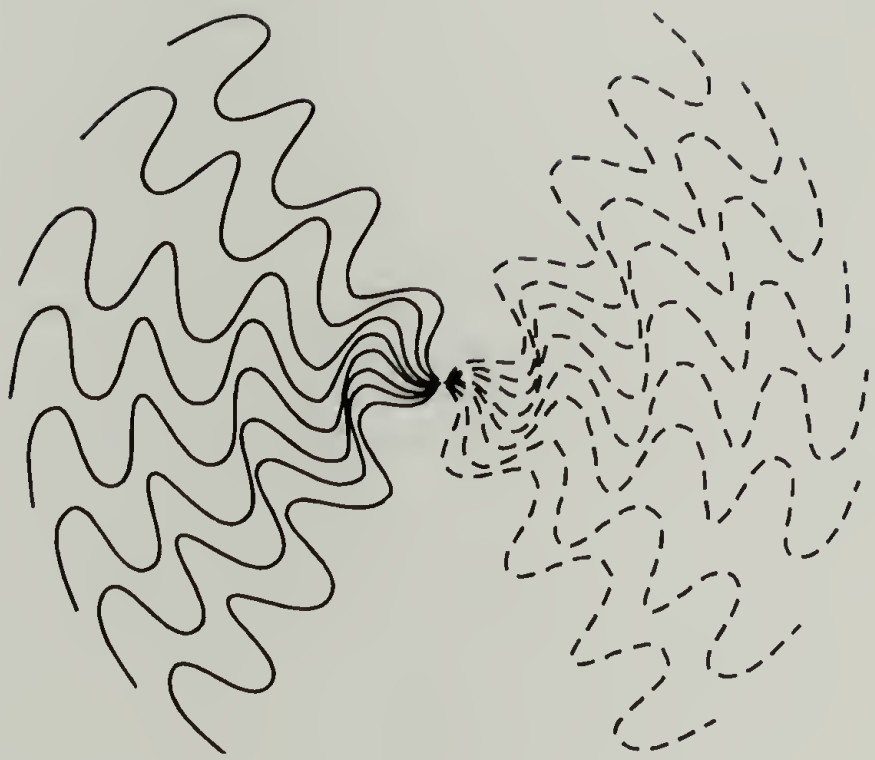

Figure 2.1. Schematic of an A_8B_8 "Vergina" star, the 16-armed miktoarm star block copolymer architecture with 8 PS arms (solid) and 8 PI arms (dashed).

Figure 2.2. TEM image of the lamellar morphology of sample VS1.

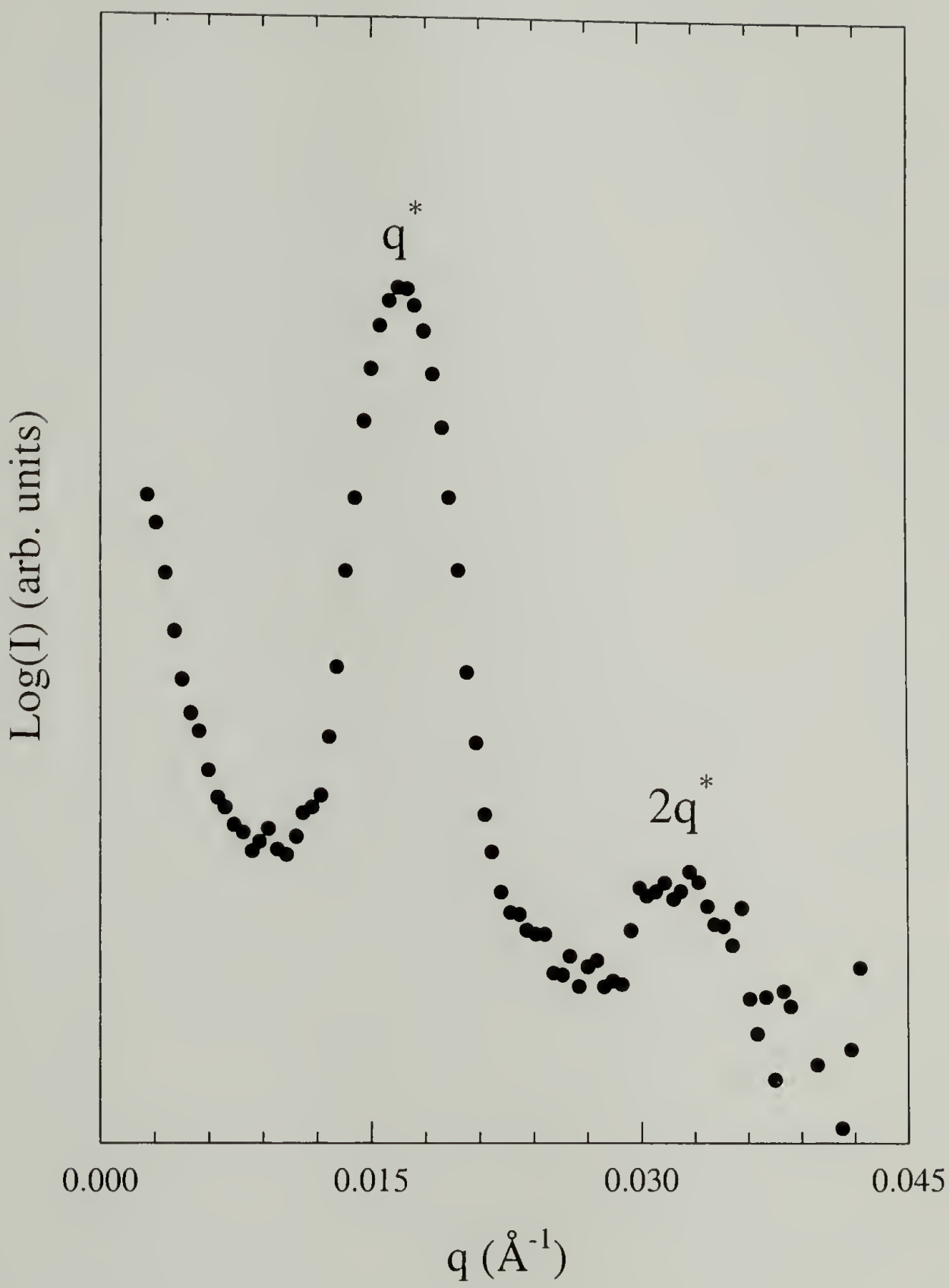

Figure 2.3. SANS data for sample VS1, indicating the formation of a lamellar morphology.

Figure 2.4. TEM image of the lamellar morphology of sample VS2.

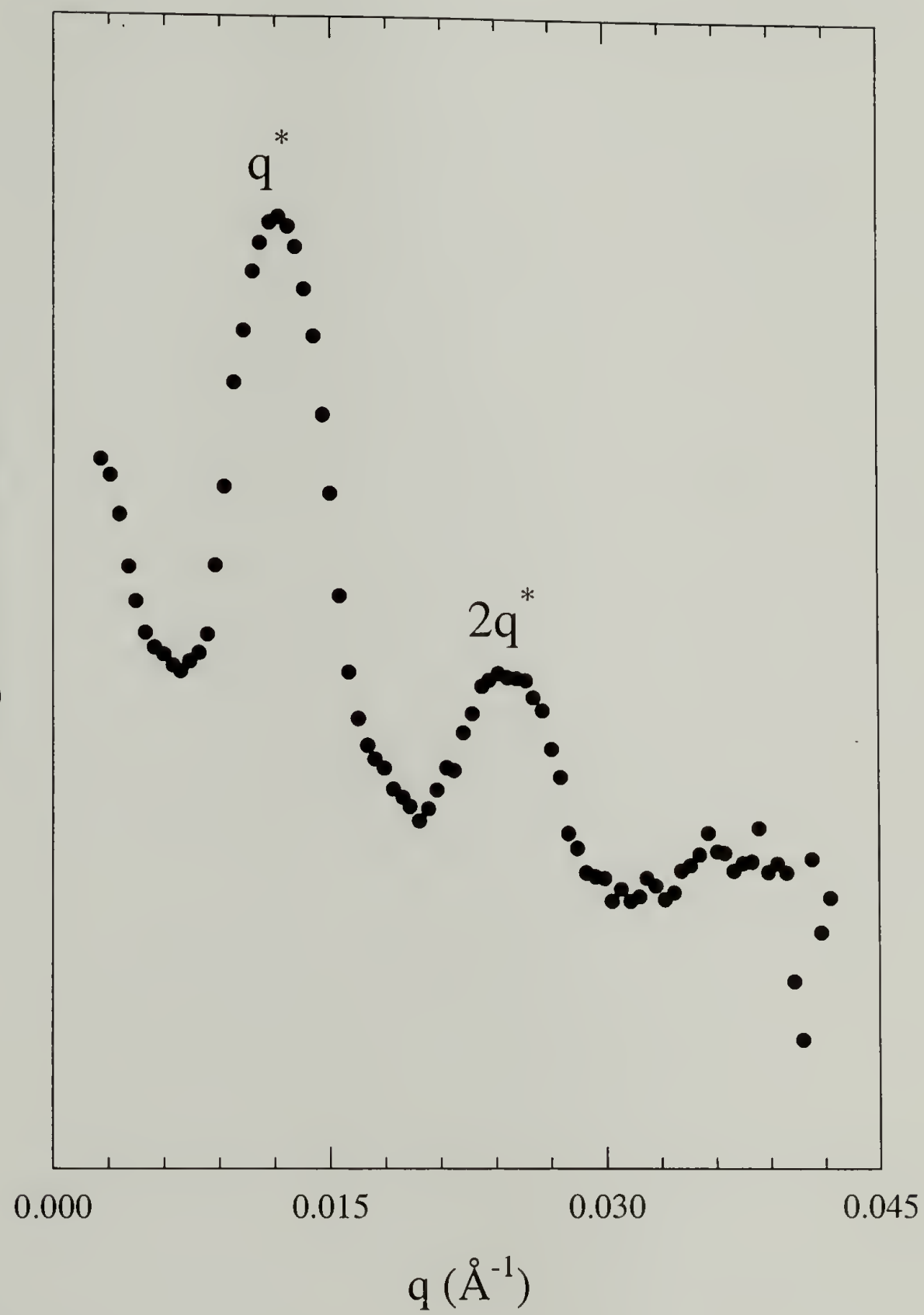

Figure 2.5. SANS data for sample VS2, indicating the formation of a lamellar morphology.

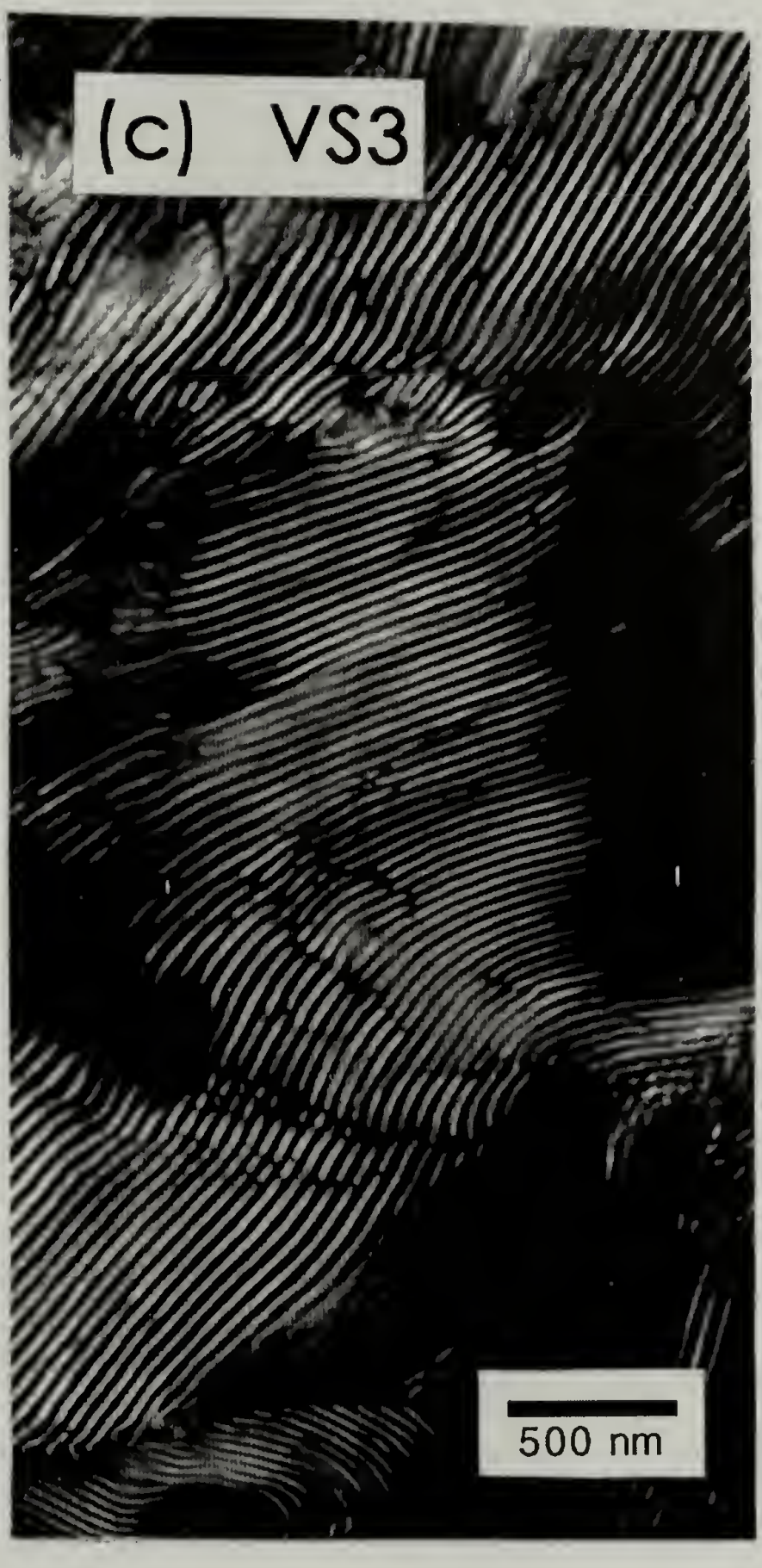

Figure 2.6. TEM image of the lamellar morphology of sample VS3.

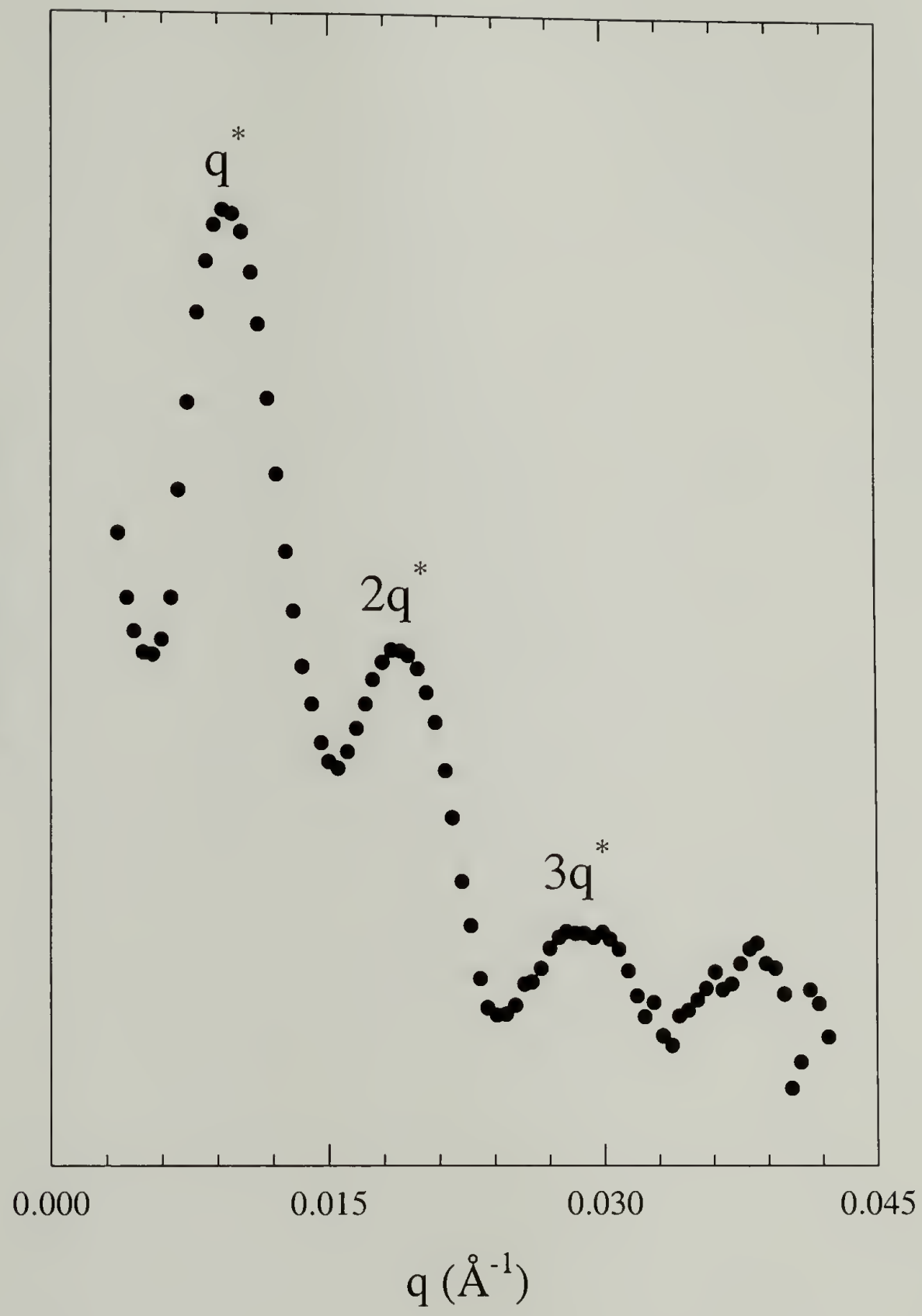

Figure 2.7. SANS data for sample VS3, indicating the formation of a lamellar morphology.

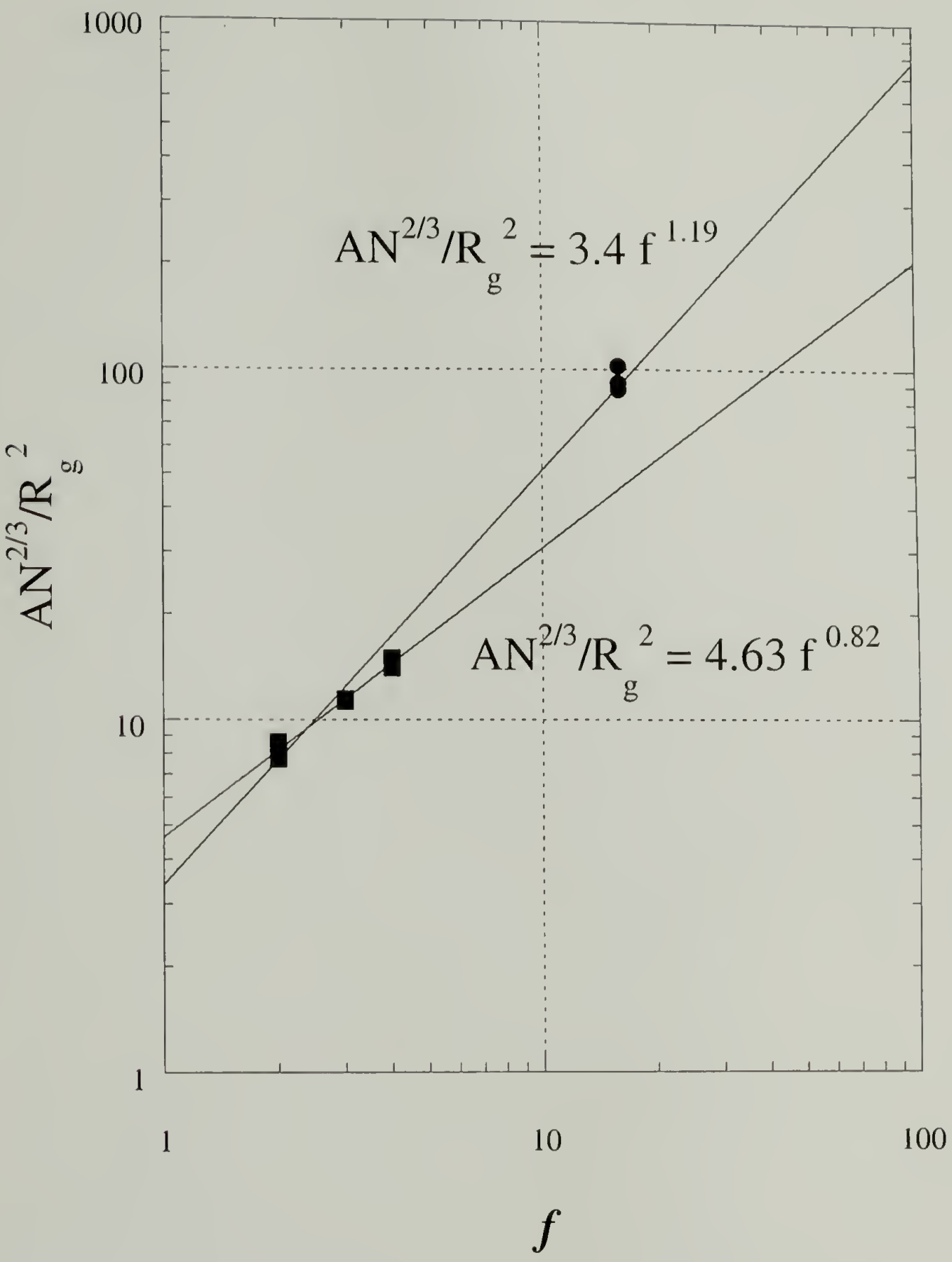

Figure 2.8. Log-log plot of $AN^{2/3}/R_g^{\ 2}$ vs. graft point functionality, f, for diblocks, three armed, and four armed miktoarm stars, and the Vergina stars.

CHAPTER 3

MORPHOLOGICAL BEHAVIOR OF A_2B_2 MIKTOARM STAR BLOCK COPOLYMERS

3.1 Abstract

A series of A_2B_2 four arm miktoarm stars of polystyrene and polyisoprene has been synthesized. The morphological behavior of these materials has been characterized using TEM, SAXS, and SANS, and was found to agree in general with the predictions of Milner's theory for miktoarm star morphological behavior. One sample was found to exhibit a cylindrical morphology where lamellae were predicted; this behavior is similar to other discrepancies observed in previous studies of miktoarm star morphological behavior. A second sample, predicted to form a bicontinuous morphology, is found to exhibit hexagonally packed cylinders. The tetrafunctional junction point also results in an increase in spacing for the lamellar sample in this series over that of an AB diblock but not as great as the increase previously observed for A_8B_8 stars.

3.2 Introduction

The morphology and microphase separation physics of block copolymers with non-linear architectures, such as star blocks and graft copolymers, have been the focus of a considerable amount of recent work.[1,2,4-6,9,51,59-61] These non-linear architectures have been demonstrated to allow control of morphology independent of the familiar composition windows in which linear diblocks form various structures. An approximate method has also been developed which models complex graft copolymer architectures with multiple graft points in terms of *corresponding block copolymers* containing single

junction points, which are representative of the junction point effect on morphology in the more complex molecules.[5] The present paper reports on the morphology of A_2B_2 four arm miktoarm star materials (Figure 3.1a). These materials are the constituting block copolymer model materials for a class of multiple graft copolymers with tetrafunctional branch points (Figure 3.1b), which are currently also being investigated.[62]

In previous studies of miktoarm star and graft architecture, a model by Milner (strictly applicable to miktoarm stars with only a single junction point in the strong segregation limit) has been used as a guide to understanding the effect of architecture on morphology.[8] The morphology diagram shown in Figure 3.2 was generated using this model. Morphology is predicted as a function of the volume fraction of component B, ϕ_B, and a molecular asymmetry parameter, ε. This asymmetry parameter incorporates both architectural and conformational asymmetries, and is calculated as $\varepsilon = (n_A/n_B)(l_A/l_B)^{1/2}$. Here, n_A and n_B are the numbers of arms of block materials A and B linked at a junction point, and $l_i = (V_i/R_i^2) = v_i/b_i^2$. V_i and R_i are the volume and radius of gyration of one arm of polymer *i*, while v_i is the segmental volume and b_i the statistical segment length of component *i*. As indicated in Figure 3.2, a shift in the volume fraction ranges in which the various morphologies are found is predicted as molecular asymmetry increases. In general, the predictions of this model have been confirmed by experiment, although specific samples have been found to disagree with the predictions of this model.[1,9]

In previous studies of miktoarm star and graft architecture, a model by Milner (strictly applicable to miktoarm stars with only a single junction point in the strong segregation limit) has been used as a guide to understanding the effect of architecture on morphology.[8] The morphology diagram shown in Figure 3.2 was generated using this

model. Morphology is predicted as a function of the volume fraction of component B, ϕ_B, and a molecular asymmetry parameter, ε. This asymmetry parameter incorporates both architectural and conformational asymmetries, and is calculated as $\varepsilon = (n_A/n_B)(l_A/l_B)^{1/2}$. Here, n_A and n_B are the numbers of arms of block materials A and B linked at a junction point, and $l_i = (V_i/R_i^2) = v_i/b_i^2$. V_i and R_i are the volume and radius of gyration of one arm of polymer *i*, while v_i is the segmental volume and b_i the statistical segment length of component *i*. As indicated in Figure 3.2, a shift in the volume fraction ranges in which the various morphologies are found is predicted as molecular asymmetry increases. In general, the predictions of this model have been confirmed by experiment, although specific samples have been found to disagree with the predictions of this model.[1,9]

In this work, the morphologies of a series of miktoarm star block copolymers having an A_2B_2 architecture have been characterized. While several studies have examined the behavior of miktoarm star block copolymers having different numbers of arms of components A and B ($n_A \neq n_B$), the behavior of architecturally symmetric miktoarm stars ($n_A = n_B$) has been little studied. Three samples having an A_8B_8 architecture[59] have been characterized, and at least three other A_2B_2 star materials have been studied.[60,63] These samples formed lamellar morphologies, leaving the broader question of overall morphological behavior unanswered. The Milner model suggests that in the strong segregation limit that A_nB_n molecules would behave in a similar manner to AB linear diblocks of the same volume fractions, but this has not been confirmed experimentally. Combining domain spacing data for the lamellar forming A_2B_2 material in the present study along with data from previous studies involving lamellar forming A_2B_2 and A_8B_8 materials is allowing us to gain some insight into the effect of the junction

point on chain conformation in the microphase separated state. This junction point effect, which is not specifically accounted for in the Milner theory, is the likely cause of the deviations of some previous experimental data in miktoarm stars and graft copolymers from the theoretical predictions.[1,5,9]

The samples considered in the present work are comprised of two polyisoprene (PI) and two polystyrene (PS) arms linked at a common junction point. The conformational asymmetry between PS (the A component) and PI (the B component) is the only contributor to the molecular asymmetry, resulting in an asymmetry value of $\varepsilon \approx 1.18$.[1]

3.3 Experimental

3.3.1 Synthesis

A series of five A_2B_2 miktoarm stars was synthesized using methods similar to those reported by Iatrou and Hadjichristidis.[64] In the present work, however, stoichiometric quantities of tetrachlorosilane were used, eliminating the need to remove excess silane. All manipulations were performed under high vacuum in all-glass, *n*-butyllithium-washed, benzene-rinsed reactors with breakseals for introduction of reactants and constriction seal-offs for sampling of intermediate products. Polystyryllithium and polyisoprenyllithium were separately prepared in benzene using *sec*-butyllithium initiator. In the linking reactor, tetrachlorosilane in benzene was chilled in an ice bath for ten minutes. Polystyryllithium was then added to the chlorosilane from a side flask at room temperature; more than one equivalent was added quickly with stirring and then the contents was stirred at 0°C for twenty minutes. During this time the reduced vapor pressure in the reactor prevented transfer of the volatile silane to the side

flask. The reactor was then warmed to room temperature and small incremental additions of polystyryllithium were made from the same side flask until essentially pure coupled product, as determined by size-exclusion chromatography (SEC) on sampled aliquots, was obtained. Steric effects and the slow addition of polystyryllithium prevented the formation of detectable amounts of three or four arm PS stars. Addition of more than twofold polyisoprenyllithium and subsequent fractionation yielded the A_2B_2 copolymer samples.

3.3.2 Molecular Characterization

The molecular characteristics of the arms and fractionated miktoarm stars are reported in Table 3.1. SEC was performed in tetrahydrofuran (THF) at 30°C using a Waters Model 510 pump, Waters Model 410 differential refractometer, and ultrastyragel columns with a continuous porosity range from 10^6 to 10^3 Å. For calculation of M_n values, calibration with absolute standards was performed. Membrane osmometry (MO) using a Jupiter Model 231 recording membrane osmometer was conducted in toluene distilled from CaH_2. Low-angle light scattering (LALLS) was performed in THF distilled from sodium, using a Chromatix KMX-6 instrument operating at 633 nm. Matrix-assisted laser desorption/ionization time-of-flight mass spectroscopy (MALDI/TOF/MS) was performed in trans-retinoic acid with silver trifluoroacetate using a Perseptive Biosystems Voyager Elite DE instrument. Proton nuclear magnetic resonance (^{1}H-NMR) was carried out in $CDCl_3$ using a Bruker 300 MHz instrument. Ultraviolet spectroscopy (UV) was conducted in THF using a Waters Alliance 2690 separations module and Waters 996 photodiode array detector.

3.3.3 Morphological Characterization

Bulk films of each sample were cast from dilute solutions of about 5 wt. % polymer in toluene, a nonselective solvent for PI and PS block copolymers.[54] Solvent evaporation was regulated to occur steadily over a period of two weeks, producing solid films approximately 1 mm in thickness. Residual solvent present in the bulk material was allowed to evaporate over an additional period of one week, at which time the films were transferred to a vacuum oven and held under vacuum for an additional week. To further promote the formation of equilibrium morphologies, the bulk films were annealed under vacuum at 120°C. The films were then cooled slowly to room temperature.

Transmission electron microscopy (TEM) and small-angle scattering techniques were used to characterize the morphologies of the samples. To prepare specimens for TEM, each film was sectioned using a Leica cryoultramicrotome with a diamond knife, operated at –110°C. Sections approximately 500 Å thick were collected on TEM specimen grids and stained four hours in OsO_4 vapor. TEM was performed using either a JEOL 100CX or JEOL 2000FX, both operated at an accelerating voltage of 100 kV.

Both small-angle neutron scattering (SANS) and small-angle X-ray scattering (SAXS) were performed to characterize the structure of the materials. SANS was performed at the National Institute for Standards and Technology (NIST), Gaithersburg, MD, on the NG-7 30 m SANS instrument. Data in the momentum transfer, q, region from 0.004 $Å^{-1}$ to 0.04 $Å^{-1}$ were collected using a wavelength of 6 Å and a camera length of 15.32 m. Data in the higher q region were collected using a camera length of 1.5 m. In both cases, the detector was offset from the incident beam by 20 cm to facilitate measurements at higher scattering angles. SAXS data were collected at the University of Massachusetts Amherst using a Rigaku rotating Cu anode X-ray generator equipped with

a Ni filter. Data were acquired using a Siemans 2D area detector and the Siemans General Area Detector Diffraction Software (GADDS) program. For a wavelength of 1.54 Å and camera length of 93.17 cm, data were collected over an inverse scattering angle, q, range of 0.016 $Å^{-1}$ to 0.22 $Å^{-1}$. The SANS data are shown because for a number of samples, the primary reflections were obscured by the beam stop in the SAXS instrument. The SANS data in these cases provided direct observation of the primary peak.

3.4 Results

A summary of the morphological behavior of all of the A_2B_2 miktoarm star block copolymer samples is given in Table 3.1. This table also lists the degree of segregation, χN, for each sample. Following the method of Olvera de la Cruz and Sanchez,[50] χN was calculated using the degree of polymerization, N, of the total A_nB_n star, while χ for PS and PI was taken from Mori and coworkers.[65] The A_2B_2 samples were found to lie in the strong segregation regime, meeting the requirements of Milner's model. Mapping each sample onto the morphology diagram in Figure 3.2 shows their predicted morphological behaviors. The samples are located according to their volume fraction of PI.

Figures 3.3 through 3.12 show the morphological data collected for each sample. Beginning with sample A_2B_2-1, Figure 3.3 shows a representative TEM micrograph indicating a morphology of small, randomly oriented grains of hexagonally packed PS cylinders in a PI matrix. Regions of this micrograph show the hexagonal packing of cylinders viewed along the cylinder axis, while other areas show alternating PS and PI domains such as one would observe if viewing a cylindrical morphology normal to the cylinder axis. Using SANS data from Figure 3.4, q^*, the inverse scattering angle of the

first order Bragg reflection, is found to be 0.0227 $Å^{-1}$, corresponding to a (100) spacing of 277 Å and a hexagonal lattice constant of 320 Å. This characterization is supported by SAXS data shown in Figure 3.4, with clear Bragg maxima located at q^* and $q^*\sqrt{3}$. An additional broad, higher order peak probably results from a combination of form factor scattering and higher order lattice scattering in the vicinity of $q^*\sqrt{13}$.

Figure 3.5 shows a representative TEM micrograph obtained from sample A_2B_2-2, also revealing a morphology of PS cylinders in a PI matrix. SANS data shown in Figure 3.6 allow determination of q^*, 0.0197 $Å^{-1}$, indicating a cylindrical morphology with a (100) spacing of 319 Å and a lattice constant of 368 Å. SAXS data shown in Figure 3.6 confirm the well ordered cylindrical morphology, with Bragg reflections at $q^*\sqrt{3}$ and $q^*\sqrt{7}$. An additional, higher scattering angle peak in the vicinity of $q^*\sqrt{19}$ probably results from both form factor scattering and lattice scattering.

The morphology of sample A_2B_2-3, shown by TEM in Figure 3.7, is lamellar. Multiple Bragg reflections in both SAXS and SANS (Figure 3.8) at integral multiples of q^* clearly demonstrate the lamellar character of this sample's microstructure. Using the spacing of q^* from SANS, the lamellar repeat is found to be 363 Å.

A representative TEM micrograph of the morphology of sample A_2B_2-4 is given in Figure 3.9, showing grains of hexagonally packed PI cylinders in a PS matrix in different orientations. SANS data shown in Figure 3.10 allow accurate determination of the (100) spacing and hexagonal lattice constant, found to be 326 Å and 376 Å, respectively. Particularly clear in SAXS (Figure 3.10) are Bragg reflections at $q^*\sqrt{3}$ and $q^*\sqrt{7}$, confirming the morphology to be hexagonally packed cylinders. Again an additional higher order peak is observed around $q^*\sqrt{19}$.

Finally, a TEM image of the morphology of sample A_2B_2-5 is shown in Figure 3.11. While the majority of this sample appears to be microphase separated but not ordered on a lattice, isolated grains of spheres on a cubic lattice (assumed to be BCC) are observed. One of these ordered regions is visible. The SAXS data for this sample (Figure 3.12) show a single reflection, indicative of a characteristic periodicity in the material of $2\pi/q^* = 230$ Å, as well as a weak shoulder and a broad, weak maximum at $q \approx 0.067$. To confirm the formation of spherical domains of PI, the form factor scattering from a single sphere is compared to the scattering data shown in Figure 3.12.[66] The domain size of the spherical particle was calculated by assuming the formation of a body-centered cubic lattice of spheres whose primary spacing is q^*. Using $\phi_{PS} = 0.865$, a spherical domain radius of 84 Å is calculated. As shown in Figure 3.12, the form factor scattering profile compares favorably with the SAXS data, predicting a peak which is coincident with the second, broad maximum. A shoulder is observed on the primary maximum, which may represent weak higher order interparticle scattering from the small cubic arrays formed, such as illustrated in Figure 3.11. The position of this shoulder is consistent with broad and overlapping reflections at $q^*\sqrt{2}$ and $q^*\sqrt{3}$. Similar behavior has been reported previously for block copolymers and blends of block copolymer and homopolymer.[67,68]

3.5 Discussion

In general, the morphologies of the A_2B_2 materials are well-ordered, as indicated by the number and strength of Bragg reflections observed in SAXS. Samples A_2B_2-1 (PS cylinders) and A_2B_2-3 (lamellae) agree explicitly with the predictions of the Milner theory. Sample A_2B_2-2, which was predicted to form a lamellar morphology, was found

instead to form cylinders of PS. This discrepancy may be the result of several factors, including the use of bulk densities for neat PI and PS to calculate the PI and PS volume fractions. However, the observation of a morphology predicted to occur in a higher volume fraction range is consistent with previous studies of miktoarm star morphology.[1,2,9]

The effect of the junction point on morphological behavior may be probed more directly by considering miktoarm stars exhibiting lamellar morphologies. Figure 3.13 shows a plot of lamellar spacing for A_nB_n materials, where n is equal to 1 (linear diblock data from Hashimoto and coworkers[55]), 2 (A_2B_2-3 and data from Turner and coworkers[60]), and 8 (A_8B_8 star data[59]). These spacings are plotted vs. the number average molecular weight divided by n, i.e. the molecular weight of a hypothetical diblock consisting of one arm of each type of material. This plot allows for a direct observation of the effect of the functionality of the junction point on the degree of stretching of the arms normal to the interface. The same comparison was made in a previous publication[5] using the diblock and A_8B_8 data only. Clearly the result of effectively bundling together eight diblocks into a Vergina star is to substantially increase the lamellar spacing. This occurs due to crowding near the junction point which can be partially reduced by more chain stretching normal to the interface. In Figure 3.13, data for two lamellar forming A_2B_2 materials are added to this picture. Interestingly, these materials result in an increase in the lamellar spacing over AB diblocks which just about splits the difference between the diblock and A_8B_8 behavior. Thus even the crowding resulting from having two arms of each type per molecule results in a substantial increase in chain stretching normal to the interface. These results illustrate the importance of the junction point on chain conformation and morphology in miktoarm star materials. In materials with A_nB

architectures, the multiple arms of A on one side of the interface, linked to a common junction point, are more highly stretched than predicted by the Milner theory, which neglects the effect of the junction point on conformation. That this junction point effect is not explicitly included in the Milner model may underlie the deviations of experimental results.[1,5,9]

In Figure 3.13, the diblock (A_1B_1) data fall on a lamellar long period (d) vs. molecular weight (M_n) power law with an exponent of 2/3, as one would expect for diblocks in strong segregation. The A_2B_2 and A_8B_8 data tentatively can be modeled by applying a positive correction to the A_1B_1 curve. This correction term decays exponentially as arm molecular weight increases; thus at sufficiently high molecular weight, where the influence of the junction point becomes negligible, all A_nB_n architectures must follow the standard 2/3 power law. The curves for A_2B_2 and A_8B_8 architectures shown in Figure 3.13 are as follows: $d_{A_2B_2} = d_{A_1B_1} + 70 \cdot \exp[-(M_n/n)/100{,}000]$, and $d_{A_8B_8} = d_{A_1B_1} + 99 \cdot \exp[-(M_n/n)/350{,}000]$. The arguments of the exponentials are the negative of a ratio between effective diblock molecular weight, M_n/n, and a constant parameter which represents effective diblock molecular weights above which the junction point influence on morphology becomes negligible. This characteristic molecular weight value is found by fitting the experimental data and is also close to the point of intersection on a log-log plot of best fit lines (power laws) for the A_1B_1 and A_nB_n data. That this characteristic molecular weight is much higher for A_8B_8 materials (350,000) than for A_2B_2 materials (100,000) makes sense since the effect of chain crowding at the eight arm junction point of the A_8B_8 is likely to be greater and to perturb chain formations further from the interface than the tetrafunctional junction point of the A_2B_2 architecture. Thus substantially higher arm molecular weights are needed for

the A_8B_8 architecture when compared to the A_2B_2 architecture to escape the influence of the junction points on lamellar spacing and morphology. Due to the small number of data points, these curves and conclusions are tentative.

Sample A_2B_2-4, with $\phi_{PS} = 0.684$, falls just within the volume fraction range in which the cubic bicontinuous morphology is predicted, but forms instead hexagonally packed PI cylinders. Recently, Matsen and Bates found that although the double gyroid bicontinuous morphology is stable at intermediate segregation, it becomes unstable in the strong segregation regime as a result of increased packing frustration.[29,48,49] The ordered bicontinuous double diamond (OBDD) morphology used in the Milner model is not found to correspond to an equilibrium structure. Chain packing considerations favor block copolymer morphologies in which the domains are of uniform thickness. Morphologies such as the gyroid that result in relatively large deviations from this regular thickness. Systems which are intermediately segregated are more able to tolerate deviation from the mean thickness in the gyroid because the variation in location of junction points along the interface between microphase separated domains reduces the chain stretching required for space to be filled. Cylindrical morphologies, as in A_2B_2-4, however, require almost no deviation from mean domain thickness, rendering them stable in strong segregation.

The majority of sample A_2B_2-5 is microphase separated, but not ordered on a lattice. The TEM projection in Figure 3.11 does not allow one to tell conclusively whether the microphase separated domains are spherical in shape or form a more chaotic morphology. The projections observed are consistent with what is expected for disordered arrangements of microphase separated spherical domains. Additionally, the comparison between calculated form factor scattering from a spherical domain and the

SAXS data support the conclusion that although not ordered on a lattice, spherical domains are formed. Grains of material with lattice ordering are also present in this sample. Their images are consistent with TEM projections expected for cubic packings of spheres. The behavior of A_2B_2-5 is similar to that found recently for multigraft block copolymers,[62,69] where SAXS and TEM data indicated the presence of microphase separated domains in a disordered arrangement.

3.6 Conclusions

The morphological behavior of a series of five A_2B_2 miktoarm star block copolymers was characterized by TEM and SAXS. The samples, which were composed of PS and PI arms, ranged from 14 volume % to 87 volume % PS. The strong segregation regime theory of Milner was used to predict the behavior of the samples. Two samples, A_2B_2-1 and A_2B_2-3, were found to agree with their predicted behavior. Sample A_2B_2-2, which was predicted to form lamellae, was found instead to form a cylindrical morphology. This behavior may in part result from the effect of the junction point chain conformation is in agreement with previously reported discrepancies to this model. Sample A_2B_2-4 exhibited a cylindrical morphology where a bicontinuous morphology was predicted, consistent with recent findings that bicontinuous morphologies are unstable in strongly segregated systems. Sample A_2B_2-5 exhibited a microphase separated morphology that generally lacked long-range lattice order with the exception of isolated grains of spheres on a cubic lattice.

			A_2B_2-1	A_2B_2-2	A_2B_2-3	A_2B_2-4	A_2B_2-5
PS Arm	SEC	M_n (g/mol)	9,080	16,400	20,500	37,300	39,700
		PDI[§]	1.03	1.03	1.03	1.03	1.03
	MALDI	M_n (g/mol)	8,740	16,930	21,500	40,040	-
		PDI	1.011	1.006	1.004	1.008	-
	MO	M_n (g/mol)	-	-	20,500	39,000	38,400
PI Arm	SEC	M_n (g/mol)	41,000	33,000	30,800	12,900	6,300
		PDI	1.02	1.03	1.03	1.03	1.04
	MALDI	M_n (g/mol)	-	-	-	-	6,360
		PDI	-	-	-	-	1.033
	MO	M_n (g/mol)	43,000	34,400	30,700	13,100	-
Miktoarm Star	SEC	PDI	1.01	1.01	1.03	1.01	1.01
	MO	M_n (g/mol)	106,000	104,000	99,000	104,000	94,000
	LALLS	M_w (g/mol)	103,000	105,000	95,000	107,000	98,000
	^{1}H-NMR	Mass % PS	16.1	30.6	38.6	71.4	88.1
	UV	Mass % PS	16.9	31.0	37.7	73.0	84.5
		Mass % PS[†]	17.5	33.1	40.8	74.9	86.1
		Vol. % PS[‡]	14.3	27.6	35.3	68.4	86.5
		χN	165	154	156	131	114
		Observed Morphology	C	C	L	C	S/Dis
		q^* (Å^{-1})	0.0227	0.0197	0.0173	0.0193	0.027

[§] Polydispersity index, PDI = M_w/M_n.
[†] Calculated from arm M_n values.
[‡] Calculated from ^{1}H-NMR mass % values and densities.

Table 3.1. Molecular and morphological characteristics of A_2B_2 stars and their component PS and PI block copolymers.

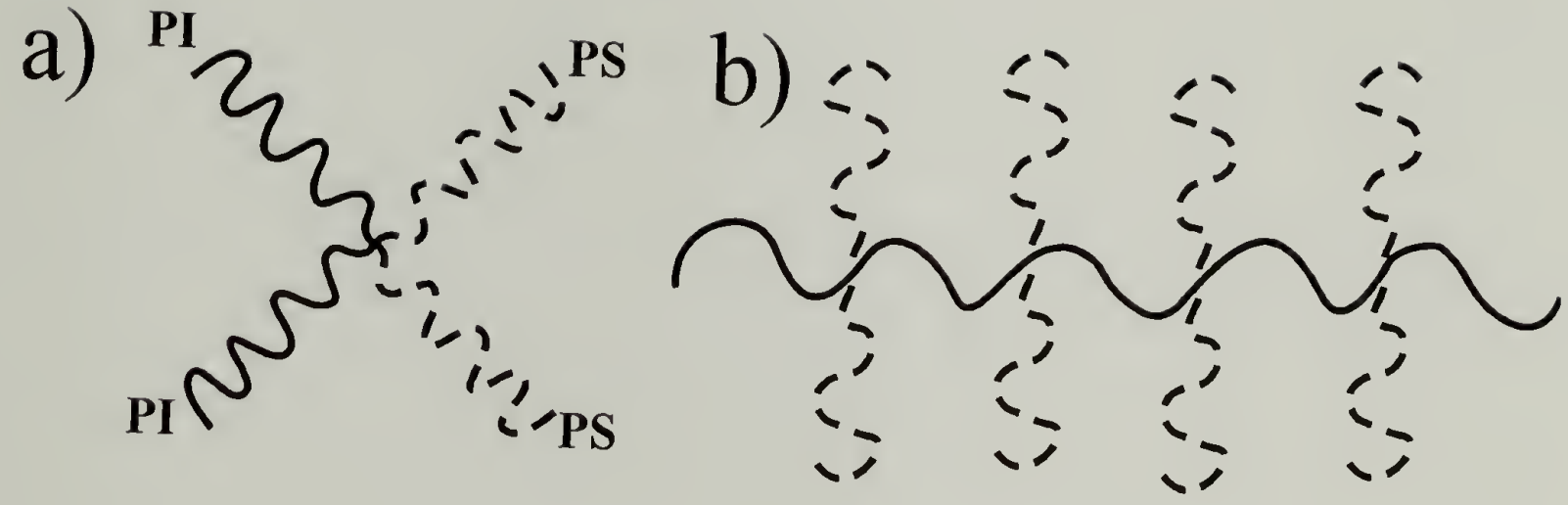

Figure 3.1. Illustrations of a) the A_2B_2 miktoarm star block copolymer architecture, and b) a multiple-graft block copolymer with regularly spaced, tetrafunctional branch points.

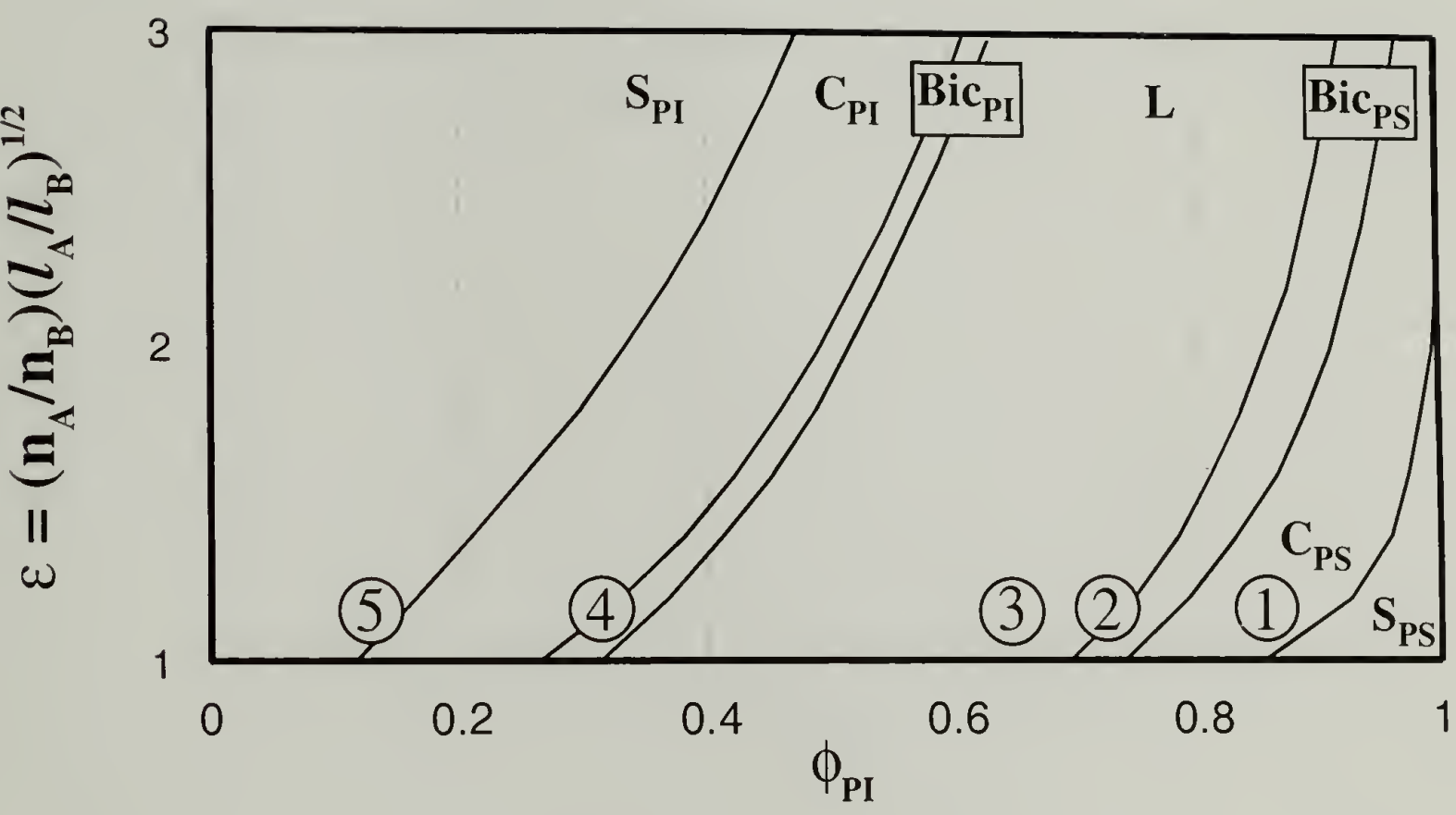

Figure 3.2. Morphology diagram from Milner's theory, including A_2B_2 star block copolymer samples.

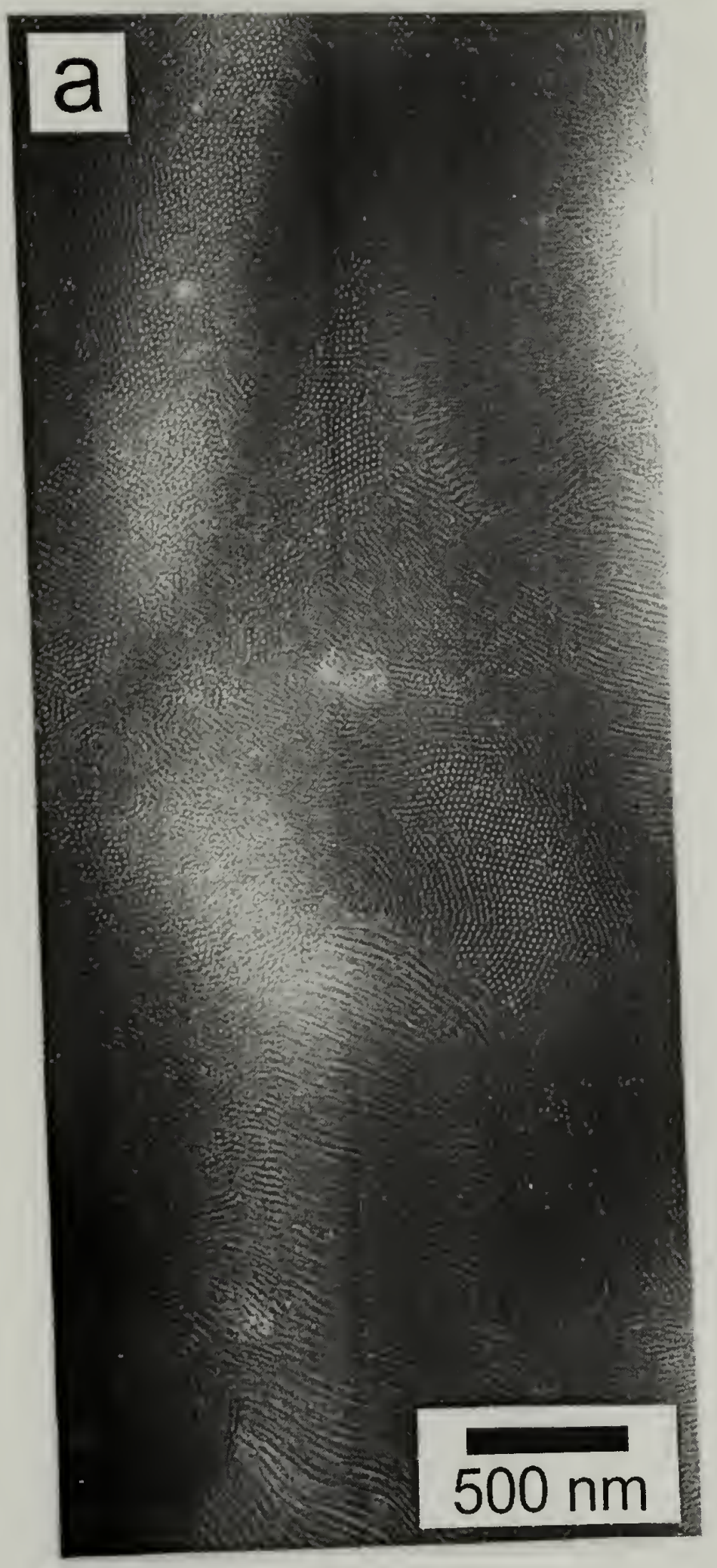

Figure 3.3. TEM micrograph illustrating the cylindrical morphology of sample A_2B_2-1.

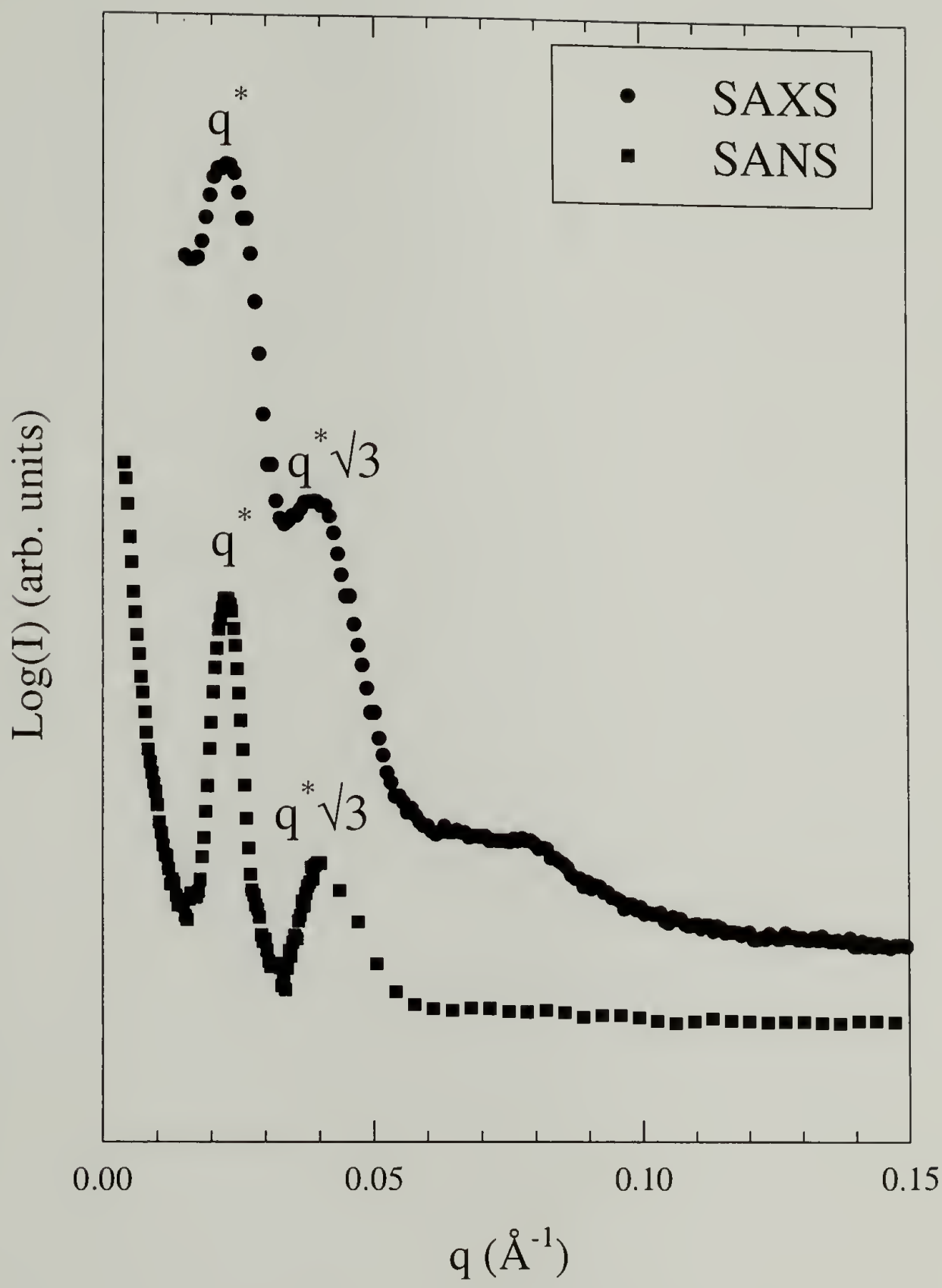

Figure 3.4. SAXS and SANS data for sample A_2B_2-1.

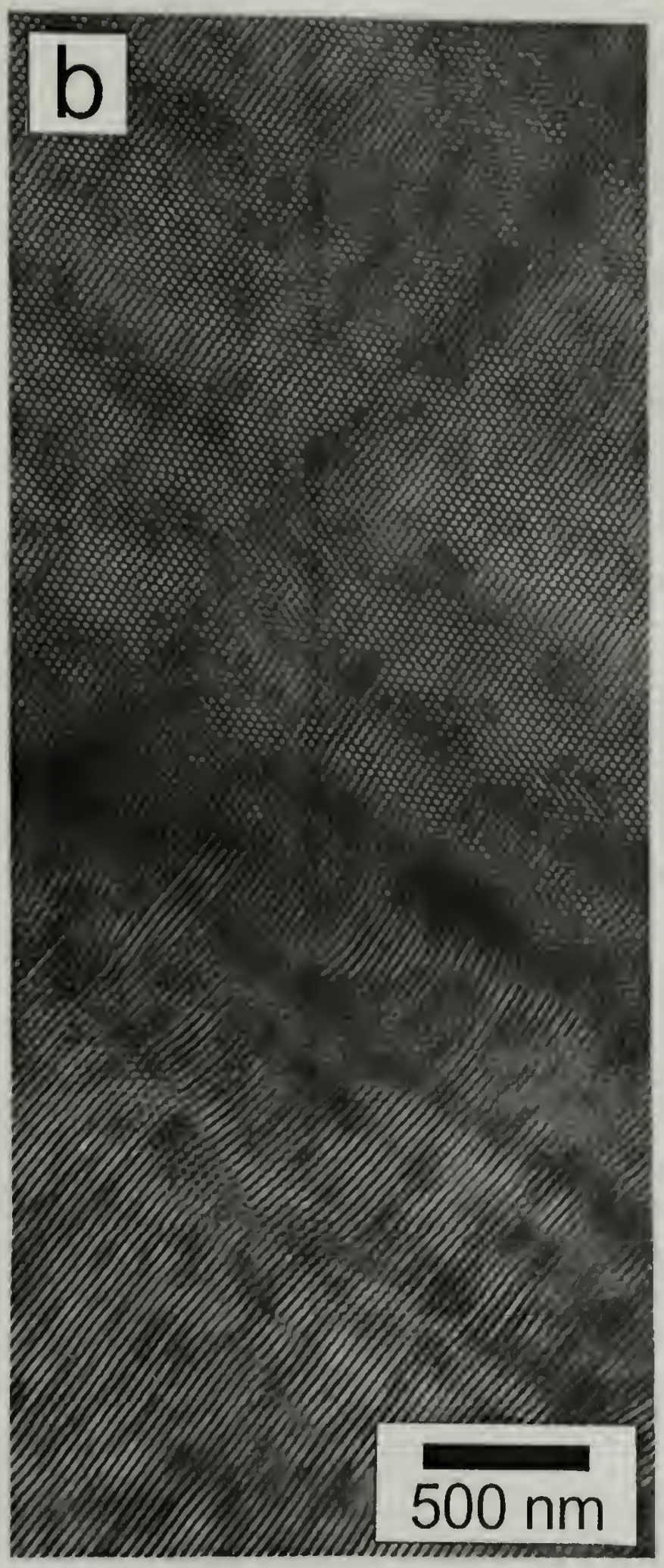

Figure 3.5. TEM micrograph illustrating the cylindrical morphology of sample A_2B_2-2.

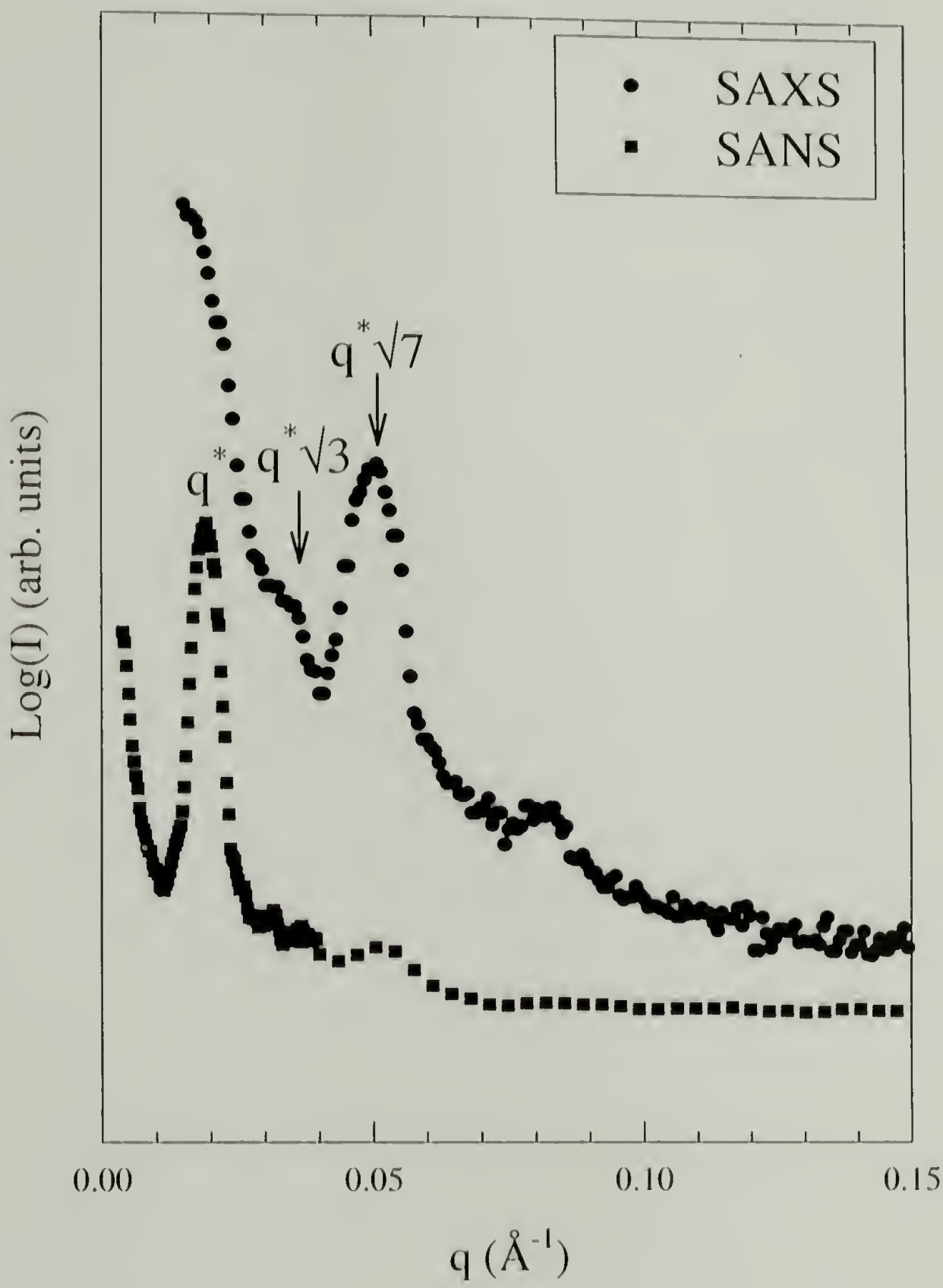

Figure 3.6. SAXS and SANS data for sample A_2B_2-2.

Figure 3.7. TEM micrograph illustrating the lamellar morphology of sample A_2B_2-3.

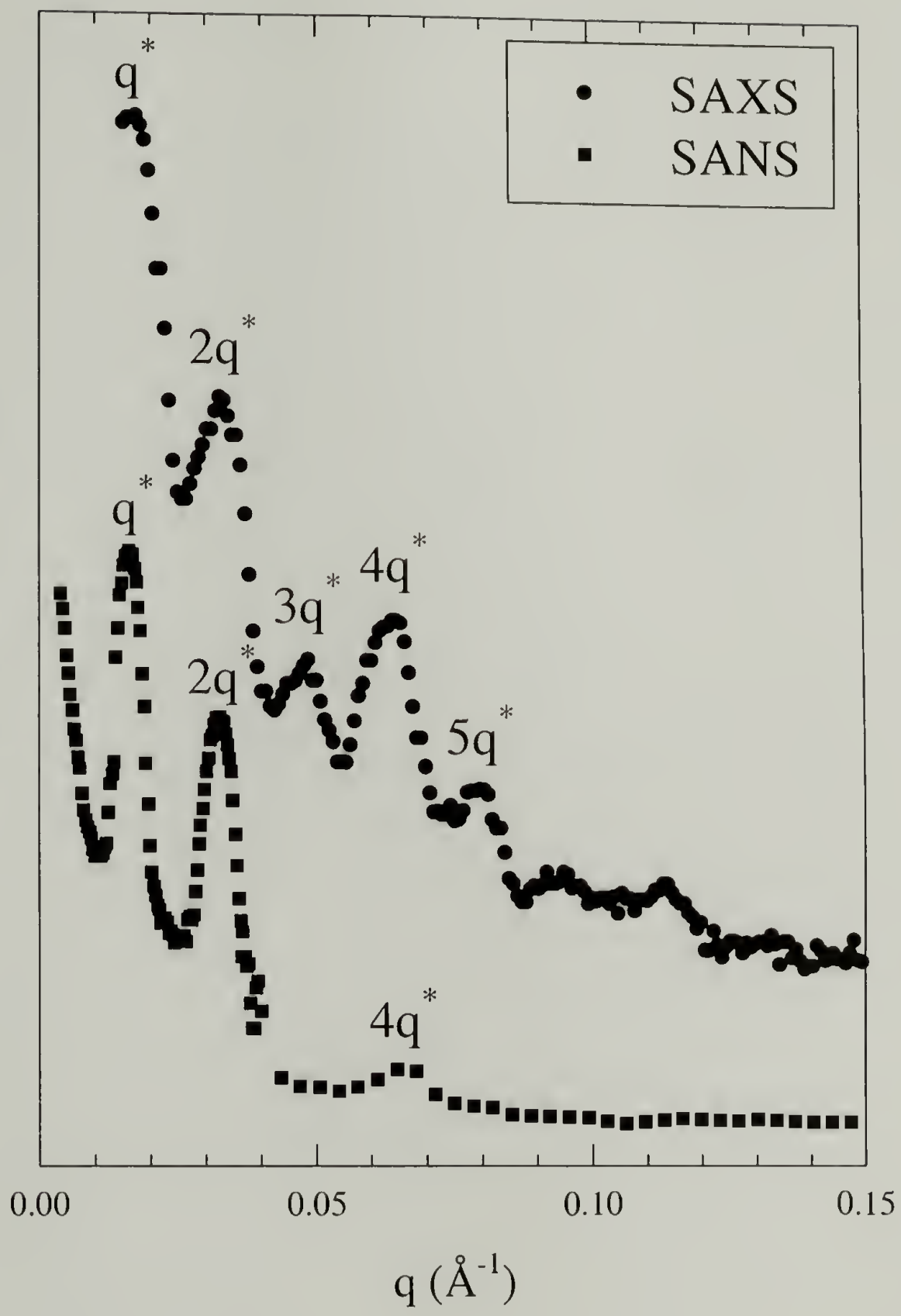

Figure 3.8. SAXS and SANS data for sample A_2B_2-3.

Figure 3.9. TEM micrograph illustrating the cylindrical morphology of sample A_2B_2-4.

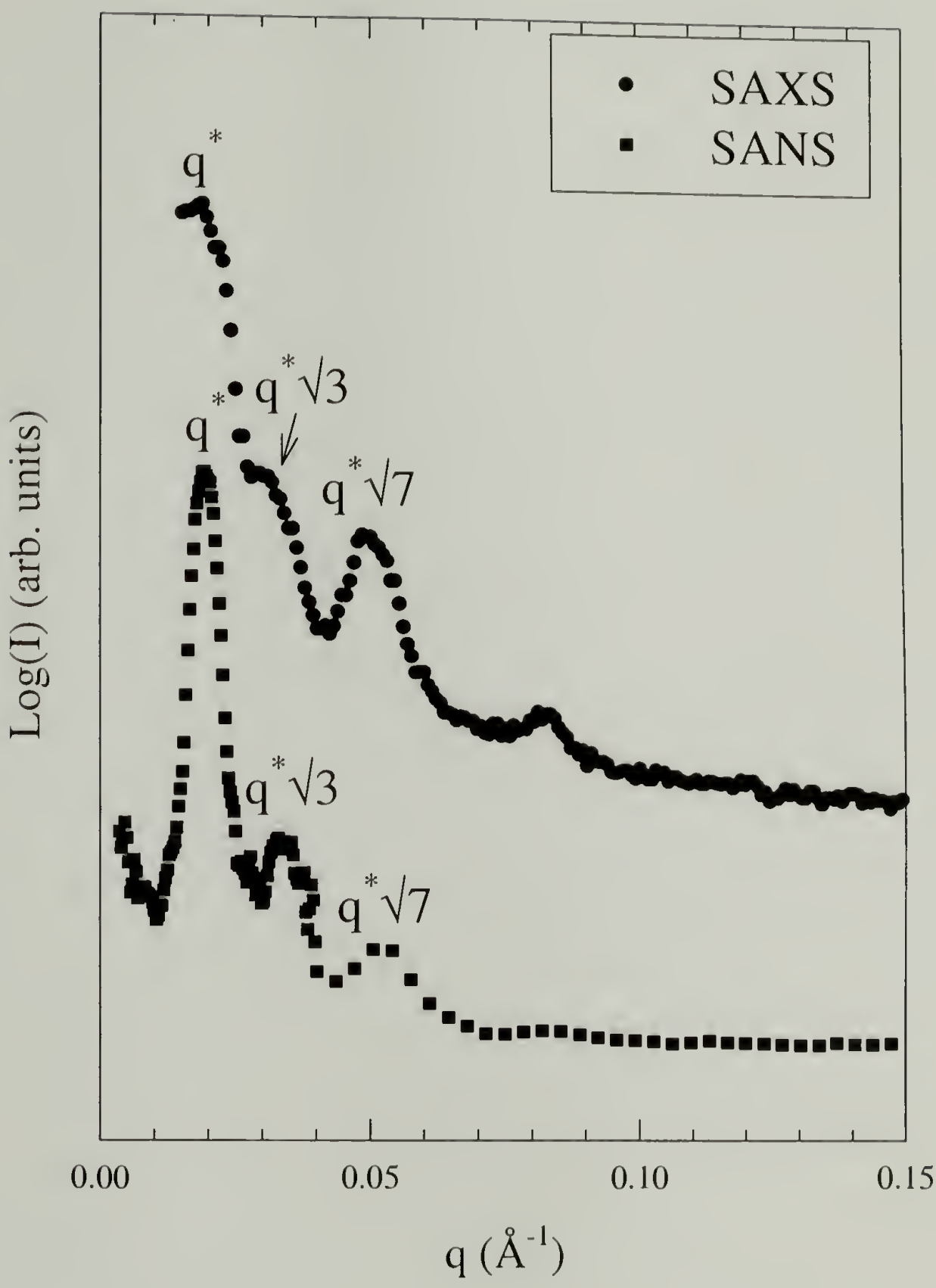

Figure 3.10. SAXS and SANS data for sample A_2B_2-4.

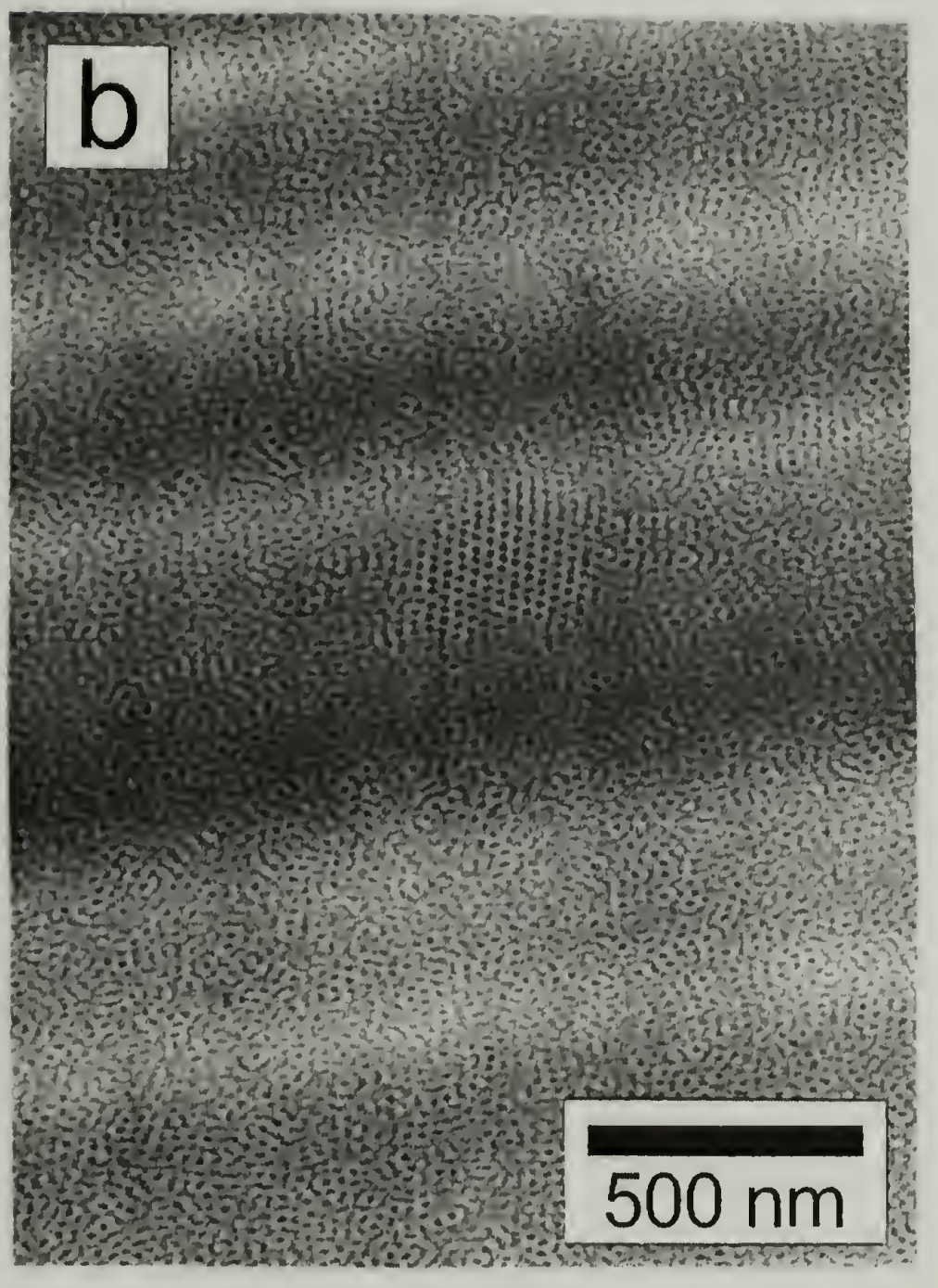

Figure 3.11. TEM micrograph illustrating the microphase separated, but disordered morphology of sample A_2B_2-5. The central portion of the micrograph shows a small region of spheres packed on a cubic lattice.

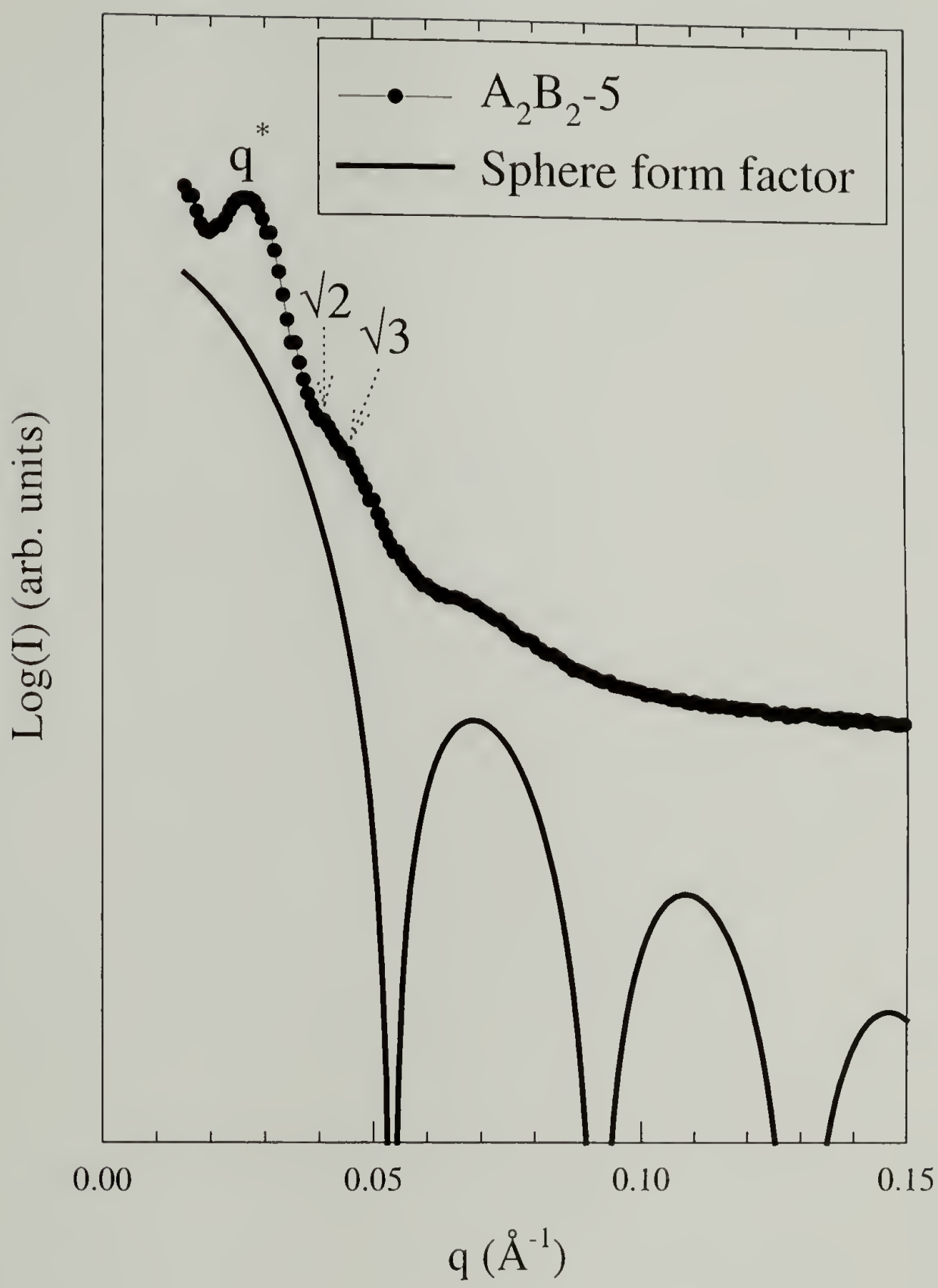

Figure 3.12. SAXS data for sample A_2B_2-5, including form factor calculated for a spherical domain.

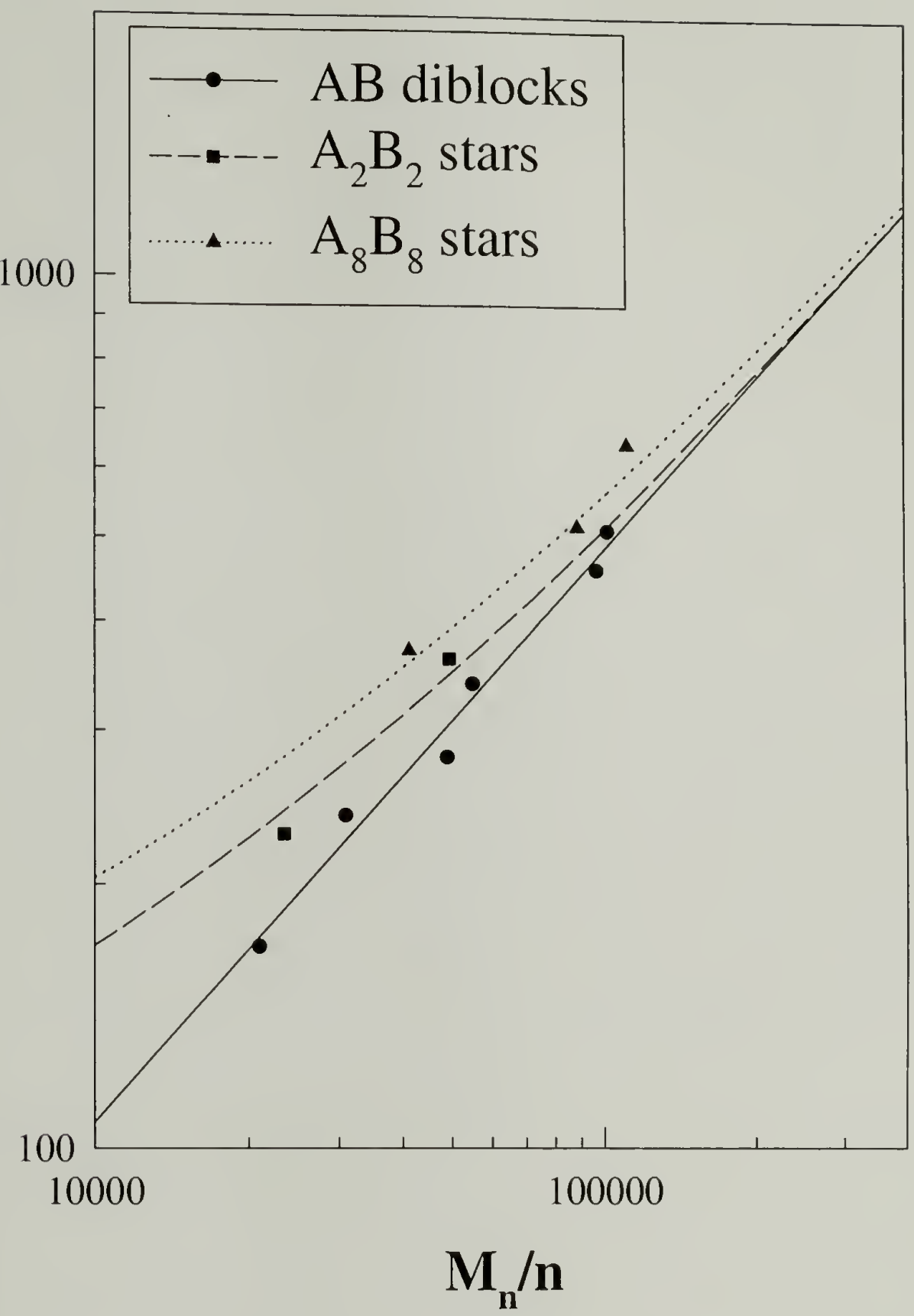

Figure 3.13. Plot of lamellar long spacing, d (Å), as a function of number average molecular weight, M_n (g/mol), for linear diblocks, A_8B_8 stars, and two lamellar A_2B_2 stars. Molecular weight is normalized by *n* for the A_nB_n-type star architecture to give the molecular weight of the equivalent linear AB diblock.

CHAPTER 4

MORPHOLOGICAL BEHAVIOR OF A_5B MIKTOARM STAR BLOCK COPOLYMERS

4.1 Abstract

A morphological study of three A_5B, six-arm miktoarm star block copolymers is presented. The miktoarm stars are comprised of five arms of polyisoprene and one arm of polystyrene joined together at a single junction point. The strong segregation limit theory for the morphological behavior of miktoarm stars, predicts that these materials should form cylindrical (two samples) and lamellar (one sample) morphologies, but only lamellar morphologies were observed by TEM and SAXS. These results are similar to previously reported discrepancies between miktoarm star morphological behavior and the predictions of the theory. Combining the data of this study with that of previous morphological studies of miktoarm star materials we can track the increasing discrepancy between the experimentally observed morphology and theoretical predictions as the molecular asymmetry parameter, ε, increases. The A_5B materials in this study were also observed to form exceptionally well ordered morphologies.

4.2 Introduction

Branched and grafted molecular architecture been shown to be an additional factor (in addition to volume fraction and degree of segregation) which affects the morphological behavior of block copolymers. Guided by the predictions of a mean field theory derived by Milner[8,45] for the morphological behavior of A_nB_m-type, miktoarm star block copolymers, work has focused on molecules with an array of architectures

including A_2B stars,[1,2,6,51] A_3B stars,[9] A_nB_n stars,[59,60,70] and multigraft architectures which may be considered to be linear combinations of miktoarm stars.[4,5,69] These studies have borne out the predictions of the model in general, but have revealed systematic discrepancies. The purpose of this study is to examine A_5B miktoarm star block copolymers, whose architecture is illustrated in Figure 4.1. These materials have the highest architectural asymmetries investigated thus far.

In the current work, three A_5B miktoarm stars of polyisoprene (PI) and polystyrene (PS) have been characterized. Their bulk morphology is predicted by the Milner theory, which is strictly applicable only in the strong segregation limit. Figure 4.2 shows the morphology diagram generated by this model. For architecturally and conformationally asymmetric block copolymer stars of type A_nB_m, the theory predicts morphology as a function of B component volume fraction, ϕ_B, and a molecular asymmetry parameter, $\varepsilon = (n_A/n_B)(l_A/l_B)^{1/2}$. Here, n_A and n_B are the numbers of arms of block materials A and B, and $l_i = (V_i/R_i^2) = v_i/b_i^2$. V_i and R_i are the volume and radius of gyration of one arm of polymer *i*, while v_i is the segmental volume and b_i the statistical segment length of component *i*.

The materials in this study, A_5B stars of PI and PS, have five arms of PI and one arm of PS per molecule, joined to each other at a single junction point. Using segmental volumes of 132 Å^3 (PI) and 176 Å^3 (PS) and Kuhn lengths of 6.8 Å (PI) and 6.9 Å (PS), an ε of 4.4 is calculated for these materials.[71,72] The samples characterized have PS volume fractions of 0.60 (I_5S-1), 0.69 (I_5S-2), and 0.77 (I_5S-3).

4.3 Experimental

Three A_5B miktoarm stars of PI and PS were synthesized using anionic polymerization and controlled chlorosilane chemistry. The synthesis of the A_5B stars has been described in detail elsewhere.[73] All manipulations were performed in glass reactors under high vacuum. The reactors were previously washed with benzene solution of *n*-butyllithium and rinsed with benzene. Benzene was the solvent for all polymerizations and linking reactions. The PS and PI arms were synthesized separately using *sec*-butyllithium as initiator and then linked together with the hexafunctional chlorosilane 1,2-bis-trichlorosilylethane.

Table 4.1 lists the molecular characteristics of each sample. Membrane osmometry (MO) was performed in toluene at 35°C. Size-exclusion chromatography with both refractive index (SEC) and UV (UV-SEC) detectors (λ = 262 nm) was performed in tetrahydrofuran (THF) at 30°C. Vapor pressure osmometry (VPO) was performed in toluene at 50°C. Proton nuclear magnetic resonance (^{1}H-NMR) was used to determine the weight fraction of PS in each sample. Finally, the weight fraction PS in each sample was calculated by dividing the PS arm M_n, as measured by SEC, by the total M_n of the star, $M_n(\mu) = 5\cdot(M_n(PI)) + M_n(PS)$. Volume fraction PS was calculated for each sample using the mass % PS measured by ^{1}H-NMR and bulk densities.[74]

Bulk films were cast from 4 weight % solution in toluene, a nonselective solvent for PI and PS.[54] Films approximately 2 mm thick were formed by allowing the solvent to evaporate slowly over a period of two weeks. The films were let stand at room temperature and atmospheric pressure for an additional week, then placed under vacuum at room temperature for one week to remove any residual solvent from the bulk material. The samples were subsequently annealed under vacuum for one week at 120°C. The

samples were then cooled under vacuum to room temperature over a period of several hours.

Sample morphology was characterized using a combination of transmission electron microscopy (TEM) and small-angle X-ray scattering (SAXS). To prepare thin sections for microscopy, a Leica Ultracut UCT microtome equipped with a Leica EM FCS cryogenic sample chamber operated at –110°C was used to cut sections approximately 500 Å in thickness. The sections were collected on TEM grids and stained four hours in OsO_4 vapor. A JEOL 100CX TEM, operated at an accelerating voltage of 100 kV, was used to image the stained sections. SAXS data were collected at the Advanced Polymers Beamline (X27C), located at the National Synchrotron Light Source at Brookhaven National Labs (BNL), Upton, NY. Two-dimensional scattering patterns were collected on Fujitsu image plates, then read by a Fujitsu BAS 2000 image plate reader. Custom software at BNL was used to subtract background noise and perform circular averaging. Data were collected for a wavelength of 1.307 Å and a camera length of 1410 mm.

4.4 Results

The results of the morphological characterization for the three I_5S materials are collected in Table 4.1. Representative TEM micrographs for samples I_5S-1, I_5S-2, and I_5S-3, indicating the formation of lamellar morphologies, are shown in Figures 4.3, 4.5, and 4.7. SAXS data are shown in Figures 4.4, 4.6, and 4.8 for samples I_5S-1, I_5S-2, and I_5S-3 respectively. A two-dimensional SAXS pattern collected for sample I_5S-3 is shown in Figure 4.9. The remarkable long range order exhibited by these materials results in 8 or 9 orders of the lamellar repeat, with the scattering vectors of the peaks occurring at

integral multiples of the scattering vector of the primary reflection (q^*), as expected for lamellae. In the SAXS data for I_5S-3, the primary reflection is obscured by the beam stop and thus the first observed peak is at $2q^*$. The values of q^* for I_5S-1 and I_5S-2 were found to be 0.0147 $Å^{-1}$ and 0.0131 $Å^{-1}$, corresponding to lamellar long periods of 427 Å and 479 Å, respectively. Using the observed reflections for I_5S-3, q^* is calculated to be 0.0099 $Å^{-1}$, corresponding to a lamellar repeat of 635 Å.

4.5 Discussion

In addition to samples from three previous works involving A_2B, A_3B, and A_2B_2 miktoarm star block copolymers,[1,9,70] the three samples characterized in this paper are plotted on the morphology diagram in Figure 4.2. Those samples reported to have morphological behavior differing from their predicted morphologies are shaded. This figure reveals an increase in the frequency of discrepancies between predicted and observed behaviors with increasing molecular asymmetry. As indicated in Figure 4.2, the Milner model predicts that only one of the three I_5S samples, I_5S-3, has the correct volume fraction of PS to exhibit a lamellar morphology. Both samples I_5S-1 and I_5S-2 are predicted to form cylinders of PS but are found experimentally to form lamellae. This discrepancy is in agreement with the general trend observed in prior studies which tested lower ε portions of the morphology diagram.

As with previous studies, samples that disagree with theoretical predictions exhibit morphologies that should occur at lower ε for a given ϕ_B, or at a higher ϕ_B for a given ε. For example, Tselikas *et al.*[9] found that their I_3S-55 sample formed lamellae instead of the predicted cylinders of PS. While ε for I_3S-55 was calculated to be approximately 2.7, for the same volume fraction, lamellae occur at a maximum of $\varepsilon \approx 2.2$.

Alternately, for $\varepsilon = 2.7$, lamellae are predicted to occur for ϕ_B greater than 0.6, but are observed at ϕ_B of 0.55. If similar comparisons are made for all the samples which disagree with the theory, one finds that the overestimation of morphological shift increases with asymmetry; slight discrepancies at low values of ε become greater as asymmetry increases. This is represented graphically in Figure 4.9, which shows a plot of $\Delta\varepsilon$ as a function of increasing ε, where $\Delta\varepsilon$ is the negative shift in ε required to bring a sample into agreement with the diagram. The I_3S-55 sample, for example, would have a $\Delta\varepsilon$ of 2.7 - 2.2 = 0.5. Plotted as a function of ε, the maximum in this shift increases with ε. These trends can only be represented approximately given the limited experimental data available, i.e. the data points available do not necessarily represent the limits of the discrepancy between theory and experiment at each value of ε.

4.6 Conclusions

As seen in prior studies, the Milner theory exhibits a systemic tendency to overestimate the effect of architectural and conformational molecular asymmetry of block copolymer morphology. This tendency becomes exaggerated with increasing asymmetry as in the I_5S samples of this study. Additionally the three I_5S samples self assembled to form remarkable long range order in their lamellar morphologies as indicated by the unusual number of Bragg reflections observed in SAXS data.

			I_5S-1	I_5S-2	I_5S-3
PS arm	M_n (g/mol)	MO	76,000	106,000	167,500
	PDI	SEC	1.02	1.03	1.03
PI arm	M_n (g/mol)	VPO	10,400	9,700	9,700
	PDI	SEC	1.03	1.04	1.04
Miktoarm Star	M_n (g/mol)	MO	126,000	152,000	218,000
	M_n (g/mol)	Calc.	128,000	154,500	216,000
	PDI	SEC	1.05	1.05	1.05
	Mass % PS	^{1}H-NMR	63	70	79
	Mass % PS	UV-SEC	61	67	75
	Mass % PS	Calc.	60	69	77
	Vol. % PS	Calc.	59.9	67.2	76.8
	q^* (Å^{-1})		0.0147	0.0131	0.0099
	d (Å)		427	479	629
	Predicted Morphology		C	C	L
	Observed Morphology		L	L	L

Table 4.1. Molecular and morphological characterization information for the three I_5S miktoarm stars.

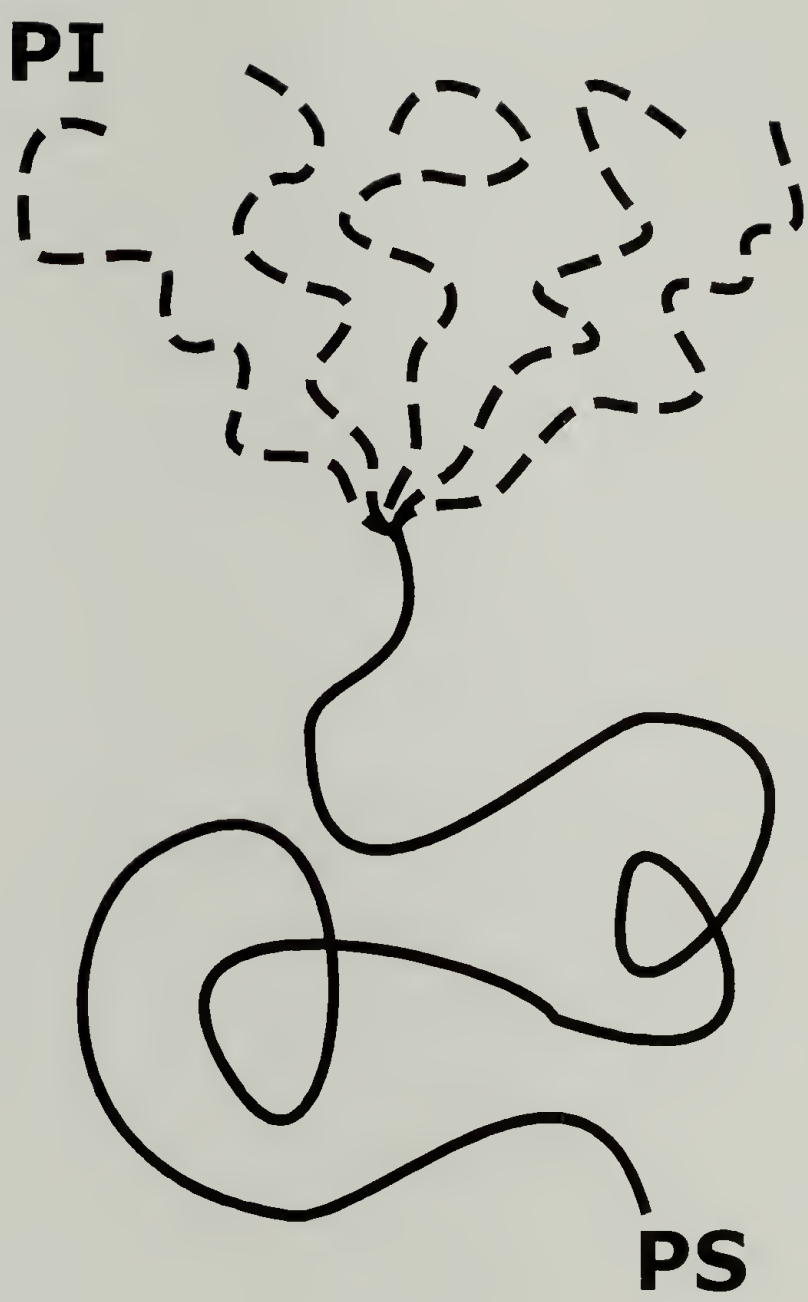

Figure 4.1. Illustration of the molecular architecture of an A_5B miktoarm star block copolymer. In this study, the A_5B stars are comprised of five PI arms and one PS arm joined at a single junction point.

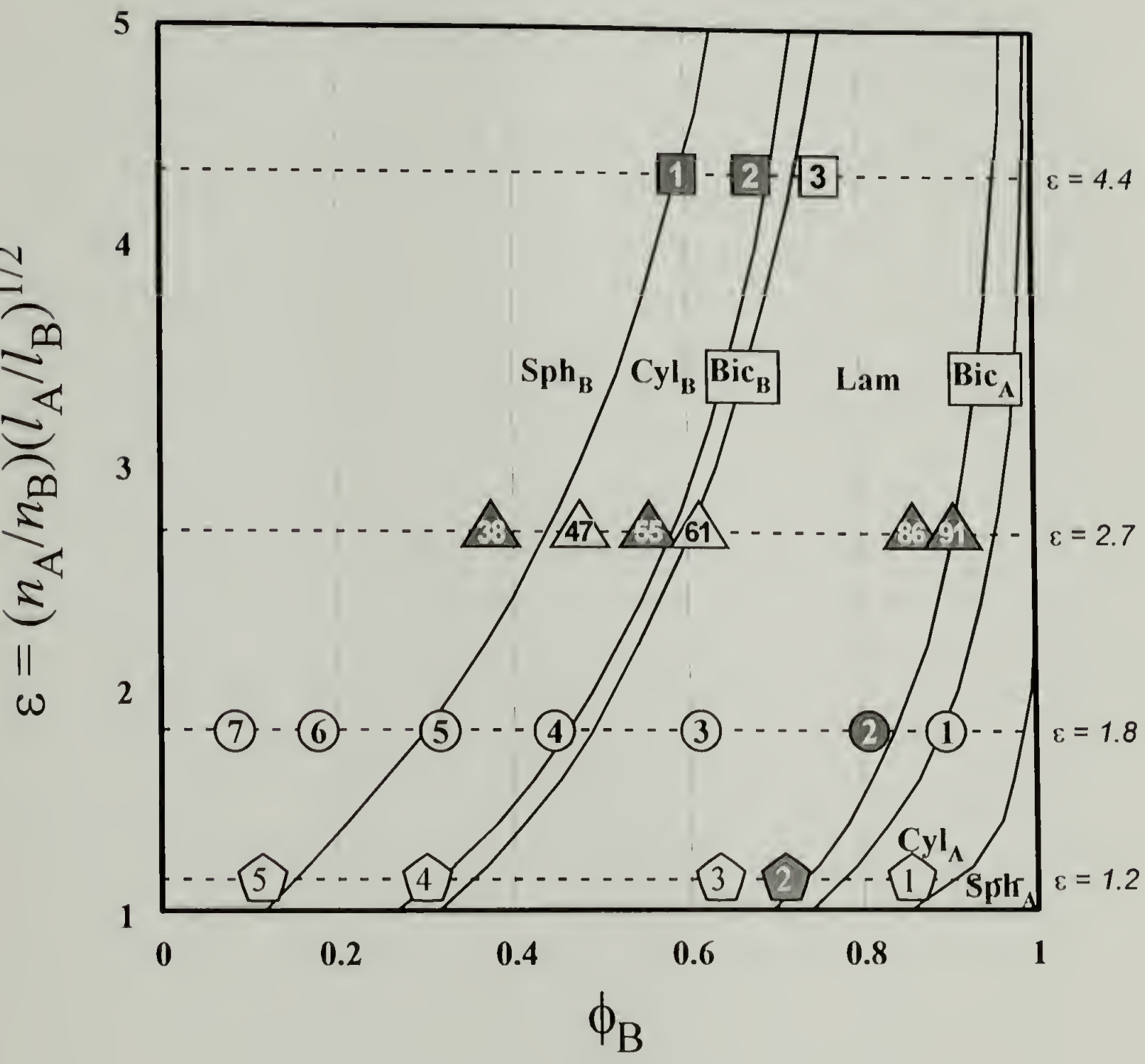

Figure 4.2. The morphology diagram generated by the Milner model. Morphology is given for the volume fraction of the B component, ϕ_B, and molecular asymmetry, ε. The A_5B stars are represented by squares while A_2B stars are represented by circles, A_3B stars by triangles, and A_2B_2 stars by pentagons. Shaded symbols indicate samples whose morphologies disagree with that predicted by theory.

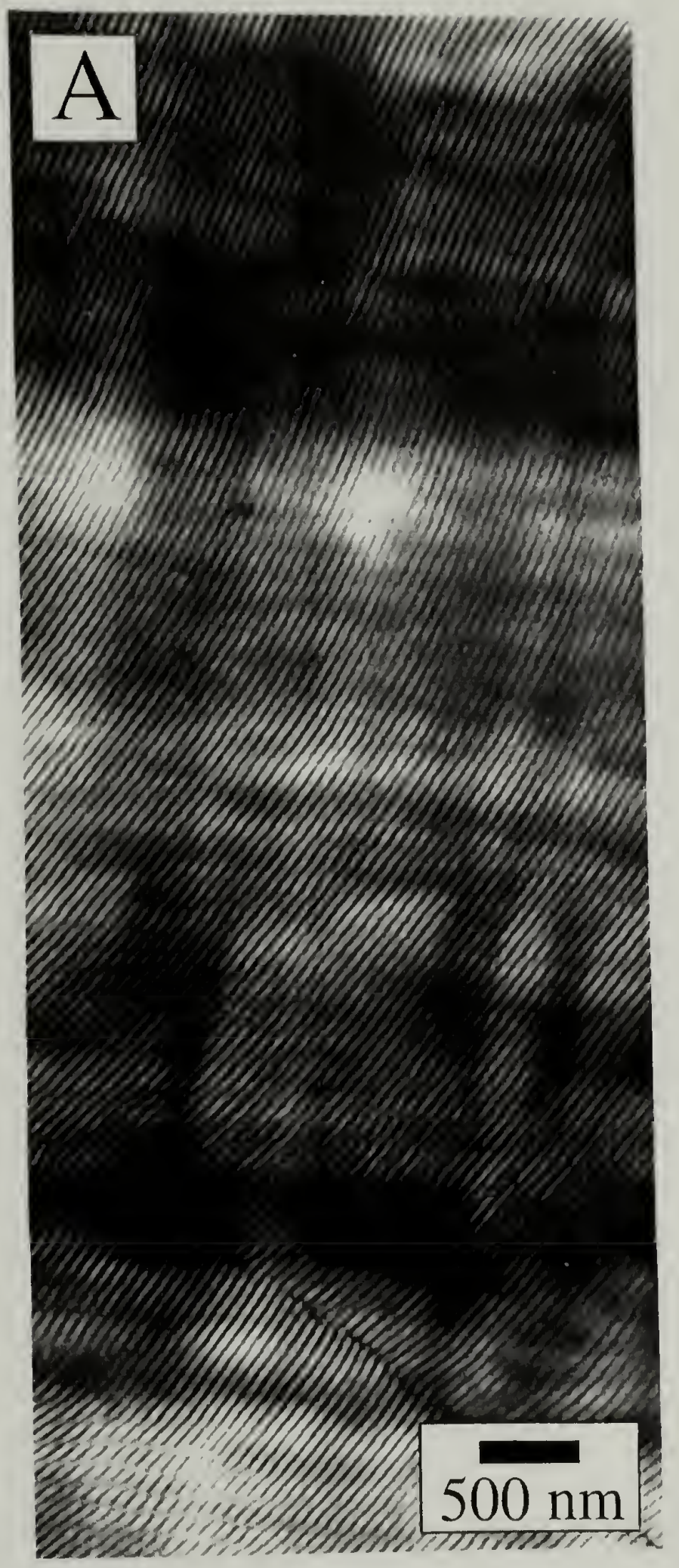

Figure 4.3. TEM micrograph of sample I_5S-1.

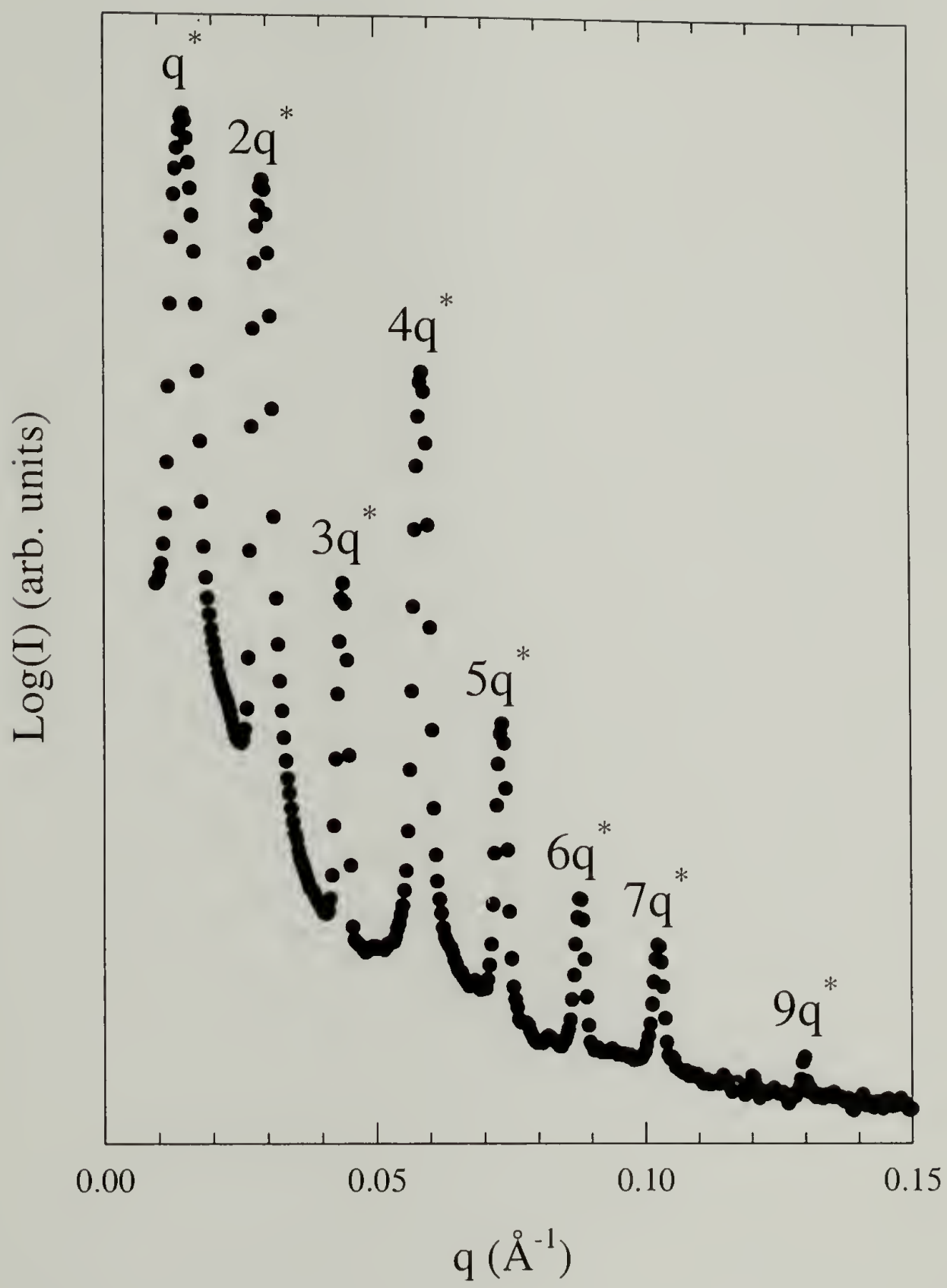

Figure 4.4. SAXS data for sample I_5S-1.

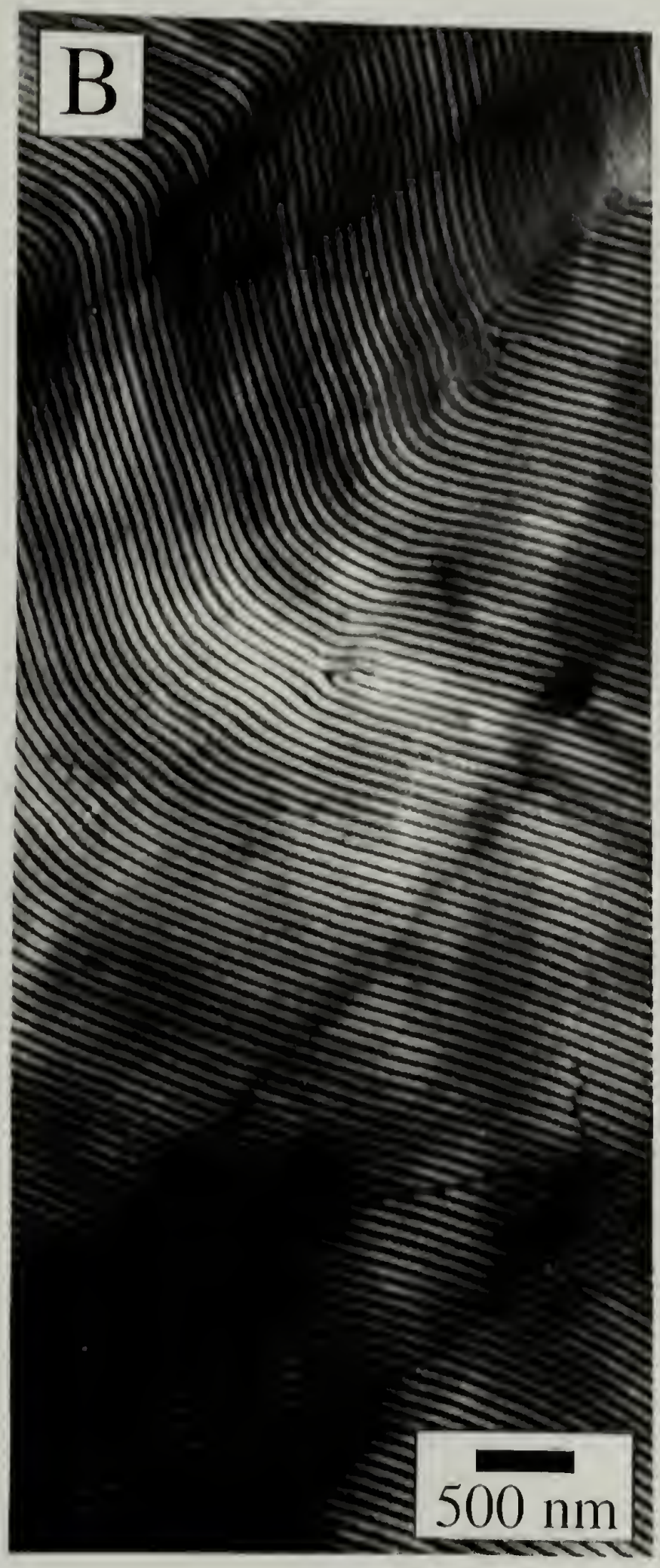

Figure 4.5. TEM micrograph of sample I_5S-2.

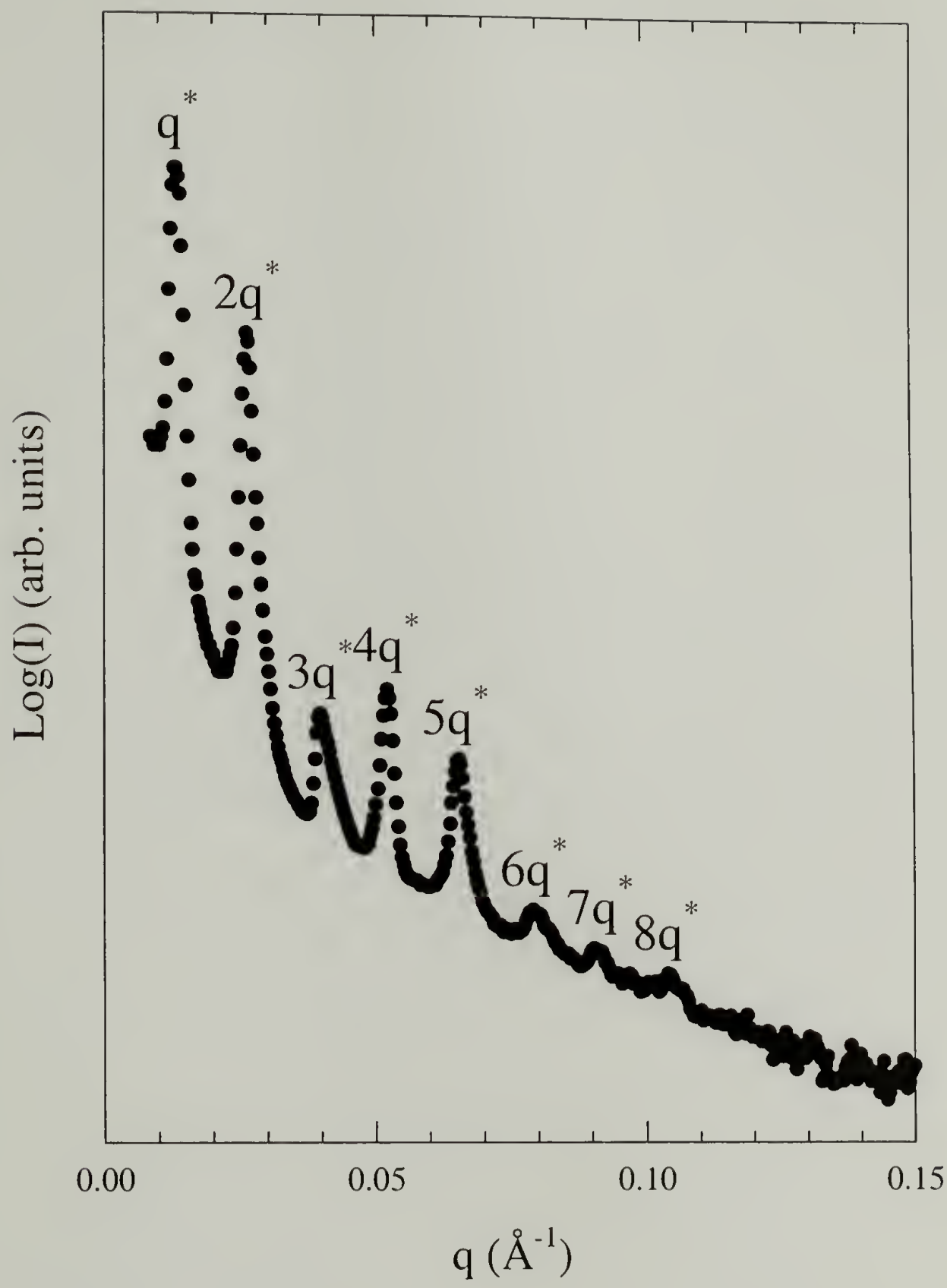

Figure 4.6. SAXS data for sample I_5S-2.

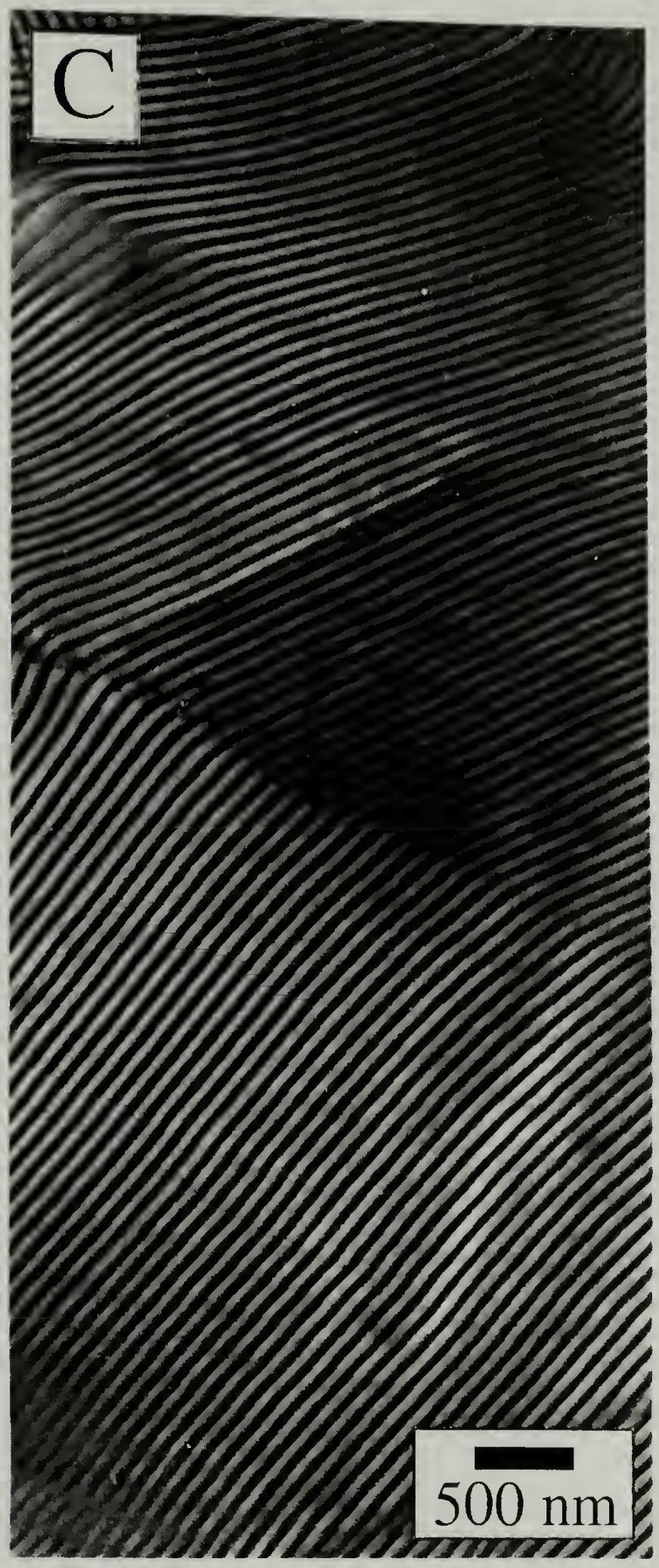

Figure 4.7. TEM micrograph of sample I_5S-3.

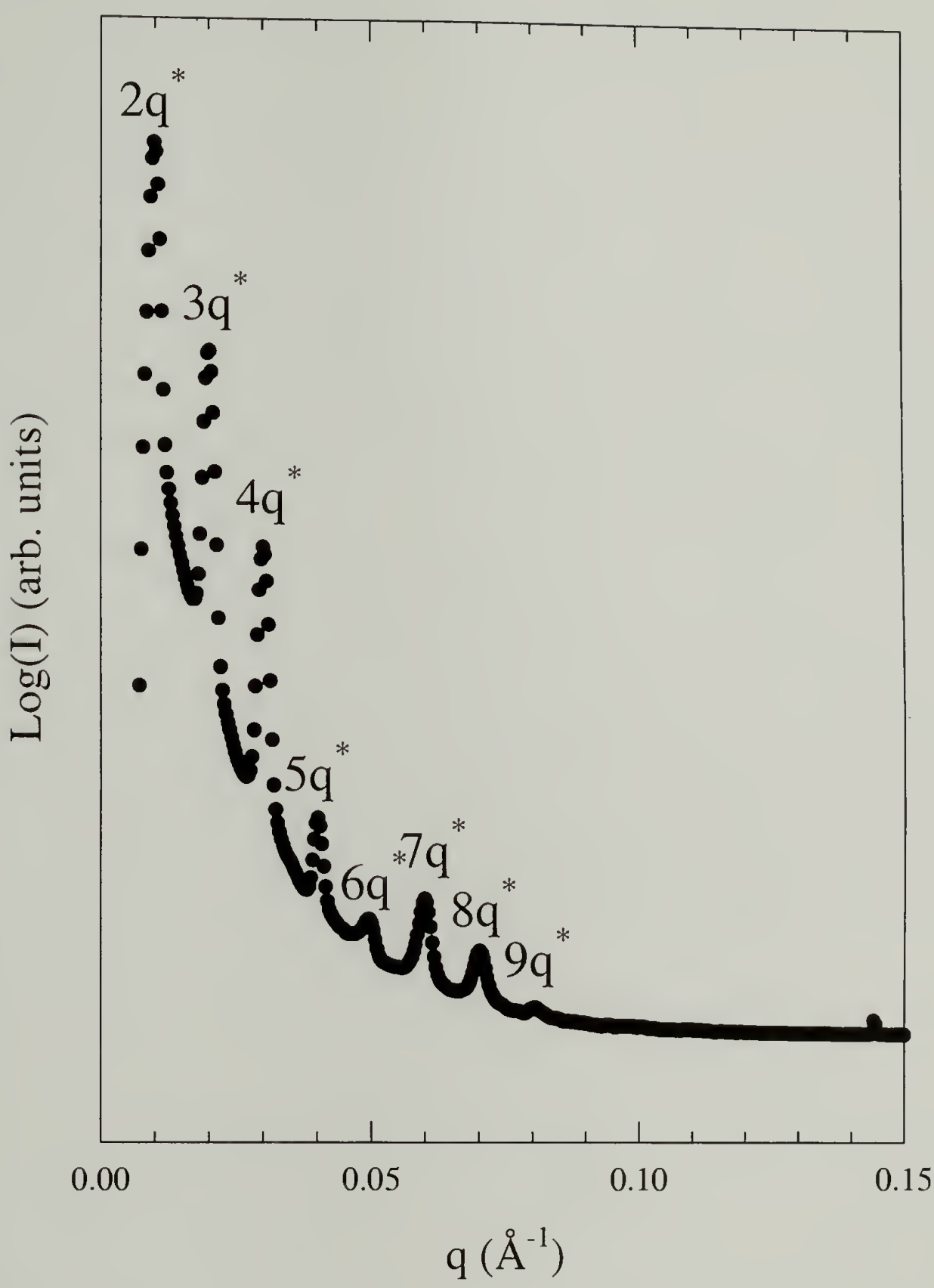

Figure 4.8. SAXS data for sample I_5S-3.

Figure 4.9. Two-dimensional SAXS data collected for sample I_5S-3, illustrating the unusual degree of long-range order present in these materials.

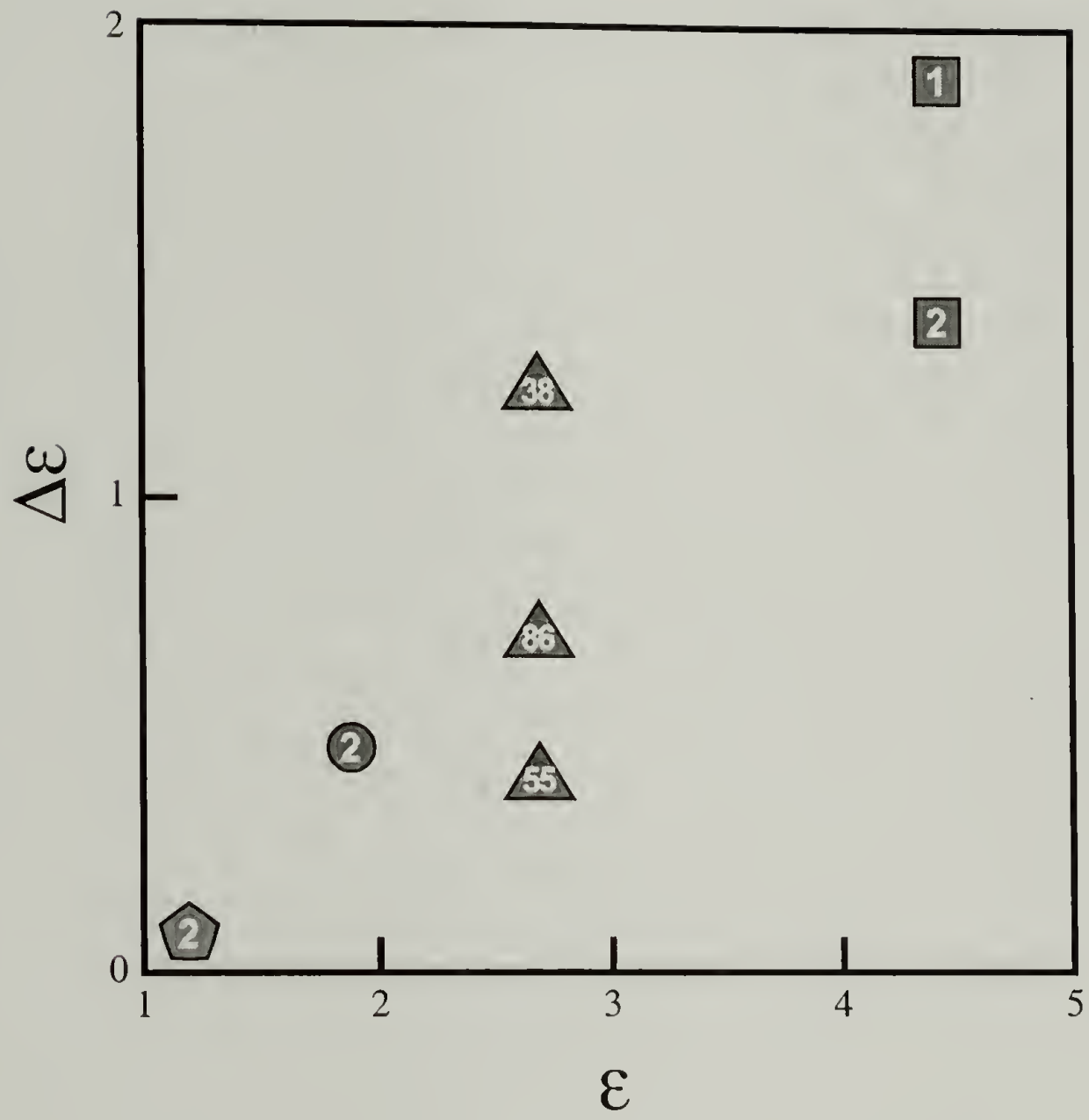

Figure 4.10. Values of $\Delta\varepsilon$ for samples exhibiting morphologies other than those predicted by theory, as a function of ε, for the data shown in Figure 4.2.

CHAPTER 5

MORPHOLOGICAL BEHAVIOR OF RANDOM MULTIGRAFT BLOCK COPOLYMERS

5.1 Abstract

The morphologies of two series of model graft copolymers were studied using transmission electron microscopy (TEM) and small angle X-ray scattering (SAXS). Both series of materials have monodisperse polybutadiene (PB) backbones and monodisperse polystyrene (PS) graft blocks. In one series there are on average five trifunctional junction points randomly distributed along the PB backbone. Each junction point grafts one PS block to the backbone. In the other series there are on average four tetrafunctional junction points randomly distributed along the PB backbone. Each junction point grafts two PS blocks to the backbone. A range of overall PB and PS volume fractions was investigated for both series. These materials simulate a controlled and known degree of architectural disorder. Current theory cannot rigorously predict the morphological behavior for these complex molecular architectures. However, it is found that an approximate extension of existing theory utilizing the constituting block copolymer (fundamental building block) concept allows a rational explanation of the effect of architecture on morphology in these materials. The materials form the domain shape (spheres, cylinders, or lamellae) which is predicted by theory, but spherical and cylindrical morphologies lack the long-range lattice order found in diblocks and other simpler block copolymer molecular architectures. When lamellar morphologies are formed, however, at least some long-range order is always present due to the space filling requirements of the lamellar domains.

5.2 Introduction

This work reports morphological characterization results for two model series of architecturally well defined graft copolymer with polybutadiene (PB) backbones and polystyrene (PS) grafted blocks. The first series of materials, illustrated in Figure 5.1a, has monodisperse PB backbones and one monodisperse PS graft block per branch point. These trifunctional branch points are randomly distributed along the PB backbone and there are, on average, five per molecule. The second series of materials, illustrated in Figure 5.1b, has monodisperse PB backbones and two monodisperse PS graft blocks per branch point. These tetrafunctional branch points are randomly distributed along the PB backbone and there are, on average, four per molecule. Thus both these series of materials are graft copolymers with a limited degree of randomness in their molecular architecture. They are a departure from the well defined molecular architectures which we have studied in previous work on graft copolymer morphology,[1,3-5,51,52,61] but they are also a logical and important extension of this previous work toward materials of more commercial importance.

Linear AB diblock copolymers and ABA triblock copolymers form different, well characterized, nanoscale, phase separated domain morphologies depending on the relative volume fractions of the two block materials. In strongly segregated systems, the type of structure formed is tied to a specific volume fraction dependence which limits the flexibility in designing new materials for new applications. A way to uncouple block copolymer morphology from its rigid dependence on component volume fractions is to introduce another variable into the system by varying molecule architecture in novel ways. One might suppose that a plurality of new block copolymer molecular structures

would introduce a plurality of new variables to be considered in the morphological behavior. However, it is the contention of the authors that a large number of the possible variations can be represented by a single molecular asymmetry parameter. This asymmetry parameter, which Gido and coworkers have been developing[3-5,51] as an extension of that proposed by Milner for miktoarm (mixed arm) star architectures,[8] contains a factor describing the conformational asymmetry between the two block materials and another factor describing the asymmetry inherent in the molecular architecture (the way in which component blocks are linked together). The problem is to figure out how to calculate the architectural asymmetry part of the general asymmetry parameter for all the various architectures encountered. Large molecular asymmetries are accessible by linking common block materials such as PB or polyisoprene (PI), and PS together in graft copolymer geometries. Figure 5c in the publication of Lee and coworkers[5] shows a morphology of alternating nanoscale, thick and thin lamellae; the volume percents of the dark OsO_4 stained PI domains and the light PS domains are 74 % and 26 % respectively. This unusual lamellar structure was formed by an H-shaped, S_2IS_2, double-graft copolymer.

The overall goal of this graft copolymer research is to systematically build a knowledge of graft copolymer morphological behavior beginning from the very simplest single-graft molecules shown in Figures 5.2a and 5.2b. The molecule in Figure 5.2a has a single PS graft placed in the middle of a PI backbone. Alternatively, this molecule may be interpreted as a three armed miktoarm star with two PI arms of identical length and one PS arm. This architecture is referred to as the symmetric single-graft or I_2S. The architecture in Figure 5.2b has a single PS graft placed asymmetrically along a PI backbone. In the notation of Olvera de la Cruz and Sanchez,[50] the molecule in Figure

5.2a corresponds to a single-graft structure in which $\tau = 0.5$, where τ is the fractional distance along the PI backbone at which the PS graft occurs. In Figure 5.2b, τ is not equal to 0.5, and this type of structure is referred to as an asymmetric single-graft (ASG). Once an understanding of the effect of single-graft architecture on morphology was developed, the next step was to investigate double-graft architectures, two of which are shown in Figures 5.2c and 5.2d. The double-graft architectures may be thought of as two single-graft molecules linked together in different ways. The architecture in Figure 5.2c, the H double-graft molecule or S_2IS_2, can be imagined as two symmetric single-graft molecules linked together at the ends of the grafted blocks, PI in this case. The architecture in Figure 5.2d, the π double-graft molecule or (SI)I'(SI), can be imagined as two single-graft molecules linked together by the ends of their PI backbones.

To discuss architectural effects on morphology from an overall perspective, the concept of dividing complex graft architectures of the types shown in Figures 5.1, 5.2c, and 5.2d into component parts, which will be called constituting block copolymers, is formalized. Assuming a lamellar morphology for simplicity, in linear diblock copolymers, each domain consists of two brushes grafted from the two opposite interfaces. Both A and B domains contain free chain ends which are generally clustered near the middle of the domains. For more complicated molecular architectures, "bridges", which are blocks with one end grafted from each of the two opposite interfaces, and "loops", which are blocks with both ends grafted from the same interface, are formed. For example, the B domains of ABA triblock copolymers contain no free chain ends, only loops and bridges. The A domains, by contrast contain only free chain ends. Cutting the loops and bridges in half results in a system consisting of the constituting block copolymers. For example, the symmetric ABA triblock copolymer has

A(½B) as the constituting block copolymer. This notation specifies a diblock copolymer composed of an A block equal to one of the A blocks of the original triblock and a B block equal to half of the B block of the original triblock.

It has been shown by both experiments and theoretical calculations that, for high molecular weights, symmetric ABA triblock copolymers, $(AB)_n$ star copolymers,[27,75-77] and ...ABAB... infinite multiblock copolymers[78,79] have the same morphology as their constituting linear diblock copolymers which are obtained by imagining the molecules to be cut in the middle of all loops and bridges in the morphologies.[5,51] The small amount of information that exists for cyclic AB block copolymers suggests that the morphological behavior may also be similar to that of linear constituting diblocks.[80,81] The connections in the microphase separated domains which loops and bridges provide may strongly influence other material properties,[82] but they have only a slight effect on the morphological behavior. The constituting block copolymer of a graft copolymer architecture with trifunctional branch points is an I_2S single-graft copolymer or an off-center single-graft copolymer[3,4,51] rather than a linear diblock.

The I_2S symmetric single-graft structure is a special case of the general A_nB_m miktoarm star architecture. The effect of miktoarm architecture on the volume fraction ranges in which various morphologies are formed was investigated by Milner[8] with a self-consistent field theory in the strong segregation limit ($\chi N > 100$). Connecting different numbers of A and B arms at one junction point creates an asymmetry in the way that the opposing A and B block materials fill space. Corresponding block copolymers are defined as materials which differ in architecture but have the same overall component volume fractions and total molecular weight. Compared to a corresponding linear diblock, block copolymers with two or more arms on the same side of the interface in a

microphase separated structure experience lateral crowding of the multiple blocks. This in turn results in more chain stretching normal to the interface on the side with multiple arms. There is a shift in interfacial curvature preference in order to alleviate this asymmetry in chain stretching; the interface tends to increase in curvature (mean curvature) when viewed from the side of the block material with higher arm number. This statement takes into account the sign convention for interfacial mean curvature which assigns a negative sign to curvature on the concave side of the interface and a positive sign to curvature on the convex side of the interface.[61,83,84] If the higher arm number occurs on the concave side of the interface, the interface will tend to be less concave (less negative curvature) than it would be in a corresponding linear diblock copolymer. If the higher arm number occurs on the convex side of the interface, then the interfacial curvature will tend to be more convex (more positive curvature) than it would be in a corresponding linear diblock copolymer.[61]

These curvature preferences, as illustrated in a mean-field morphology diagram for A_nB_m type block copolymers calculated by Milner, result in a shift of the morphological transition lines toward higher volume fractions of the lower arm number component. In this calculation, the asymmetry caused by the difference in A and B arm numbers was lumped with the conformational asymmetry inherent in the A and B polymer chains into one asymmetry factor, $\varepsilon = (n_A/n_B)(l_A/l_B)^{1/2}$. Here (n_A/n_B) is the ratio of arm numbers of the two block types and represents the asymmetry due to the architecture. The conformational asymmetry between the two block materials is expressed by the ratio, $(l_A/l_B)^{1/2}$, where l_i is the ratio of segmental volume to the square of statistical segment length for the block material *i*.

The I_2S and ASG, as well as model double-graft copolymer, architectures have been experimentally demonstrated to produce a shift in the volume fraction ranges in which the various well known block copolymer morphologies (A spheres, A cylinders, lamellae, B cylinders, B spheres) are observed to higher volume fractions of the graft block material.[1,3-5] The results of these studies are in general agreement with the theoretical predictions embodied in the Milner morphology diagram, and they validate the constituting block copolymer concept. Those few samples which do not agree with the predictions of the Milner diagram are part of an overall trend, also observed in I_3S miktoarm stars,[9] indicating a tendency of the Milner morphology diagram to slightly overestimate the shift in volume fraction windows of the various morphologies due to architectural asymmetry.

Graft copolymers have long been of interest as a result of their application as interface compatibilizers in blends. Several studies of graft copolymers have been carried out previously.[85,86] However, previous studies have been limited to samples that have been prepared in similar fashion as those commonly used as blend compatibilizers, which produces a polydisperse sample of ill-defined architecture. More careful synthesis has been performed,[87] but in no case has a systematic attempt been made to elucidate the morphological behavior of this class of copolymer. The present study of the effect on morphology of graft architecture with controlled amounts of randomness is a start in this direction and also is a logical extension of our previous work on more well-defined architectures.

5.3 Experimental

5.3.1 Synthesis

The random trifunctional and tetrafunctional multigraft copolymers were prepared via living anionic polymerization and hydrosilylation chemistry.[16] A study has been carried out involving the hydrosilylation of PB in the presence of platinum divinyltetramethyldisiloxane complex in xylene (Petrarch PC072), which selectively catalyzes the hydrosilylation of the vinyl C=C bonds of the PB.

The synthetic procedure was based on coupling hydrosilylated PB backbones with living PS arms. The PB backbone and the PS arms were prepared by anionic polymerization[64] using high vacuum techniques in evacuated, *n*-BuLi-washed and benzene-rinsed reactors. The PB backbone was hydrosilylated with chlorodimethylsilane in the presence of Petrarch PC072 catalyst. The resultant chlorosilylated PB was coupled with living PS. In the case of tetrafunctional multigrafts, dichloromethylsilane was used instead of chlorodimethylsilane. To relieve the steric hindrance and facilitate the addition of two PS arms per branch point, the living arms were capped with 3-4 units of butadiene before the coupling reaction with the multifunctional backbone. Details are given elsewhere.[16]

5.3.2 Molecular Characterization

The molecular weight distributions and the purities of the final multigrafts were evaluated by size-exclusion chromatography (SEC) at 30°C. The weight-average molecular weight was determined by low-angle laser light scattering (LALLS) in THF at 25°C. The compositions of the copolymers were determined by SEC-UV at 260 nm and ^{1}H-NMR spectroscopy. The results of these molecular characterization studies are given

in Tables 5.1 and 5.2. The nomenclature for these samples gives a rough description of the molecular architecture. In the name RMG-3-5-62, "RMG" in the first position stands for "random multiple-graft," "3" in the second position indicates that the graft points have a single PS block attached and are thus trifunctional, "5" in the third position indicates that there are an average of five graft points per PB backbone, and "62" in the fourth position indicates a total composition of 62 volume % PS. Samples with a "4" in the second position have two PS arms attached at each tetrafunctional branch point. The molecular characterization results conclusively establish that the samples possess the predicted architecture and can be characterized as model materials due to their well-defined structures.

5.3.3 Morphological Characterization

Solid films of the graft copolymer material, approximately 2 mm thick were cast from solution in toluene, a non-preferential solvent for PS and PB[54], over a period of two weeks. In an effort to enhance the development of long-range order the samples were thermally annealed at 120°C under vacuum for one week. These casting and annealing conditions have been found to promote self-assembly of well-ordered, nanostructured morphologies in our previous studies of single and double-graft copolymers. After annealing, ultrathin sections approximately 500-1000 Å thick were prepared for TEM observation by cryoultramicrotoming. The sections were stained four hours in OsO_4 vapor to allow TEM imaging of the structures. Small-angle X-ray scattering (SAXS) experiments were performed to determine the lattice symmetries, domain shapes, and spacings of the morphologies. SAXS was performed at the Advanced Polymers Beamline (APB, X27C) at the National Synchrotron Light Source (NSLS), Brookhaven

National Laboratory (BNL). The 3 mm^2 beam had a wavelength of 1.307 Å. The camera length was 1.410 m. Two-dimensional scattering patterns were recorded on Fujitsu HR-V image plates and were digitized using a Fujitsu BAS 2000 image plate reader. Background was subtracted, circular averaging was performed, and the data were converted to a log intensity scale in order to generate plots of log(I) vs. q.

5.4 Results

The morphological results for the series of materials with an average of five trifunctional branch points per molecule are now presented. The morphological assignments for each sample as well as dimensions determined by SAXS are summarized in Table 5.3. Figure 5.3 shows a TEM image for sample RMG-3-5-18, which displays a characteristic microphase separated but disordered morphology. Viewing stereo pair images of this structure suggests, although not conclusively, that the structure consists of randomly packed spherical domains. The SAXS for RMG-3-5-18 is shown in Figure 5.4 along with form factor scattering curves for spherical and cylindrical domains. The initial peak indicates an average intersphere correlation of 290 Å. The scattering vector of the Bragg peak with the lowest scattering angle is referred to as q^*, and q_n are the series of peaks, in order of increasing scattering angle, beginning with q^*. The ratios of q_n/q^* for the series of peaks in a diffraction pattern are characteristic of the lattice symmetry when Bragg scattering is present. The SAXS data for RMG-3-5-18 display a second broad maximum centered at q_n/q^* equal to 2.4, which is not consistent with the symmetries of any of the lattices known to be formed by block copolymers (cubic, hexagonal). This maximum does, however, coincide very well with the second form factor maximum for spherically shaped domains.

To calculate the form factors, the radii of the spherical or cylindrical domains in the morphology must be known. When block copolymer microdomains are well-ordered on a lattice, domain radius is best determined from the spacings of the primary scattering peaks. Calculations of domain sizes require the assumption of a lattice packing symmetry and also use the known volume fractions of the two domain materials. Measuring domain sizes on TEM micrographs is generally less desirable due to the possibilities of dimensional changes caused by staining as well as projection artifacts. However, in the present situation, since no lattice is formed, the calculation of domain sizes from a single scattering peak and volume fractions is also approximate. It requires the assumption of some type of lattice order or unit cell as a basis for the calculation.

For these reasons, it was found that more accurate domain dimensions were obtained for the microphase separated but randomly ordered structures in the present study by taking measurements directly from TEM images. Form factors were calculated and compared to the experimental SAXS data for both spheres and cylinders with radii determined from the domain size measured in the micrographs. The spherical form factor gave a better fit to the second broad maximum than the cylindrical form factor calculated for the same (measured) radius. The first minimum of the spherical form factor more accurately coincided with the depression in the scattering curve which precedes (occurs at slightly lower q than) the second maximum. Thus a disordered packing of spherical domains is the structure assigned to RMG-3-5-18. For all samples in this study, the domain radii (spheres or cylinders) upon which the best fit form factor calculations are based are also listed in Table 5.3.

TEM images of the morphologies for RMG-3-5-34 and RMG-3-5-41 appear nearly identical; only the image for RMG-3-5-41 is shown in Figure 5.5. Stereo pair

TEM images from both these samples suggest a tangle of disordered cylindrical domains of the white PS graft material in a dark PB matrix. The SAXS data for these samples are shown in Figures 5.6 and 5.7. Both show a strong initial peak and a broad second maximum at scattering vector ratios of 2.3 (RMG-3-5-34) and 2.8 (RMG-3-5-41), which are inconsistent with Bragg scattering. Form factors for cylindrical and spherical domains are also plotted in Figures 5.6 and 5.7; domain sizes were measured from TEM micrographs as discussed previously. The agreement of the second form factor peak for cylinders with the second broad experimental scattering maximum in both RMG-3-5-34 and RMG-3-5-41 confirms the assignment of a disordered cylindrical morphology to these two samples.

The lamellar morphologies formed by samples RMG-3-5-48 (Figure 5.8) and RMG-3-5-62 (Figure 5.10) are among the most ordered morphologies displayed by any of the randomly grafted materials in this study. These lamellar phases are, however, clearly much less well-ordered than typical lamellae in diblock copolymers or model graft materials of simpler and more regular molecular architecture.[3-5,88,89] The SAXS data for RMG-3-5-48 (Figure 5.9) clearly show four Bragg peaks with scattering vector ratios of 1, 2, 3, and 4, consistent with the lamellar morphology. The SAXS data from RMG-3-5-62, shown in Figure 5.11, have four distinct Bragg peaks which represent the first, second, third, and fifth orders of the lamellar long period.

The morphological results for the series of materials with an average of four tetrafunctional branch points per molecule are now presented, with quantitative dimensions listed in Table 5.3. Sample RMG-4-4-16 displays a microphase separated but disordered morphology similar to that observed in previously discussed materials with disordered spherical and cylindrical structures. A TEM image of this sample is shown in

Figure 5.12 and the SAXS data is shown in Figure 5.13. The SAXS data for RMG-4-4-16 show a single maximum falling off slowly at higher scattering angle. This scattering, coupled with the placement of this sample at the ODT (described in the discussion section) suggests that the morphology consists of immobilized and stained composition fluctuations. It is interesting to note that the TEM image of these composition fluctuations is not much different from the images produced by more strongly segregated spherical and cylindrical samples which lack lattice symmetry. Only from the scattering data can one tell the difference.

The TEM image of RMG-4-4-28 (Figure 5.14) shows a similar microphase separated structure with a lack of lattice ordering. The SAXS data for this sample (Figure 5.15) show the primary peak, a broad shoulder around q of 0.04, and another broad maximum at q of about 0.07. These features can be attributed to the form factor for a cylindrical domain shape. Sample RMG-4-4-43 displays a lamellar morphology with considerably greater long-range order than the other samples in this series. This can be seen in the TEM image in Figure 5.16. The SAXS data for this sample (Figure 5.17) show four peaks consistent with the first, second, fourth, and fifth orders of the lamellar long period. In TEM (Figure 5.18), sample RMG-4-4-61 shows a microphase separated but poorly ordered morphology which displays some small regions of limited lattice-like order. The SAXS data for this sample (Figure 5.19) show a primary peak and a second broad maximum which correlates well with the second maximum of the cylinder form factor.

5.5 Discussion

That the random multigraft copolymer materials investigated in this study exist in the intermediate and weak segregation regimes at the conditions under which they were annealed and then observed complicates the interpretation of the results as compared with Gido and coworkers' previous studies of more strongly segregated model graft copolymers.[1,3-5,51,52] The Milner morphology diagram onto which we have mapped the constituting single-graft copolymers in these previous studies is only strictly applicable to strongly segregated materials. Calculations of intermediate segregation morphological behavior of diblock copolymers have been carried out by Vavasour and Whitmore,[90] Matsen and Schick,[91] Lescanec and Muthukumar,[92] and Matsen and Bates.[29] These theories have not been extended to graft molecular architectures. One can, however, still use what theoretical work does exist as an approximate guide for interpreting the current experimental results.

The current results point to the importance of the constituting graft copolymer concept in determining the effect of graft molecular architecture on both the morphology and the degree of segregation. The RMG-3-5 series is the more strongly segregated set of samples in this study, based on χN values calculated for the average constituting block copolymers. The theoretical work of Balazs and coworkers[12] indicates that it is the χN of the average constituting single-graft copolymer which determines the proximity to the ODT. These χN values are listed in Table 5.3 for three different temperatures: 120°C (annealing temperature), 100°C (T_g of bulk PS), and 25°C (room temperature). The value of χ as a function of temperature for PS and PB was obtained from the work of Wolff *et al.*[93] Since after annealing the samples were slowly cooled to room temperature over the course of about a day, it is suspected that the degree of segregation at the

temperature where the PS domains approach T_g is the most relevant to the morphology which we observe. The T_g of bulk PS at high molecular weight is about 100°C and thus values for this temperature are included in the table. Additionally, T_g of PS in small microphase separated domains may be different from that of bulk PS. That some of the PS graft block molecular weights are quite low (around 5,000 to 10,000 g/mol) will lead to a suppression of T_g as given by the Fox-Flory equation.[94] The PS T_g values calculated with this equation as well as the corresponding χN values are also listed in Table 5.3. It is apparent that T_g suppression due to low molecular weight does not significantly increase χN over the value at 100°C. Low molecular weight may not, however, be the only factor influencing T_g of the PS domains. Confinement effects, interfacial energy and perturbed chain conformation may all effect the T_g of PS in these microphase separated systems. These effects are not currently well understood, and thus χN values calculated for 100°C will be used in this work.

At 100°C, χN ranges from 39 for RMG-3-5-18 to 68 for RMG-3-5-62.

Unfortunately the only theories available for comparison are the strong segregation calculations of Milner[8] for miktoarm stars and the weak segregation calculations of the order-disorder transition for A_2B single-grafts (Olvera de la Cruz and Sanchez;[50] Floudas *et al.*[95]) and comb-shaped multiple-graft copolymers (Balazs and coworkers[12]). Calculations of the ODT and order-order transitions for model star and multiple-graft copolymers by Dobrynin and Erukhimovich[96] are unfortunately confined to the weak segregation region. Of these theories, only the Milner calculation provides for any comparison to the morphologies actually formed. The other theories are, however, useful in that they allow us to estimate the strength of microphase separation in grafted morphologies by how far they are above the ODT. The calculations of Olvera de la Cruz

and Sanchez, and Floudas *et al.* indicate that in the A_2B architecture with a graft (B block) volume fraction of 0.2 that the ODT is shifted upward to a χN value of about 32.5, placing sample RMG-3-5-18 in a weakly segregated state. All the other RMG-3-5 samples have degrees of segregation in the intermediate regime.

Figure 5.20 shows the Milner morphology diagram with symbols plotted at the volume fractions of the PS grafts corresponding to the samples in the RMG-3-5 series. We are unsure of the value of the molecular asymmetry parameter, ε, which is appropriate for our materials. The conformational asymmetry between the PS and PB block materials may be relatively strong, about 0.6.[90] We assume an average constituting block obtained by assigning a single PS graft to the average length of backbone obtained by dividing the total backbone length by the average number of grafts per molecule. It is unclear whether this average constituting graft copolymer should be considered symmetric ($\tau = 0.5$) or asymmetric. If it is symmetric, then $\varepsilon = 2 \cdot 0.6 = 1.2$. Otherwise, $\varepsilon = f(\tau) \cdot 0.6$, where τ represents the appropriate average asymmetry in the constituting graft copolymer, and $f(\tau) \leq 2$.[3,4,51] The data for all the samples agree with the diagram in a band ranging between ε values of about 1.5 and 1.7, which is shaded on the diagram. Any quantitative comparison is at best uncertain from the error inherent in the composition information about the graft copolymers, the estimation of χN, the estimation of conformational asymmetry, and from the application of a strong segregation model to intermediately segregated polymers. However, it is clear that there is a morphological shift brought about by the random graft architecture. Samples RMG-3-5-18, RMG-3-5-34, and RMG-3-5-44 display morphologies which are shifted from those of diblock copolymers or other symmetric molecular architectures at the same composition. One should, however, keep in mind that intermediate segregation is likely to shift all the

order-order transition lines in the Milner diagram closer to the center of the diagram as is the case in morphology diagrams calculated for simpler molecular architectures in intermediate segregation.[29,90,91] Thus, the order-order transitions on the left side of the Milner diagram, which impact on the morphologies of the RMG-3-5 series, will be shifted slightly to the right. This would shift the range of agreement with experiment to slightly lower ε values.

The RMG-4-4 series is less strongly segregated, as can be appreciated by both the calculated χN values and by the morphological results. The average constituting graft copolymers for this series are A_2B_2 stars and the spinodal curves for materials of general A_nB_n architecture have been calculated by Olvera de la Cruz and Sanchez.[50] In this calculation they use the degrees of polymerization of only a single A and a single B block to calculate χN. Application of this χN calculation to the RMG-4-4 series results in values at 100°C ranging from 24 to 42. Comparison of Figures 3 and 5 from Olvera de la Cruz and Sanchez[50] suggests that the morphological behavior of the A_2B_2 molecules is quite similar to that of simple AB diblocks. This conclusion agrees with the observation that both types of molecules are architecturally symmetric as opposed to asymmetric architectures with trifunctional branch points.

Because of this similarity and because weak and intermediate segregation calculations of order-order transitions are not available for the A_2B_2 architecture of the constituting graft copolymer, in this work an approximate comparison of experimentally observed morphologies with the weak and intermediate segregation results calculated by Vavasour and Whitmore for conformationally asymmetric AB diblock copolymers.[90] Similar morphology diagrams including the gyroid morphology have been calculated by Matsen and Schick,[91] and Matsen and Bates.[29] However, since no bicontinuous

morphologies are definitively identified, the diagram of Vavasour and Whitmore which includes only spheres, cylinders, and lamellae will be used. Figure 5.21 shows the experimental points of the RMG-4-4 series plotted on the morphology diagram calculated by Vavasour and Whitmore for a conformational asymmetry of 0.6. Here f_A must refer to the PB volume fraction. This conformational asymmetry approximately matches that which as been reported for the PS-PB block materials.[90] The architectural asymmetry (n_A/n_B) for the PS_2PB_2 constituting architecture is unity. The experimental observation that sample RMG-4-4-18 produces a chaotic morphology with no long-range order and no characteristic domain shape is consistent with the placement of the average constituting graft copolymer for this material close to, but below the ODT. Samples RMG-4-4-28 and RMG-4-4-43 were observed to form disordered cylinders and lamellae respectively, in agreement with their placement on the morphology diagram. Finally, sample RMG-4-4-61, at 61 vol. % PS, maps onto the cylinder region of the morphology diagram, again in agreement with our experimental findings. A conformationally symmetric diblock or A_2B_2 architecture at this composition would be lamellar. That cylinders are observed is a manifestation of the effect of the PS-PB conformational asymmetry.

It is interesting to compare the effect of graft molecular architecture on the degree of segregation for the trifunctional branch points of the RMG-3-5 series and the tetrafunctional branch points of the RMG-4-4 series. The work of Olvera de la Cruz and Sanchez[50] indicates that the appropriate way to calculate χN for A_2B architectures is based on the total degree of polymerization of both A arms and the B arm. For the tetrafunctional random multigraft architectures, χN is calculated based an A_1B_1 diblock. While calculation of χN for the tetrafunctional multigraft should be that of the

constituting A_2B_2 star, in this case it is found that the A_2B_2 star χN is below the strong segregation regime limit. In this situation, unable to apply the Milner model for miktoarm star behavior and resorting to the weak and intermediate segregation model of Vavasour and Whitmore, the appropriate measure of χN is that of the A_1B_1 linear diblock. This leads to significantly lower values of χN for graft copolymers with tetrafunctional branch points, as compared to materials of the same composition and total molecular weights of both A and B components but with trifunctional branch points. An experimental verification of this effect can be appreciated by comparing the χN values for pairs of samples, one from the RMG-3-5 series and one from the RMG-4-4 series, which have the same overall volume fractions and approximately the same total amount of PS grafted at each junction point. The following pairs of samples permit such a comparison: (RMG-3-5-18 and RMG-4-4-16), (RMG-3-5-34 and RMG-4-4-28), and (RMG-3-5-41 and RMG-4-4-43). The χN values for the samples with tetrafunctional branch points are about 40% lower than those of the corresponding materials with trifunctional branch points. Olvera de la Cruz and Sanchez show that the ODT occurs at slightly higher values of χN for materials with trifunctional branch points, an increase from 10.5 to 13.5 at 0.5 volume fraction. However, this does not compensate for the difference in χN between trifunctional and tetrafunctional branch points. The good agreement of the data from this series of samples with tetrafunctional branch points with the weak and intermediate segregation predictions of Vavasour and Whitmore supports the application of the constituting graft copolymer approach to these materials as well as the calculation of χN for these constituting block copolymers using the procedures of Olvera de la Cruz and Sanchez.

5.6 Conclusions

In general the morphological characterization results for all the series of samples indicate little or no long-range order for materials displaying spherical and cylindrical morphologies. The order is slightly better for materials giving lamellar morphologies. This lack of long-range order is undoubtedly the result of two factors. First, the relatively high molecular weight and multiple junction points of these materials must severely limit the molecular mobility necessary to increase long-range order during solvent casting and thermal annealing. Second, the architectural dispersity of the molecule resulting from random graft point locations along the backbone causes different parts of the molecule to locally prefer a different morphology than other parts of the same molecule which by chance have a different local graft density. Our results indicate that the molecules form the morphologies which are dictated by their average constituting single-graft copolymer structures. However, the multiple behaviors inherent in the different local parts of the molecular architecture lead to significant suppression of long-range order.

Even with the loss of long-range order, the samples, as a function of average molecular architecture (i.e. junction point density) and composition, do show a clear preference for a specific domain shape (spherical, cylindrical, or lamellar). In disordered cylindrical morphologies, it sometimes appears that the cylinders have a tendency to form three way branch points, and thus some of these structures may be more properly categorized as disordered bicontinuous structures. However, the differentiation of disordered cylinders and disordered bicontinuous structures is nearly impossible based on the projected images in TEM micrographs and on the scattering data. Essentially all that remains when long-range order is reduced or lost entirely is the general domain shape.

This is expressed as the preference for domain dimensionality: spheres 0, disordered cylinders 1, and lamellae 2.

The lamellar domain shape, when formed, appears to require the establishment of at least a modest degree of long-range order. A similar degree of lattice order does not appear to be required for the formation of spherical and cylindrical domains. This result can be simply understood in terms of the excluded volume characteristics of the spherical, cylindrical and lamellar domain shapes. Because lamellae extend over two spatial dimensions, they must pack parallel to one another or they cannot fill space to the density required of these materials. Essentially the lamellar domain shape templates its own long-range order. Spherical and cylindrical domains have more freedom to form disordered packings while still filling space to uniform density.

Sample	M_w PB[a]	PB PDI[b]	M_w PS[a]	PS PDI[b]	M_w RMG[a]	RMG PDI[b]	Vol. % PS	# branch points[c]
RMG-3-5-18	198000	1.04	10200	1.04	247000	1.06	18.1	4.9
RMG-3-5-34	198000	1.04	23200	1.03	314000	1.06	33.7	5.0
RMG-3-5-41	198000	1.04	31400	1.03	353000	1.06	40.8	4.9
RMG-3-5-48	198000	1.04	41600	1.04	420000	1.06	47.5	5.3
RMG-3-5-62	198000	1.04	73800	1.05	577000	1.07	61.6	5.1
RMG-4-4-16	198000	1.04	5500	1.04	245000	1.06	16.1	4.3
RMG-4-4-28	198000	1.04	11300	1.03	283000	1.05	28.4	3.8
RMG-4-4-43	198000	1.04	21600	1.03	383000	1.05	43.1	4.4
RMG-4-4-61	198000	1.04	44500	1.04	554000	1.06	60.7	4.0

[a] LALLS in THF at 25°C.
[b] SEC in THF at 30°C.
[c] Per backbone chain, calculated from M_w values of PB backbones, PS branches, and graft copolymers (from LALLS).

Table 5.1. Molecular characteristics of trifunctional and tetrafunctional random multigrafts.

Sample	Wt. % PS by ^{1}H-NMR[a]	Wt. % PS by UV-SEC[b]	Wt. % PS by dn/dc[c]	Calculated wt. % PS[d]
RMG-3-5-18	21	20	20	20
RMG-3-5-34	37	36	36	37
RMG-3-5-41	44	44	42	43
RMG-3-5-48	50	52	51	53
RMG-3-5-62	64	64	66	66
RMG-4-4-16	17	17	18	19
RMG-4-4-28	29	29	30	30
RMG-4-4-43	45	45	46	48
RMG-4-4-61	62	63	64	64

[a] NMR in $CDCl_3$ at 30°C.
[b] SEC in THF at 30°C.
[c] Calculated from $dn/dc = w\cdot(dn/dc)_{PS} + (1-w)\cdot(dn/dc)_{PB}$ using the values of the differential refractive index, dn/dc, of the PS and the PB graft copolymers determined in THF at 25°C.
[d] Calculated from the M_w values of PB backbones, PS branches, and the multigraft copolymers, as determined by LALLS.

Table 5.2. Weight % PS in trifunctional and tetrafunctional random multigrafts.

Sample RMG-	χN (120°C)	χN (100°C)	T_g PS arm (°C)[a]	$\chi N(T_g$ PS arm)	χN (25°C)[a]	d^* (Å)[b]	Domain Radius (Å)	Morph-ology
3-5-18	40	42	81	44	52	290	94	PS Sph.
3-5-34	45	47	92	48	59	307	84	PS Cyl.
3-5-41	49	52	94	53	65	369	110	PS Cyl.
3-5-48	51	54	95	55	68	439	-	Lam.
3-5-62	67	70	97	71	88	498	-	Lam.
4-4-16	22	24	65	26	30	302	-	Dis.
4-4-28	28	29	83	31	37	341	75	PS Cyl.
4-4-43	29	31	91	32	39	461	-	Lam.
4-4-61	41	44	96	44	55	595	130	PB Cyl.

[a] T_g of PS arm calculated using the Fox-Flory Equation, assuming $M_w = M_n$.
[b] Primary SAXS reflection, $d^* = 2\pi/q^*$.

Table 5.3. Morphological characteristics of trifunctional and tetrafunctional random multigrafts.

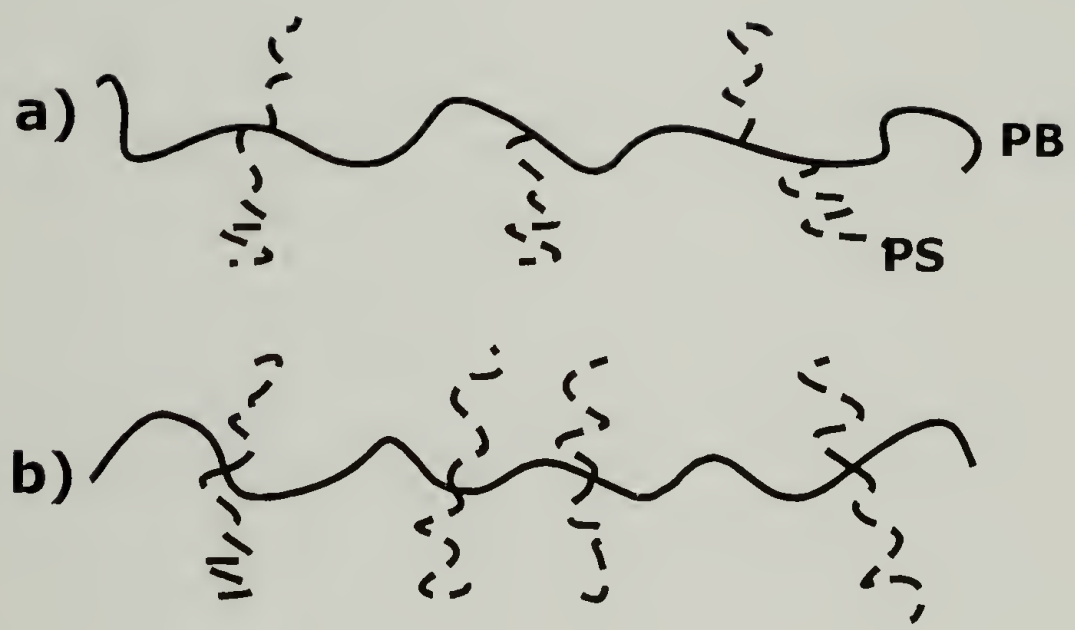

Figure 5.1. Random multigraft copolymer architectures with a) trifunctional branch points and b) tetrafunctional branch points.

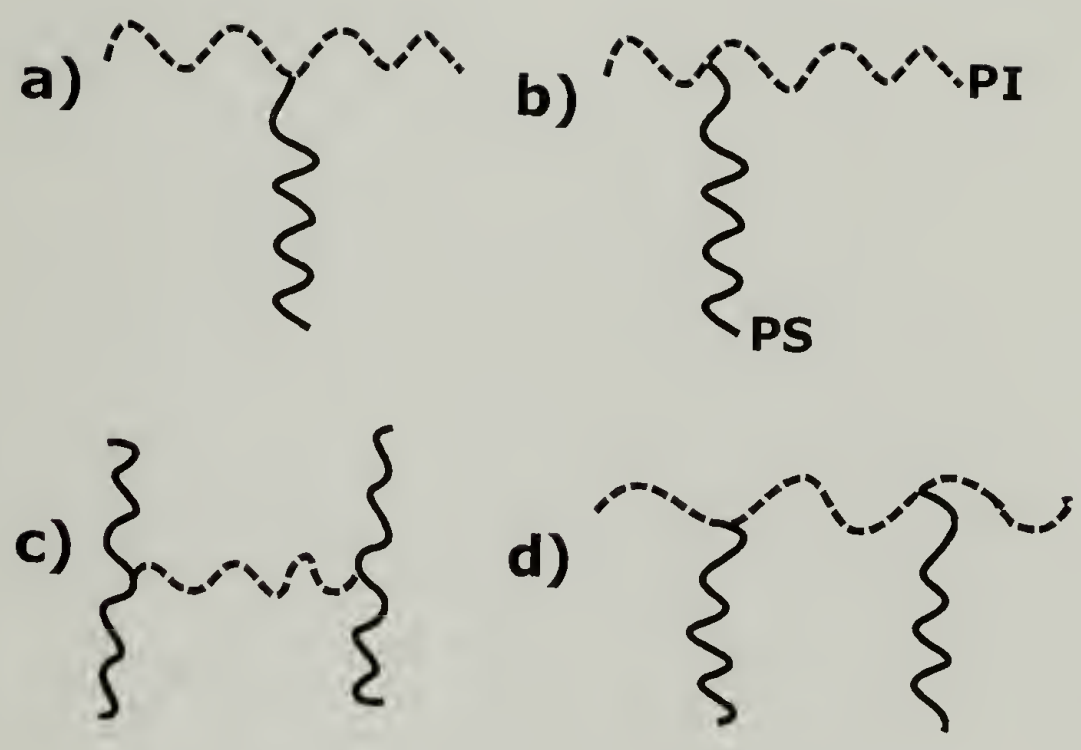

Figure 5.2. Single-graft copolymer architectures. a) single-graft, b) asymmetric single-graft, c) H double-graft, and d) π double-graft.

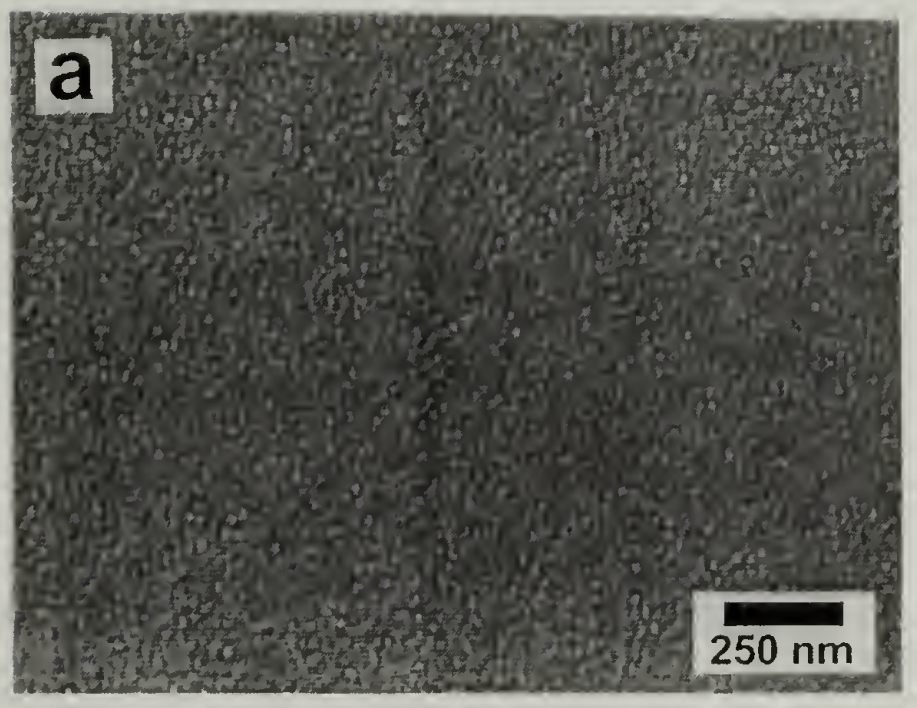

Figure 5.3. Representative TEM micrograph of sample RMG-3-5-18.

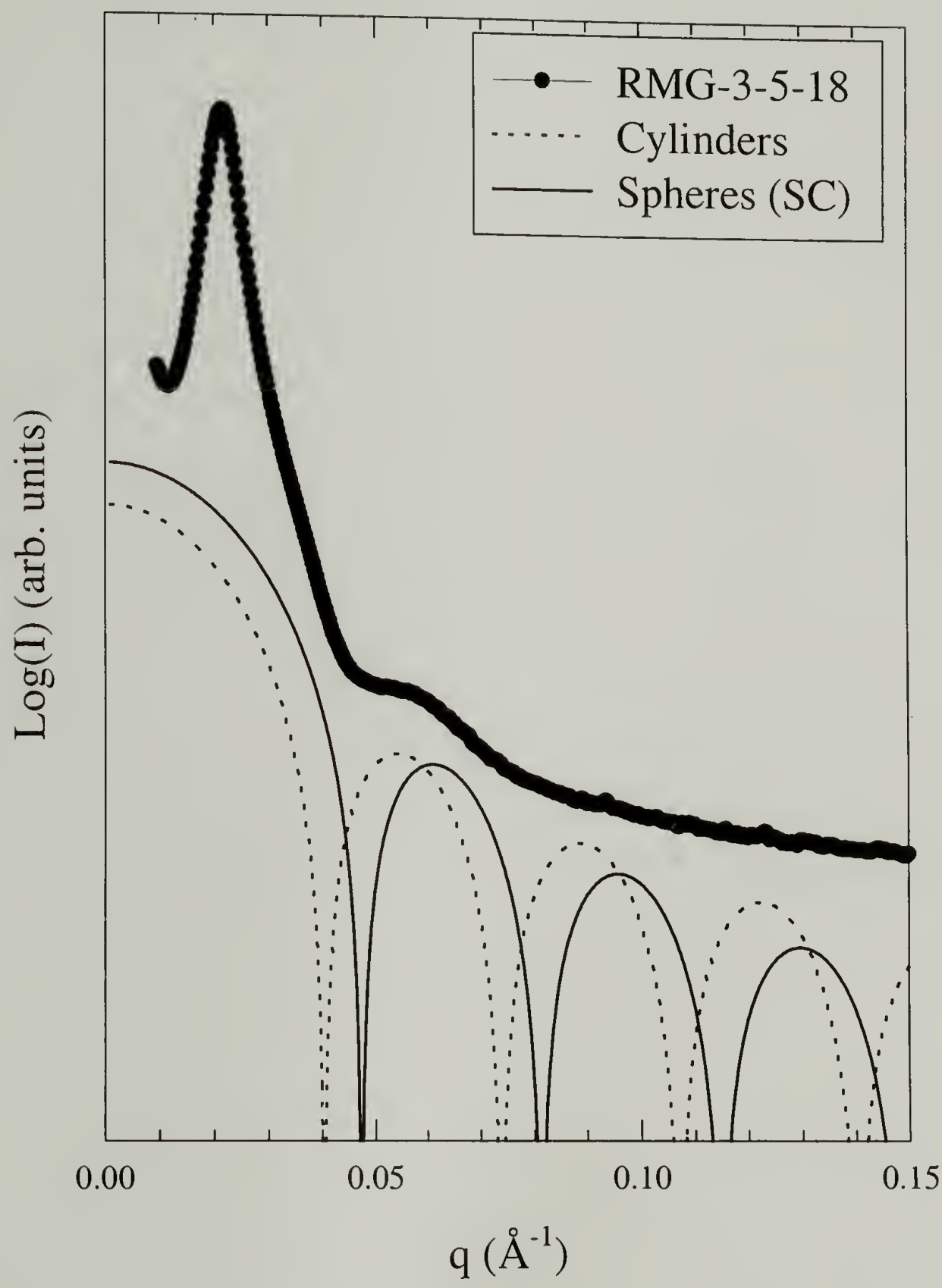

Figure 5.4. SAXS and form factors for sample RMG-3-5-18.

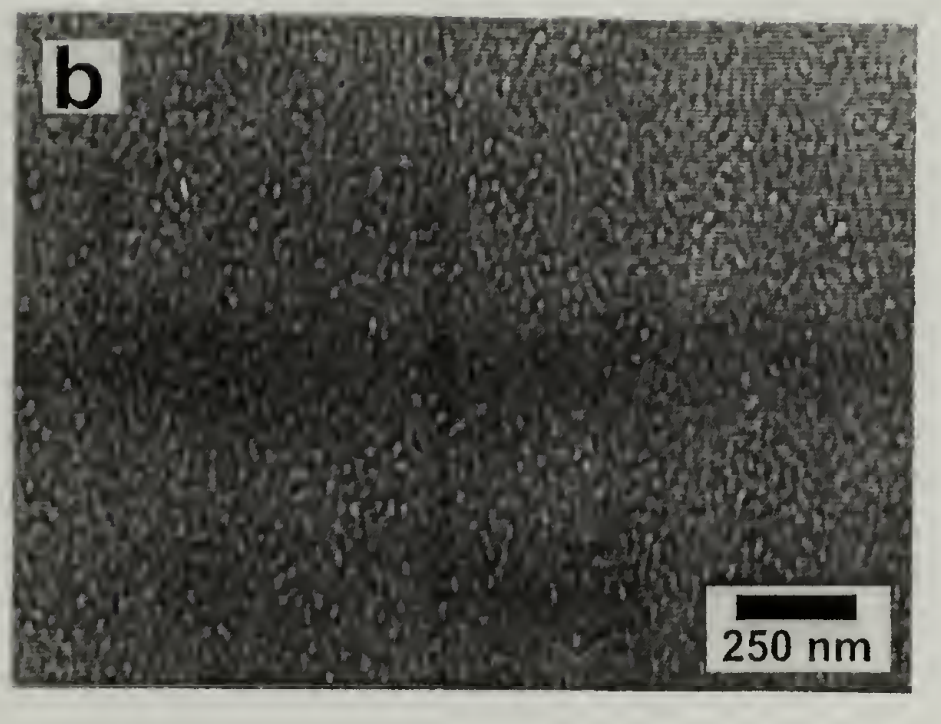

Figure 5.5. Representative TEM micrograph of sample RMG-3-5-41.

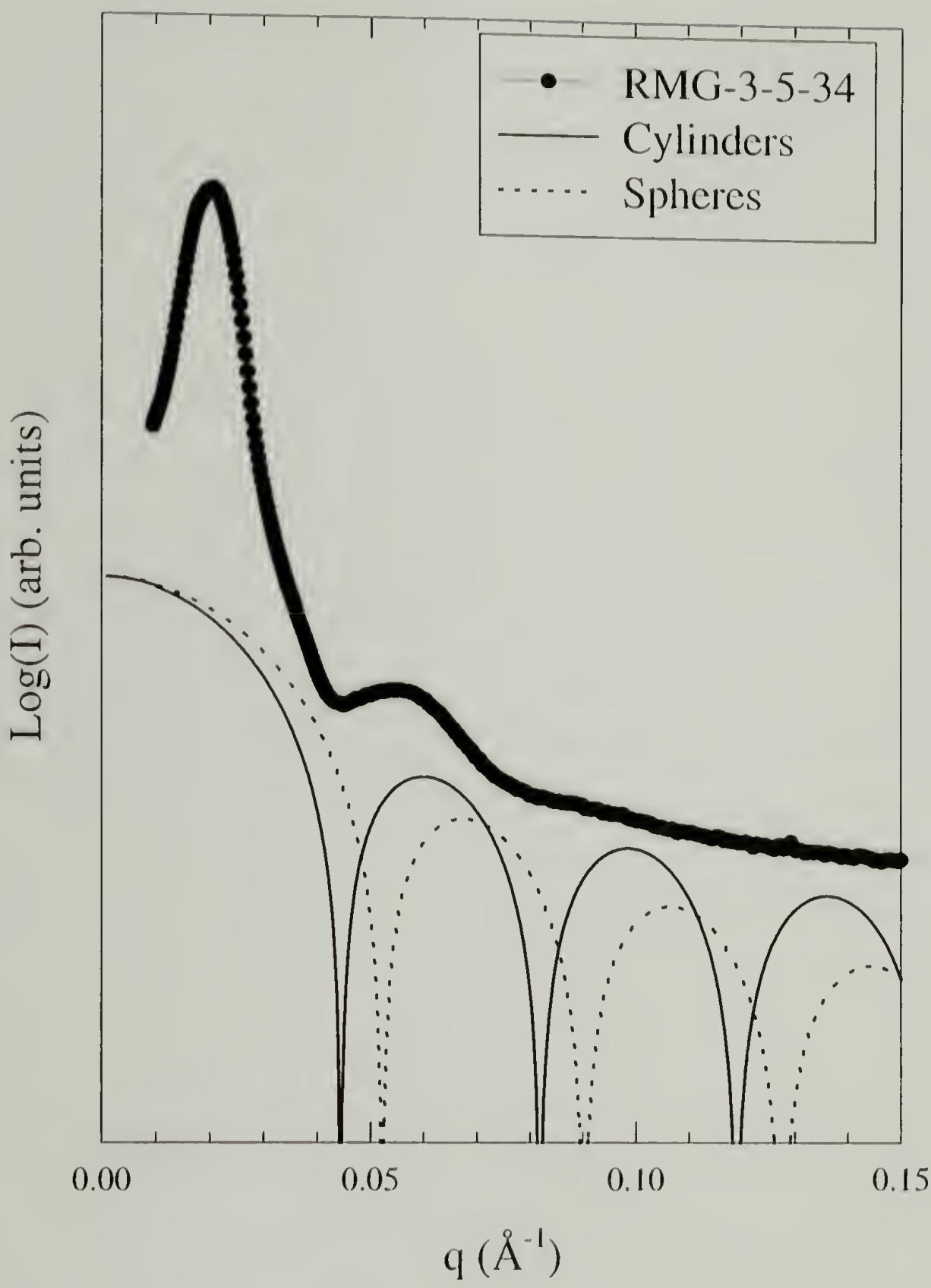

Figure 5.6. SAXS and form factors for sample RMG-3-5-34.

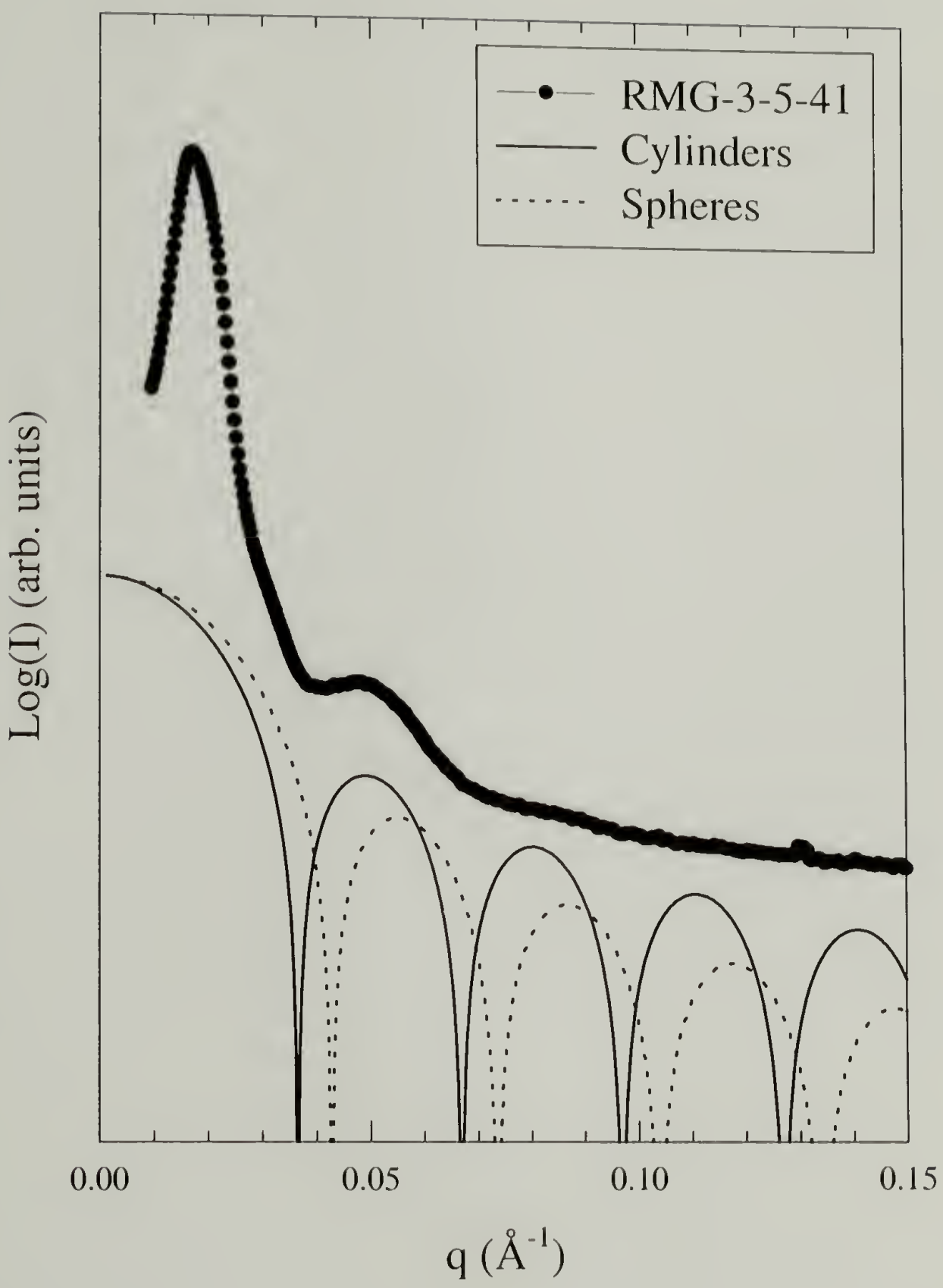

Figure 5.7. SAXS and form factors for sample RMG-3-5-41.

Figure 5.8. Representative TEM micrograph of sample RMG-3-5-48.

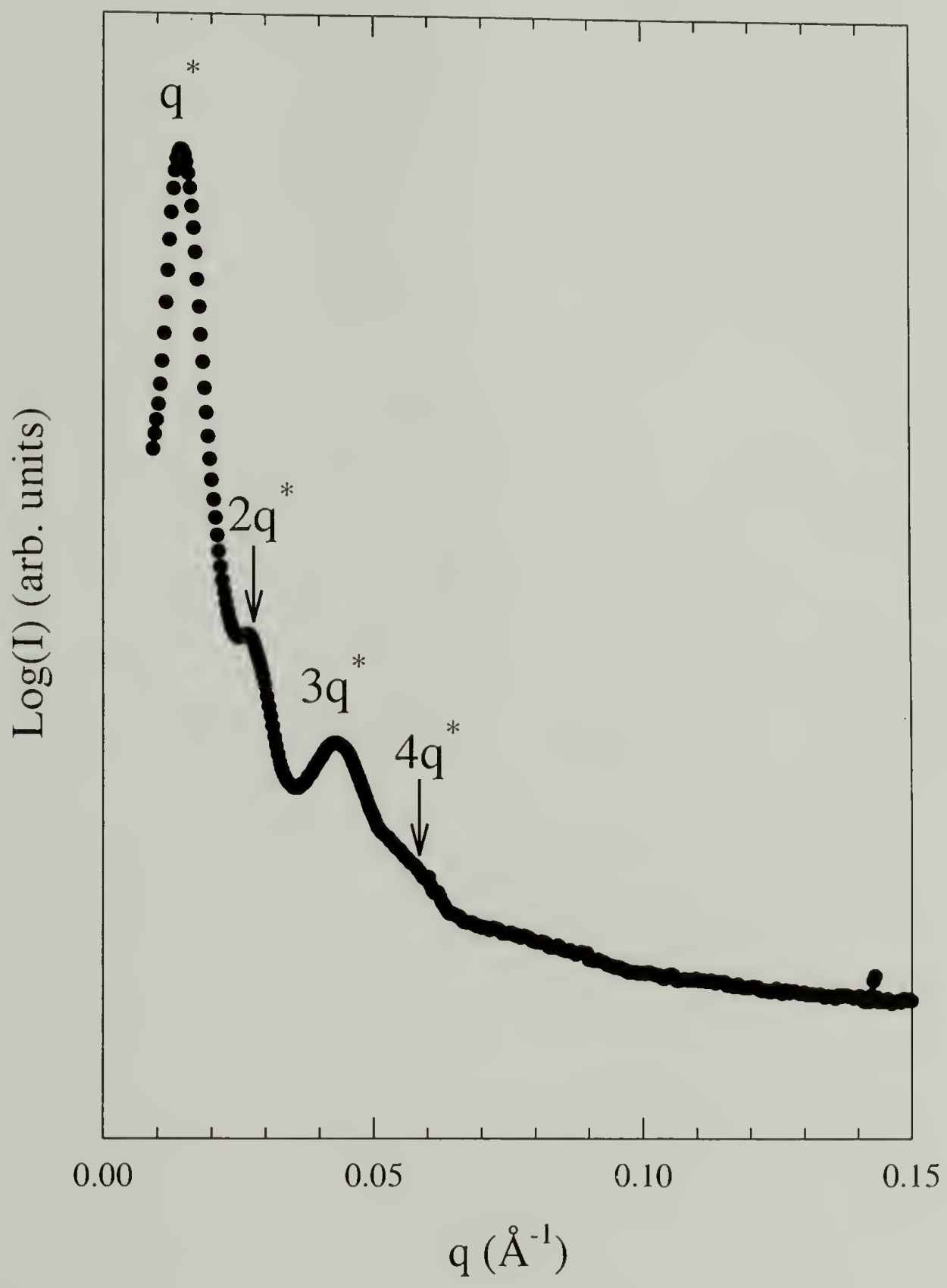

Figure 5.9. SAXS data for sample RMG-3-5-48.

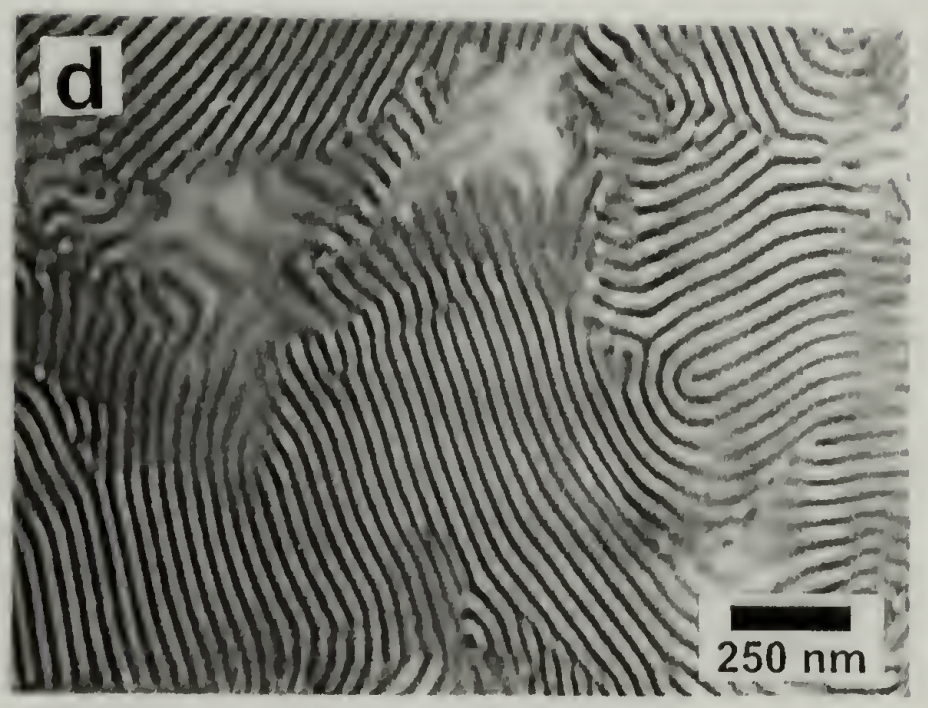

Figure 5.10. Representative TEM micrograph of sample RMG-3-5-62.

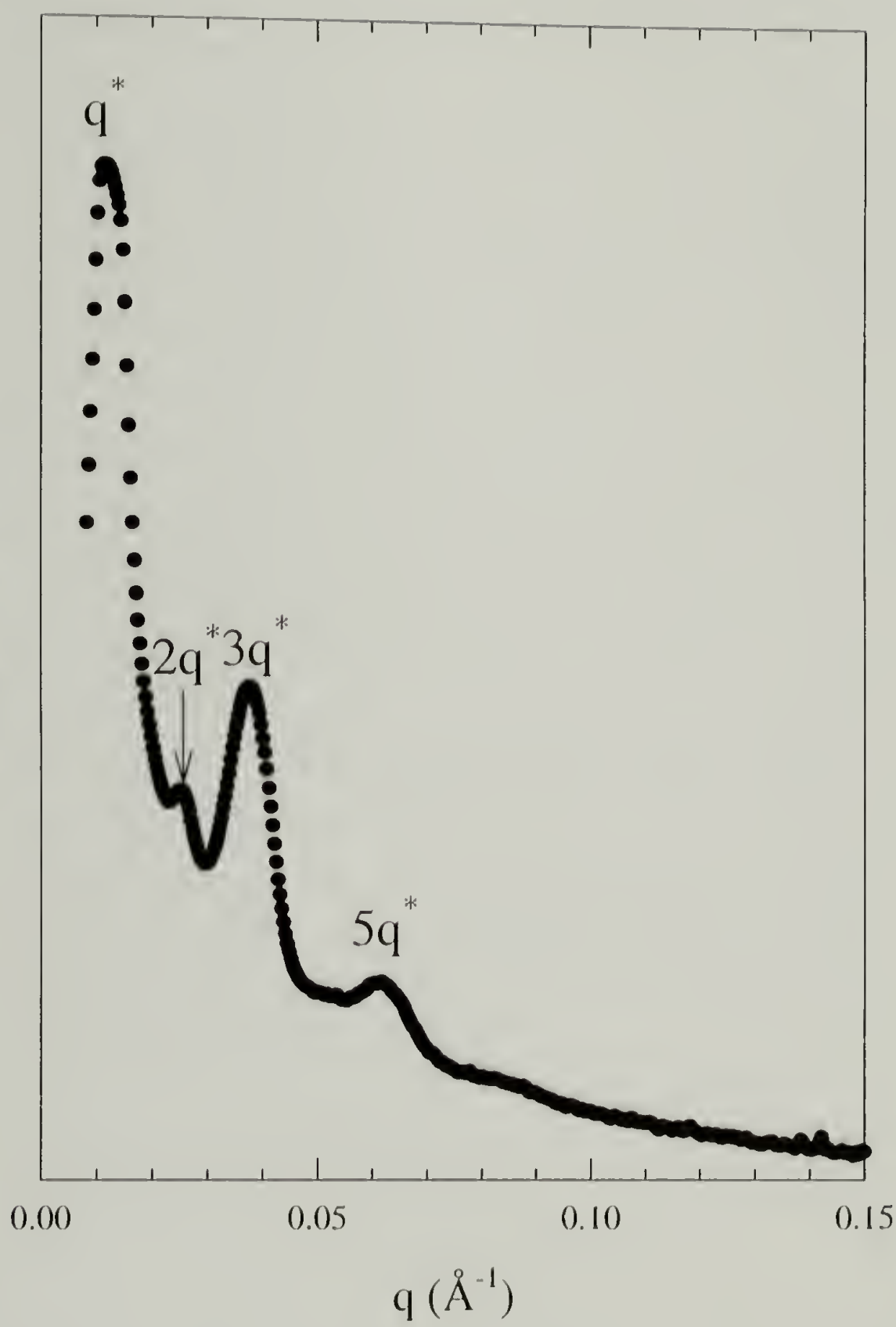

Figure 5.11. SAXS data for sample RMG-3-5-62.

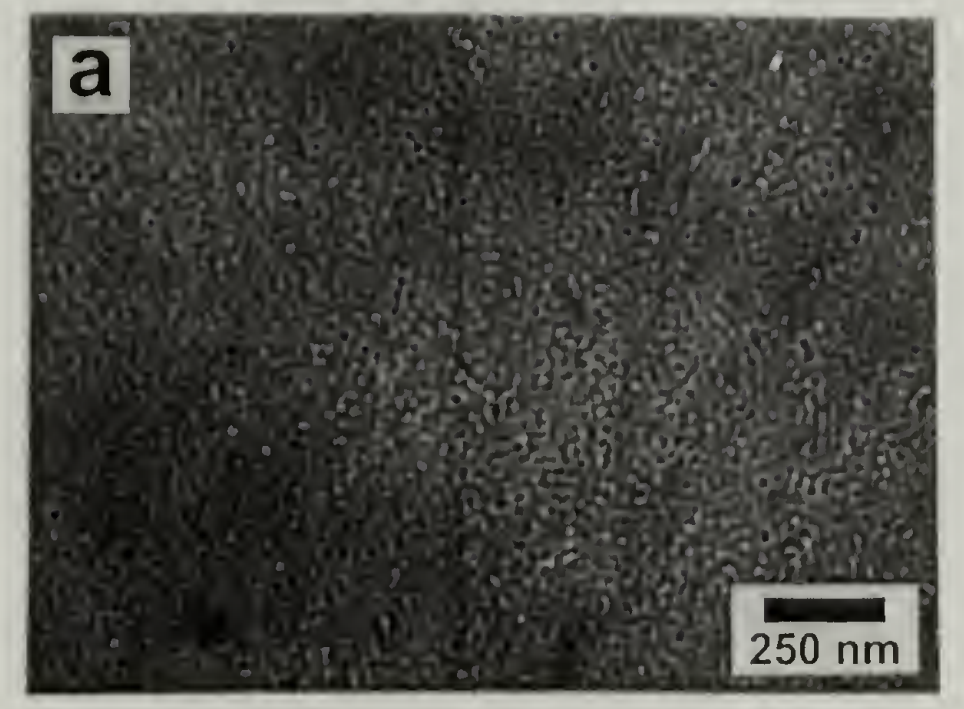

Figure 5.12. Representative TEM micrograph of sample RMG-4-4-16.

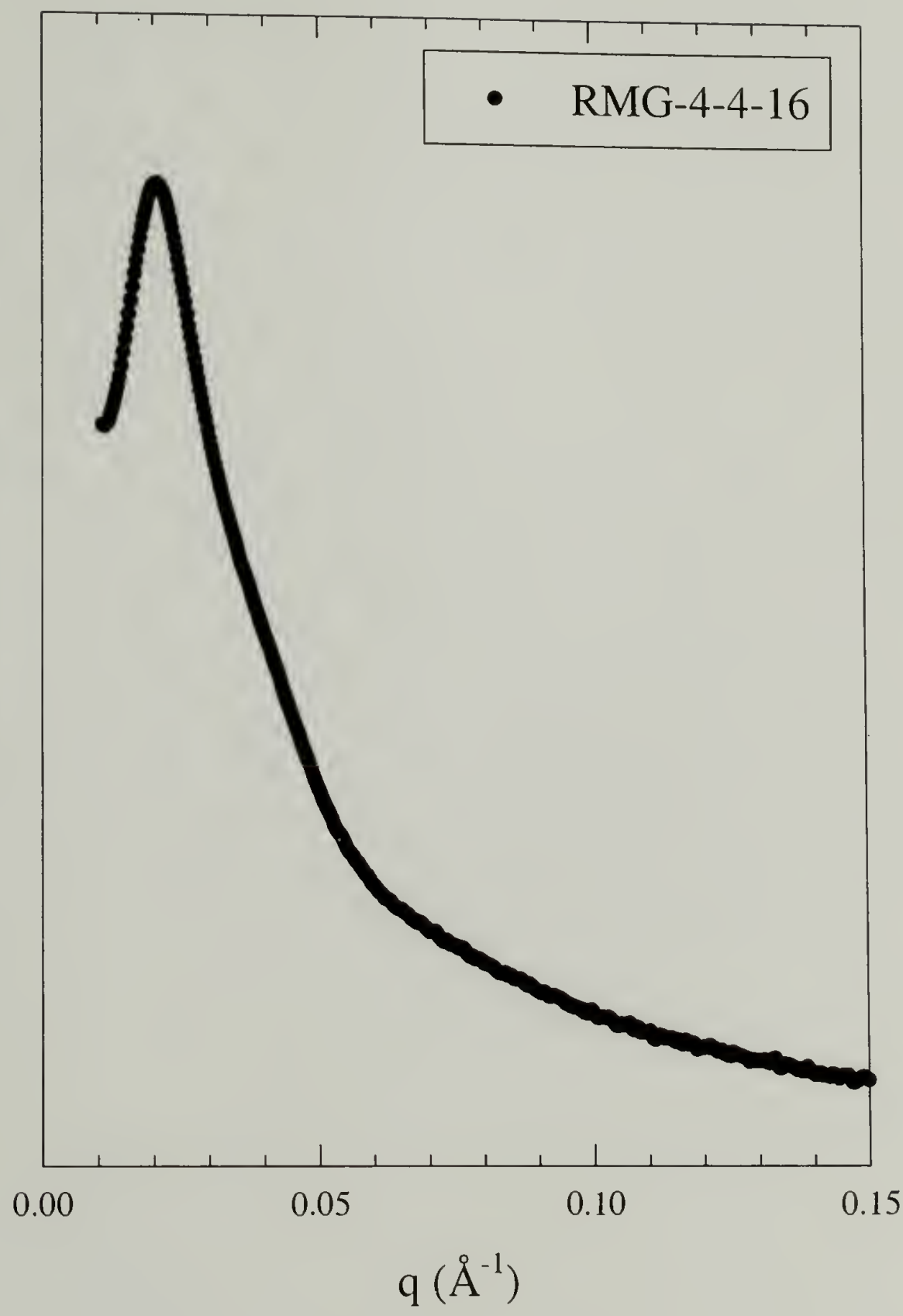

Figure 5.13. SAXS for sample RMG-4-4-16.

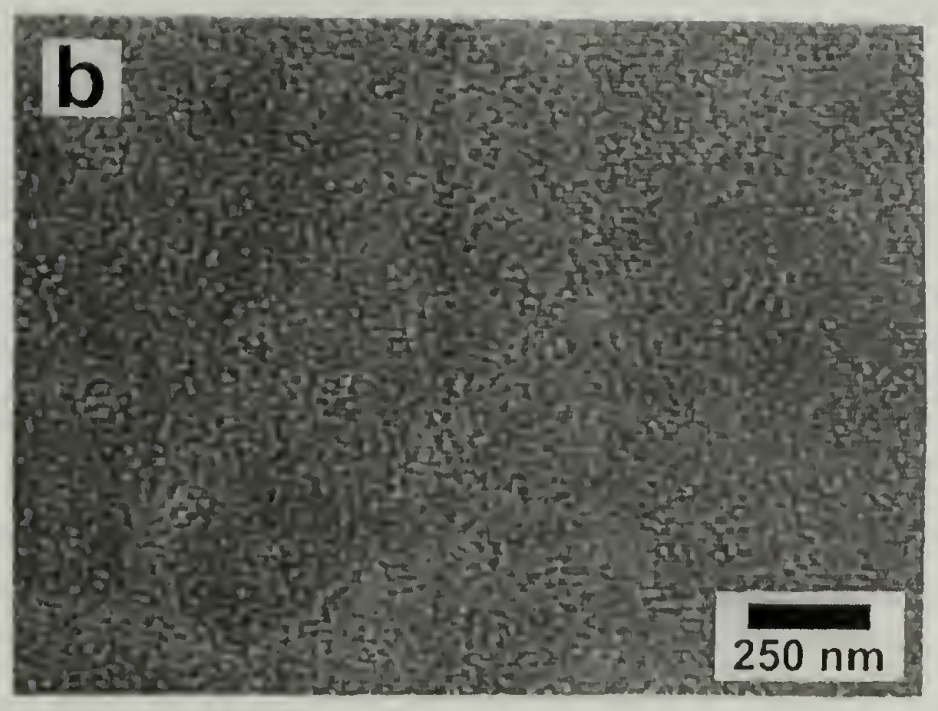

Figure 5.14. Representative TEM micrograph of sample RMG-4-4-28.

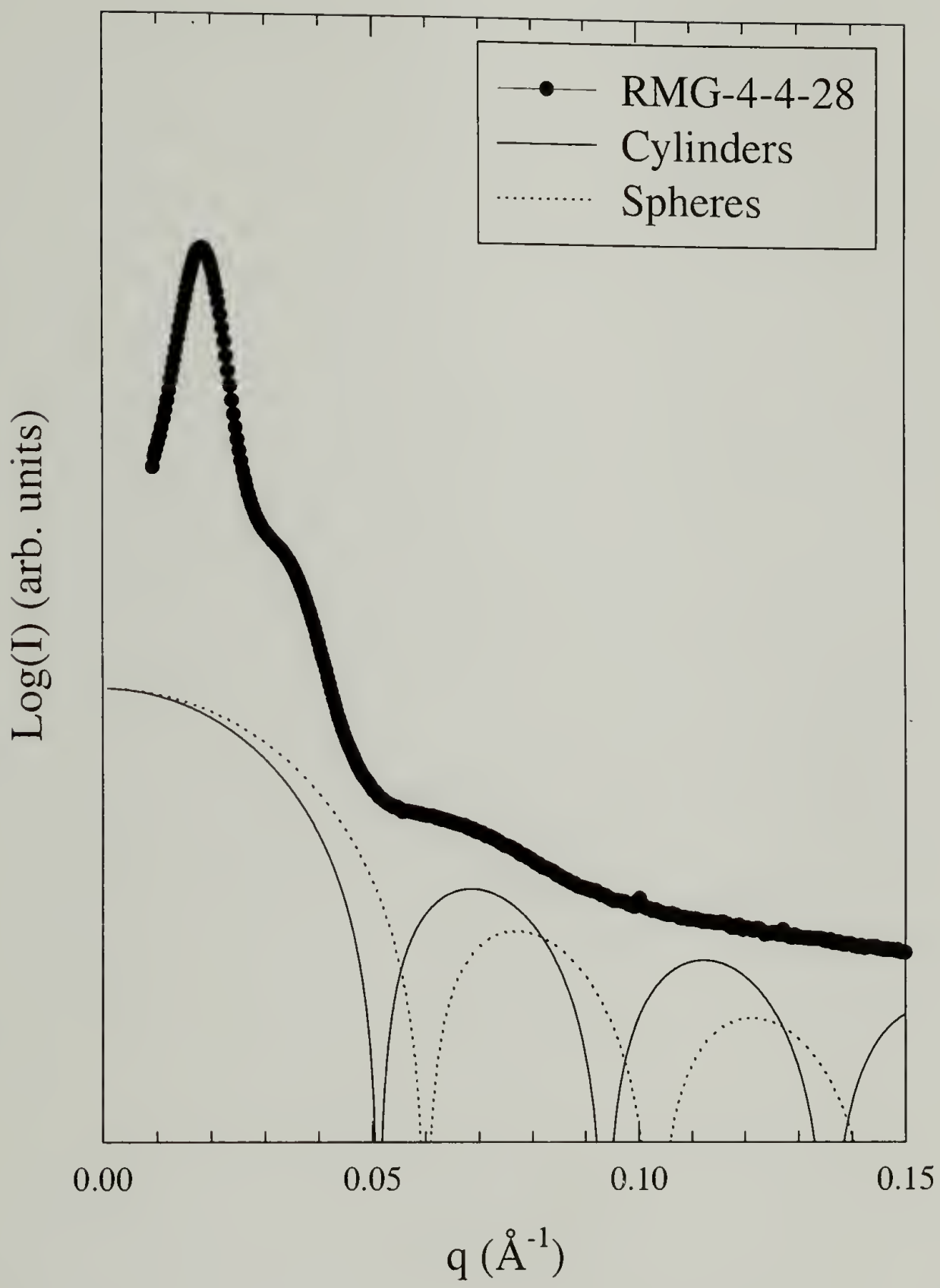

Figure 5.15. SAXS and form factors for sample RMG-4-4-28.

Figure 5.16. Representative TEM micrograph of sample RMG-4-4-43.

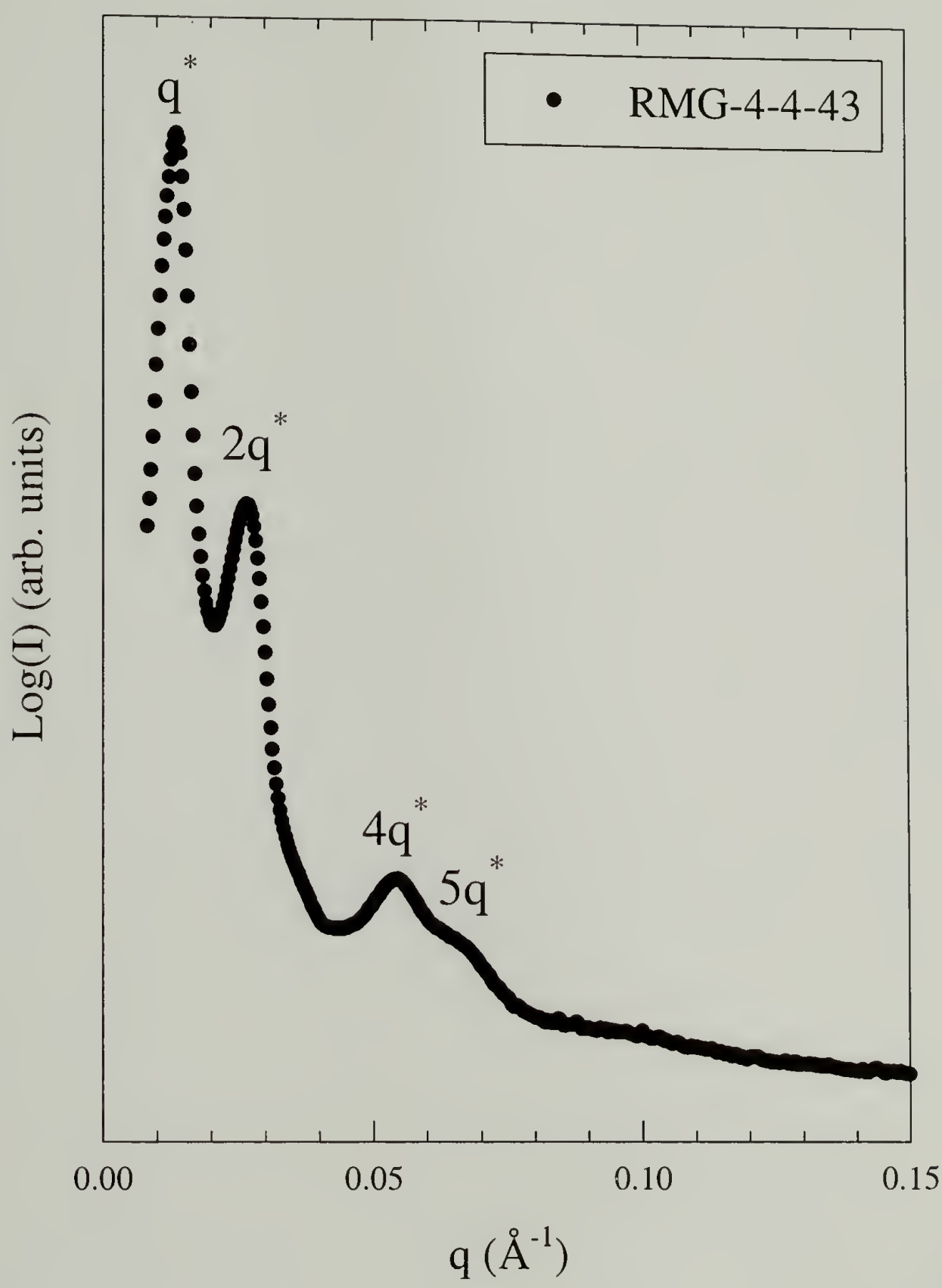

Figure 5.17. SAXS for sample RMG-4-4-43.

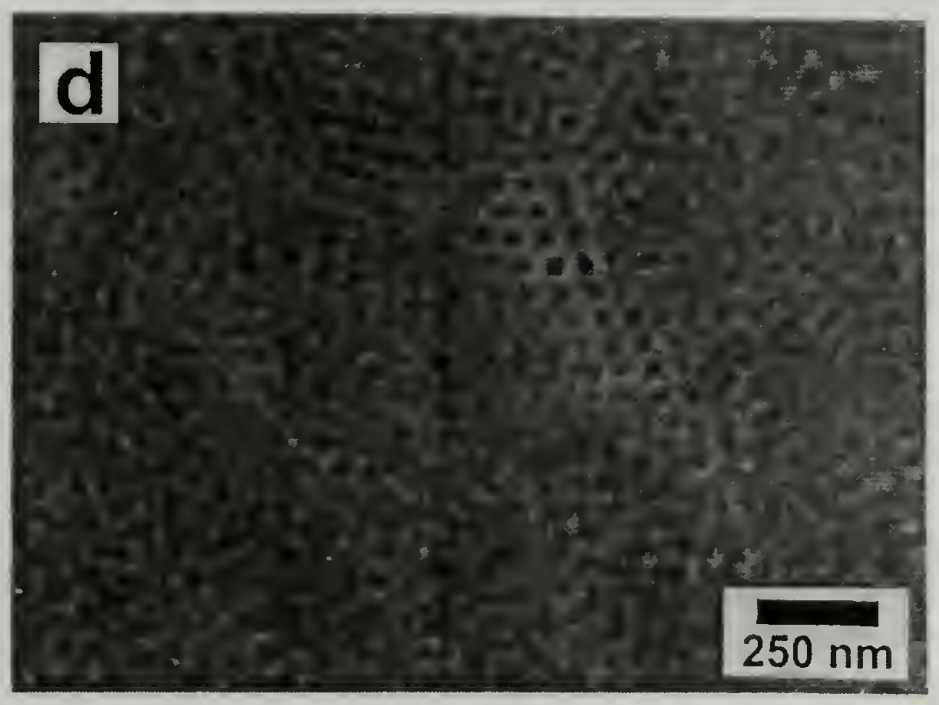

Figure 5.18. Representative TEM micrograph of sample RMG-4-4-61.

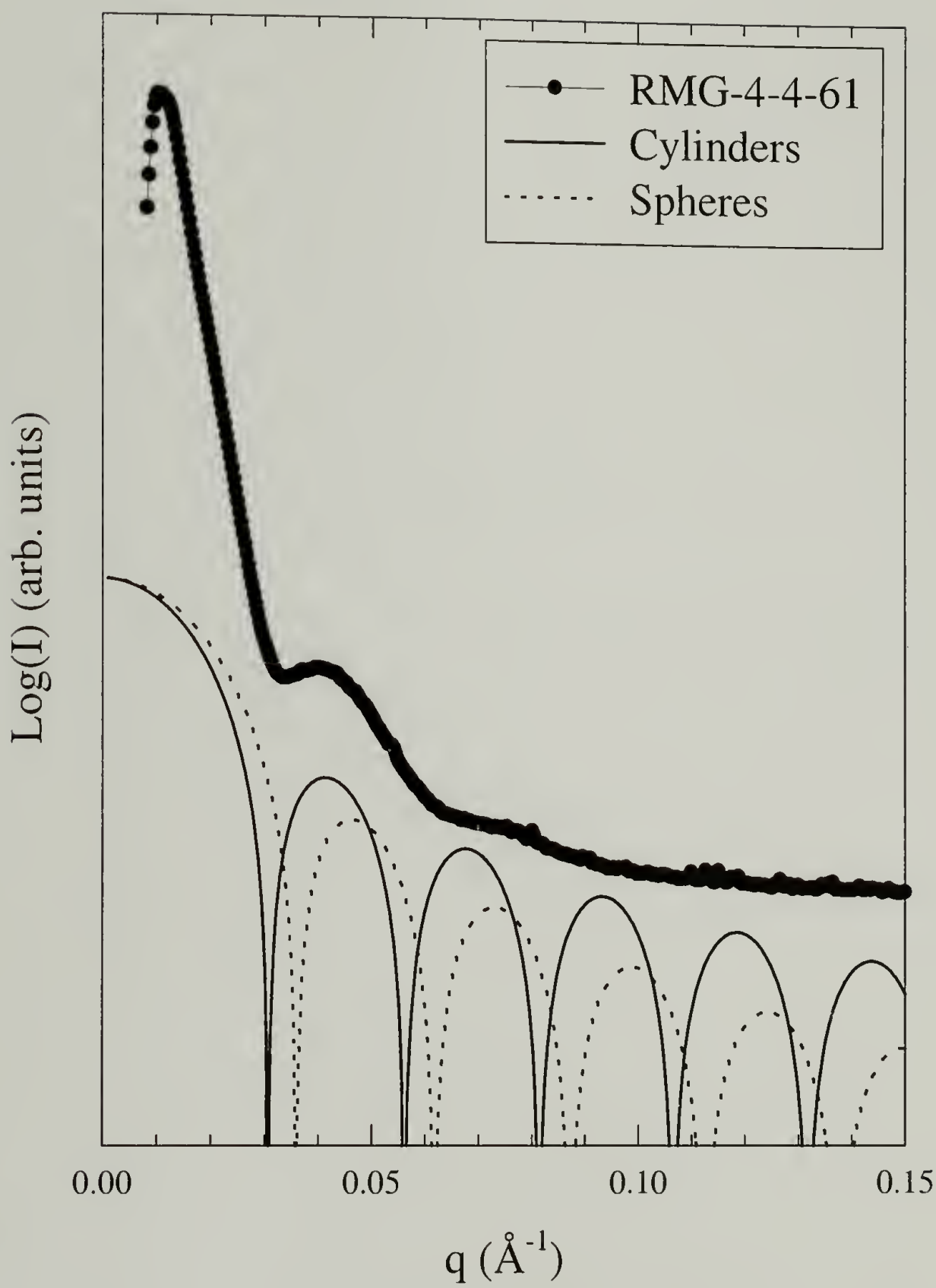

Figure 5.19. SAXS and form factors for sample RMG-4-4-61.

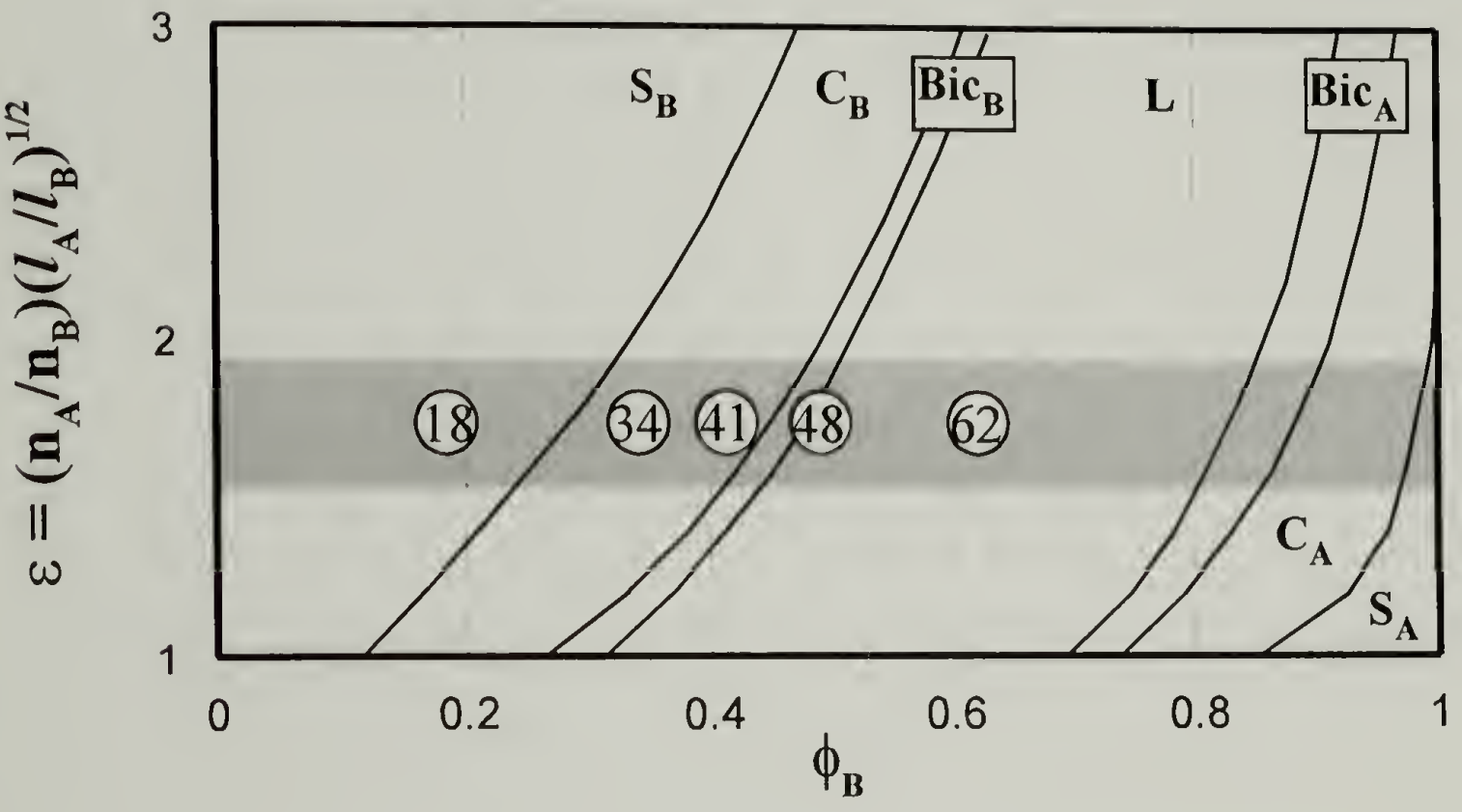

Figure 5.20. Milner morphology diagram with RMG-3-5 series samples plotted assuming an A_2B constituting block copolymer. The shaded band indicates the range of molecular asymmetries, ε, in agreement with morphological characterization. The box symbols map the RMG-3-5 samples onto the diagram; the numbers in the boxes are the volume percent PS in these samples.

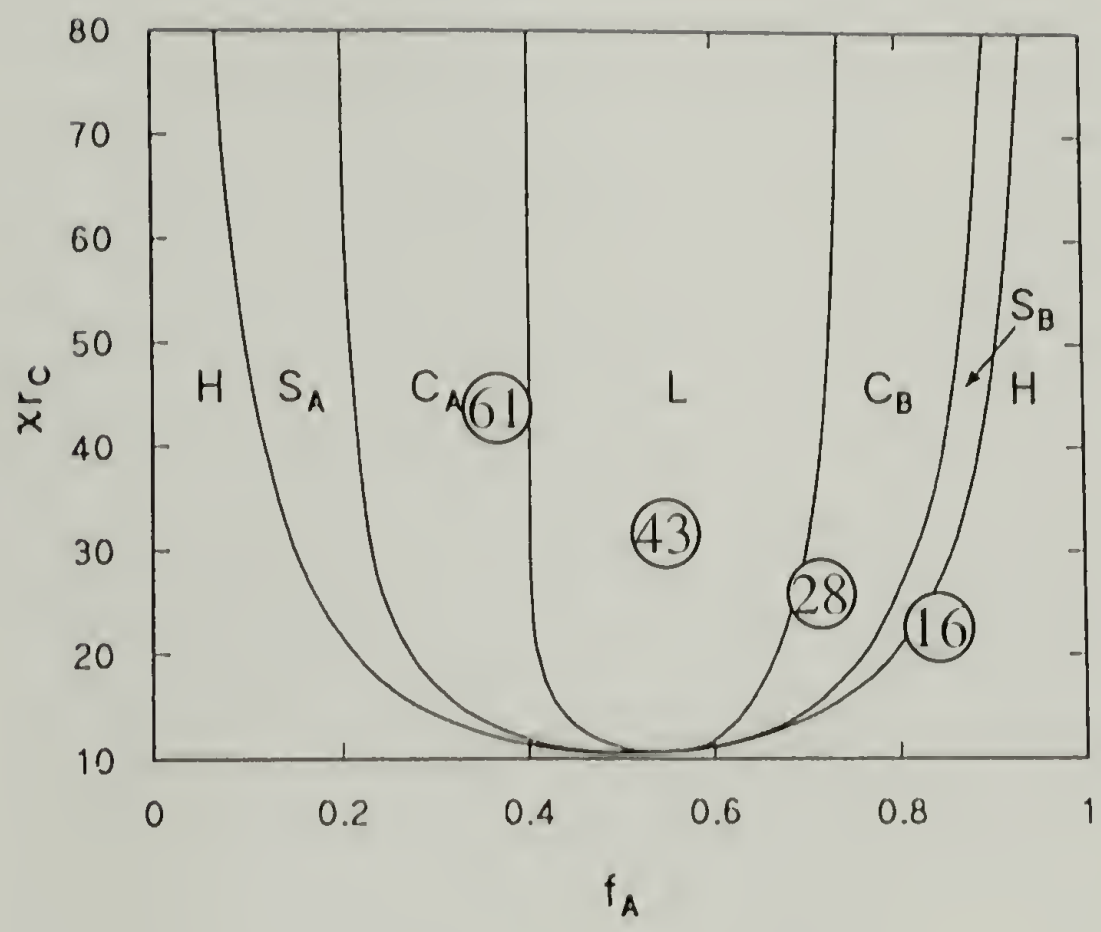

Figure 5.21. Morphology diagram from Vavasour and Whitmore, including RMG-4-4 series samples, plotted assuming a linear diblock constituting block copolymer.

CHAPTER 6

MORPHOLOGICAL BEHAVIOR AND GRAIN STRUCTURE OF REGULAR, TETRAFUNCTIONAL MULTIGRAFT BLOCK COPOLYMERS

6.1 Abstraet

An investigation of the morphologieal behavior of a series of graft eopolymers having multiple regularly spaeed, tetrafunetional braneh points has been earried out. The behavior of these materials, eomprised of polyisoprene baekbones with two polystyrene arms grafted to the backbone at eaeh braneh point, is shown to be effeetively modeled by eonsidering the behavior of smaller, arehitectural subunits based on the local environment of each junetion point (eonstituting block eopolymer). Morphologieal behavior was eharaeterized using TEM and SAXS. Well-ordered eylindrieal and lamellar morphologies were observed. Several samples appear to form eylindrieal domains in disordered arrangements. Samples predicted to form spheres form instead a mierophase separated "mesh" morphology. Lamellar grain size and shape were also investigated and lamellar grain orientation eorrelation lengths were determined. These measurements show a deerease in grain size with increasing number of branch points per moleeule. They also indieate that the grains formed are anisotropie in shape.

6.2 Introduetion

Moleeular architeeture has been demonstrated to be an important faetor in the morphological behavior of bloek eopolymers. Systematie studies of the relationship between moleeular architecture and morphology have been largely restrieted to diblock and triblock eopolymers due to the unavailability of model graft eopolymer materials

with precisely controlled architectures. Common methods of producing block copolymers often yield materials with heterogeneous, ill-defined architectures. As illustrated in Figure 6.1a, characteristics of such materials included polydisperse backbones and arms, irregular placement of branch points, and variation in the number of branch points per molecule.[10]

New synthetic techniques allow synthesis of graft block copolymers having well-defined molecular architectures.[16,17] These techniques provide precise control over backbone molecular weight, arm molecular weight, arm polydispersity, the placement of the branch points along the backbone, and the number of arms grafted to each branch point. Molecules with specific, incremental backbone lengths are produced, allowing multiple-grafts with well-defined architectures to be isolated and characterized.

An empirical framework for predicting and interpreting the morphological behavior of block copolymers with complex architectures has been developed.[4,5,51,69] This framework, the *constituting block copolymer hypothesis*, proposes that the morphological behavior of a graft copolymer with a complex architecture is governed by the behavior of smaller block copolymer units (the constituting block copolymers) associated with each junction point. Existing theories for miktoarm stars,[8,45] or conformationally asymmetric linear diblocks,[90,97] are used to predict the behavior of the constituting block copolymer, which is then applied to the overall multigraft architecture. The constituting block copolymer hypothesis for strongly segregated graft copolymers is reminiscent of the calculations of Benoit and Hadziioannou for graft copolymers in the homogenous state and at the spinodal.[98] They found that the scatting profiles for multigraft copolymers as well as the spinodal curves were relatively insensitive to the total number of constituting units, approaching a limiting value at high numbers of these

units. Additionally, they found that the relevant value of χN for controlling phase behavior was that of the constituting unit rather than of the whole graft copolymer. A similar result was found by Balazs and coworkers when considering the order-disorder transition behavior of comb copolymers.[12]

Recently we studied the morphological behavior of multiple-graft block copolymers with monodisperse polybutadiene (PB) backbones, monodisperse polystyrene (PS) arms, and branch points located randomly along the PB backbone.[69] The average number of branch points per molecule was controlled as described by Xenidou and Hadjichristidis.[16] Each branch point was either trifunctional, allowing one arm of PS to be grafted to the PB backbone, or tetrafunctional, allowing two PS arms to be grafted to the PB backbone at the same point. The tetrafunctional random multigraft illustrated in Figure 6.1b represents a moderate level of architectural heterogeneity, intermediate between the precisely defined architectures of the molecules examined in this work and the case of common multiple-graft architectures with much more heterogeneous molecular architectures. It was observed that while the constituting block copolymer hypothesis, based on the average environment around each junction point, correctly predicted domain shape preferences, only lamellar morphologies formed with long-range order. When non-lamellar morphologies were predicted, the samples were observed to form microphase separated morphologies, characterized by form factor scattering indicating the formation of specific domain shapes (spheres or cylinders) which were not, however, ordered on lattices. These preferred domain shapes agreed with the predictions made using the constituting block copolymer hypothesis.

In the present study, the morphological behavior of a series of multiple-graft block copolymers with regularly spaced branch points is characterized. These

multigrafts, illustrated in Figure 6.1c, have monodisperse polyisoprene (PI) backbones, monodisperse PS arms, and tetrafunctional branch points. As shown in Figure 6.2, the molecular architecture of these materials may be thought of as serial combinations of I_2S_2 miktoarm stars. The synthesis utilizes a polycondensation reaction that connects the constituting block copolymer I_2S_2 units.

Several issues are considered. First, the effectiveness of the constituting block copolymer hypothesis for the regular multigraft block copolymer architecture is evaluated. Second, the polycondensation technique used to produce the regular multigraft copolymers produces a distribution of molecular weights but with all molecules having the same exact composition because they are all based on the same constituting unit. This allows an important self-consistency check to the constituting block copolymer hypothesis. Specifically, different average molecular weight fractions based on the same constituting block copolymer can be isolated and should form the same morphology. It is expected that as molecular weight (number of junction points per molecule) increases, long-range order will decrease but the domain shape should be conserved. Thus the internal consistency of the constituting block copolymer hypothesis can be evaluated even if the samples at a particular volume fraction are found to disagree with predictions of theories such as that of Milner.[8]

The decrease in long-range order with increasing numbers of junction points per molecule is investigated quantitatively for a series of three regular multigraft fractions all based on the same constituting block copolymer unit and all forming lamellar morphologies. This is achieved by measuring the average grain size by analysis of TEM images of the morphologies of these materials. Additionally, the grain shape anisotropy in these samples is measured.

6.3 Experimental

6.3.1 Synthesis

A series of multigrafts having regularly spaced, tetrafunctional branch points was synthesized as described by Iatrou, Mays, and Hadjichristidis.[17] The synthesis of these materials is a multiple-step process beginning with the polymerization of monodisperse PI dianions by living anionic polymerization. PS arms are also polymerized separately by living anionic polymerization. The molecular characteristics of the component PI blocks and PS arms for each composition are given in detail in Table 6.1. A macrocoupling agent is then created by joining two PS arms with a tetrafunctional chlorosilane coupling agent, leaving two functionalized sites on the silicon. In the final reaction, PI dianions and PS macrocoupling agents are reacted to form multigrafts with regularly spaced branch points, where the PI blocks form a backbone with two PS arms at each branch point. Stoichiometry is adjusted to assure that the regular multigraft has PI blocks at both ends. The polycondensation nature of this final step produces a most-probable, Flory-Schultz distribution of multigraft molecular weights, equivalent to a distribution in number of branch points and in number of constituting block copolymer units per molecule. Each species has nearly identical volume fractions of PS, and has the same constituting block copolymer. Through solvent-nonsolvent fractionation, two or three average molecular weight fractions are obtained from each overall polycondensation product. Four compositions were examined, with 10 samples studied in all, as indicated in Table 6.2.

6.3.2 Molecular Characterization

The molecular characteristics of the component blocks and the regular multigrafts were determined using a variety of techniques. Size-exclusion chromatography (SEC) was performed for solutions in tetrahydrofuran (THF) at 30°C using a Waters Model 510 pump, Waters Model 410 differential refractometer, and ultrastyragel columns with a continuous porosity range from 10^6 to 10^3 Å. Ultraviolet size-exclusion chromatography (SEC-UV) was performed on solutions in THF at 30°C and a flow rate of 1 mL/min using a Waters Alliance Separations Module 2690 and a Waters Photodiode Array Detector 996. Multi-angle laser light scattering size-exclusion chromatography (SEC-MALLS) was performed using a Waters Alliance Separations Module 2690, Waters Refractive Index Detector 2410, and a Wyatt Technology Dawn DSP Laser Photometer with solutions in THF at 30°C with a flow rate of 1 mL/min. Low-angle laser light scattering (LALLS), used to obtain an independent measure of weight-average molecular weight, was performed on multigraft solutions in THF at 22°C using a Chromatix KMX-6 instrument with $\lambda = 633$ nm. Membrane osmometry (MO) using a Jupiter Model 231 recording membrane osmometer was conducted in toluene distilled from CaH_2. Matrix-assisted laser desorption/ionization time-of-flight mass spectroscopy (MALDI/TOF/MS) was performed in trans-retinoic acid with silver trifluoroacetate using a Perseptive Biosystems Voyager Elite DE instrument. Finally, nuclear magnetic resonance (NMR) was used to determine overall weight fractions of PS in each sample. The molecular characterization data are listed in Tables 6.1 and 6.2.

To describe molecular architecture, the following notation is used: MG-*f*-*n*-ϕ, where MG stands for *multigraft*, *f* describes the functionality of the branch points, *n* gives the average number of branch points per molecule in a particular fraction, and ϕ is the

overall volume fraction of PS in the sample. This nomenclature differs from that used by Iatrou, Mays, and Hadjichristidis,[17] but is consistent with the previous work on random multigrafts.[69]

6.3.3 Morphological Characterization

For multigrafts having tetrafunctional branch points, an A_2B_2 miktoarm star of PI and PS (I_2S_2) is the appropriate constituting block copolymer. The two PI arms in the constituting I_2S_2 are each ½ the length of a single PI connector. To calculate the number of branch points per molecule in a given fraction, the average molecular weight of the fraction, less the molecular weight of one PI connector, is divided by the molecular weight of the constituting block copolymer. Even after fractionation, the samples obtained contain a distribution of molecular weights and of number of constituting units per molecule. Polydispersities for all samples are listed in Table 2. The degrees of segregation, χN, are calculated for the constituting block copolymers, where χ is the Flory-Huggins parameter, and N is the degree of polymerization for the constituting block copolymer. These values, listed in Table 2, place all the samples in the strong segregation limit. These χN valued are expected to accurately represent the degrees of segregation for the various multigraft copolymers.[50,51]

Morphological characterization of each sample followed established techniques for block copolymers. Solid films approximately 1 mm thick were cast from 2.5 wt. % solutions in toluene, a non-preferential solvent for PS and PI.[54] To promote the formation of equilibrium morphologies, solvent evaporation was restricted to allow approximately 8 weeks for the solidification of a bulk film. To further promote the formation of equilibrium morphologies, the samples were annealed at 120°C under vacuum for a

period of two weeks. These casting and annealing conditions allow a much greater period of time for self-assembly than is usual for block copolymers having simple architectures. To allow for comparison of long-range order and grain size, all samples in the study were cast and annealed together, ensuring that they experienced identical conditions. After annealing, thin sections approximately 500-1000 Å thick were prepared by ultramicrotoming the bulk films using a Leica EM-FCS microtome, equipped with a cryogenic sample chamber operated at -110°C. The sections were stained 4 hours in OsO_4 vapors for transmission electron microscopy (TEM) imaging of the structures. TEM was performed using either a JEOL 100CX TEM or a JEOL 2000FX TEM, both operated at an accelerating voltage of 100 kV.

Small-angle X-ray scattering (SAXS) experiments were performed to determine the lattice symmetries, domain shapes, and spacings of the morphologies. SAXS was performed on the Advanced Polymers Beamline (X27C), at the National Synchrotron Light Source, Brookhaven National Laboratory, Upton, NY. The incident beam had an area of 3 mm^2 at the sample and a wavelength of 1.307 Å. The sample-to-detector distance was 1.410 m. Two-dimensional scattering patterns were recorded on Fujitsu HR-V image plates and digitized using a Fujitsu BAS 2000 image plate reader. Background was subtracted, circular averaging performed, and the data converted to a logarithmic intensity scale for plots of log(I) vs. q.

6.3.4 Grain Structure Analysis

Quantitative estimates of grain size were obtained for the lamellar samples in this study (MG-4-5-36, MG-4-9-36, and MG-4-12-36) using procedures described by Garetz, Balsara, and coworkers.[99] TEM micrographs were digitized using an UMAX 1220S

digitizer. The azimuthal angles, $\phi(\mathbf{r})$, which describe the local orientation of the lamellar normal at various points in the images, relative to a fixed reference direction, were computed by a local, two-dimensional Fourier analysis. Each image was divided into overlapping 245 nm × 245 nm squares with centers separated by 76.5 nm, and the image within this square was stored as a 32 × 32 element array of 8-bit integers. The correlation function, C(r), was obtained using two models:

6.3.4.1 Model 1

$C(|\mathbf{r} - \mathbf{r}'|) \approx \langle\cos[2\{\phi(\mathbf{r}) - \phi(\mathbf{r}')\}]\rangle$. Random pairs of points, $\mathbf{r}$ and $\mathbf{r}'$, were chosen on a digitized micrograph, and the local Fourier transform analysis gave $\phi(\mathbf{r})$ and $\phi(\mathbf{r}')$. The ensemble averages, $\langle\cos[2\{\phi(\mathbf{r}) - \phi(\mathbf{r}')\}]\rangle$, were computed by repeating this procedure 10^6 times per micrograph. The distance scale, $r = |\mathbf{r} - \mathbf{r}'|$, was discretized into 76.5 nm interval bins. $C(|\mathbf{r} - \mathbf{r}'|)$ was determined for 12 images of MG-4-5-36, 13 images of MG-4-9-36, and 11 images of MG-4-12-36. For each sample, the correlation function was found by nonlinear regression to be approximately exponential with a baseline: $C(r) = \exp(-r/\kappa) + b$. The baseline values, b, were 0.041 (MG-4-5-36), 0.024 (MG-4-9-36), and 0.021 (MG-4-12-36).

6.3.4.2 Model 2

$C(|\mathbf{r} - \mathbf{r}'|)$ is the probability that both $\mathbf{r}$ and $\mathbf{r}'$ lie in the same grain. The correlation function was computed by choosing a random location, $\mathbf{r}$, on a digitized micrograph, and computing $\phi(\mathbf{r})$. Then one travels along a random direction in the image examining $\phi(\mathbf{r}')$. The discretization of $r = |\mathbf{r} - \mathbf{r}'|$ and the images used here were the same

as those used to compute C(r) from Model 1. If $|\phi(\mathbf{r}) - \phi(\mathbf{r}')|$ was less than a prescribed tolerance, $\Delta\phi$, then $\mathbf{r}$ and $\mathbf{r}'$ were considered to lie within the same grain and one was input in the corresponding bin, and $\mathbf{r}'$ was increased. When $\mathbf{r}' = \mathbf{r}^*$ was reached such that $|\phi(\mathbf{r}) - \phi(\mathbf{r}^*)| > \Delta\phi$, then zeros were input into all the remaining bins. This procedure was repeated 10^4 times for different $\mathbf{r}$ locations on each micrograph and C(r) was obtained by the averaging of these results. This method was used on the same 36 TEM micrographs as Model 1. For each micrograph, the calculation was done for $\Delta\phi$ = 10°, 15°, and 30°.

Photographic enlargements were made at different magnifications for each lamellar multigraft sample. A representative enlargement for sample MG-4-5-36 showed approximately 50 lamellar grains in an area of 100 μm^2. Each enlargement for sample MG-4-9-36 allowed examination of approximately 200 lamellar grains in an area of about 90 μm^2. Sample MG-4-12-36 was characterized using enlargements which showed an average of 30 μm^2 and approximately 400 grains each.

Grain size for the lamellar samples was also measured by a manual method. This provides a consistency check for the results obtained from the computerized image analysis. It also allows measurement of the grain shape anisotropy which could not be obtained by the current computer program. Photographic enlargements of the same TEM micrographs used for the computer analyses of grain size were overlaid with clear plastic sheets and the outlines of grains were traced with a pen. The lamellar grains of the MG-4-n-36 samples are generally anisotropic. They are longer in the direction normal to the lamellae than parallel to the lamellae, consistent with previous results reported by Hashimoto and coworkers.[100,101] Additionally, within each micrograph the long axes of the grains approximately line up in the same directions. The transparent overlays of the grain outlines were oriented with the long axis of the grains along one principal direction

and the short axis, orthogonal to the long axis, along the other. The overlays were digitally scanned and analyzed with a computer program which calculated the mean intercept lengths of test lines passed across the image in the two principal directions. These mean intercept lengths are proportional to, but not equal to, the actual average grain sizes in the two principal directions. The proportionality (constant of order one) between the mean intercept lengths and true average grain dimensions depends on the details of the grain shape.[102] Lacking a good model for grain shape, mean intercept lengths are taken as approximate indicators of grain size.

6.4 Results

To predict the morphological behavior of the regular multigrafts examined in this study, the morphological behavior for the appropriate constituting block copolymer was predicted using existing theory. For miktoarm star constituting block copolymers in the strong segregation limit ($\chi N > 100$), a theory derived by Milner models the effect of molecular architecture and composition on morphology.[8] For architecturally and conformationally asymmetric block copolymer stars of type A_nB_m, this theory predicts morphology as a function of component B volume fraction, ϕ_B, and a molecular asymmetry parameter, $\varepsilon = (n_A/n_B)(l_A/l_B)^{1/2}$. Here, n_A and n_B are the numbers of arms of block materials A and B (n and m in the A_nB_m notation) linked at a junction point, and $l_i = V_i/R_i^2 = v_i/b_i^2$. V_i and R_i are the volume and radius of gyration of one arm of polymer i, while v_i is the segmental volume and b_i is the statistical segment length of component i. Figure 6.3 shows the morphology diagram, indicating a shift in the volume fraction ranges in which a given morphology is observed with increasing molecular asymmetry. The I_2S_2 constituting block copolymer has no architectural asymmetry because n_A and n_B

are equal. The conformational asymmetry between PS and PI raises the total molecular asymmetry to $\varepsilon \approx 1.2$.[1] In this ease, PS is the A component and PI is the B eomponent so that $\varepsilon > 1$. The four volume fraetions of the regular multigrafts in this study are loeated on the diagram at their volume fraction of PI, but are labeled by their volume percent PS in keeping with previous block eopolymer nomenelature. Using the Milner theory and the constituting block copolymer argument, the samples having 67 vol. % PS are predicted to form cylinders of PI, or possibly a bicontinuous morphology. The samples having 37 vol. % PS are predicted to form lamellar morphologies. Those having 21 vol. % PS are predicted to form cylinders of PS, and those having 9 vol. % PS are predieted to form spheres of PS. Table 6.3 lists the predicted morphologies and summarizes the results of the morphological characterization described below.

Figures 6.4 and 6.6 show representative TEM micrographs from samples MG-4-10-67 (6.4) and MG-4-14-67 (6.6). These samples both have 67 volume % PS with on average 10 (MG-4-10-67) and 14 (MG-4-14-67) constituting block copolymer units per molecule. The morphology diagram in Figure 6.3 indicates that these samples are located near the cylinder/bicontinuous boundary. The representative TEM micrograph for MG-4-10-67, shown in Figure 6.4, shows a cylindrical morphology. Figure 6.6 shows a slightly less well-ordered cylindrical morphology formed by MG-4-14-67. SAXS data for both samples, shown in Figures 6.5 and 6.7, exhibit strong primary reflections at q^*, and higher order reflections at $2q^*$ and $q^*\sqrt{7}$, consistent with hexagonally packed cylinders. The absence of the reflection expected for a hexagonal lattice at $q^*\sqrt{3}$ is due to a minimum in the cylindrical form factor. The SAXS data indicate that MG-4-10-67 has a (100) interplanar spacing of 373 Å and a hexagonal lattice parameter of 431 Å, while

sample MG-4-14-67 has a (100) interplanar spacing of 349 Å and a hexagonal lattice parameter of 403 Å.

Samples MG-4-5-36, MG-4-9-36, and MG-4-12-36 were all predicted to form lamellar morphologies. Figures 6.8, 6.10, and 6.12 show representative TEM micrographs for each sample, and the corresponding SAXS data are shown in Figures 6.9, 6.11, and 6.13. While sample MG-4-4-36 exhibits a well-ordered lamellar morphology, with four strong Bragg reflections at integral multiples of q^*, sample MG-4-9-36 was found to have a markedly less well-ordered morphology. SAXS data for this sample, shown in Figure 6.11, still exhibit Bragg reflections at $2q^*$, $3q^*$, and $4q^*$ which indicate a lamellar morphology, but their reduced intensities and increased width relative to the SAXS data for MG-4-5-36 results from the poorer ordering evident in Figure 6.10 for MG-4-9-36. Figure 6.12 shows the morphology of sample MG-4-12-36 to be microphase separated but generally not ordered on a lattice. A few very small regions which appear to be forming extremely small grains with some limited lamellar order are visible. Bragg reflections, indicative of well developed order, are absent from the SAXS data for MG-4-12-36, shown in Figure 6.13. The lamellar spacings of MG-4-5-36 and MG-4-9-36 are 410 Å and 354 Å, respectively.

Figures 6.14 through 6.19 show representative TEM micrographs and SAXS data for the samples having 21 volume % PS: MG-4-4-21, MG-4-7-21, and MG-4-9-21. These samples were predicted to form cylindrical morphologies. As seen in Figures 6.14, 6.16, and 6.18, each of these three samples formed a microphase separated morphology which appears to lack long-range order. As was seen frequently in the study of random multigrafts,[69] the SAXS data for all samples in the MG-4-n-21 series exhibit a strong primary maximum followed by a weak, broad secondary maximum at approximately

$2.5 \cdot q^*$, which does not correspond to a Bragg reflection for any known block copolymer morphology.[103] However, such scattering profiles are similar to intraparticle scattering which results from disordered arrangements of domains of a specific shape. Form factors for spheres and cylinders of the appropriate domain size were generated and compared to the scattering data. Domain sizes were obtained by using the primary peak to get an average center-to-center distance between neighboring domains. For samples MG-4-4-21, MG-4-7-21, and MG-4-9-21 these distances were found to be 297 Å, 288 Å, and 279 Å respectively. This spacing along with the known PS and PI volume fraction can be used to calculate sphere and cylinder radii provided that a model for how the domains fill space is assumed. For the purposes of these calculations cylinder radii were obtained assuming a hexagonal packing and sphere radii were determined using both BCC and SC lattice packings.[66,104] The use of a lattice in this calculations is an approximation to allow calculation of domain size; it does not imply that that sample is actually ordered on a lattice. As in Figure 6.15, the form factors for spheres (both BCC and SC) fit the data poorly, predicting maxima where there are none, and extinctions coincident with the second maximum. The form factor for a cylinder, however, fits the data better, with the form factor maximum corresponding with the observed secondary maximum. This suggests that the sample is composed of cylindrical, worm-like domains in a disordered arrangement. Similar calculations for samples MG-4-7-21 and MG-4-9-21, illustrated in Figures 6.17 and 6.19, also support a preference for cylindrically shaped domains.

Samples MG-4-4-9 and MG-4-8-9 both formed the same unusual morphology, TEM images of which are given in Figures 6.20 and 6.22. It may be described as a microphase separated mesh of PS struts or worm-like domains in a PI matrix. SAXS data for samples MG-4-4-9 and MG-4-8-9, shown in Figures 6.21 and 6.23, are consistent

with a disordered, mesh-like structure with average mesh sizes of 249 Å and 252 Å respectively.

The SAXS and TEM data demonstrate that the domain shape of the graft copolymers is essentially independent of the number of constituting units, *n*. However, it is evident that increasing *n* decreases the coherent order or grain size of the microstructure. This is clearly visible in the three lamellar forming samples with PS volume fractions of 0.36. Figure 6.24 shows the correlation functions, C(r), obtained using Model 2 with a tolerance $\Delta\phi = 10^{\circ}$ from 3 separate micrographs of MG-4-5-36. The results from the different micrographs are in reasonable agreement and the correlation functions are exponentials to a good approximation: $C(r) = \exp(-r/\kappa)$, where κ is the correlation length. The lines in Figure 6.24 represent least squares fits to this equation.

In Figure 6.25, the correlation functions from a single micrograph are presented using Model 2 with different values of $\Delta\phi$. The correlation functions remain exponential, and, as expected, the correlation length, κ, increases with increasing tolerance, $\Delta\phi$. Correlation functions for MG-4-5-36, MG-4-9-36, and MG-4-12-36, using Model 2 with $\Delta\phi = 10^{\circ}$, are shown in Figure 6.26. It is evident that κ decreases with increasing molecular weight; the long-range order in the samples is adversely affected by the increase in number of constituting block copolymer units. This trend is supported in Figure 6.28, where the correlation functions obtained from Model 1 are plotted.

In Figure 6.28, the average values of κ, over all the TEM images analyzed, using the five methods outlined above (Model 1, Model 2 with different $\Delta\phi$ values, and manual), are plotted against *n*, the average number of junctions or constituting block copolymer units per molecule. The average grain size κ decreases with increasing *n*. The

least square power law fit utilizing all of the data in Figure 6.28 (essentially averaging over all the different grain size measurement techniques) yields

$$\kappa \sim n^{-2.0} \tag{1}$$

The uncertainty in this power law exponent was estimated by looking at the range of exponents obtained by independent fits to the grain size data from the different measurement methods, and was found to be ± 0.4.

Because the grain structure is anisotropic, the manual method gives two length scales, L_1 parallel to the lamellae and L_2 perpendicular to the lamellae. The grains are systematically larger perpendicular to the lamellae than parallel to the lamellae for all three samples. The ratio L_2/L_1 gives the aspect ratio of the grains, which is plotted in Figure 6.29 as a function of the number of junction points. The aspect ratio decreases from 1.6 for MG-4-5-36 to 1.1 for MG-4-12-36. Table 6.4 lists the grain size results for all samples studied and all the methods used.

6.5 Discussion

Of the ten multigraft samples examined in this work, seven exhibited some degree of agreement with predictions made by the constituting block copolymer hypothesis and the Milner theory (Table 6.3). Samples of type MG-4-n-67 (hexagonal cylinders) and MG-4-n-36 (lamellae) formed the morphologies predicted by theory. Samples of type MG-4-n-21, which were predicted to form hexagonally packed cylinders, instead formed a microphase separated structure of worm-like cylindrical domains without lattice ordering. This indicates that the preference for the theoretically predicted domain shape persists even as the long range order is lost due presumably to decreased molecular mobility in these high molecular weight, multi-junction point materials. The loss of

lattice ordering before the loss of domain shape preference was also observed in the previous study of random multiple graft copolymers.[69] Only the MG-4-n-9 samples showed no agreement with theory at all, instead forming a microphase separated mesh structure. This mesh, which looks like the early stages of spinodal decomposition although on a much smaller length scale, may result from a lack of molecular mobility in these materials with high molecular weight and many branch points.

The results of this study show that the constituting block copolymer hypothesis is self-consistent. In each of the four sets of samples based on four different constituting block copolymer units, all the fractions containing different average numbers of these units formed the same morphology. There was of course a progressive decrease in the degree of order in these structures with increasing number of constituting block units, but the structural similarities were clear. Also, within the lamellar (MG-4-n-36) and the two cylindrical (MG-4-n-67 and MG-4-n-21) sets of samples there was a noticeable decrease in the measured lattice constants or interdomain spacings with increasing n. Whether this is kinetic or thermodynamic in origin remains unclear.

The fact that the grain size of the lamellar MG-4-n-36 materials decreases with increasing number of junction points per molecule is to be expected. The fact that the grain shape anisotropy decreases with increasing number of junction points is perhaps less expected.

6.6 Conclusions

The usefulness of the constituting block copolymer hypothesis to predict morphological behavior of the regular multigrafts has been demonstrated. The self-consistency of the morphological behavior of molecules having the same constituting

block copolymer confirm that the behavior of molecules with large, complex architectures is dictated by the behavior of the smaller architectural subunits from which they are comprised. The main effect of increasing the number of constituting block copolymer units per chain was to decrease the coherent order of the morphologies as measured by grain size.

The role of branch point location along the backbone can be examined by comparing the behavior of multigrafts with regularly located branch point to that of multigrafts with randomly located branch points.[69] In the study of multigrafts with random junction point placement, only lamellar morphologies formed any kind of long range order. Cylindrical and spherical domain shapes formed, but were not ordered on a lattice. Due to excluded volume considerations, the lamellar domain shape templates its own long range order to a much greater degree than spheres or cylinders.[69] The observation of limited lattice ordering in cylindrical samples in the regular multigraft series of this study indicates that regularity of graft placement improves the ability of multiple-graft copolymers to form long range order. This is most likely a thermodynamic, rather than a kinetic, effect because both the random and regular multigraft materials had similar molecular weights and similar numbers of branch points per molecule. The multigraft materials with random junction point locations are frustrated due to the fact that different regions of the molecule want to form different morphologies due to the fluctuating local junction point density. This undoubtedly suppresses the driving force for the formation of the structure based on the average constituting block copolymer over the case of the regular multigrafts, where every local region of every molecule wants to do exactly the same thing.

Sample	PS branch					PI connector		
	SEC		MALDI		MO	SEC		MO
	M_n (g/mol)	PDI	M_n (g/mol)	PDI	M_n (g/mol)	M_n (g/mol)	PDI	M_n (g/mol)
MG-4-x-9	6500	1.05	6790	1.029	-	100600	1.17	91600
MG-4-x-21	13400	1.03	14070	1.014	-	82800	1.15	72700
MG-4-x-36	23900	1.03	25500	1.005	28800	60300	1.22	61800
MG-4-x-67	29100	1.02	31900	1.009	34400	26100	1.35	27400

Table 6.1. Molecular characteristics of the PI and PS connectors and arms comprising the regular multigrafts.

Sample	Wt. % PS (NMR)	Wt. % PS (SEC-UV)	Vol. % PS[a]	Total M_w (SEC-MALLS, kg/mol)	Total M_w (LALLS, kg/mol)	PDI (SEC)	M_n Const-ituting Unit (kg/mol)	# Branch points[b]
MG-4-4-9	10.3	12.0	9.1	589	540	1.24	113.6	4.3
MG-4-8-9	10.8	11.9	9.6	994	1020	1.22	113.6	7.9
MG-4-4-21	23.6	24.9	21.3	565	600	1.29	109.6	4.4
MG-4-7-21	23.8	25.2	21.5	798	830	1.23	109.6	6.5
MG-4-9-21	23.9	25.6	21.6	1094	1170	1.26	109.6	9.2
MG-4-5-36	40.2	41.4	37.0	570	600	1.41	108.1	4.7
MG-4-9-36	39.3	41.6	36.2	983	950	1.32	108.1	8.5
MG-4-12-36	38.6	40.1	35.5	1351	1260	1.37	108.1	11.9
MG-4-10-67	69.6	70.3	66.7	827	800	1.26	84.3	9.5
MG-4-14-67	69.4	70.4	66.5	1166	1220	1.28	84.3	13.5

[a] Calculated using wt. % PI from NMR, $\rho_{PI} = 0.91$ g/cm^3, and $\rho_{PS} = 1.05$ g/cm^3.
[b] Number of branch points calculated as (Total $M_{w(SEC\text{-}MALLS)}$ – PI connector $M_{n(SEC)}$)/(Constituting block copolymer M_n).

Table 6.2. Molecular characteristics of the regular multigraft block copolymers with tetrafunctional branch points.

Sample	χN of Constituting Unit	Predicted Morphology	Observed Morphology	q^* ($Å^{-1}$)	Primary Spacing (Å)	Lattice Parameter (Å)
MG-4-4-9	192	PS Sp. / PS Cyl.	Dis. / "mesh"	0.0252	249	-
MG-4-8-9	192	PS Sp. / PS Cyl.	Dis. / "mesh"	0.0249	252	-
MG-4-4-21	177	PS Cyl.	Dis. Cyl.	0.0211	297	-
MG-4-7-21	177	PS Cyl.	Dis. Cyl.	0.0218	288	-
MG-4-9-21	177	PS Cyl.	Dis. Cyl.	0.0225	279	-
MG-4-5-36	161	Lam.	Lam.	0.0153	410	-
MG-4-9-36	161	Lam.	Lam.	0.0177	354	-
MG-4-12-36	161	Lam.	Dis.	-	-	-
MG-4-10-67	113	PI Cyl. / Bicont.	PI Cyl.	0.0194	373	431
MG-4-14-67	113	PI Cyl. / Bicont.	PI Cyl.	0.0208	349	403

Table 6.3. Morphological characterization results for the 10 regular, tetrafunctional multigrafts.

Sample	Model 1	Model 2			Manual method	
	κ (μm)	κ, Δϕ = 10° (μm)	κ, Δϕ = 15° (μm)	κ, Δϕ = 30° (μm)	L_1 (μm)	L_2 (μm)
MG-4-5-36	0.189	0.202	0.231	0.344	0.281	0.469
MG-4-9-36	0.059	0.091	0.099	0.147	0.069	0.103
MG-4-12-36	0.034	0.047	0.047	0.058	0.038	0.041

Table 6.4. Summary of the characteristic length scales (κ) and mean intercept lengths (L) collected using Model 1, Model 2, and manually.

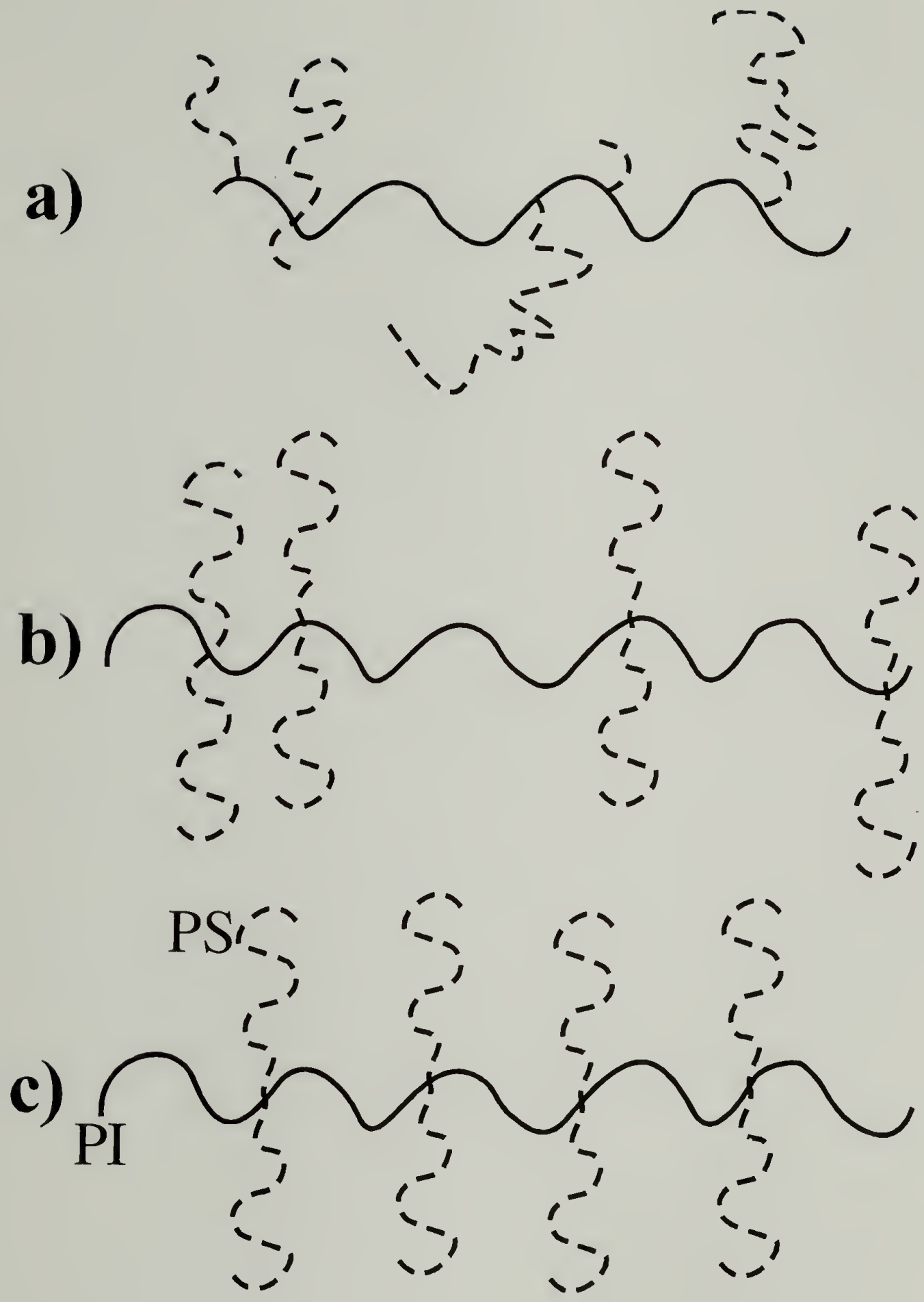

Figure 6.1. Illustrations of a) a multigraft having a heterogeneous, ill-defined architecture, b) a multigraft with randomly placed, tetrafunctional branch points, and c) a multigraft of PI and PS with regularly placed, tetrafunctional branch points.

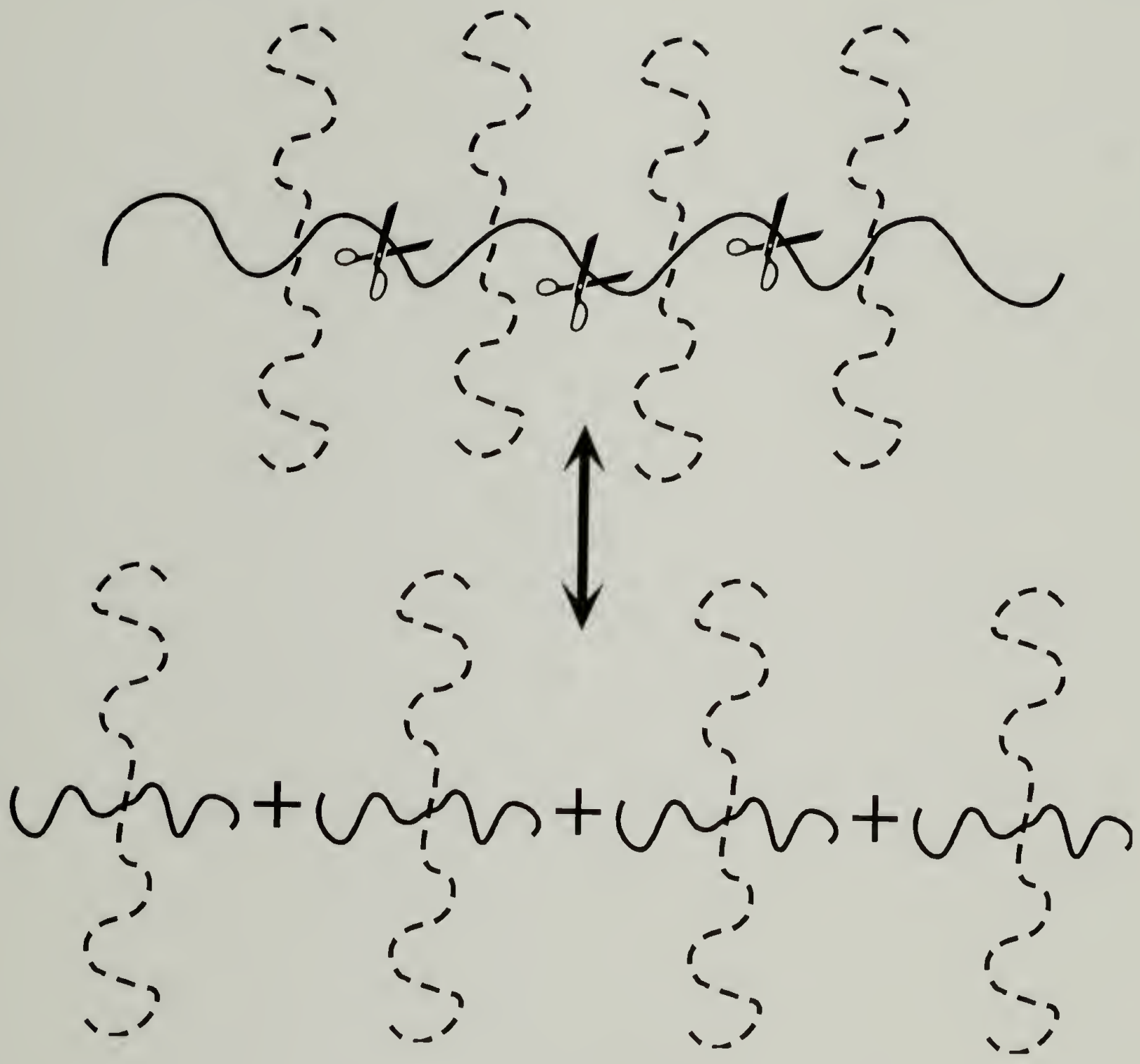

Figure 6.2. Illustration of the constituting block copolymer hypothesis as applied to a regular multigraft having tetrafunctional branch points. Imaginary division of the tetrafunctional regular multigraft produces identical A_2B_2 miktoarm star block copolymers.

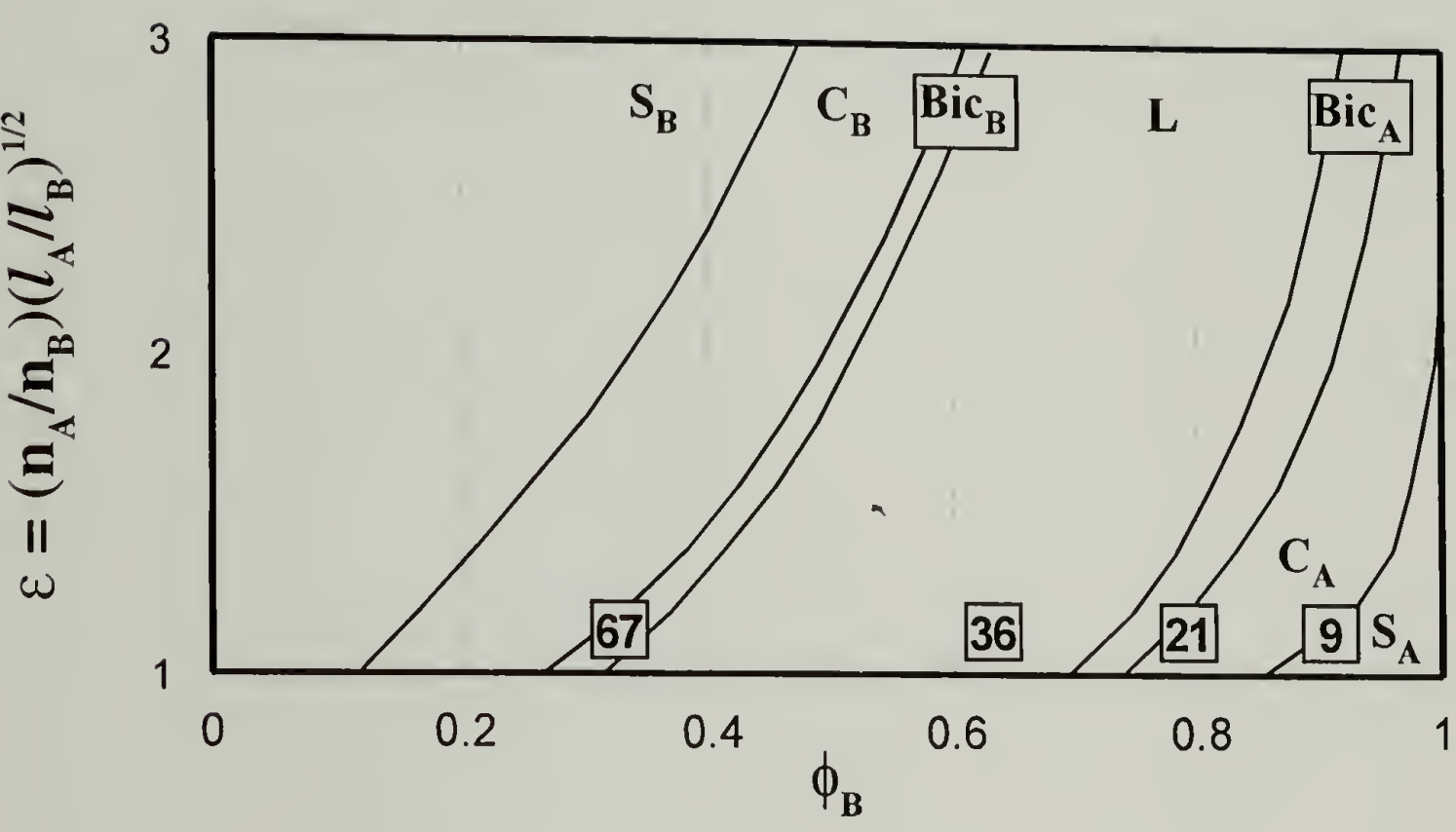

Figure 6.3. Morphology diagram generated by the Milner model for architecturally and conformationally asymmetric miktoarm stars of type A_nB_m, having volume fraction ϕ_B and unified asymmetry parameter ε. In this study, PS is component A and PI is component B, such that $\varepsilon \approx 1.2$. The four different volume fractions of samples considered in this work are placed on the diagram by their PI volume fraction, but are labeled by their PS volume percent.

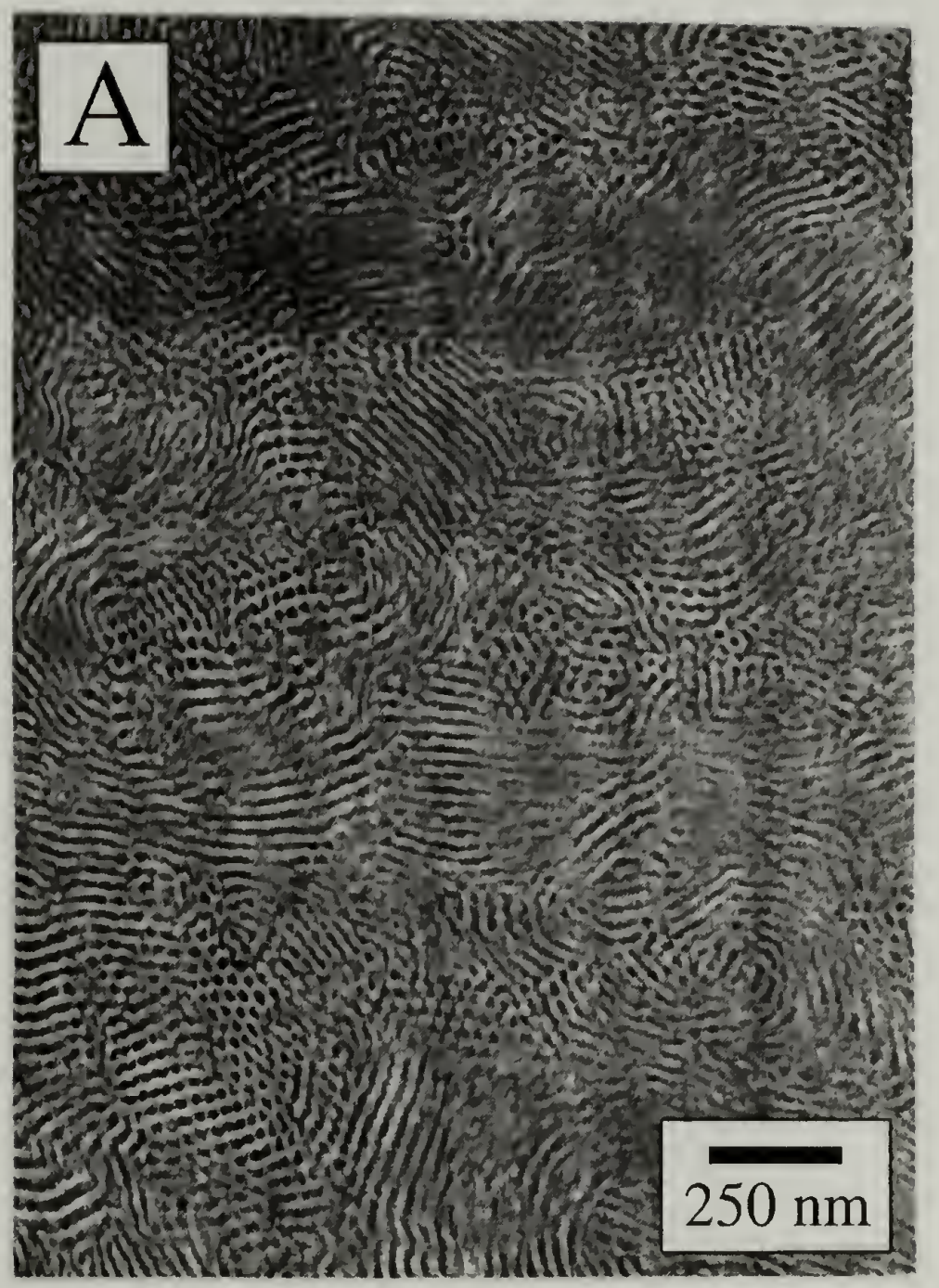

Figure 6.4. TEM micrograph for sample MG-4-10-67.

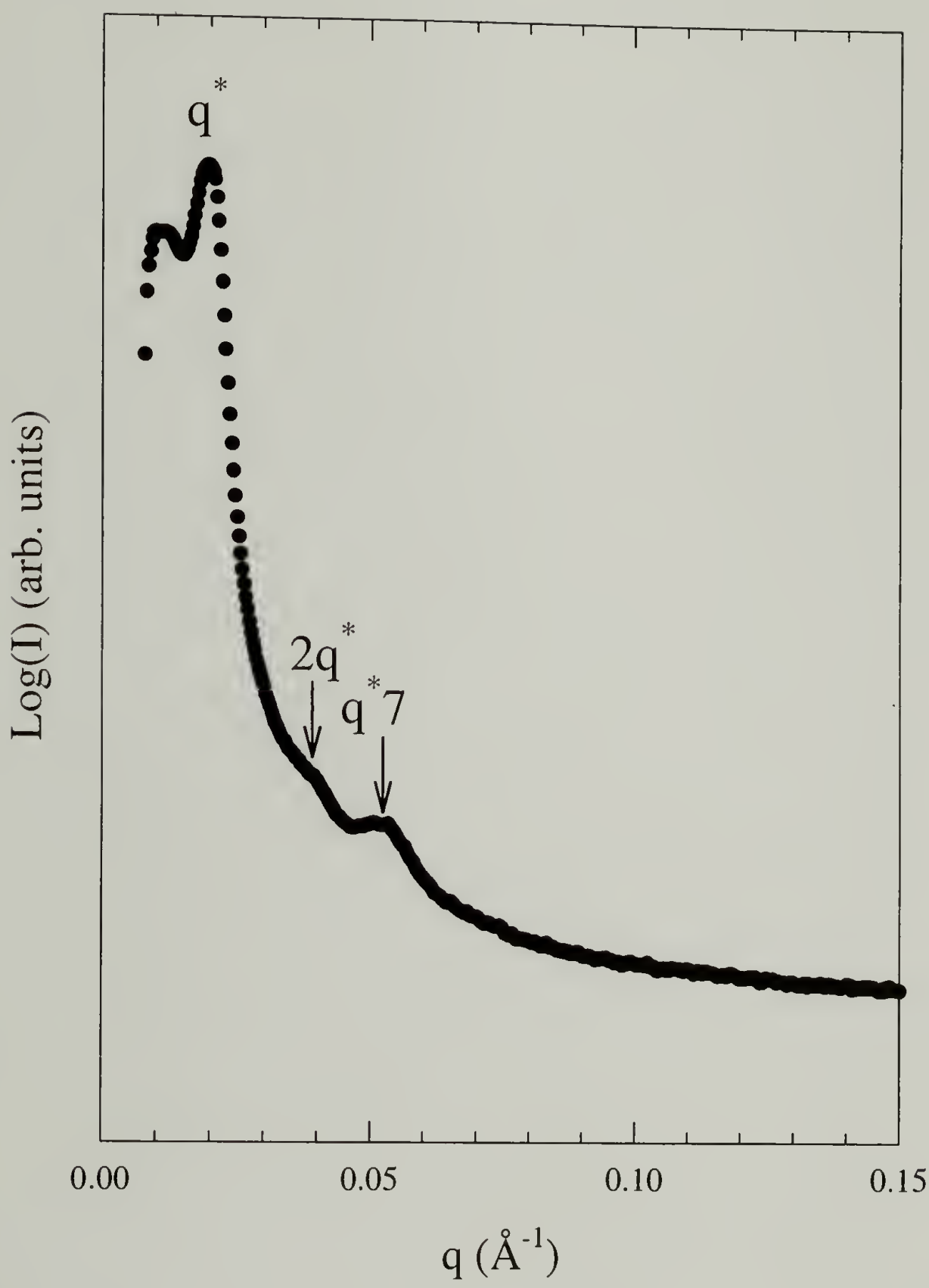

Figure 6.5. SAXS data for sample MG-4-10-67.

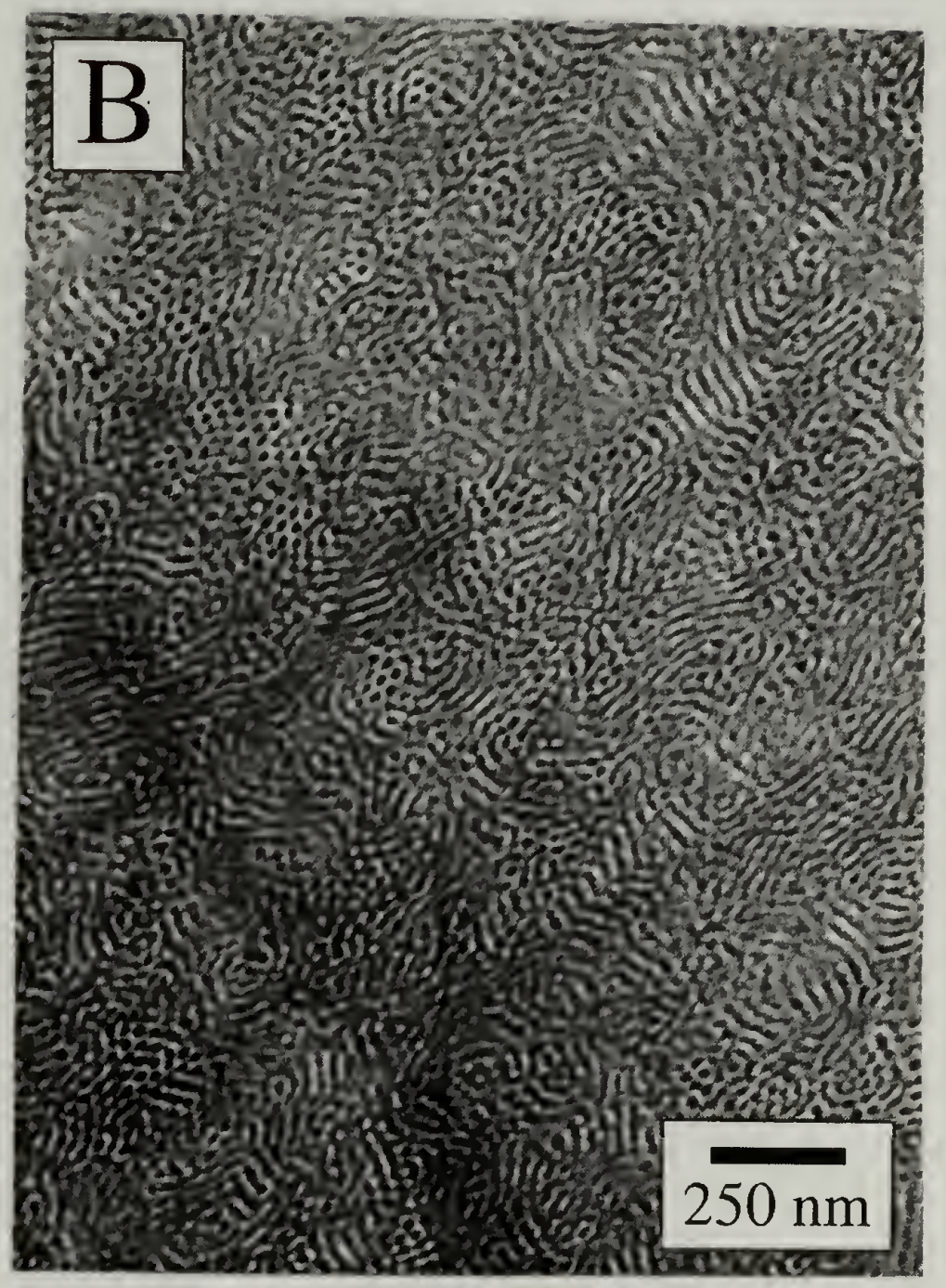

Figure 6.6. TEM micrograph for sample MG-4-14-67.

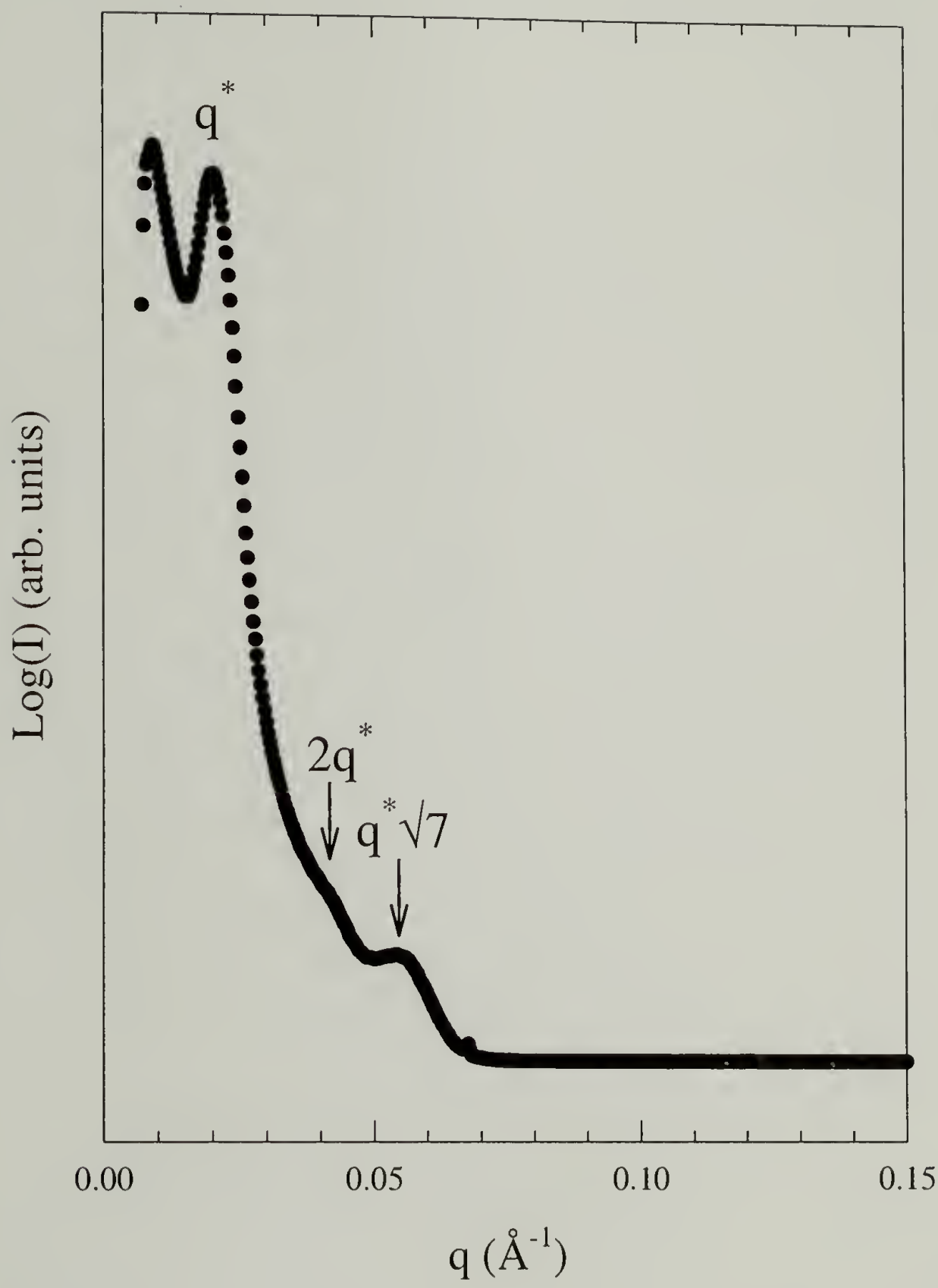

Figure 6.7. SAXS data for sample MG-4-14-67.

Figure 6.8. TEM micrograph for sample MG-4-5-36.

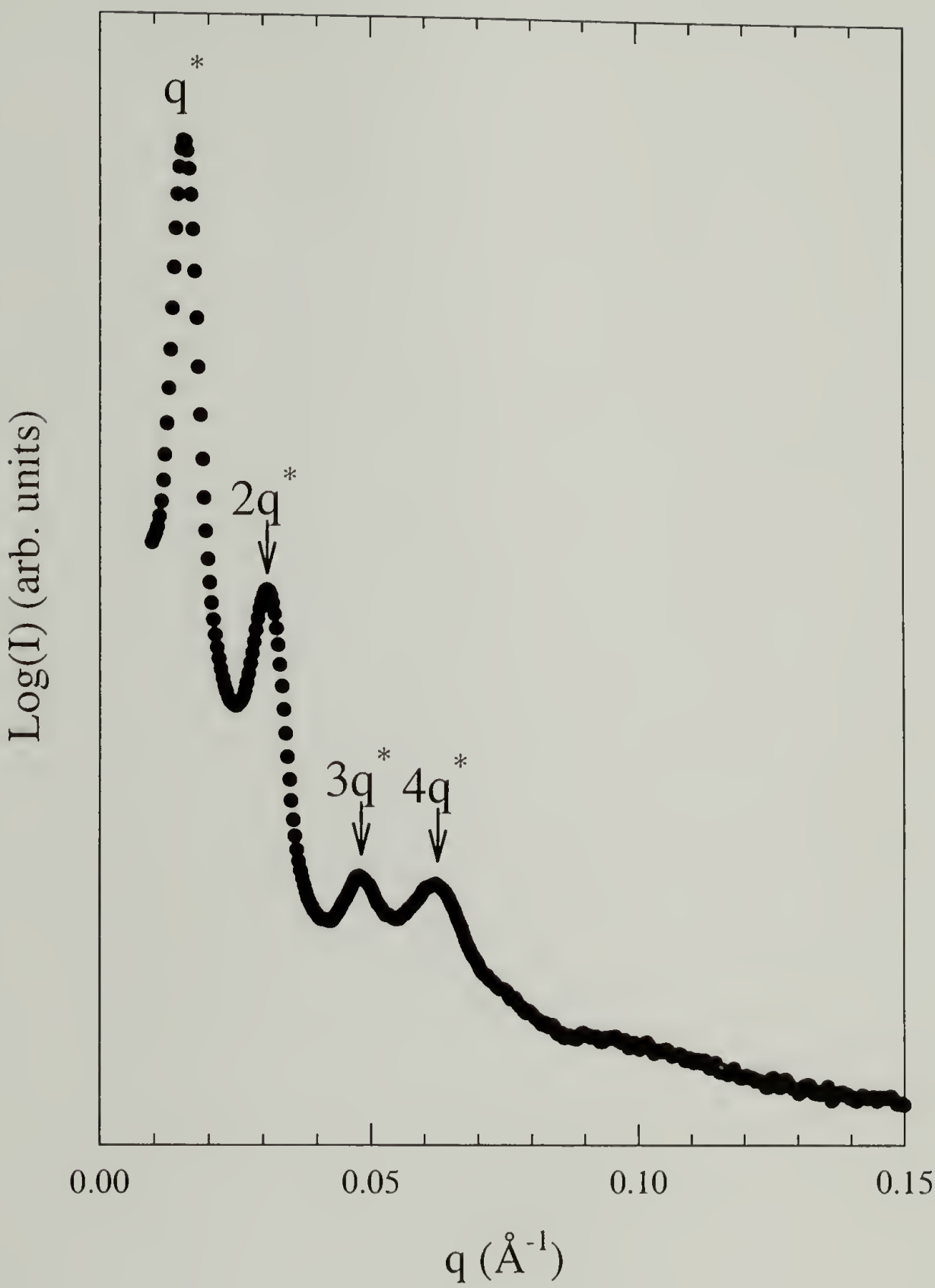

Figure 6.9. SAXS data for sample MG-4-5-36.

Figure 6.10. TEM micrograph for sample MG-4-9-36.

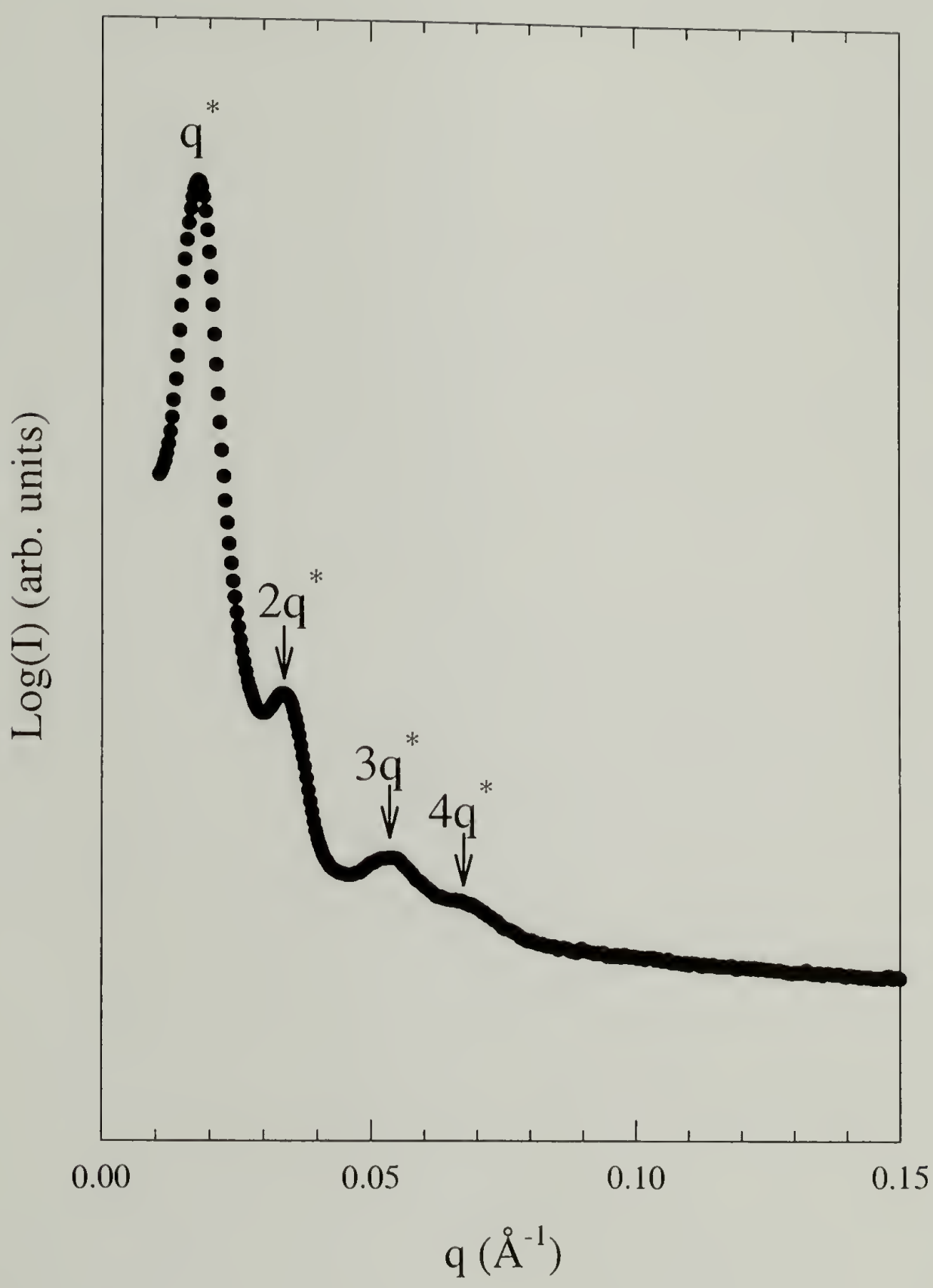

Figure 6.11. SAXS data for sample MG-4-9-36.

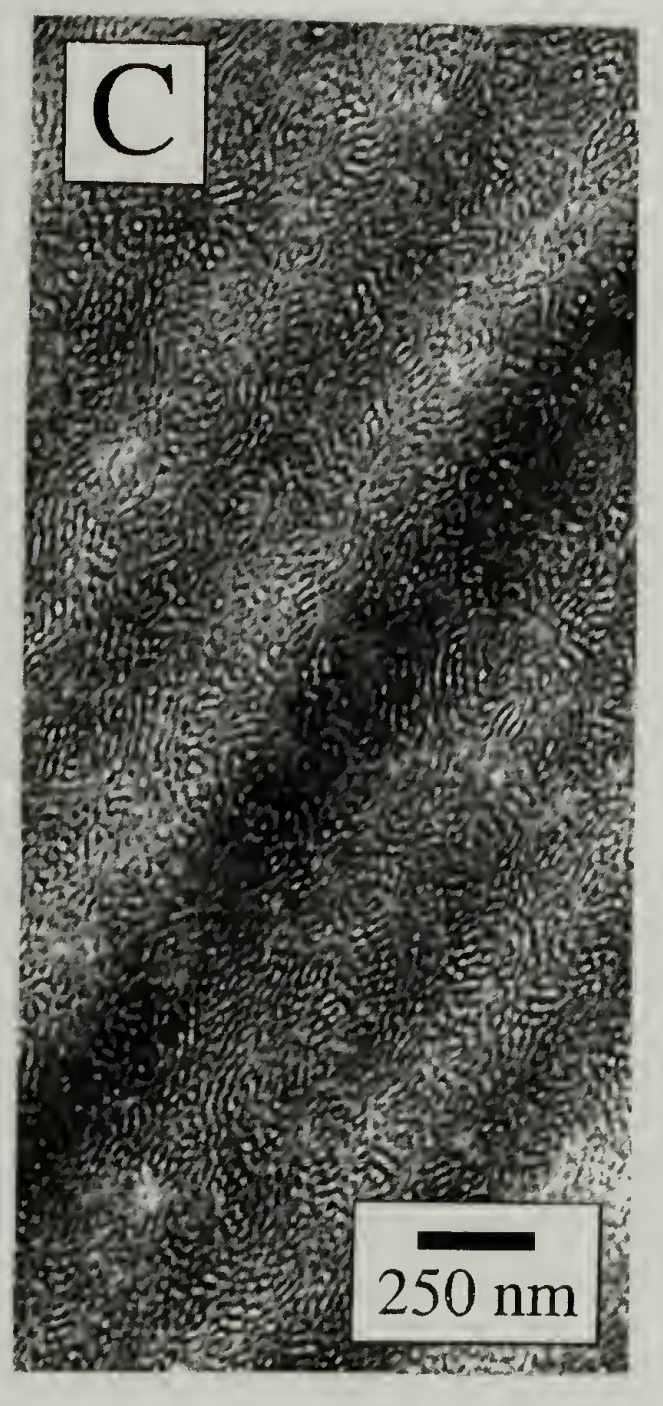

Figure 6.12. TEM micrograph for sample MG-4-12-36.

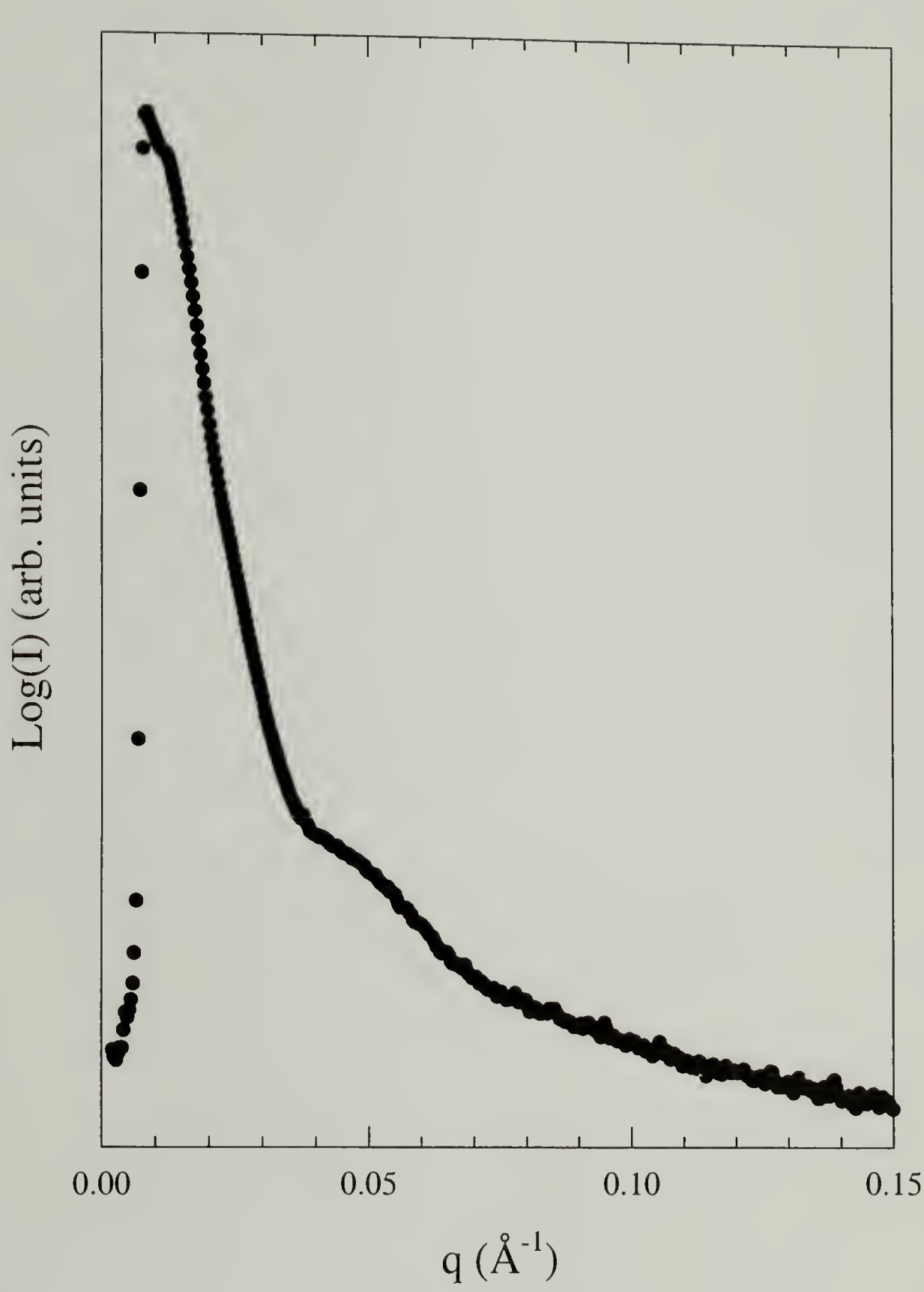

Figure 6.13. SAXS data for sample MG-4-12-36.

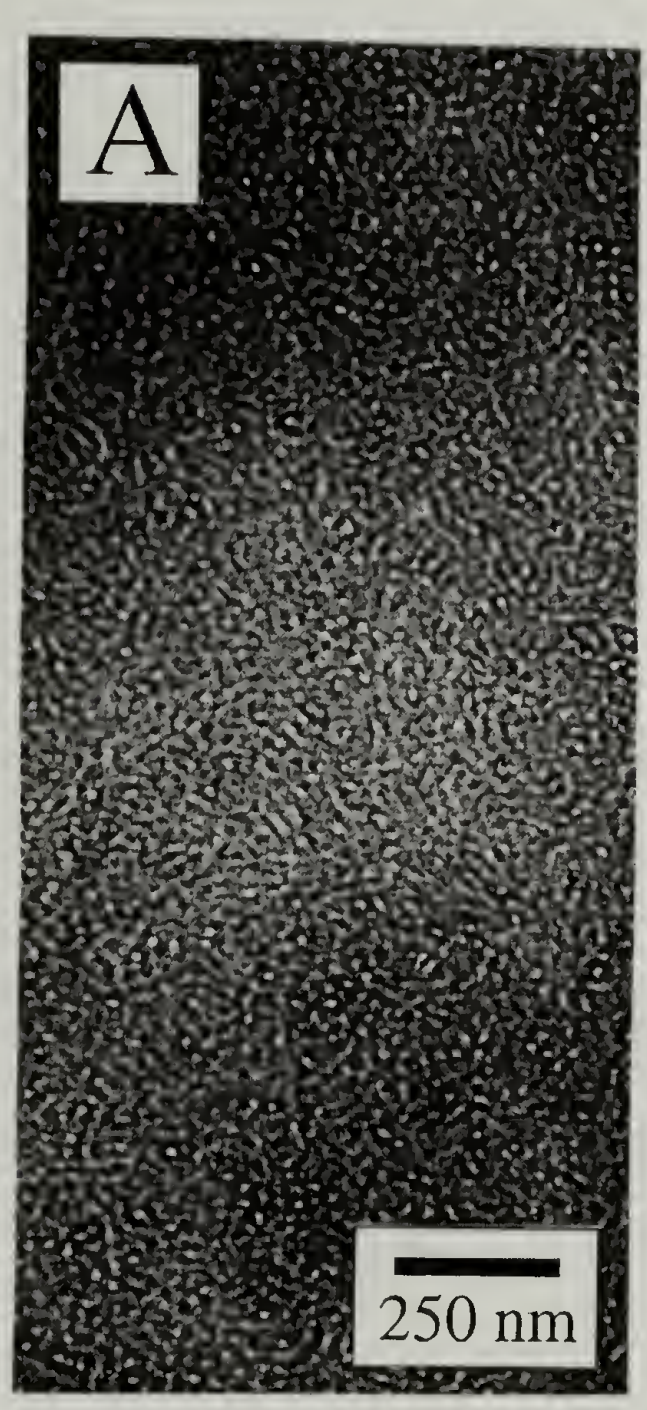

Figure 6.14. TEM micrograph for sample MG-4-4-21.

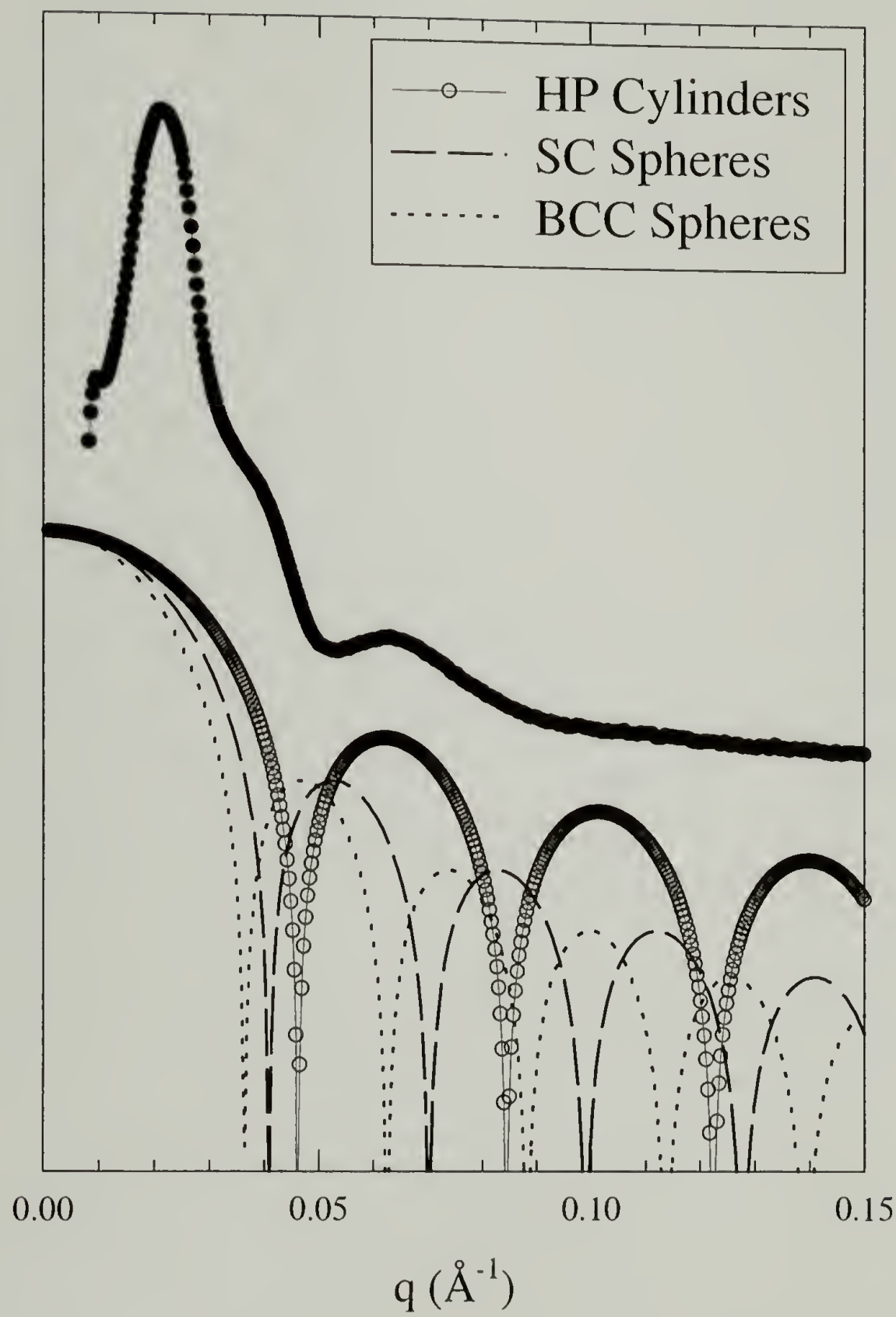

Figure 6.15. SAXS data for sample MG-4-4-21, with form factor profiles for hexagonally packed cylinders (open circles), SC spheres (dashed), and BCC spheres (dotted).

Figure 6.16. TEM micrograph for sample MG-4-7-21.

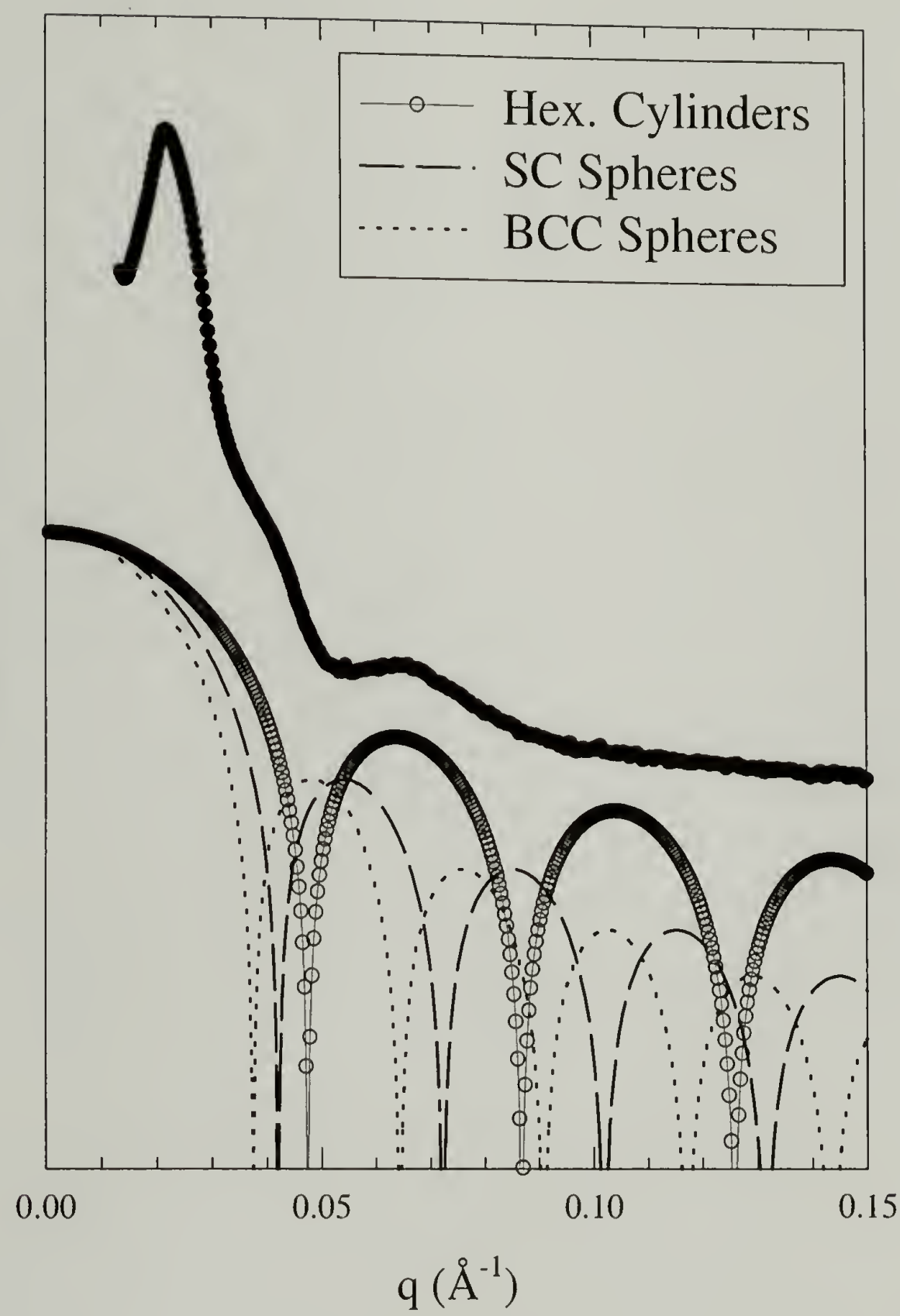

Figure 6.17. SAXS data for sample MG-4-7-21, with form factor profiles for hexagonally packed cylinders (open circles), SC spheres (dashed), and BCC spheres (dotted).

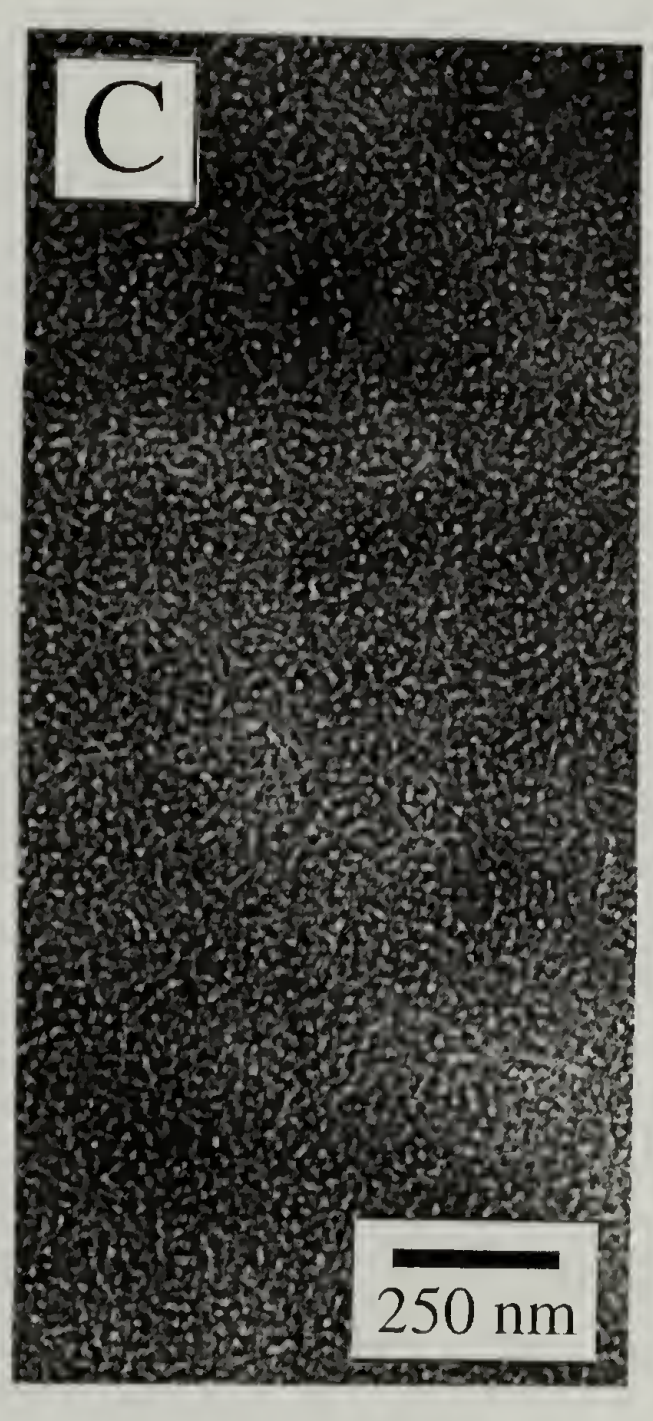

Figure 6.18. TEM micrograph for sample MG-4-9-21.

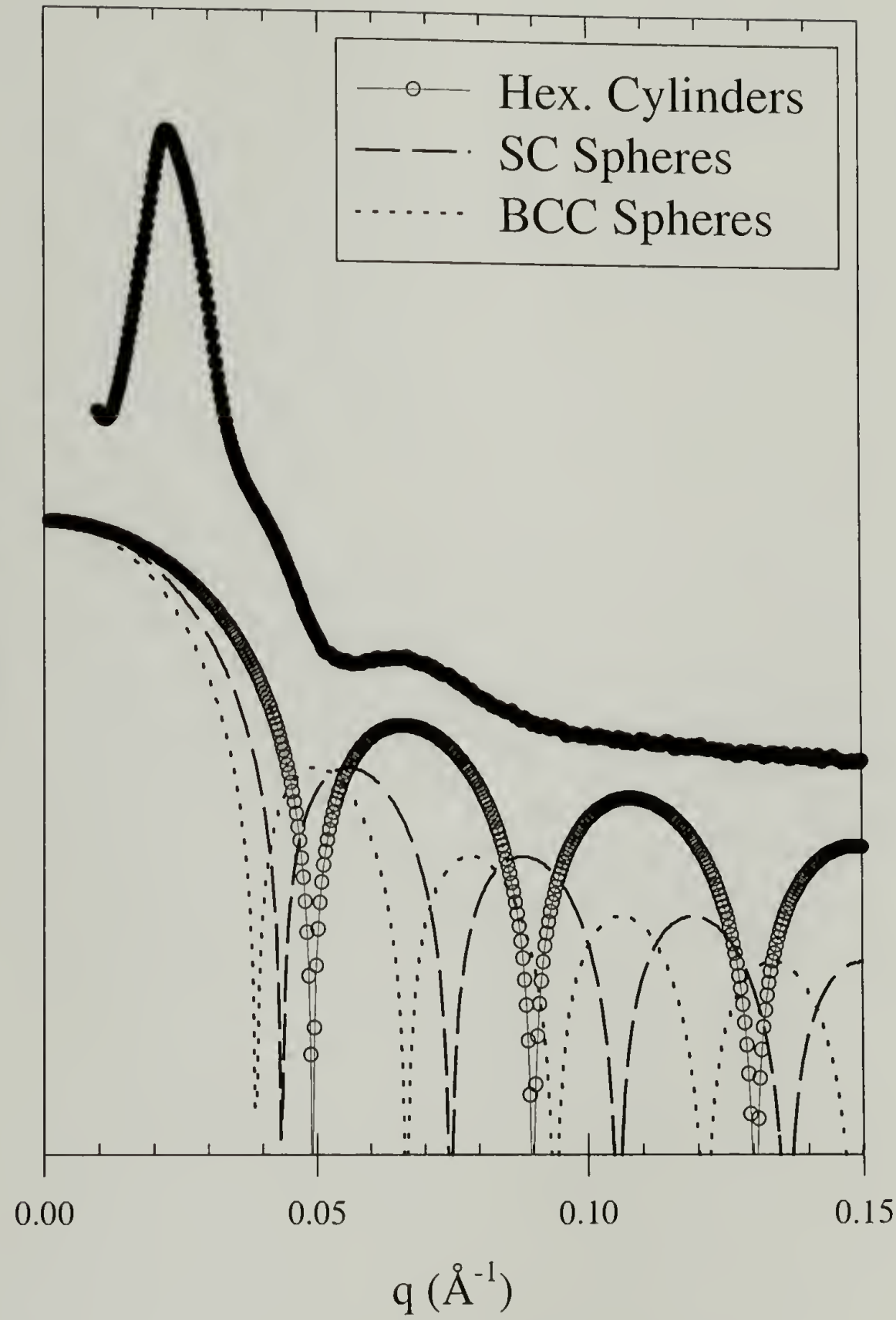

Figure 6.19. SAXS data for sample MG-4-9-21, with form factor profiles for hexagonally packed cylinders (open circles), SC spheres (dashed), and BCC spheres (dotted).

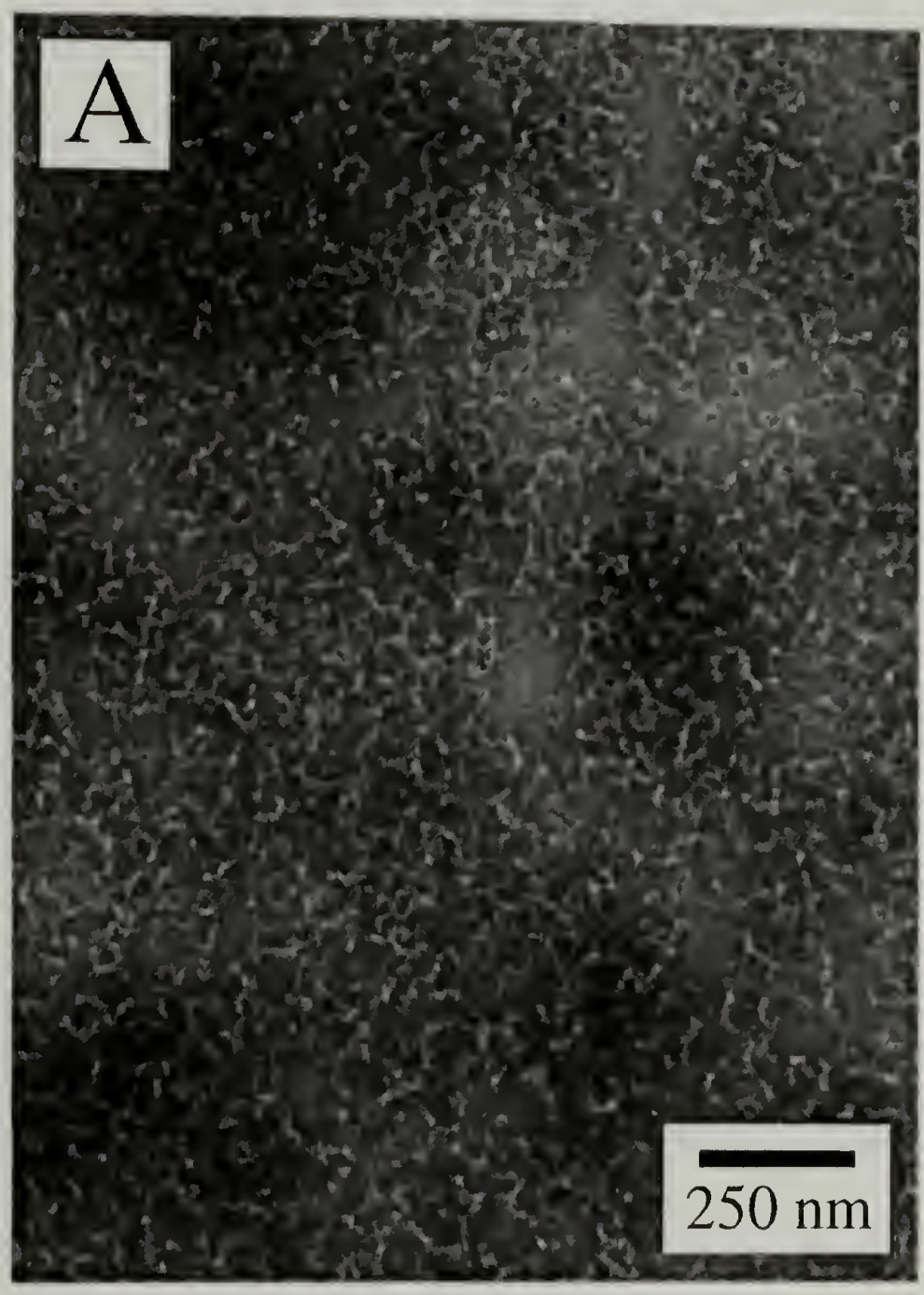

Figure 6.20. TEM micrograph for sample MG-4-4-9.

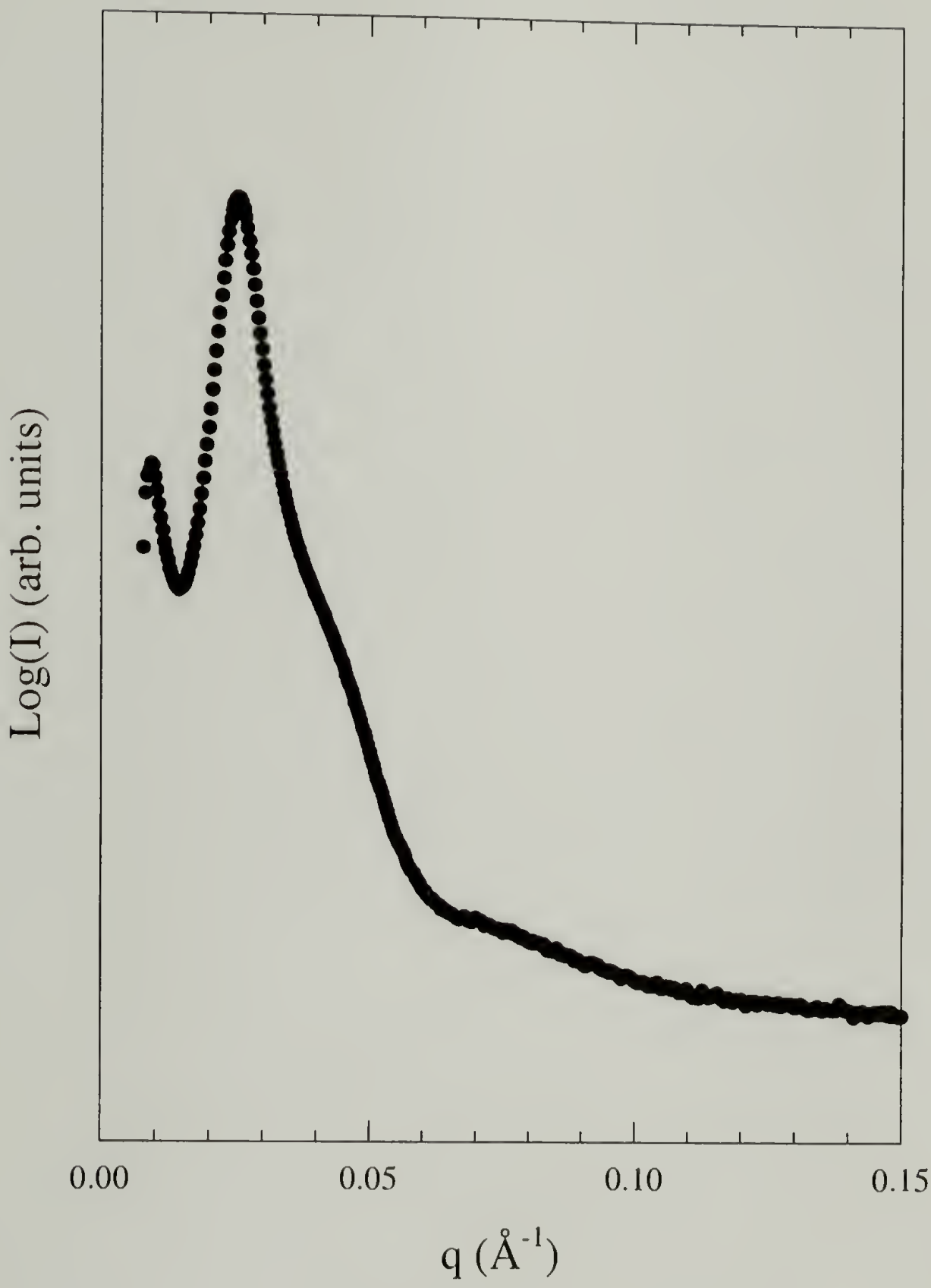

Figure 6.21. SAXS data for sample MG-4-4-9.

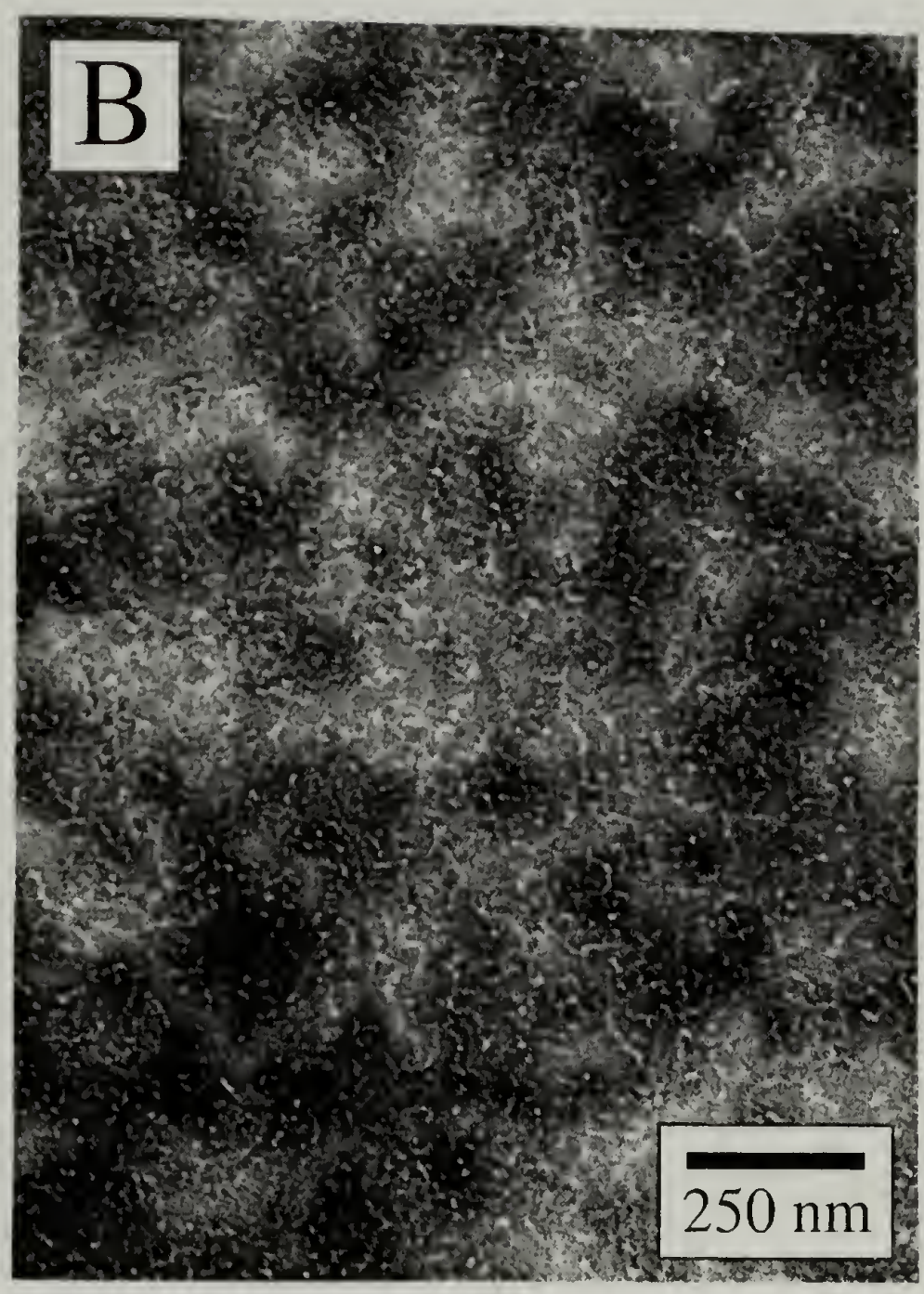

Figure 6.22. TEM micrograph for sample MG-4-8-9.

Figure 6.23. SAXS data for sample MG-4-8-9.

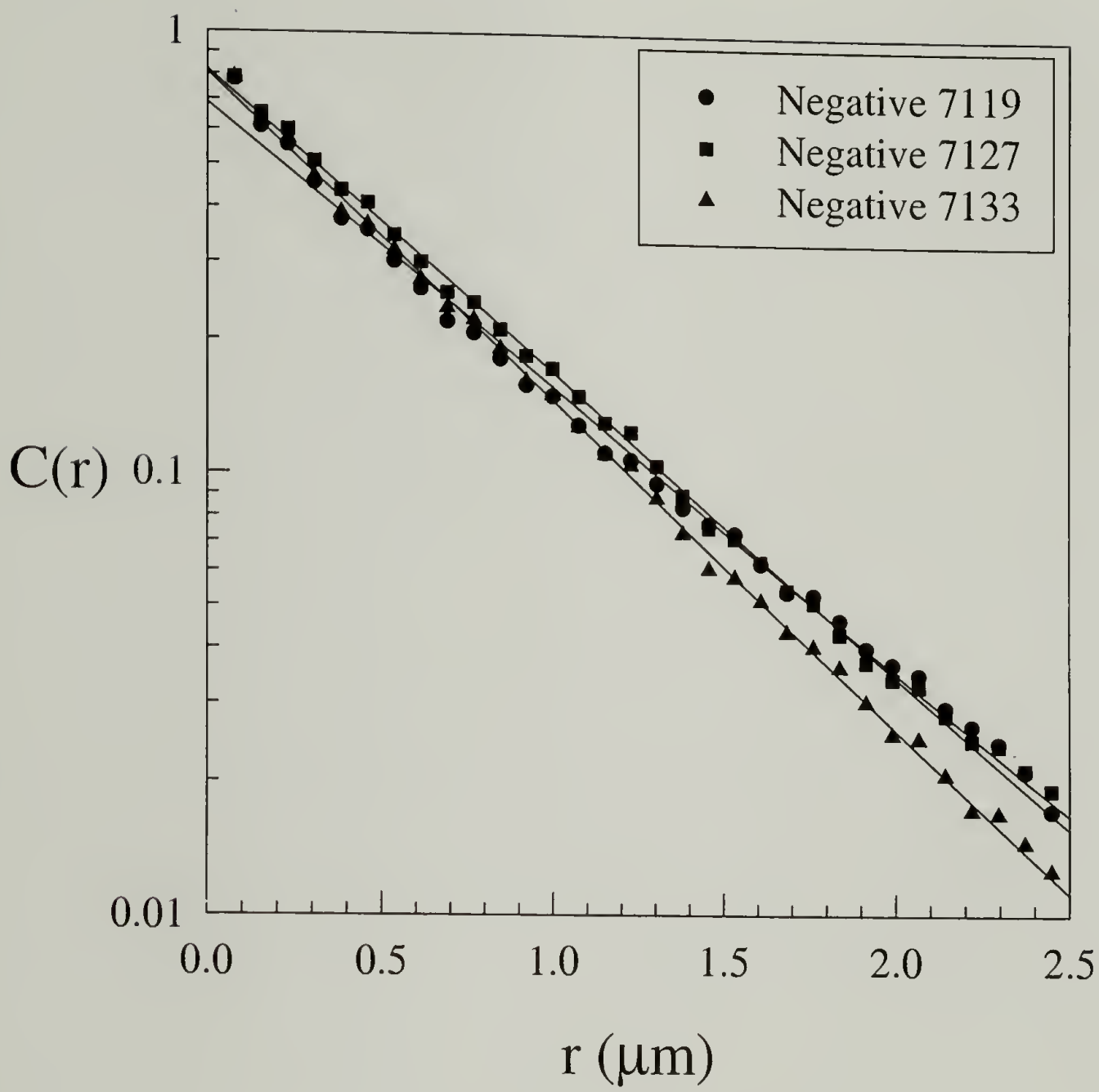

Figure 6.24. Correlation functions, C(r), for MG-4-4-36 generated using Model 2 with $\Delta\phi = 10^{o}$ from three separate micrographs.

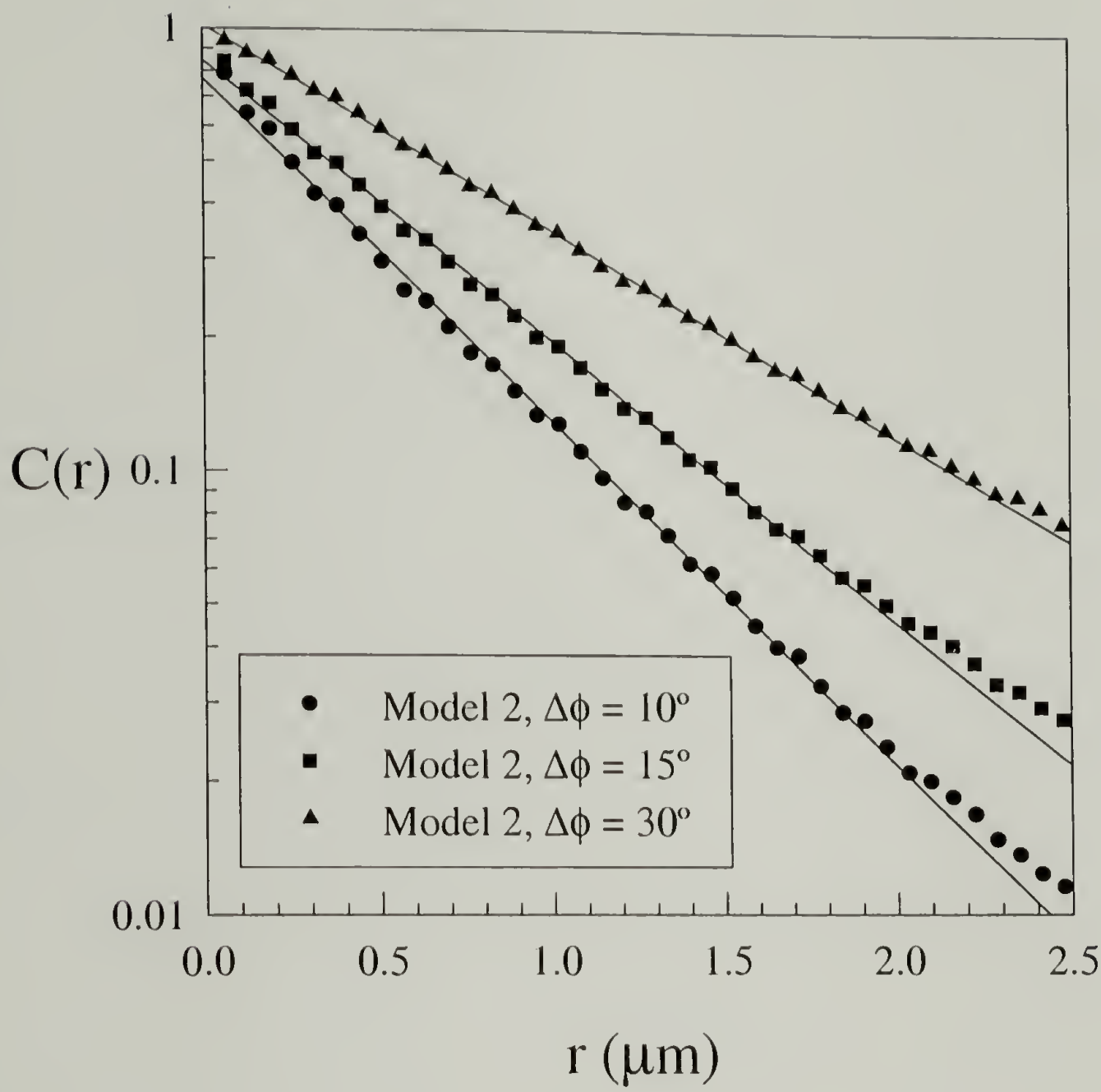

Figure 6.25. Correlation functions, C(r), for MG-4-4-36 generated using Model 2 with $\Delta\phi = 10^{\circ}$, 15°, and 30°.

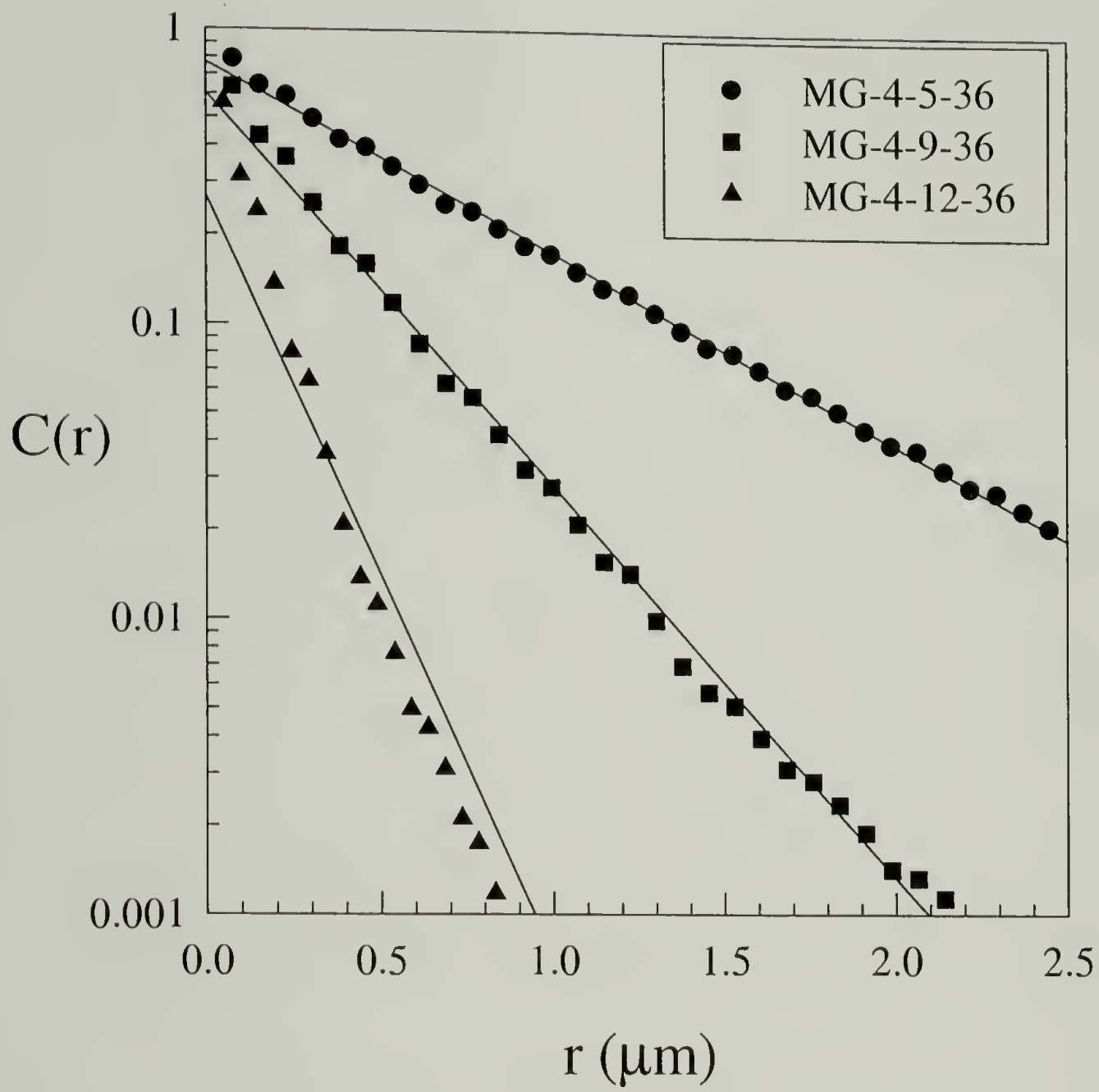

Figure 6.26. Correlation functions, C(r), generated for MG-4-4-36, MG-4-7-36, and MG-4-9-36 using Model 2 with $\Delta\phi = 10^{o}$.

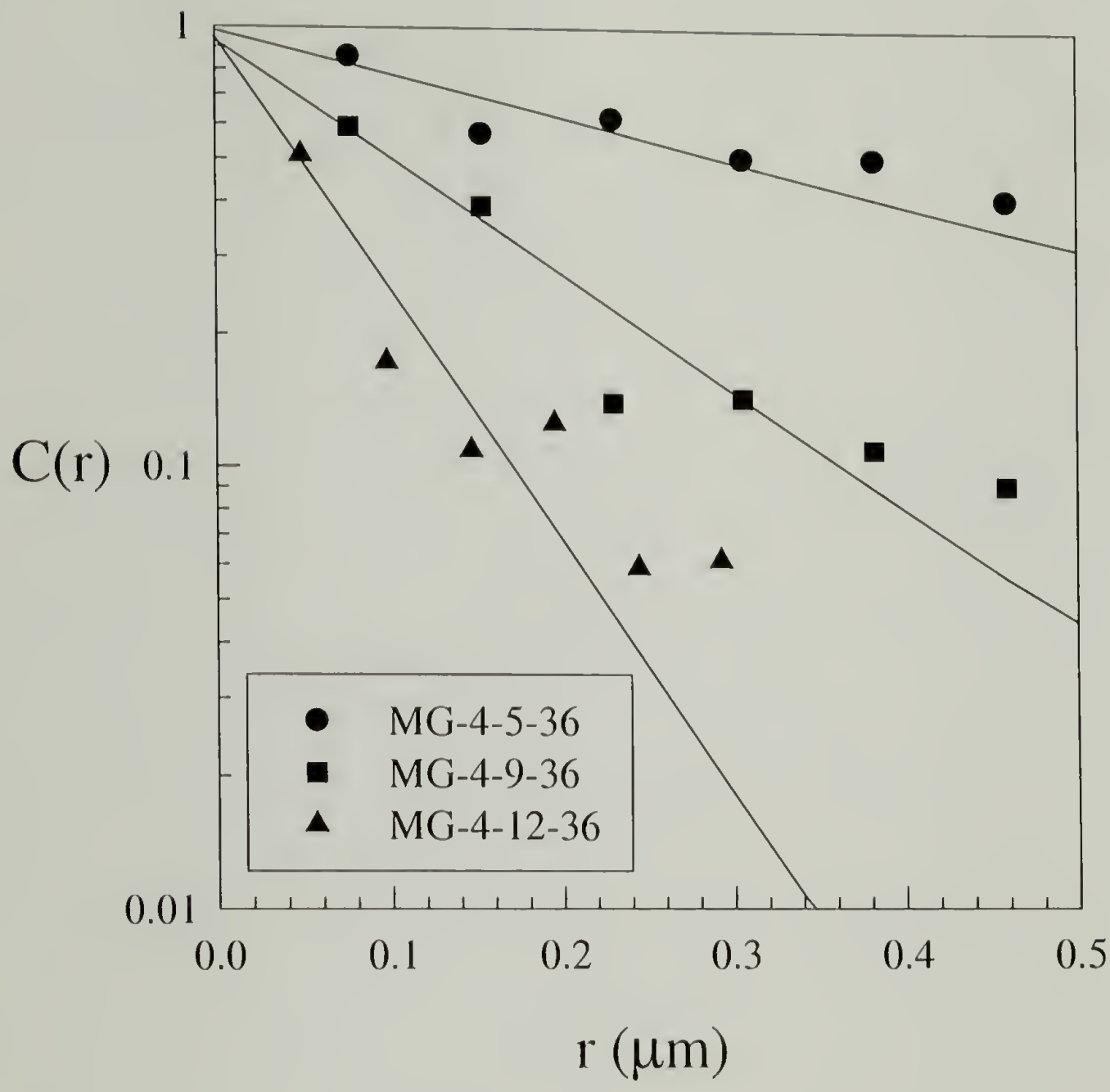

Figure 6.27. Correlation functions, C(r), for MG-4-5-36, MG-4-9-36, and MG-4-12-36 generated using Model 1.

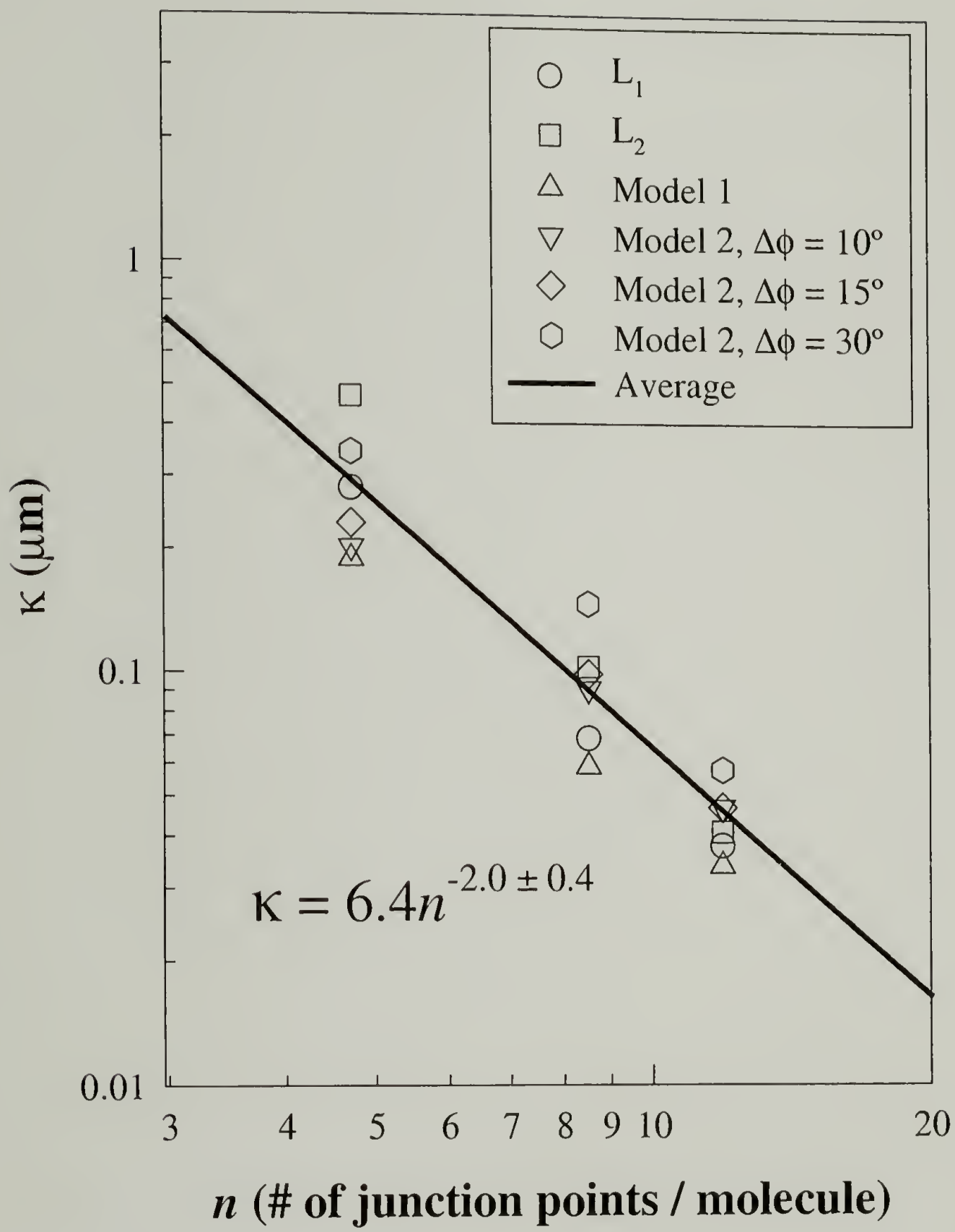

Figure 6.28. Power law fit to all correlation lengths (k) and mean intercept lengths (L) for lamellar multigrafts MG-4-5-36, MG-4-9-36, and MG-4-12-36. κ is found to scale as $n^{-2.0}$, with an uncertainty in the exponent of ± 0.4.

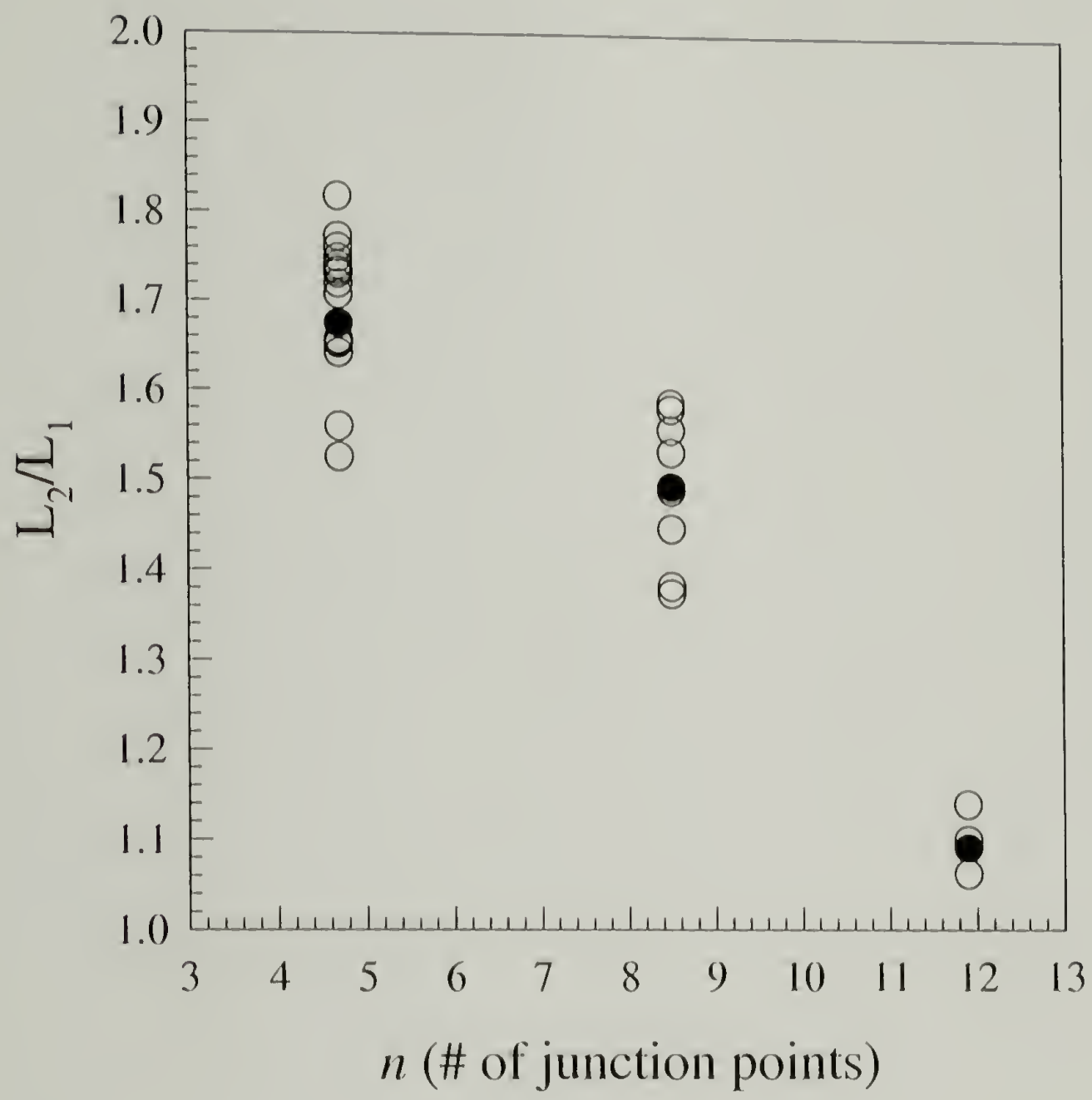

Figure 6.29. Lamellar grain aspect ratios (L_2/L_1), measured manually, given as a function of the number of junction points per molecule. Filled symbols are the average value for each sample.

CHAPTER 7

CONCLUSIONS

7.1 Miktoarm Star Block Copolymers and the Milner Model

Although the Milner model had been proven to be generally correct in its predictions for the morphological behavior of miktoarm stars, two points of contention had arisen by the start of this work. First, the predictions of the Milner theory had not been examined in the low asymmetry (ε) regime. This region, where $1 < \varepsilon < 1.5$, is the regime which is applicable to architecturally symmetric, A_nB_n-type stars. The interest in the predictions of the model for this type of molecule was largely a result of interest in modeling the behavior of tetrafunctional multigrafts with A_2B_2 miktoarm stars.

The second issue that had arisen was the ability of the model to correctly predict behavior at high levels of asymmetry. As indicated by the shaded symbols in Figure 4.2 (p. 76), evidence of a systematic overestimation of the shift in morphological behavior caused by asymmetry had emerged. Several samples at given values of ϕ and ε had been found to exhibit morphologies predicted to occur at greater ϕ or lower ε. Resolution of this issue would provide better understanding of the effects of molecular architecture on the physical behavior of miktoarm stars.

7.1.1 The Low-ε Regime

To examine the low-ε regime of the Milner model, two sets of samples were examined. A set of three A_8B_8 stars were characterized.[59] These samples are illustrated in Figure 2.1 (p. 33), and are comprised of eight PI and eight PS arms per molecule. The range of volume fraction examined by the three samples was limited, from 37 volume %

PS to only 47 volume % PS. However, having a molecular asymmetry of $\varepsilon \approx 1.2$ places these samples on the Milner diagram in the desired regime, illustrated in Figure 7.1. All three samples were predicted to form lamellar morphologies, and were confirmed by TEM and SANS to do so.

A more thorough investigation of the low-ε regime was conducted with a series of A_2B_2 stars, also composed of PI and PS (see Figure 3.1a, p. 55). There were five samples in this series, spanning a compositional range from 14 volume % PS to nearly 87 volume % PS. The location of these samples on the Milner morphology diagram is also shown in Figure 7.1. As illustrated, the samples were predicted to form a variety of morphologies, from spheres of PI in a PS matrix to cylinders of PS in a PI matrix. Three of the five samples were found to exhibit the predicted morphology. Sample A_2B_2-2, predicted to form lamellae, instead exhibited well-ordered cylinders of PS in a PI matrix. This behavior, while disagreeing with the predictions of the theory, was consistent with previous reports of discrepancies with the model. A second sample, A_2B_2-4, was predicted to form the OBDD bicontinuous morphology, but formed cylinders. This was attributed to the relative instability of bicontinuous morphologies in the SSR. Therefore, while clearly not completely accurate, the Milner model was found to predict miktoarm star behavior in this low-ε regime fairly well in general, and certainly constitutes a useful tool for interpreting the morphological behavior of A_nB_m stars of low to moderate asymmetry (ε).

A second result emerged when the data collected for the A_2B_2 stars was examined in combination with the data from the A_8B_8 stars. As first observed by Lee, Gido, and coworkers,[5] the A_nB_n molecular architecture appears to have an effect on morphological behavior as illustrated in Figure 3.13 (p. 67). In this figure, the lamellar long period (d,

Å) is plotted as a function of M_n/n, the number average molecular weight of the total molecule (A_nB_n) divided by n, the number of arms of A or B. The lamellar A_8B_8 stars, sample A_2B_2-3, an A_2B_2 star characterized by Turner and coworkers,[60] and seven lamellae-forming linear diblocks characterized by Hashimoto *et al.*[55] are included on the figure. The classical behavior of linear AB diblock domain scaling, where $d \sim N^{2/3}$, is found for the lamellar diblocks. However, the lamellar periods for all five miktoarm stars fall above the power-law fit to the AB diblock behavior.

Figure 7.2 illustrates the reason for this behavior. The increase in lamellar domain spacing can be understood by considering the effect of the junction point on the space filling behavior of the individual arms of the star. By joining two corresponding linear diblocks, whose A and B arms are the same lengths as those in the A_2B_2 star, to form an A_2B_2 star, the number of unfavorable A-B contacts at and near the junction point in increased. This, combined with simple steric interactions, increases the driving force for the arms to stretch away from the interface, resulting in an increase in lamellar period. For an A_2B_2 star, this effect is moderate. Combining eight AB linear diblocks into one A_8B_8 star has the same effect, but to a greater extent; the increase in lamellar period is more significant.

7.1.2 The High-ε Regime

To investigate the behavior of A_nB_m stars with $\varepsilon > 2.7$, and to address the apparently systematic discrepancies to predictions of the Milner model observed in earlier works, a set of samples having a high value of ε were needed. For this purpose, three A_5B stars of PI and PS were synthesized, having five short arms of PI and one long arm of PS per molecule. The A_5B stars fall in the high-ε regime, with $\varepsilon \approx 4.4$. The

results of the characterization of the A_5B stars of PI and PS are also illustrated in Figure 7.1. While not examining a broad range of volume fraction, the samples fall in a complicated region of the diagram, and are predicted to form morphologies ranging from cylinders of PS in a PI matrix to lamellae.

All three samples were found to form lamellae. This finding confirmed the expectation that the previously reported deviations from predicted morphological behavior are systematic, and appear to become increasingly large as molecular asymmetry increases. A second interesting observation for these materials was that the long-range order exhibited for these lamellar materials is profound, with a minimum of seven Bragg reflections exhibited in SAXS.

Taken with the data for the A_2B_2 stars and previously published data for A_2B and A_3B miktoarm stars,[1,2,9] a pattern of discrepancies was clearly developed. As architectural and conformational asymmetry increase, the Milner model overestimates the effect of these asymmetries on morphological behavior. These discrepancies may also be considered in terms of the effective molecular asymmetry, ε', of a sample which exhibits a morphology other than that predicted, where ε' is the value of ε which brings the observed behavior into agreement with predicted behavior at the specific volume fraction of the sample. This effect is illustrated in Figure 4.10 (p. 84) by considering $\Delta\varepsilon = \varepsilon - \varepsilon'$ as a function of ε. The maximum $\Delta\varepsilon$ increases with increasing ε.

The cause of this effect is not revealed conclusively by the data collected in this work. However, two omissions from the Milner model which may account for part of this overestimation have been identified. First, the confinement of more than two polymer blocks to a single junction point alters the conformational (chain stretching) behavior of the arms in the star. Conclusive evidence for this may been seen in Figure

3.13 (p. 67) and is discussed above. Additionally, the Milner model accounts for conformational behavior simply by the calculation of the term l_i, where $l_i = (V_i/R_i^2)^{1/2} = (v_i/b_i^2)^{1/2}$. In this formulation, the measures of segmental volume, v_i, and statistical segment length, b_i, are based on measurements for neat component i in the bulk. Thus, the calculation of molecular asymmetry, ε, neglects not only the effect of the components being part of a block copolymer, but the additional effects of the junction point in a miktoarm star are neglected entirely.

The Milner model also incorrectly models the junction point of the miktoarm star in a second manner. The Milner model is based on polymer brush theory and applies concepts of polymer brush theory to describe the manner in which the individual polymer blocks (arms) are "attached" to the interface between microphase separated domains. The height of the brush is calculated, which in turn determines the height of the Gaussian wedge, the location of the interface between microphase separated domains, and thus the interfacial contribution to the free energy of the system. While adequate, an apparently important detail is neglected in this calculation. Figure 7.3a shows a schematic of the molecule actually modeled in this way. The method by which the star arms are added to the appropriate side of the interface represents not a miktoarm star, with arms grafted together at a single junction point, but rather a star whose arms are attached simply to the interface between domains, as in a polymer brush.

The effect of the junction point, then, is illustrated by comparing Figure 7.3b with Figure 7.3a. Bringing both the arms on one side of the interface together at the same junction point affects the conformational statistics of the component blocks. This results in increased chain stretching, which raises the free energy of the morphology, but allows the curvature of the interface to decrease. The effect is manifest on the Milner

morphology diagram by evidence of a less dramatic shift in the volume fraction ranges at which the classical morphologies are observed. Alternatively, the molecular asymmetry of a given molecular (ε) is actually less than that calculated by the Milner model.

7.1.3 Proposed Research

The results of these studies of miktoarm star morphological behavior lead to several interesting questions. First, regarding the effect of the junction point of the conformational behavior of the component arms in the miktoarm star block copolymers, limited data is available. Only three lamellar A_8B_8 stars and two lamellar A_2B_2 stars have been examined. This gives rise to two questions. If one considers the effect of the junction point on the conformational statistics of A_nB_n-type miktoarm stars, the effect may reasonably by viewed as a local effect. This concept is illustrated in Figure 7.2. To minimize the unfavorable segmental contacts created by bringing $2n$ polymer chains of A and B together at a single junction point, the chains stretch immediately away from the interface. However, at some distance from the interface, the chains are no longer affected by the unfavorable enthalpic interactions with the opposite component material, and so can logically be expected to return to a more bulk-like conformational state. As the molecular weight of the arms in the star increases, the contribution to the total lamellar period of the highly stretched chain segments near the interface becomes less and less. When considered in terms of lamellar period as a function of M_n/n, for $n > 1$, the behavior should approach that of linear diblocks asymptotically as M_n/n increases. This result is predicted in Figure 3.13 (p. 67). However, with only 3 data points for A_8B_8 stars, and 2 for A_2B_2 stars, the fit of the exponentially decaying deviation from the

power-law behavior of linear AB diblocks is strictly hypothetical. In fact, even the actual behavior of these A_nB_n-type systems is not necessarily strictly certain.

To fully investigate this behavior, two sets of lamellar A_nB_n stars, with n constant, over a range of total M_n. If a sufficient number of samples could be examined, the functional form of lamellar period for A_nB_n stars with $n > 1$ might be revealed. For example, examining a series of A_8B_8 stars of PI and PS having a composition of 50 volume % PS, and total molecular weights of 100,000 g/mol, 200,000 g/mol, 400,000 g/mol, 500,000 g/mol, and 600,000 g/mol, as well as a set of A_2B_2 stars also of 50 volume % PS, would provide data with which to consider this question.

A second interesting question which arises from Figure 7.3 is that of the scaling of lamellar period with n, rather than M_n/n. To date, only AB, A_2B_2, and A_8B_8 stars have been characterized. From this data, the effect of increasing n on lamellar period appears to diminish as n increases. To examine this behavior, an appropriate series to examine would be a series of A_nB_n stars where the molecular weights of the A and B component blocks are held constant while n is increased, i.e. a series comprised of an A_2B_2 star, A_3B_3 star, A_4B_4 star, and so on, with the lengths of A and B constant throughout the series.

In addition to a straightforward morphological study of these materials, utilizing microscopy and small-angle scattering techniques to characterize morphology, these materials might also exhibit interesting behavior regarding the thickness of the interface between the microphase separated domains of A and B. Recent work by Anastasiadis and coworkers[105] indicates that the presence of additional blocks of polymer at the interface may cause the interface thickness to decrease. Such a series of samples would be ideal for considering this question. The effect could be studied using neutron

reflectivity techniques, which are sensitive to interfaces between domains of different neutron scattering length densities, such as between PI and P(d-Styrene).[106]

Finally, regarding the Milner model, the main task of exploring the morphological behavior of miktoarm stars has been accomplished. However, a complete examination of a high-ε set of samples, such as the A_5B stars, has not been finished. A_5B stars of PI and PS should be synthesized which complete the study begun in this work. The best results will be obtained by examining a large set of samples having controlled architectures and low polydispersity. The closer the samples are in volume fraction to one another, the more accurate the understanding of the morphological behavior in this regime will be.

7.2 Multigraft Block Copolymer Morphological Behavior

The central results from the study of multiple-graft block copolymers involve the validity of the constituting block copolymer hypothesis as a tool for predicting morphological behavior, the effects of architectural heterogeneity on multigraft self-assembly, and the observation of domains having specific shapes but not forming ordered arrays.

7.2.1 Constituting Block Copolymer Hypothesis

The constituting block copolymer hypothesis argues that the behavior of molecules with complex molecular architectures is governed by the behavior of the smaller architectural subunits comprising the larger architecture. The first result illustrating this is the agreement between observed behavior of the multigrafts and the predictions made using existing theory. In the case of the tetrafunctional regular multigrafts, agreement was found for seven of ten samples examined. The behavior of

two samples agreed explicitly with the predicted behavior. Partial agreement, where domains of the predicted shape were formed but not arrayed on a lattice, was found for five regular multigrafts. The remaining three samples formed a disordered morphology and, in the case of samples MG-4-4-9 and MG-4-8-9, an unusual "mesh" morphology. The behavior of these three samples is reasonable given the very asymmetric compositions for those with 9 volume % PS, and the high molecular weight of sample MG-4-12-36. For the random multigrafts, both trifunctional and tetrafunctional series produced good agreement with predicted behaviors. Although only lamellar morphologies were observed with appreciable long-range order, eight of the nine regular multigrafts formed a minimum of domain shapes in agreement with the predicted behavior.

The second result confirming the constituting block copolymer hypothesis was the self-consistent behavior observed for tetrafunctional, regular multigrafts. The synthesis of these materials produces samples which have the same volume fraction and constituting block copolymer, but a distribution in the number of constituting block copolymer subunits per molecule. The high molecular weights of the PI connector blocks and PS arms in these materials allow them to be fractionated according to the number of constituting block copolymer units per molecule. Because the different fractionations have the same constituting block copolymer, they are predicted to have the same morphological behavior.

This was found to be true. As shown in Table 6.3 (p. 150), for each volume fraction of regular multigrafts, the behavior of the samples is self-consistent. Where the morphological behavior is not predicted by the Milner model, such as for the two samples

having 9 volume % PS, the behaviors of these two samples are consistent even while disagreeing with the predictions of the model.

These two studies, particularly when combined with earlier studies of double-grafts, clearly establish the constituting block copolymer hypothesis as a valid and useful tool for predicting the morphological behavior of block copolymers whose architectures may be considered to be combinations of simpler architectural building blocks.

7.2.2 Disordered Arrangements of Specific Domain Shapes

In both studies of multigraft morphological behavior, small-angle scattering evidence was found indicating the formation of domains with specific shapes but without any lattice ordering. The evidence for such behavior was always the observation of a strong scattering maximum, usually with a shoulder at slightly higher q, followed by a broad, weak secondary maximum. The location of this secondary maximum was typically at approximately $2\frac{1}{2} \cdot q^*$, where q^* is the scattering angle of the primary reflection. Figure 5.15 (p. 123) illustrates this characteristic scattering behavior. Such scattering has been observed previously for diblocks which form spheres and blends of block copolymer and homopolymer which form spherical micelles,[67,68] but attempts to model the scattering behavior of the multigrafts in this way proved unsatisfactory. However, it was possible to compare the SAXS data collected for the multigrafts exhibiting this characteristic behavior to form factor scattering profiles generated for spheres and cylinders.[66] By measuring domain diameters directly from real space images of the morphology, or by using $2\pi/q^*$ as a lattice constant and assuming a specific packing of domains (hexagonal cylinders, BCC spheres, SC spheres), form factor scattering profiles were generated. Comparisons of these scattering profiles with SAXS

data in each case indicated that, although long-range order was not achieved, self-assembly into domains of specific shapes was occurring. In each case, the most favorable comparison was to the form factor scattering from the domain shape predicted using the constituting block copolymer hypothesis.

For both random and regular multigrafts, lamellar morphologies were observed, where formed, to exhibit appreciable long-range order. However, only two samples forming non-lamellar morphologies exhibit similar long-range order. These samples formed cylindrical morphologies. An explanation for this behavior derives from the incompressibility boundary condition and in the process of mesophase self-assembly. The formation of a lamellar domain is unique in that any lamellar domain acts as a very effective template, guiding the self-assembly of adjacent lamellae so that their orientation is the same as the original lamella. The results in the growth of an automatically well-ordered morphology. This characteristic is reflected in both the anisotropic shape of lamellar grains and in the anisotropic nature of lamellar grain growth.[100,101] Non-lamellar domains such as cylinders and spheres are unlike lamellae in that they can form and fill space while not arranged on a lattice. While not the most efficient way to fill space, for a system that has high molecular weight or a complex architecture that may impede molecular motion such as reptation, the efficiency of the spatial arrangement is less important than incompressibility.

7.2.3 Effect of Architectural Variables on Self-assembly

The effects of two architectural variables on multigraft morphological behavior were considered in this work, as illustrated in Figure 1.3 (p. 15). Branch point functionality (trifunctional versus tetrafunctional) and the effects of branch point location

(regular versus random) were considered. Practical difficulties prevented an examination of multigraft block copolymers with regularly placed, trifunctional branch points. These materials are currently being synthesized, using the same technique which allowed synthesis of regular multigrafts having tetrafunctional branch points, by Kunlun Hong at the University of Alabama at Birmingham. These materials will provide much needed information for a more complete understanding of multigraft behavior.

However, the effect of branch point regularity on self-assembly is noticeable in the data currently available. The lack of well-ordered non-lamellar morphologies was noted and described above. Two samples did form non-lamellar morphologies with appreciable long-range order. These materials were regular multigrafts with 67 volume % PS, MG-4-10-97 and MG-4-14-67. The observation of hexagonally packed cylindrical domains indicates that multigrafts with regularly placed branch points are more capable of forming well-ordered, non-lamellar morphologies than are similar multigrafts with randomly placed branch points. The closest random multigraft to which this behavior may be compared is RMG-4-4-61, which formed a microphase separated but disordered morphology with cylindrically shaped domains.

Several factors complicate this comparison. First, the random multigraft is calculated to be intermediately segregated, with $\chi N \approx 44$, while the regular multigrafts are expected to be strongly segregated ($\chi N > 100$). This difference may account for the relative disorder of the random multigraft. Second, the number of branch points per molecule differs between the regular and random multigrafts. The random multigraft has only four constituting block copolymer units per molecule while the regular multigrafts have seven and ten. This difference favors the deleterious effect of randomly located branch points. As observed in Chapter 6, multigrafts with fewer the branch points form

more well-ordered the morphologies. Only a regular multigraft with four constituting block copolymer units per molecule would allow direct comparison, but such a multigraft would reasonably be expected to form very well ordered cylinders, indicating that randomly located branch points inhibit self-assembly.

The second architectural variable, the effect of branch point functionality, is more difficult to discern from the present data. Direct comparison between samples having trifunctional and tetrafunctional branch points is limited due to the lack of trifunctional, regular multigrafts. Based only on the behavior of the random multigrafts characterized in this work, one must conclude that branch point functionality does not significantly impact the ability of multigrafts to self-assemble.

7.2.4 Long-range Order and Lamellar Grain Anisotropy

Finally, an interesting relationship between the number of constituting block copolymer units per molecule and the long-range order exhibited by that sample was found. Although the morphological behavior of the constituting block copolymer was shown to govern the morphological behavior of the multigraft, the number of constituting block copolymer units per molecule is correlated with the long-range order obtained by that sample. Comparison of samples having the same constituting block copolymer, but in different number, such as between samples MG-4-5-36, MG-4-9-36 and MG-4-12-36, revealed that as the number of constituting block copolymers increases, grain size (or long-range order) diminishes. This observation was be attributed directly to the kinetic barriers to self-assembly that arise as molecular weight increases.

However, it was also found that the lamellar grains were anisotropic in shape, having a larger dimension in the direction normal to the plane of the lamellae. In this

case, an interesting correlation between anisotropy and number of constituting block copolymer units per molecule was revealed. As shown in Figure 6.29 (p. 180), the lamellar grains become more anisotropic as the number of constituting block copolymer units per molecule decreases. Because the samples with higher numbers of constituting block copolymer units per molecule are essentially in a kinetically trapped, non-equilibrium state, this is equivalent to the grains becoming more anisotropic as they grow.

7.2.5 Proposed Research

The lingering questions concerning the morphological behavior of multigraft block copolymers considered in this work can be answered largely by completion of the investigation of the behavior of regular multigrafts with trifunctional branch points. A set of samples spanning a significant range of volume fraction should be synthesized in such a manner to that the number of possible comparisons to existing data is maximized. First, the samples should be designed so that their constituting block copolymers are strongly segregated ($\chi N > 100$). Second, if possible no fewer than five volume fractions should be considered, ideally matching those of the A_2B stars characterized by Pochan, Gido, and coworkers.[1] While there is little question that the constituting block copolymer argument is a successful tool for predicting and interpreting morphological behavior, prudence dictates that where possible, existing literature and data should be used to the fullest advantage. Finally, care should be taken to fractionate species having different numbers of constituting block copolymers so that the polydispersity of the fractionated samples is minimized, and if possible at least three viable fractionations are available for each volume fraction.

This series of samples should provide useful information on many of the results and questions posed by the work presented in this work. The effect of branch point functionality should become clear from comparison with data from the tetrafunctional regular multigrafts. The effect of regular branch point location will be best understood if samples having five branch points per molecule can be isolated for direct comparison with the existing data from the RMG-3-5-ϕ series.

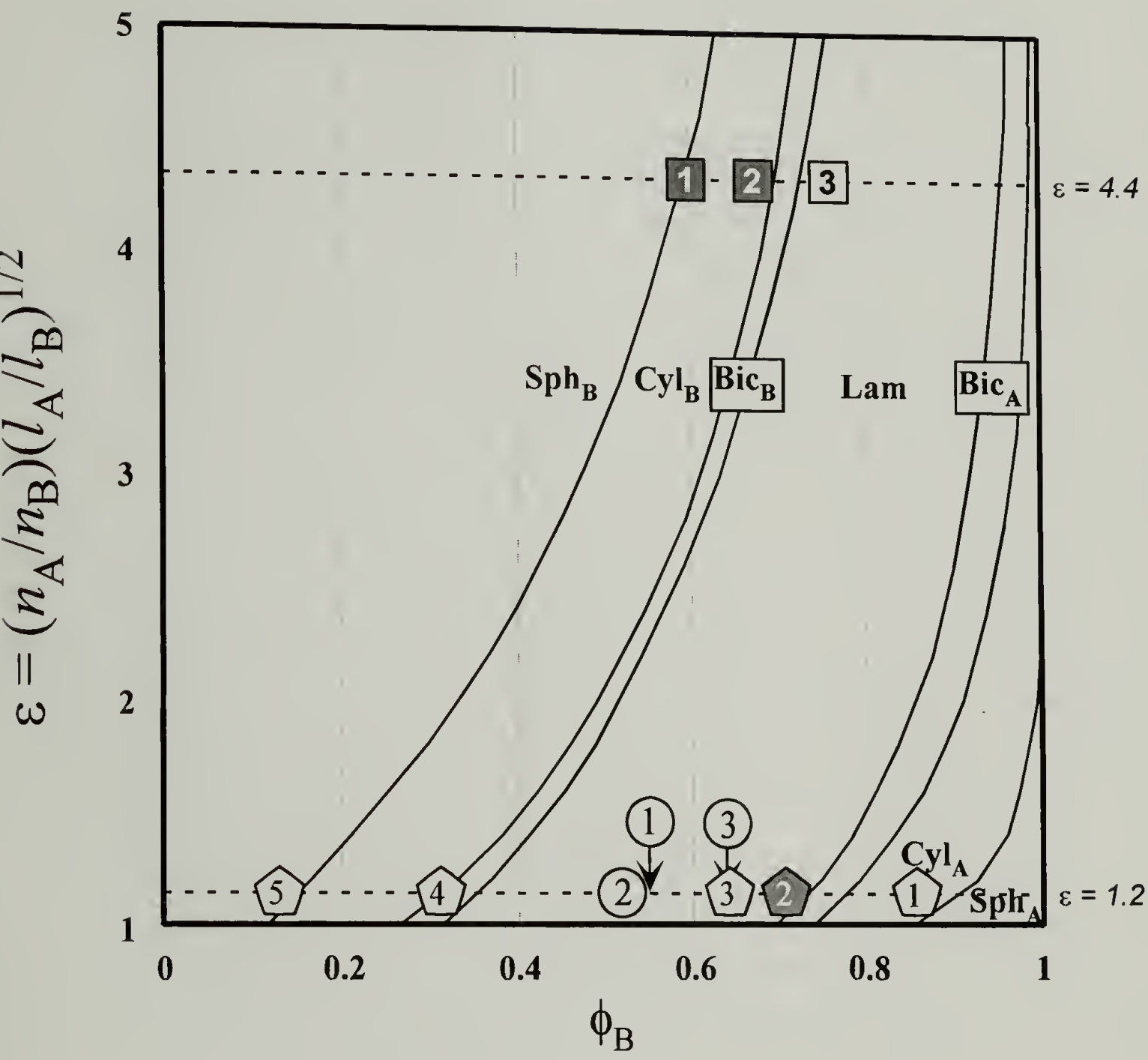

Figure 7.1. Milner morphology diagram showing the locations of the A_8B_8 Vergina stars, A_2B_2 stars, and A_5B stars examined in this work. Shaded symbols represent samples which exhibited morphologies other than that predicted by the model. A_2B_2 stars are represented by pentagons, Vergina stars by circles, and A_5B stars by squares.

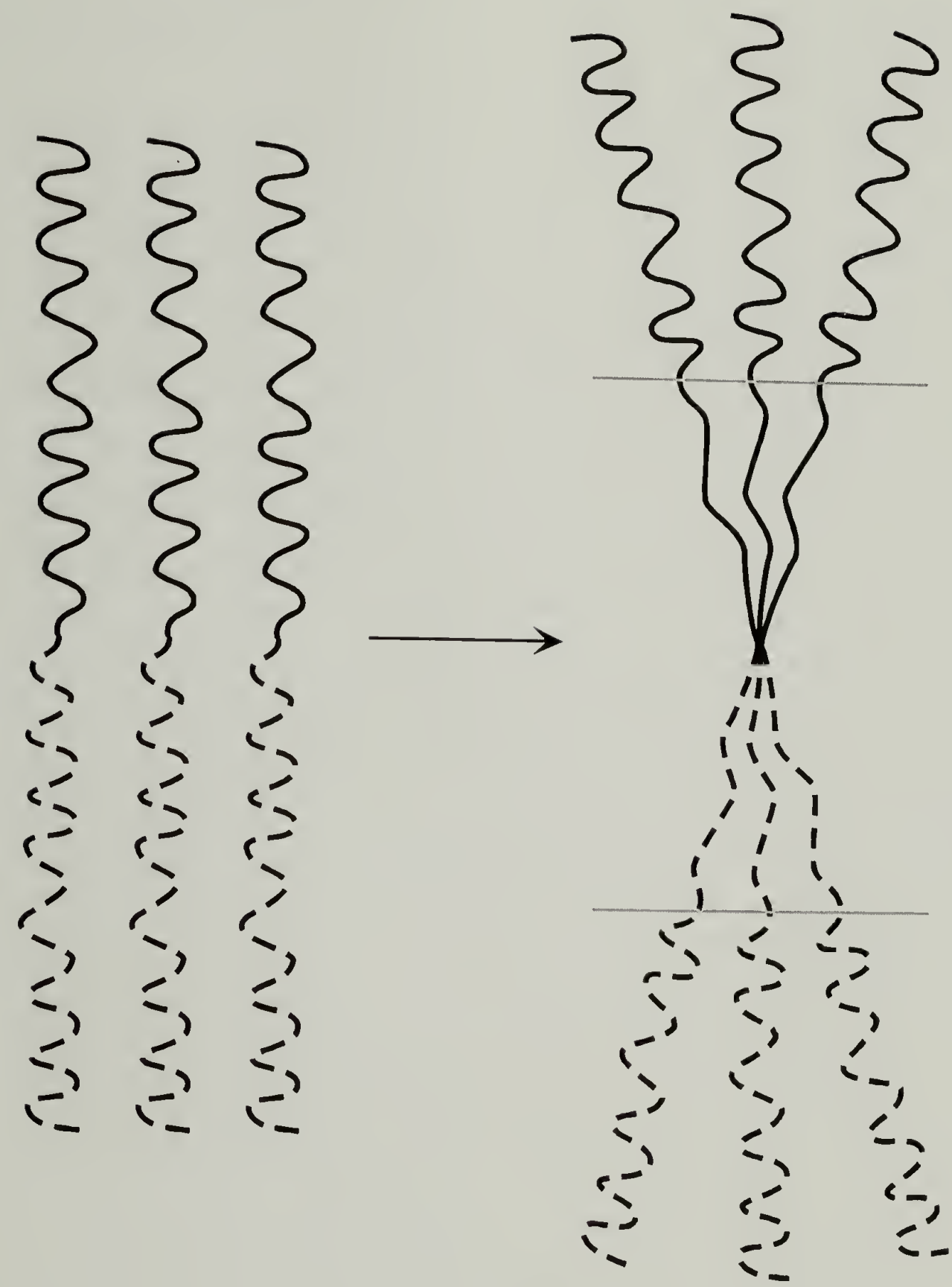

Figure 7.2. Illustration of the effect of the junction point on the conformational behavior of the A and B component arms in an A_nB_n miktoarm star where $n = 3$. The gray lines represent the boundaries of the region in which the effect of the junction point is felt.

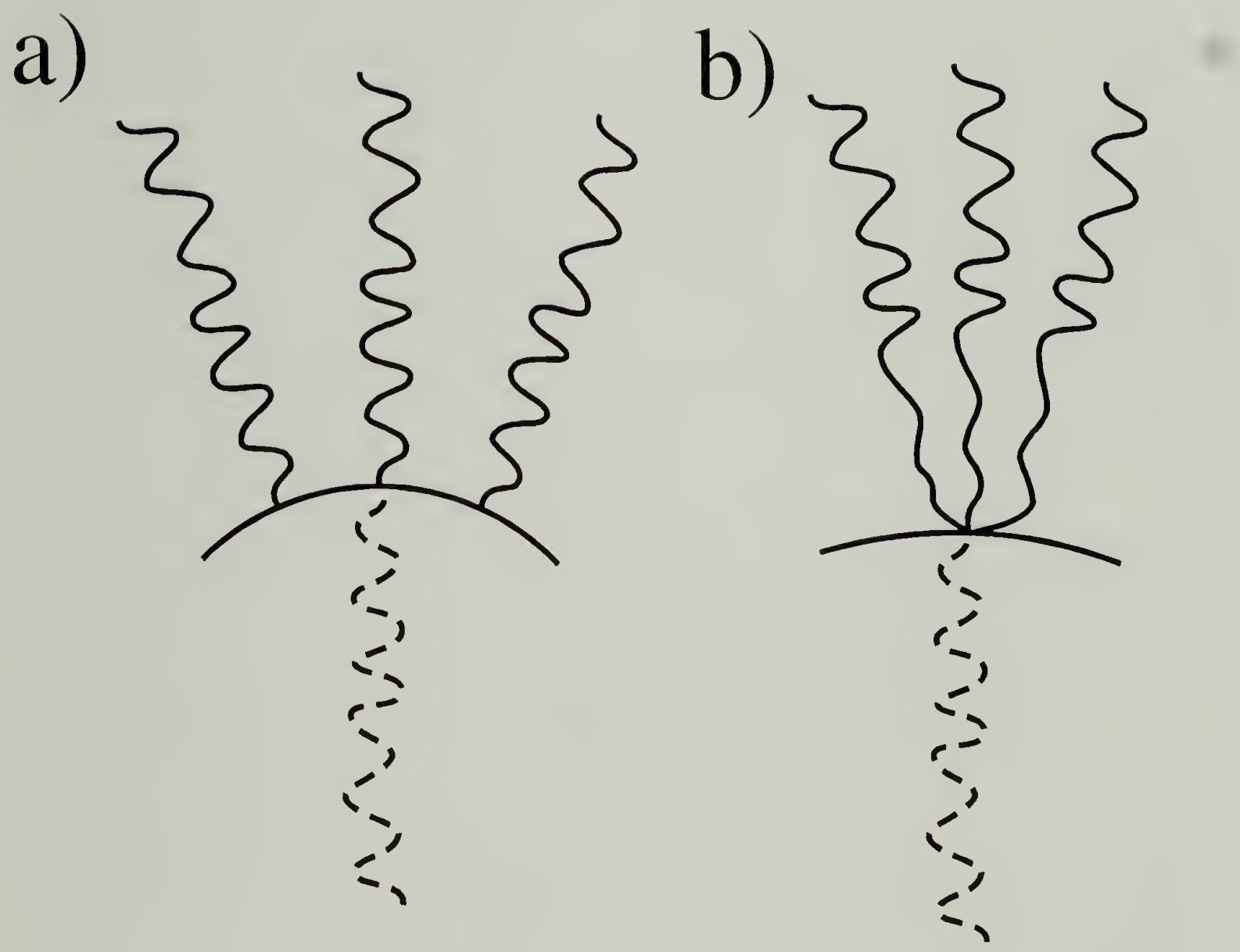

Figure 7.3. Illustration of a) the manner in which the Milner model represents an A_3B star when calculating free energy for a given Gaussian wedge, and b) a more realistic representation of the same miktoarm star.

BIBLIOGRAPHY

(1) Pochan, D. J.; Gido, S. P.; Pispas, S.; Mays, J. W.; Ryan, A. J.; Fairclough, J. P. A.; Hamley, I. W.; Terrill, N. *Macromolecules* **1996**, *29*, 5091.

(2) Hadjichristidis, N.; Iatrou, H.; Behal, S. K.; Chludzinski, J. J.; Disko, M. M.; Garner, R. T.; Liang, K. S.; Lohse, D. J.; Milner, S. T. *Macromolecules* **1993**, *26*, 5812.

(3) Lee, C.; Gido, S. P.; Pitsikalis, M.; Mays, J. W.; Beck Tan, N.; Trevino, S. F.; Hadjichristidis, N. *Macromolecules* **1997**, *30*, 3732.

(4) Lee, C.; Gido, S. P.; Poulos, Y.; Hadjichristidis, N.; Beck Tan, N.; Trevino, S. F.; Mays, J. W. *Polymer* **1998**, *39*, 4631.

(5) Lee, C.; Gido, S. P.; Poulos, Y.; Hadjichristidis, N.; Beck Tan, N.; Trevino, S. F.; Mays, J. W. *J. Chem. Phys.* **1997**, *107*, 6460.

(6) Matsushita, Y.; Noda, I. *Macromol. Symp.* **1996**, *106*, 251.

(7) Hadjichristidis, N. *J. Polym. Sci., Pt. A: Polym. Chem.* **1999**, *37*, 857.

(8) Milner, S. T. *Macromolecules* **1994**, *27*, 2333.

(9) Tselikas, Y.; Iatrou, H.; Hadjichristidis, N.; Liang, K. S.; Mohanty, K.; Lohse, D. J. *J. Chem. Phys.* **1996**, *105*, 2456.

(10) Noshay, A.; McGrath, J. E. *Block Copolymers: Overview and Critical Survey*; Academic Press: New York, 1977.

(11) Odian, G. *Principles of Polymerization*; 3rd ed.; John Wiley & Sons: New York, 1991.

(12) Shinozaki, A.; Jasnow, D.; Balazs, A. C. *Macromolecules* **1994**, *27*, 2496.

(13) Lyatskaya, Y.; Gersappe, D.; Balazs, A. *Macromolecules* **1995**, *28*, 6278.

(14) Lyatskaya, Y.; Balazs, A. *Macromolecules* **1996**, *29*, 7581.

(15) Lyatskaya, Y.; Gersappe, D.; Gross, N. A.; Balazs, A. C. *J. Phys. Chem.* **1996**, *100*, 1449.

(16) Xenidou, M.; Hadjichristidis, N. *Macromolecules* **1998**, *31*, 5690.

(17) Iatrou, H.; Mays, J. W.; Hadjichristidis, N. *Macromolecules* **1998**, *31*, 6697.

(18) Atkins, P. W. *Physical Chemistry*; 5th ed.; W. H. Freeman and Company: New York, 1994.

(19) Bates, F. S.; Frederickson, G. H. *Ann. Rev. Phys. Chem.* **1990**, *41*, 525.

(20) Frederickson, G. H.; Bates, F. S. *Ann. Rev. Mat. Sci.* **1996**, *26*, 501.

(21) Hamley, I. W.; Koppi, K. A.; Rosedale, J. H.; Bates, F. S.; Almdal, K.; Mortensen, K. *Macromolecules* **1993**, *26*, 5959.

(22) Hamley, I. W.; Gehlsen, M. D.; Khandpur, A. K.; Koppi, K. A.; Rosedale, J. H.; Schulz, M. F.; Bates, F. S.; Almdal, K.; Mortensen, K. *J. de Phys. II* **1994**, *4*, 2161.

(23) Disko, M. M.; Liang, K. S.; Bheal, S. K.; Roe, R. J.; Jeon, K. J. *Macromolecules* **1993**, *26*, 2983.

(24) Schulz, M. F.; Bates, F. S.; Almdal, K.; Mortensen, K. *Phys. Rev. Lett.* **1994**, *73*, 86.

(25) Forster, S.; Khandpur, A. K.; Zhao, J.; Bates, F. S.; Hamley, I. W.; Ryan, A. J.; Bras, W. *Macromolecules* **1994**, *27*, 6922.

(26) Hajduk, D. A.; Harper, P. E.; Gruner, S. M.; Honeker, C. C.; Kim, G.; Thomas, E. L. *Macromolecules* **1994**, *27*, 4063.

(27) Thomas, E. L.; Alward, D. B.; Kinning, D. J.; Martin, D. C.; D.L. Handlin, J.; Fetters, L. J. *Macromolecules* **1986**, *19*, 2197.

(28) Hasegawa, H.; Tanaka, K.; Yamasaki, K.; Hashimoto, T. *Macromolecules* **1987**, *20*, 1651.

(29) Matsen, M. W.; Bates, F. S. *Macromolecules* **1996**, *29*, 1091.

(30) Young, R. J.; Lovell, P. A. *Introduction to Polymers*; 2nd ed.; Chapman & Hall: New York, 1991.

(31) Helfand, E.; Tagami, Y. *J. Chem. Phys.* **1972**, *57*, 1812.

(32) Helfand, E.; Tagami, Y. *J. Chem. Phys.* **1972**, *56*, 3592.

(33) Helfand, E. *Macromolecules* **1975**, *8*, 552.

(34) Helfand, E.; Wasserman, Z. R. *Macromolecules* **1976**, *9*, 879.

(35) Helfand, E.; Wasserman, Z. R. *Macromolecules* **1978**, *11*, 960.

(36) Helfand, E.; Wasserman, Z. R. *Macromolecules* **1980**, *13*, 994.

(37) Leibler, L. *Macromolecules* **1980**, *13*, 1602.

(38) Semenov, A. N. *Sov. Phys. JETP* **1985**, *61*, 733.

(39) Milner, S. T. *J. Polym. Sci., Pt. B: Polym. Phys.* **1994**, *32*, 2743.

(40) Milner, S. T.; Witten, T. A.; Cates, M. E. *Europhys. Lett.* **1988**, *5*, 413.

(41) Milner, S. T.; Witten, T. A.; Cates, M. E. *Macromolecules* **1988**, *21*, 2610.

(42) Milner, S. T.; Witten, T. A. *J. de Phys.* **1988**, *49*, 1951.

(43) Milner, S. T. *J. Chem. Soc., Fara. Trans.* **1990**, *86*, 1349.

(44) Milner, S. T. *Science* **1991**, *251*, 905.

(45) Olmsted, P. D.; Milner, S. T. *Macromolecules* **1998**, *31*, 4011.

(46) Semenov, A. N. *Sov. Phys. JETP* **1985**, *88*, 1242.

(47) Olmsted, P. D.; Milner, S. T. *Phys. Rev. Lett.* **1994**, *72*, 936.

(48) Matsen, M. W.; Bates, F. S. *Macromolecules* **1996**, *29*, 7641.

(49) Matsen, M. W.; Bates, F. S. *J. Chem. Phys.* **1997**, *106*, 2436.

(50) Olvera de la Cruz, M.; Sanchez, I. C. *Macromolecules* **1986**, *19*, 2501.

(51) Gido, S. P.; Lee, C.; Pochan, D. J.; Pispas, S.; Mays, J. W.; Hadjichristidis, N. *Macromolecules* **1996**, *29*, 7022.

(52) Pochan, D. J.; Gido, S. P.; Pispas, S.; Mays, J. W. *Macromolecules* **1996**, *29*, 5099.

(53) Avgeropoulos, A.; Poulos, Y.; Hadjichristidis, N.; Roovers, J. *Macromolecules* **1996**, *29*, 6076.

(54) Cowie, J. M. G. In *Developments in Block Copolymers - 1*; Goodman, I., Ed.; Applied Science Publishers: New York, 1982, p. 1.

(55) Hashimoto, T.; Shibayama, M.; Kawai, H. *Macromolecules* **1980**, *13*, 1237.

(56) Yamakawa, H. *Modern Theory of Polymer Solutions*; Harper & Row: New York, 1971.

(57) Mays, J. W.; Hadjichristidis, N. *J. App. Polym. Sci.: App. Polym. Symp.* **1992**, *S1*, 53.

(58) Daoud, M.; Cotton, J. P. *J. de Phys.* **1982**, *43*, 531.

(59) Beyer, F. L.; Gido, S. P.; Poulos, Y.; Avgeropoulos, A.; Hadjichristidis, N. *Macromolecules* **1997**, *30*, 2373.

(60) Turner, C. M.; Sheller, N. B.; Foster, M. D.; Lee, B.; Corona-Galvin, S.; Quirk, R. P.; Annis, B.; Lin, J.-S. *Macromolecules* **1998**, *31*, 4372.

(61) Gido, S. P.; Wang, Z.-G. *Macromolecules* **1997**, *30*, 6771.

(62) Beyer, F. L.; Gido, S. P.; Iatrou, H.; Uhrig, D.; Mays, J. W.; Beck Tan, N.; Trevino, S. *Unpublished research* **1999**.

(63) Buzza, D. M. A.; Hamley, I. W.; Fzea, A. H.; Moniruzzaman, M.; Allgaier, J. B.; Young, R. N.; Olmsted, P. D.; McLeish, T. C. B. *Submitted to Macromolecules* **1999**.

(64) Iatrou, H.; Hadjichristidis, N. *Macromolecules* **1993**, *26*, 2479.

(65) Mori, K.; Hasegawa, H.; Hashimoto, T. *Polym. J.* **1985**, *17*, 799.

(66) Oster, G.; Riley, D. P. *Acta Cryst.* **1952**, *5*, 1.

(67) Kinning, D. J.; Thomas, E. L. *Macromolecules* **1984**, *17*, 1712.

(68) Kinning, D. J.; Thomas, E. L.; Fetters, L. J. *J. Chem. Phys.* **1989**, *90*, 5806.

(69) Xenidou, M.; Beyer, F. L.; Gido, S. P.; Hadjichristidis, N.; Beck Tan, N. *Macromolecules* **1998**, *31*, 7659.

(70) Beyer, F. L.; Gido, S. P.; Uhrig, D.; Mays, J. W.; Beck Tan, N.; Trevino, S. F. *Submitted to J. Polym. Sci., Pt. B: Polym. Phys.* **1999**.

(71) Gehlsen, M. D.; Bates, F. S. *Macromolecules* **1994**, *27*, 3611.

(72) Lin, C. C.; Jonnalagadda, S. V.; Kesani, P. K.; Dai, H. J.; Balsara, N. P. *Macromolecules* **1994**, *27*, 7769.

(73) Velis, G.; Hadjichristidis, N. *Macromolecules* **1999**, *32*, 534.

(74) *Polymer Handbook*; 3rd ed.; Wiley-Interscience: New York, 1989.

(75) Matsen, M. W.; Schick, M. *Macromolecules* **1994**, *27*, 6761.

(76) Herman, D. S.; Kinning, D. J.; Thomas, E. L.; Fetters, L. J. *Macromolecules* **1987**, *20*, 2940.

(77) Kinning, D. J.; Alward, D. B.; Thomas, E. L.; Fetters, L. J.; Handlin Jr., D. J. *Macromolecules* **1986**, *19*, 1288.

(78) Matsen, M. W. *J. Chem. Phys.* **1995**, *102*, 3884.

(79) Matsen, M. W.; Schick, M. *Macromolecules* **1994**, *27*, 7157.

(80) Lescanec, R. L.; Hajduk, D. A.; Kim, G. Y.; Gan, Y.; Yin, Y.; Gruner, S. M.; Hogen-Esch, T. E.; Thomas, E. L. *Macromolecules* **1995**, *28*, 3485.

(81) Marko, J. F. *Macromolecules* **1993**, *26*, 1442.

(82) Watanabe, H. *Macromolecules* **1995**, *28*, 5006.

(83) Safran, S. A. *Statistical Thermodynamics of Surfaces, Interfaces, and Membranes*; Addison-Wesley: Reading, Massachusetts, 1994; Vol. 90.

(84) Gido, S. P.; Thomas, E. L. *Macromolecules* **1994**, *27*, 849.

(85) Dozier, W. D.; Thiyagarajan, P.; Peiffer, D. G.; Rabeony, M.; Lin, M. Y.; Agrawal, G.; Wool, R. P. *Polymer* **1994**, *35*, 3116.

(86) Price, C.; Singleton, R.; Woods, D. *Polymer* **1974**, *15*, 117.

(87) Evans, D. C.; George, M. H.; Barrie, J. A. *Polymer* **1975**, *16*, 690.

(88) Gido, S. P.; Gunther, J.; Thomas, E. L.; Hoffman, D. *Macromolecules* **1993**, *26*, 4506.

(89) Pochan, D. J.; Gido, S. P.; Zhou, J.; Mays, J. W.; Whitmore, M.; Ryan, A. J. *J. Polym. Sci., Pt. B: Polym. Phys.* **1997**, *35*, 2629.

(90) Vavasour, J. D.; Whitmore, M. D. *Macromolecules* **1993**, *26*, 7070.

(91) Matsen, M. W.; Schick, M. *Phys. Rev. Lett.* **1994**, *72*, 2660.

(92) Lescanec, R.; Muthukumar, M. *Macromolecules* **1993**, *26*, 3908.

(93) Wolff, T.; Burger, C.; Ruland, W. *Macromolecules* **1993**, *26*, 1707.

(94) Fox, T. G.; Flory, P. J. *J. App. Phys.* **1950**, *21*, 581.

(95) Floudas, G.; Hadjichristidis, N.; Tselikas, Y.; Erukhimovich, I. *Macromolecules* **1997**, *30*, 3090.

(96) Dobrynin, A. V.; Erukhavimovich, I. Y. *Macromolecules* **1993**, *26*, 276.

(97) Whitmore, M. D.; Vavasour, J. D. *Acta Polym.* **1995**, *46*, 341.

(98) Benoit, H.; Hadziioannou, G. *Macromolecules* **1988**, *21*, 1449.

(99) Garetz, B. A.; Balsara, N. P.; Dai, H. J.; Wang, Z.; Newstein, M. C.; Majumdar, B. *Macromolecules* **1996**, *29*, 4675.

(100) Hashimoto, T.; Sakamoto, N.; Koga, T. *Phys. Rev. E* **1996**, *54*, 5832.

(101) Sakamoto, N.; Hashimoto, T. *Macromolecules* **1998**, *31*, 3815.

(102) Underwood, E. E. *Quantitative Stereology*; Addison-Wesley Publishing Company: Reading, MA, 1970.

(103) Skoulios, A. E. In *Developments on Block Copolymers - 1*; Goodman, I., Ed.; Applied Science Publishers: New York, 1982, p. 81.

(104) Oster, G.; Riley, D. P. *Acta Cryst.* **1952**, *5*, 272.

(105) Anastasiadis, S. H.; Retsos, H.; Toprakcioglu, C.; Menelle, A.; Hadziioannou, G. *Macromolecules* **1998**, *31*, 6600.

(106) Higgins, J. S.; Benoit, H. C. *Polymers and Neutron Scattering*; Oxford University Press Inc.: New York, 1994.